

BIOMEDICAL APPLICATIONS OF PHOTO RESPONSIVE LIPID-BASED GENE/DRUG DELIVERY SYSTEMS

BY

WENJIE CHEN

A THESIS SUBMITTED TO MACQUARIE UNIVERSITY

FOR THE DEGREE OF

DOCTOR OF PHILOSOPHY

DEPARTMENT OF PHYSICS AND ASTRONOMY

March 2018

Supervisor: Prof. Ewa M. Goldys; Prof. Michael Steel



MACQUARIE
University
SYDNEY · AUSTRALIA

Contents

<i>Contents</i>	<i>i</i>
<i>List of acronyms</i>	<i>iv</i>
<i>Abstract</i>	<i>vii</i>
<i>Statement of candidate</i>	<i>xi</i>
<i>Acknowledgements</i>	<i>xii</i>
1 Introduction	- 1 -
1.1 Nanotechnology and nanomedicine	- 2 -
1.2 Viral vectors for gene therapy applications	- 3 -
1.3 Nanomaterials used for nucleic acids and drug delivery	- 6 -
1.3.1 Nanoscale drug/gene delivery systems (DDS).....	- 6 -
1.3.2 Cationic polymers for gene delivery	- 8 -
1.3.3 Lipid nanoparticles for gene delivery	- 12 -
1.3.4 The transportation process and cellular uptake of the nanocarrier delivery system in human body	- 19 -
1.4 Light-induced release from synthetic nanocarrier delivery systems	- 20 -
1.4.1 Light triggered delivery systems	- 21 -
1.4.2 Mechanisms and applications of photo-induced gene release	- 22 -
1.4.3 PDT.....	- 25 -
1.5 Light-triggered liposomes for drug/gene delivery	- 26 -
1.6 Data Visualization of literature citation analysis on light-triggered gene release strategy by Citespace	- 29 -
1.7 Thesis aims and outline	- 31 -
Reference	- 34 -
2 Light triggerable liposomes for gene silencing	- 43 -
3 Liposome-polycation-DNA (LPD) for enhanced plasmid delivery	- 69 -
Supplementary material	- 84 -

4	<i>X-ray radiation-induced and targeted photodynamic therapy</i>	<i>- 91 -</i>
5	<i>X-ray radiation-induced gene release and drug delivery in vivo.....</i>	<i>- 111 -</i>
6	<i>Conclusions and perspectives</i>	<i>- 141 -</i>
6.1	<i>Conclusions.....</i>	<i>- 142 -</i>
6.2	<i>Perspectives.....</i>	<i>- 142 -</i>
6.3	<i>Future work on light-triggered liposomal delivery systems.....</i>	<i>- 144 -</i>
7	<i>List of publications.....</i>	<i>- 147 -</i>
	<i>Appendix.....</i>	<i>- 149 -</i>

List of acronyms

AAV	Adenoviruses and adeno-associated viruse
ADA-SCID	Adenosine deaminase-deficient severe congenital immunodeficiency syndrome
asODN	Antisense oligodeoxynucleotides
BPD-MA	Benzoporphyrin derivative monoacid
BPEI	Branched polyethylenimine
Cas9	Associated protein-9 nuclease
CLSM	Confocal laser scanning microscopy
CRISPR	Clustered regularly interspaced short palindromic repeats
DDS	Drug/gene delivery systems
DiI	1,1'-didodecyl-3,3,3,3'-tetramethylindocarbocyanine perchlorate
DiR	1,1'-dioctadecyl-3,3,3,3'-tetramethylindotricarbocyanine iodide
DNQ	2-diazo-1,2-naphthoquinone
DOPE	1,2-Dioleoyl-sn-glycero-3-phosphoethanolamine
DOTAP	N-[1-(2,3-Dioleoyloxy)propyl]-N,N,N-trimethylammonium methyl-sulfate
DPPC	1,2-Dipalmitoyl-sn-glycero-3-phosphocholine
DSPC	1,2-Distearoyl-sn-glycero-3-phosphocholine
DSPE	1,2-distearoyl-sn-glycero-3-phosphoethanolamine
EGFP	Enhanced green fluorescent protein
FA	Folic acid
FDA	Food and drug administration
FR	Folate receptors
LED	Light-emitting diode
LPEI	Linear polyethylenimine
LUV	Large unilamellar vesicles
miRNA	Microrna
MLV	Multilamellar vesicles

NIR	Near-infrared
PA	Phosphatidic acid
PAC1R	Pituitary adenylyl cyclase-activating peptide receptor 1
PACAP	Pituitary adenylyl cyclase-activating peptide
PC	Phosphatidylcholine
PCI	Photochemical internalization
pDNA	Plasmid DNA
PDT	Photodynamic therapy
PE	Phosphatidylethanolamine
PEG	Poly-(ethylene glycol)
PEI	Polyethylenimine
PI	Phosphatidylinositol
PLGA	Poly(D,L-lactide-co-glycolide)
PLL	Poly-L-lysine
PS	Photosensitiser
PS	Phosphatidylserine
ROS	Reactive oxygen species
sgRNA	Short guide RNA
siRNA	Small interference RNA
SUV	Single unilamellar vesicles,
TAPP	5, 10, 15, 20-Tetrakis-(4-aminophenyl) porphyrin
TEM	Transmission electronic microscopy
VP	Verteporfin
DLS	Dynamic light scattering
DCF	2', 7'-dichlorofluorescein
DCF-DA	2', 7'-Dichlorofluorescein diacetate
PBS	Phosphate-buffered saline
HEPES	4-(2-hydroxyethyl)-1-piperazineethanesulfonic acid
TAE	Tris-acetate-EDTA
HBSS	Hank's balanced salt solution
DMEM	Dulbecco's modified Eagle's medium

FBS	Fetal bovine serum
DPBS	Dulbecco's Phosphate-buffered saline
DSC	Differential scanning calorimetry
EPR	Enhanced permeability and retention
EDC	1-[3-Dimethylamino)-propyl]-3-ethyl carbodimide hydrochloride
NHS	N-hydroxysulfosuccinimide
DMSO	Dimethyl sulfoxide
SOSG	Singlet oxygen sensor green probe
CR	Cerenkov radiation
FTIR	Fourier transform infra-red spectroscopy
AOQY	Singlet oxygen quantum yield
H&E	Haematoxylin and eosin
ICP-MS	Inductively coupled plasma mass spectrometry
PTA	Phosphotungstic acid

Abstract

Gene delivery via the nonviral route (i.e., transfection) has emerged in recent decades for biomedical applications, which provides a promising approach for elucidating gene function, genetic engineering and gene therapy for cancer and genetic diseases. The success of nonviral gene delivery highly relies on the development of efficient and biocompatible delivery vectors. Among these synthetic nanoscale vectors, liposomes and polymeric nanomaterials are excellent candidates due to the advantages of safety, easy production, minimal immunotoxicity and high transfection efficiency. It can be envisioned that once these nanocarriers have reached their desired sites, the kinetics and extent of gene release from nanocarriers plays a significant role in the therapeutic performance. The targeting capability of gene delivery systems can also be considered as another important determinant of efficacy of gene action and overall treatment outcome. Therefore, development of triggerable gene delivery systems for on-demand gene release is the subject of current and future considerations to achieve better therapeutic index of gene therapy. My PhD research is mainly focused on development of lipid-based nanocarriers where the payload release can be activated by irradiation from visible light or X-ray. By using these two triggering modalities, therapeutic effect from loaded gene and/or drug was enhanced significantly, compared with traditional liposome delivery systems.

My first project focuses on gene silencing in rat PC12 cells by light-triggered liposomes. These liposomes composed of cationic and neutral lipids and a photosensitizer were utilized in asODN delivery for gene silencing. Gene silencing efficiency of the pituitary adenylyl cyclase-activating peptide (PACAP) receptor 1 (PAC1R) was enhanced by almost 40% under light irradiation compared to the non-irradiated groups. In order to assess this light-activated gene release process, the subcellular analysis was conducted through imaging-based quantitation. Endo/lysosomal escape of antisense oligonucleotides was documented at different time points based on quantitative analysis of colocalization between fluorescently labelled DNA and endo/lysosomes. This work laid a foundation for further development of more complicated liposome delivery systems.

In the second project, further modifications of these liposomes were made to deliver the larger DNA fractions, plasmid DNA (pDNA) expressing the enhanced green fluorescent protein (EGFP). Cholesterol with appropriate amount was incorporated into liposomal structure to enhance the liposome stability in physiological environment. In addition, high complexation ability of polycation molecules with the DNA molecules was also taken advantage, the designed liposome-polycation-DNA (LPD) nanocomplexes, which incorporate verteporfin (VP) in a lipid bilayer and the complex of polyethylenimine (PEI)/plasmid DNA (pDNA) encoding EGFP (polyplex) in the central cavity of the liposome. The nanocomplexes were demonstrated to obtain the light triggered release of pDNA from the liposomes upon irradiation with a near-infrared (NIR) light-emitting diode (LED) light source. The release mechanism is driven by reactive oxygen species (ROS) oxidization via the photochemical reaction from the PS, leading to the release of pDNA into the cytosol and subsequent gene transfer. Light-triggered endolysosomal escape of pDNA at different time points was confirmed by quantitative analysis of colocalization between pDNA and endolysosomes. The efficiency of this photo-induced gene transfection was demonstrated to be more than double compared to non-irradiated controls. Additionally, we observed reduced cytotoxicity of the LPD nanocomplexes compared with the polyplexes alone. We have thus shown that light-triggered and biocompatible LPD nanocomplexes enable improved control of gene delivery which will be beneficial for future gene therapies.

The third part discussed my main contributions to the following work on the drug/gene delivery platforms developed by introducing verteporfin and/or gold nanoparticles into PLGA polymers or the liposomal bilayer:

(1) Photodynamic therapy (PDT) by using X-ray triggered Poly (D, L-lactide-co-glycolide) (PLGA) polymer nanoconstructs (equal authorship contribution): A dual PDT system was developed that can be triggered by both red light at 690 nm and X-ray radiation. PLGA nanoparticles conjugated with folic acid (FA) and incorporating verteporfin, can generate cytotoxic singlet oxygen for cell killing effects and allowed for specific targeting to the HCT116 cancer cells which overexpress the folate receptors (FRs).

(2) *In vitro* and *in vivo* enhanced gene knockdown and antitumour effect by using the X-ray triggered liposomes (second authorship contribution): The same X-ray triggered liposomes loaded with a chemotherapy drug, doxorubicin killed human colorectal cancer cells more effectively than in the absence of X-ray triggering. They have been further demonstrated

better antitumor effect in the colorectal cancer *in vivo*, which indicates the feasibility of a synergistic effect in the course of standard radiotherapy combined with chemotherapy delivered via X-ray triggered liposomes.

The future work on liposome-mediated clustered regularly interspaced short palindromic repeats (CRISPR)-associated protein-9 nuclease (Cas9) delivery system is summarized in the last chapter. In this study, the light-triggered liposomal gene editing systems will be investigated in human cells and zebrafish embryos.

In summary, my PhD work is structured as a thesis by publication. The chapters are presented in the form of published peer-reviewed journal papers.

Key words: lipid-based nanovectors; gene transfection; nonviral gene delivery; drug delivery system; light induced delivery; photochemical internalization; drug delivery; photodynamic therapy; controlled release.

Statement of candidate

I certify that the work in this thesis has not previously been submitted for a degree nor has it been submitted as part of requirements for a degree to any other university or institution other than Macquarie University.

I also certify that the thesis is an original piece of research and it was authored by myself. Help and assistance that I have received in the course of my research work and in the preparation of the thesis itself has, where appropriate, been acknowledged.

In addition, I certify that all information sources and literature used in the course of this research is also indicated where appropriate in this record of my thesis.

Wenjie CHEN

Acknowledgements

Herein I wish to express my sincere appreciates to those who are directly or indirectly involved in the projects during my whole PhD candidature in Macquarie University. Without the tremendous assistance and contributions from them, I would not complete this thesis within three years. Thus I would like to thank:

Firstly my supervisors Prof. Ewa Goldys and Dr. Wei Deng. The continuous support and guidance from them contributed significantly to my completion of PhD study and thesis writing. Ewa Goldys is a professor of great personality, always easy-going, patient and encouraging, she have held the whole directions of all the projects to be on track, offered precious suggestions of problem-solving and paper corrections. Dr. Wei Deng has acted as the daily mentor of my research on almost all matters whether important or trivial. She played the role of an elder sister, being considerate and patient with every details on the experiments and manuscript writing. Both of them have offered great support when I applied the iMQRES scholarship, and have provided me a multidisciplinary atmosphere of advanced research, inspiration and encouragement of devotion into realistic applications using cutting-edge nano techniques.

Then my friends and colleagues who got involved in my projects. First, I wish to thank Prof. Haixin Cui, Dr. Xiang Zhao from the Chinese Academy of Agricultural Sciences for their generous gifts of plasmids which are crucial for my second project on plasmid gene transfer; Second, I greatly appreciate Dr. Jenny Vo, A/Prof. Andrew Piggout, Prof. Ian Paulsen and Miss Xin Xu for their kind supply of the facilities in their lab for me to do microbiology and DNA analysis work, and Jenny's guidance on the plasmid purification and molecular design did a really great help for my work. Third, I want to thank Dr. Sandhya Clement for letting me get involved in her wonderful projects so that we had an excellent cooperation working on the targeted polymer for cancer photodynamic therapy. Fourth, I would like to thank Dr. Ayad Anwer for his patient training and management on most lab facilities and experimental procedures. All these people were very supportive to my research work and they inspired me tremendously.

I also would like to thank two humorous mathematicians that I met since the beginning of my PhD, Dr. Huaiqian Li (Sichuan University) and Dr. Ji Li (MQ), and his wife, who helped me so much to get settled down in the first month when I started exploring Sydney, their patience and hospitality enabled me get familiar with the new environment such quickly. Also my office mates, home mates and friends who cared and helped me with many matters, they are Dr. Deming Liu, Dr. Lixin Zhang, Dr. Xianlin Zheng, Dr. Liuen Liang, Dr. Lianmei Jiang, Dr. Jie Lu, Dr. Yiqing Lu, Dr. Xiantao Jiang, Dr. Anna Guller, Dr. Saabah Bin Mahbub, Dr. Annemarie Nadort, Dr. Shalini Tirunagari, Ms. Minakshi Das, Dr. Ian Loke, Dr. Wan Aizuddin Bin W Razali, Ms. Lisa Pesavento, Ms. Nicole Vella, Ms. Jenny Morcom, Ms. Leonie McKay, Mr. Kaixin Zhang, Ms. Zahra Khabir, Mr. Kashif Islam, Mr. Aziz Ul Rehman, Mr. Abbas Habibalahi, Miss Yan Wang, Miss Yameng Zheng, Mr. Meng He, Dr. Ke Ma, Mr. Fei Deng, Mr. Fei Wang, Miss Fang Gao, Ms. Yuan Liu and Dr. Xiaoteng Jia, Dr. Ran Li, Dr. Xiaoxue Xu, Dr. Jinxiang Huang, Dr. Jipeng Lin, Dr. Peng Hao, Miss Mengyin Li, Dr. Bo Xu, Dr. Ting Hiu Chan, Dr. Longxiang Lin (SIAT, CAS), Miss Fang Yuan, Mr. Long Zhang, Mr. Feng Gao, Ms. Xiaomin Zhang, Ms. Nan Wang, Prof. Yulong Sun (SIAT, CAS), Miss Keke Zhang, Miss Chang Liu (SIAT, CAS), Dr. Huiqiang Cai (MDC-Berlin), Miss Yueyue Liu, Mr. Zac Kalergis, Mr. Yunhai Zhu, Miss Jingjing Ma, Miss Yang Ge, Mr. Yifeng Chen, Miss Sha Zhan, Miss Li Park Lam, Miss Fan Zhu, Miss Yujia Zhai, Miss Wei Li, Miss Ruth Sun and my friends in Melbourne Canberra and Brisbane, Miss Yiwei Xie, Mr. Yanming Pei, Dr. Li Liao, Miss Yasi Xu. Most of the time I spent with you on sports, BBQ, hiking, travelling and lovely parties brought me the biggest fun during the tough periods occupied by scientific research. Thanks a million for your support and friendship.

In addition, I also would like to thank the funding opportunities from different parties. Firstly the iMQRES scholarship from Macquarie University which supported me for three years to pursue the PhD without concerning much on living expenditure. Secondly, the HDR budget from the Physics Department offered us considerable money in research and domestic conferences, which is so important for my projects especially the first one. The PGRF from the university also allowed me the chance to attend an international conference which broad our academic frontier. Thirdly, the Overseas Chinese Youth Forum held by Chinese Academy of Sciences funded me the travel for networking and communicating with the young and intelligent Chinese scientists from many counties across the world.

Finally and most importantly, I have been always kept feeling my heartfelt gratitude to my parents, families, my twin sisters Feifei and Fangfang for their endless love and support. It is to them I dedicate this thesis. Since the day three years ago, which is my first day to go abroad and leave them so far away, I felt so homesick and missed them so much everyday especially in the first month. They always stand behind me no matter what I do and no matter where I go. I will definitely go back to stay with them and make my devotions to this harmonious family.

Sincerely

Wenjie Chen

君子食无求饱，居无求安，敏于事而慎于言，就有道而正焉，可谓好学也已。 ----孔子 (Confucius)

1

Introduction

1.1 Nanotechnology and nanomedicine

Nanotechnology is one of the new important technologies for promoting global technological innovation in the 21st century. There are many new emerging fields associated with nanoscience and nanotechnology, such as nanobiology¹, nanochemistry², nanoelectronics³, and nanomaterials⁴. As the fastest growing field of nanotechnology, various innovative nanomaterials have been widely used in biology, medicine, environment, energy and other fields⁵. Due to the special nature of nanomaterials that many traditional bulky materials do not have, they have been applied to diverse areas such as light heat absorption⁶, magnetic separation⁷, special conductors⁸, molecular sieves⁹, catalysts¹⁰, heat exchange materials¹¹ and lubricants¹². Particularly in biomedical science¹³, the advent of nanotechnology has presented its huge potential to renovate the traditional diagnosis and treatment methods, which will greatly improve the diagnostic accuracy and therapeutic efficiency¹⁴.

This thesis will mainly focus on the nanoscale gene/drug delivery systems based on the light-triggerable lipid and polymeric nanoparticles. These smart systems can help to address current challenges¹⁵ of traditional drug/gene delivery systems in biomedical applications, including:

(1) Improvement of the stability of loaded therapeutic agents. Nano-sized drug carriers can protect the cargos from external environment by loading them into delivery vehicles¹⁵. This feature can be achieved by adjusting physico-chemical properties such as nanomaterial size, the surface charge, components and the nature of the payload.

(2) Enhancement of targeting ability of delivery systems by conjugation of nanoparticle surface with targeting molecules. Targeting delivery is a very important feature in nano-based delivery systems, which can be divided into passive and active targeting¹⁶⁻¹⁷. The passive targeting¹⁷ mainly focuses on tumour blood vessels where nanoparticles have high permeability, leading to the retention of delivery systems at targeted tumour sites. This targeting activity is based on enhanced permeability and retention (EPR) effect of nanoparticle systems¹⁸. However, several factors affect the EPR effect of nanoparticles, such as a lack of targeting ligand, the surface properties of carrier systems and the scavenger receptors in the reticuloendothelial system (RES)¹⁹. Especially the RES uptake has been demonstrated to be a major barrier to the delivery of macromolecular therapeutic agents²⁰.

Hence, in order to overcome these limits, active targeting strategies have been extensively developed where targeting ligands were attached to the nanoparticle surface by various binding methods. In addition, to prolong plasma half-life of delivery systems when used in *in vivo* applications, polyethylene glycol (PEG) polymer was also attached to nanoparticle surface²¹. Compared with passive targeting, active targeting is a more desirable strategy because it can facilitate cellular uptake of nanoparticles by cells themselves. In one of my main contributed work, we conjugated PLGA nanoconstruct drug delivery system with the folic acid molecules (a targeting ligand to folate receptor) to achieve targeted photodynamic therapy (PDT) on killing colorectal cancer cells.

(3) Controllable drug release. Nanoparticle delivery systems can release payloads in a more controllable way by using various stimulus strategies, achieving on-demand drug/gene release and enhancing therapeutic effect. These strategies include endogenous stimuli (such as enzyme²², pH²³ and redox reactions²⁴, etc.) and exogenous ones (such as light, temperature, magnetic field and X-ray irradiation etc.)²⁵. Among various approaches, the light-mediated triggering method has shown great potential and feasibility for on-demand release purpose. My PhD study is mainly focused on light-triggered liposome gene delivery systems, which is discussed in Chapter 2 and 3. In addition, the X-ray irradiation induced gene or drug release systems have also been investigated for *in vitro* and *in vivo* cancer treatment, which are shown in Chapter 4 and 5.

1.2 Viral vectors for gene therapy applications

Gene therapy is a treatment based on the transgenic technique where the foreign gene materials were introduced into the targeted cells to correct or compensate the gene defects and abnormalities caused by the disease²⁶. In May 2016, Europe Commission approved the gene therapy drug Strimlevis for GlaxoSmithKline (GSK), which is used to treat adenosine deaminase-deficient severe congenital immunodeficiency syndrome (ADA-SCID)²⁷. The disease is caused by a congenital absence of a metabolic enzyme called ADA²⁸, which leads to a serious immune system defect. The function of Strimlevis is to extract the hematopoietic stem cells from the patient and introduce the ADA gene into the patient. Although the treatment is expensive (\$660,000), the company guarantees that it will not be paid if the disease cannot be cured. To date the US Food and Drug Administration has

already approved 15 gene therapy products since the first one was approved in October 18, 2017²⁹.

Generally speaking, the gene therapy efficiency highly relies on the delivering methods of the therapeutics genes³⁰. There are various viral and non-viral vectors applied for gene therapy and other applications, some representative examples are shown in the Figure 1-1.

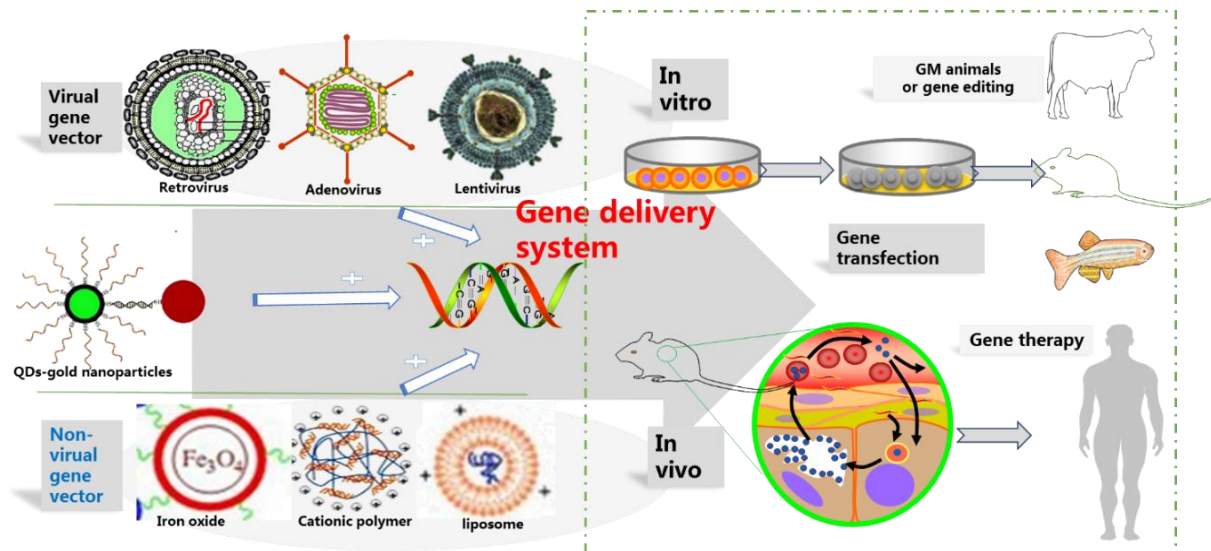


Figure 1-1 Viral and non-viral gene delivery systems.

In this part I mainly discuss viral vectors. Figure 1-2 illustrates the basic route of viral vectors used in gene therapy. In specific, the virus particle loaded with therapeutic DNA sequences attaches to and then enters a cell via receptor mediation process. The packaged

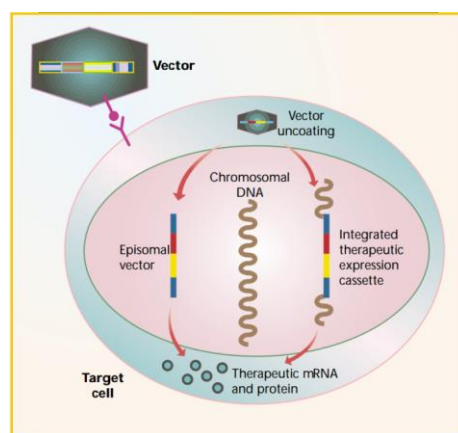


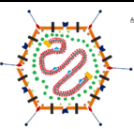
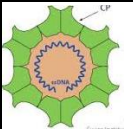
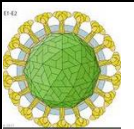
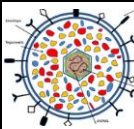
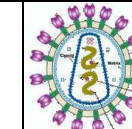
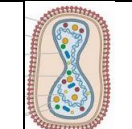
Figure 1-2 Transduction mechanism of a target cell using viral vectors³¹.

genome of virus can be integrated into the host genome or persist as an isolated episome, followed by transcription of the gene for mRNA and expression of protein³¹.

Retroviruses, adenoviruses and adeno-associated viruses (AAVs) are the main viral vectors that have been well characterized and widely used in the provision of viral gene therapy³² (Table 1-1). Retroviral vectors specifically introduce the exogenous DNA into target cells that do not undergo cell division, such as muscle cells or neurons, by reversing transcription replication, e.g., lentiviral vectors and a subclass of retroviral vectors³³. The adenovirus vector only carries viral double-stranded DNA, rather than incorporating it into the host cell genome, making it suitable for applications that require transient protein expression. The AAV vector is a small and simple package³⁴. It can transduce both non-dividing cells and split cells, making it a relatively safe and useful carrier for human gene therapy. Although AAV is non-pathogenic, and proven to be effective in gene delivery, for its long-term effects on safety, further investigation still needs to be done to avoid medical malpractice³⁵⁻³⁶.

Table 1-1 Particle characteristics and gene therapy properties of various Viral gene vectors

32

		Adenovirus	Adeno-associated virus	alphavirus	Herpesvirus	Retrovirus/Lentivirus	Vaccinia virus
Particle characteristics	Genome	dsDNA	ssDNA	ssRNA (+)	dsDNA	ssRNA (+)	dsDNA
	Coat	Naked	Naked	Enveloped	Enveloped	Enveloped	Enveloped
	Virion diameter	70-90 nm	18-26 nm	60 -70 nm	150-200 nm	80-130 nm	300-450 nm
	Genome size	39-38 kb	5 kb	12 kb	120-200 kb	3-9 kb	130-280 kb
							
Gene therapy properties	Family	Adenoviridae	Parvoviridae	Togaviridae	Herpesviridae	Retroviridae	Poxviridae
	Infection	Dividing and non-dividing cells	Dividing and non-dividing cells	Dividing and non-dividing cells	Dividing and non-dividing cells	Dividing cells	Dividing and non-dividing cells
	Host genome interaction	Non-integrating	Non-integrating	Non-integrating	Non-integrating	Integrating	Non-integrating
	Transgene expression	Transient	Potential long lasting	Transient	Potential long lasting	Long lasting	Transient
	Packaging capacity	7.5 kb	4.5 kb	7.5 kb	>30 kb	8 kb	25 kb

There are several risks and barriers that are currently hampering virus vectors-based gene therapy³⁷. First, viruses can usually infect more than one type of cells so they would transduce not only diseased cells but also the healthy cells. In addition, viruses would probably incur the wrong insert of the foreign therapeutic gene, resulting in harmful mutations to the host genome DNA or even diseased disorders. What's more, there is the possibility of randomness of transduction to many types of cell by viruses. In such cases the unintentional introduction of the foreign genes would occur to the reproductive cells, leading to undesired genetic changes that may be passed onto the next generation. Other concerns include the possibility of the overexpression of the introduced genes, the undesired immune response to the virus carriers and the potential transmission of virus between patients, other individuals and the environment³⁶.

1.3 Nanomaterials used for nucleic acids and drug delivery

1.3.1 Nanoscale drug/gene delivery systems (DDS)

In recent years, nano-based drug/gene delivery systems with various structures and functions have been widely developed and applied into medical fields. Compared with viral vectors, these nanoparticle-base delivery systems are non-immunogenic, biocompatible, easy to produce and flexible for surface modification. They have demonstrated excellent performance in nanomedicine, in particular disease treatment³⁸⁻³⁹. Many existing drugs, genetic materials (including DNA, mRNA, siRNA etc.) and biologically active molecules (such as proteins and antibodies) have been incorporated into the appropriate nanoscale carriers. Although traditional nanomaterials as a delivery platform have shown great promise in the treatment of cancer and other diseases, they are still facing complex challenges when used in clinical applications, such as inadequate curative efficiency, less control of the content release and difficult access to target sites⁴⁰. To overcome these limits, many strategies on nanomaterial modification have been developed to improve the performance of non-viral synthetic delivery systems⁴¹ (see Figure 1-3). These nanoscale carriers can be engineered to have the capabilities for controlled drug/gene release, lesions-specific targeting and other desired functions⁴². For example, to meet the requirement of controllable cargo release, many stimulus-responsive systems have been designed where active molecules are incorporated into nanomaterials to achieve the on-demand payload release (Figure 1-4). These stimuli include pH change, temperature, physical fields, or

photochemistry^{25, 43}. Among these approaches, photo-responsive methods for on-off response and even for reversible switch have attracted extensive interests due to the precise control of light parameters such as illumination wavelength, power density and illumination time⁴⁴.

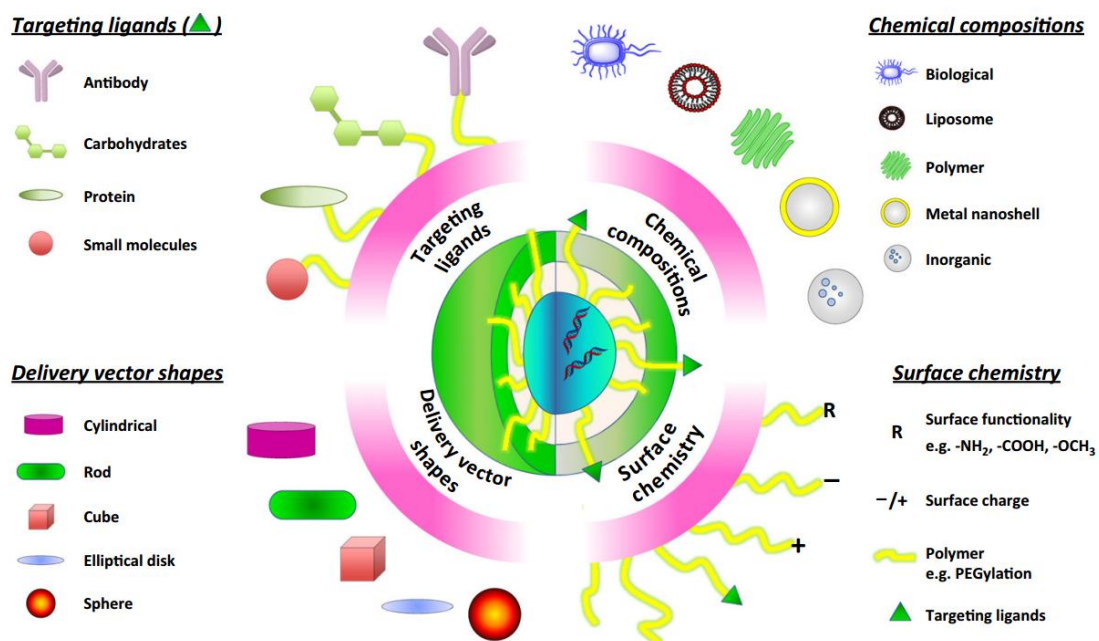


Figure 1-3 Compositional design considerations for four representative properties(target ligands, shapes, chemical compositions and surface chemistry) of nonviral gene delivery systems⁴⁵.

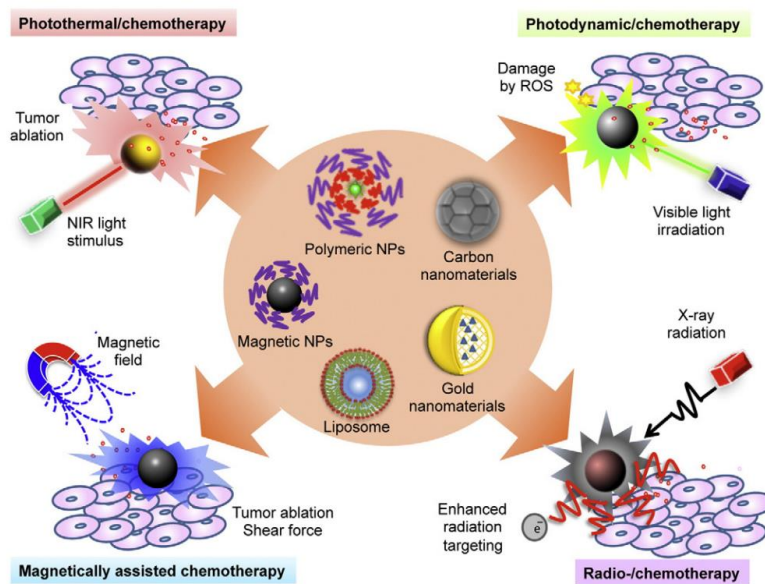


Figure 1-4 Nanocarriers combine chemotherapy with physically destructive modalities that induce tumor ablation (photothermal/magnetic)⁴⁶.

These nanoscale delivery systems are broadly classified into inorganic particles, lipid-, polymer- and peptide-based nanoparticles. In this chapter, I will mainly discuss on polymer- and lipid-based systems that are the focus of my PhD work.

1.3.2 Cationic polymers for gene delivery

Cationic polymers can bind to DNA at physiological pH to form the polymer/DNA complexes, termed as polypox that can condense the DNA molecules into small particles, facilitating the entry into the target cells. Adding polycations such as polyethylenimine (PEI), poly-L-lysine (PLL) and protamine, as a copolymer into liposome components can significantly increase *in vitro* and *in vivo* transfection efficiency⁴⁷. Cationic polymers can enhance cellular uptake by endocytosis, however their transfection efficiencies and cytotoxicity are quite different.

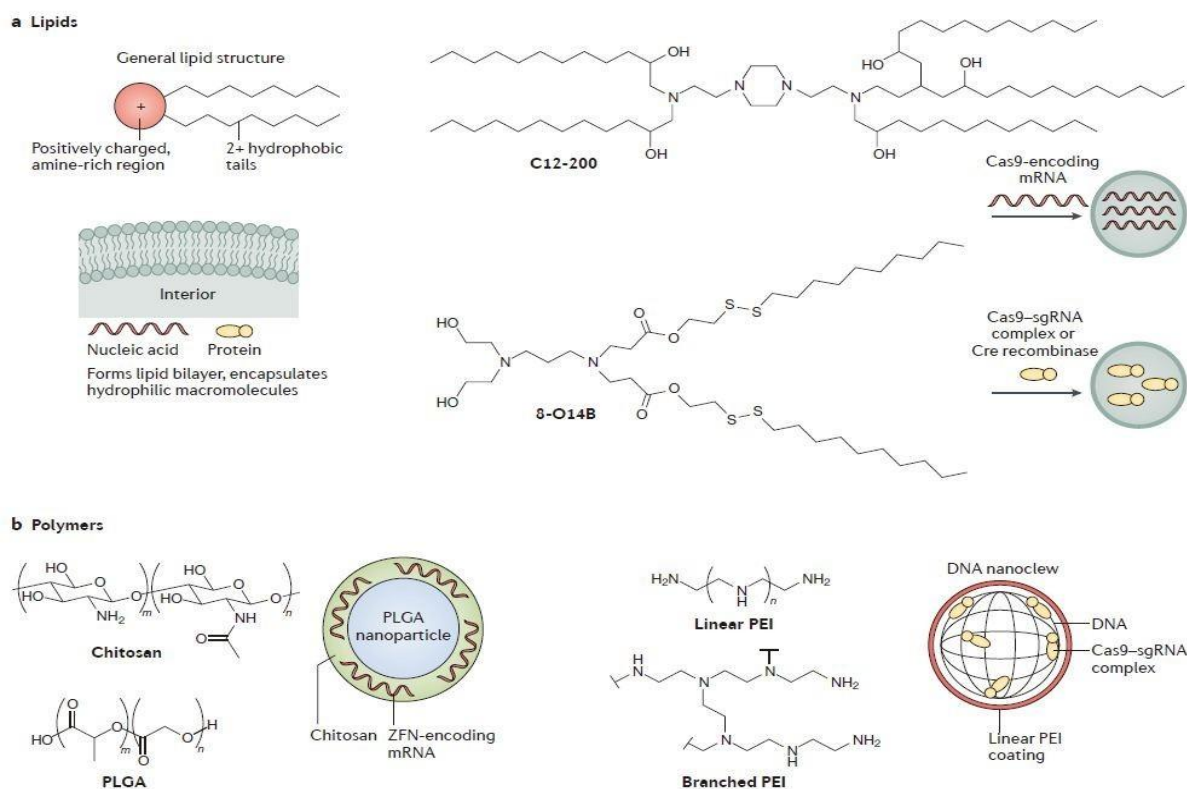


Figure 1-5 Non-viral gene vectors using sythetic lipid and polymer nanomaterials⁴⁸. Two main classes of non-viral nanoparticles are made from cationic materials: lipids (a) and polymers (b).

1.3.2.1 PEI

PEI is the mostly studied and efficient polymer gene vector. The capacity of PEI to condense DNA molecules and its proton sponge effect⁴⁹ are the vital properties of efficient gene delivery. Its transfection efficiencies vary widely different between the ones with different molecular weights and different sturcture⁵⁰. Low molecular weight PEI does not have capabilities of delivering gene. Typically 25 KD PEI is utilized as a potent copolymer for gene transfection. Many factors affect the gene transfer capacity of PEI complexes, such as: molecular weight, degree of branching, zeta potential and particle size⁵¹.

Linear and branched PEI (BPEI) have high *in vitro* transfection efficiency and moderate in vitro efficiency. Linear PEI (LPEI) has lower cytotoxicity than BPEI. Compared to BPEI/DNA, LPEI/DNA complex has higher gene transfection efficiency. This could be contributed to the less compactness that LBPI compresses DNA molecules compared BPEI does⁵². One of the disadvantages of using PEI is the non-degradable characteristics in animal body that generates toxicity⁵³. The cytotoxicity and transfection efficiency of PEI

are also determined by the physicochemical properties of structures and molecular weight. For example, branched PEI with a high molecular weight (for example, 25 kD) shows favourable transfection activity but suffers from the greater cytotoxicity, compared with PEI of lower molecular weight⁵⁴. The cell viability can be even reduced to less than 20% after treatment of Lovo cells with branched PEI (25 kD, 60 µg/mL)⁵⁵. In order to achieve the optimal balance between cytotoxicity and transfection efficiency, various strategies for PEI modification have been explored, such as combination of PEI/DNA complex with various phospholipids to form the LPD complexes (named as lipopolyplexes)⁵⁶.

The "proton sponge effect" is used to explain the gene delivery mechanism of cationic polymer, especially PEI and its derivatives. The vast majority of amino groups on PEI can not be fully protonated under physiological conditions, while in the endosomes where pH is below 6.0, it can be protonated. Protons entering the endosomes carry chloride ions and increase the osmotic pressure causing the vesicles to burst and rupture. Interestingly, neither lipids nor other cationic polymers (such as PLL, histidine and chitosan) can lead to vesicle rupture, but they can still achieve gene transfection⁵⁷. Therefore, for non-viral vector-mediated gene delivery, there are yet many mechanisms that require further study.

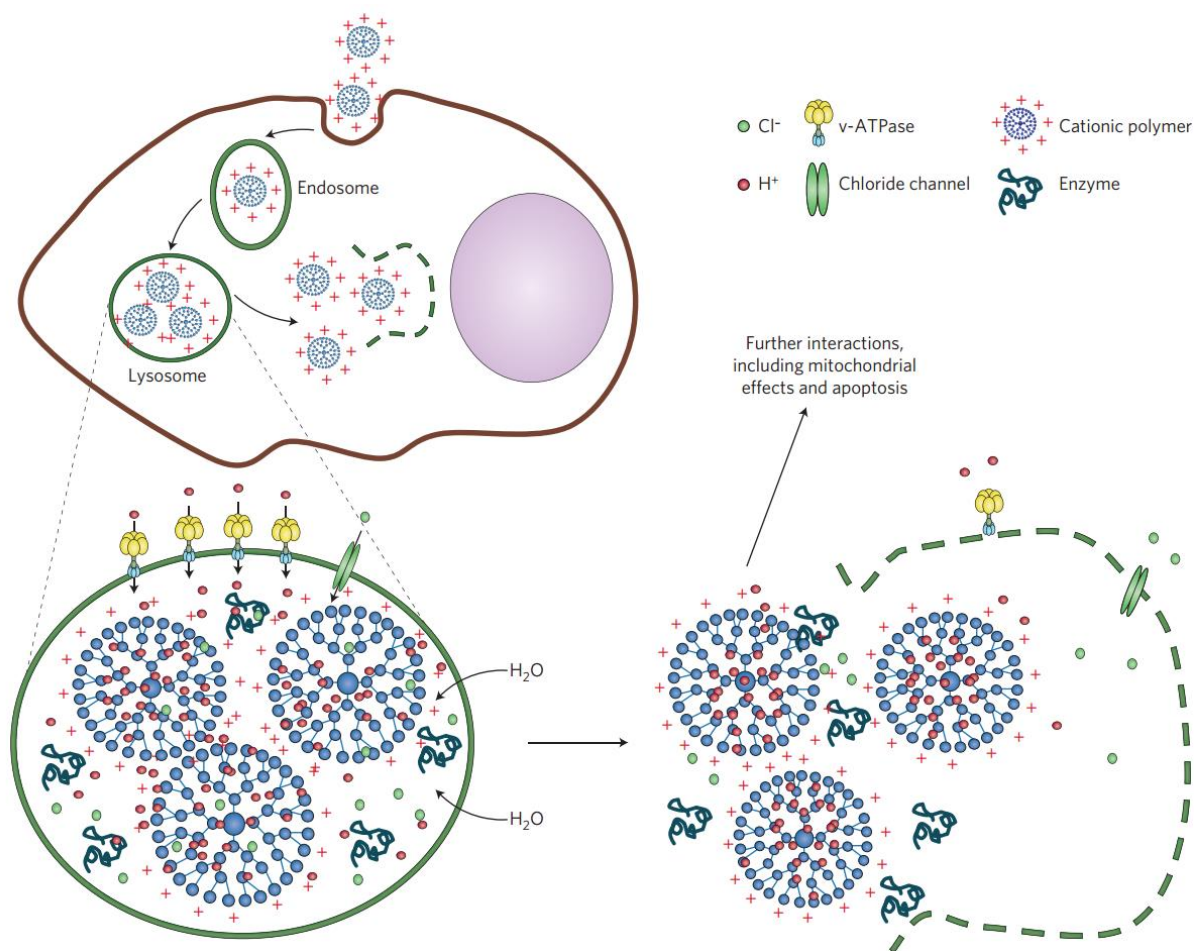


Figure 1-6 The illustration of proton sponge effect ⁵⁷.

1.3.2.2 Poly (L-lysine) (PLL)

Poly-L-lysine was the first cationic polymer to be used for gene transfer and was the one of the first cationic polymers to be used in clinic trails⁵⁸. It is a linear peptide with lysine as a repeat unit, its biodegradable feature make it has advantages *in vivo* application. However, the PLL complexes are prone to bind with hemoglobin and then to be cleared in the circulation⁵⁹. In fact, PLL's transfection efficiency is usually low without modification. In addition, successful transfection by using PLL usually needs combination with other endocytosis enhancer such as chloroquine to reduce lysosomal degradation of the complex⁶⁰.

1.3.3 Lipid nanoparticles for gene delivery

1.3.3.1 The structure of liposomes and phospholipid molecules

Nano organic delivery systems are constructed from different types of chemical materials including chitosan and its derivatives, poly lactic acid and its derivatives, liposomes, sodium alginate, collagen, cyclodextrins, amino acid polymers, hyaluronic acid and so on⁶¹. Among them, liposomes are an excellent candidate of the active nanoscale delivery systems due to their unique amphiphilic structure. The specific application of this kind of system depends on the different liposome formulations. In brief, liposomes are vesicles assembled from phospholipid bilayer membranes, simultaneously wrapping the drug or other molecules for the delivery aims⁶². Figure 1-7 shows the basic rout of making liposomes through the molecular reassembly between amphiphilic phospholipids that are the main components. Liposome preparation technologies are well demonstrated and easy to achieve large-scale products, which enable liposomes to be applicable to various fields such as pharmacy, immunomodulation, biotechnology, genetic medicine and genetic engineering. Many liposomes applied in drug formulations have been approved by FDA and more are undergoing clinical trials recently⁶³.

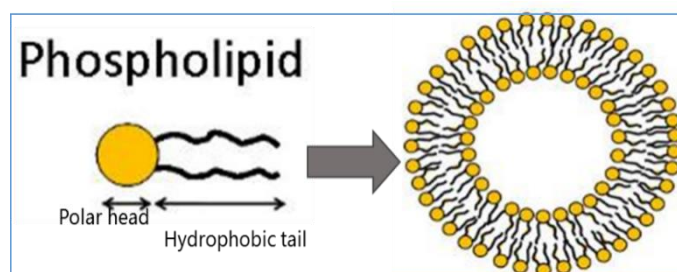


Figure 1-7 Liposome preparation by molecular reassembling.

Liposomes are mainly composed of phospholipids and cholesterol. Figure 1-8 is a schematic diagram of phospholipids where the molecule contains a hydrophilic phosphate ester group and lipophilic fatty acid chain, enabling them a category of excellent amphiphilic molecules. Based on the main structure of phospholipids, they are divided into phosphoglycerides and sphingomyelin⁶⁴. The phosphoglycerides are commonly used in the preparation of liposomes, and the following brief description of phosphoglyceride is shown in Figure 1-9⁶⁵.

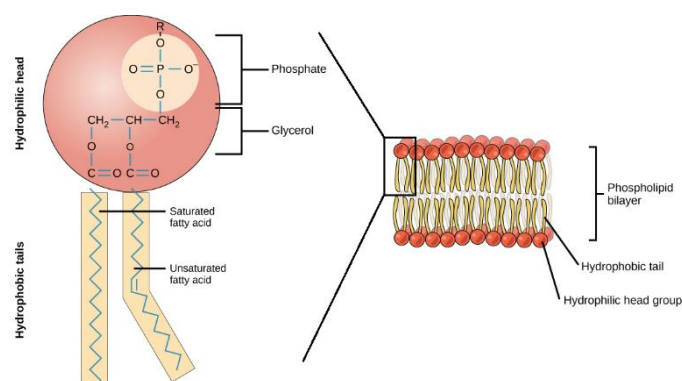


Figure 1-8 Schematic illustration of phospholipid molecule⁶⁶.

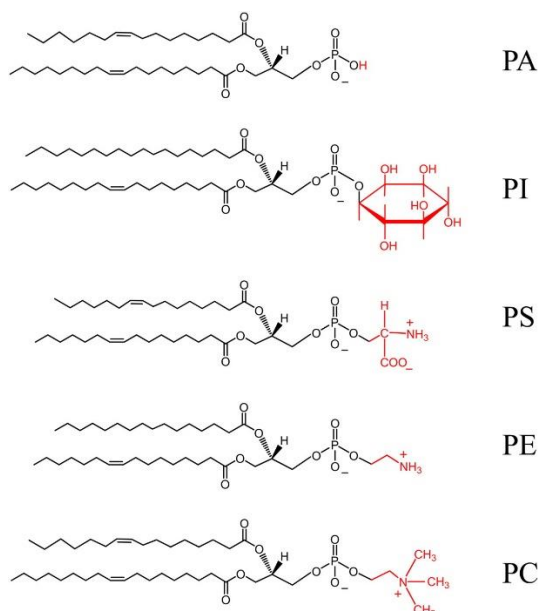


Figure 1-9 The diagram shows the structures of phosphatidic acid (PA), phosphatidylinositol (PI), phosphatidylserine (PS), phosphatidylethanolamine (PE) and phosphatidylcholine (PC) (PI, PS, PE, and PC are derived from PA)⁶⁵. The hydrophilic head groups (H, inositol, serine, ethanolamine and choline) that are attached to the basic phospholipid structure are shown in red.

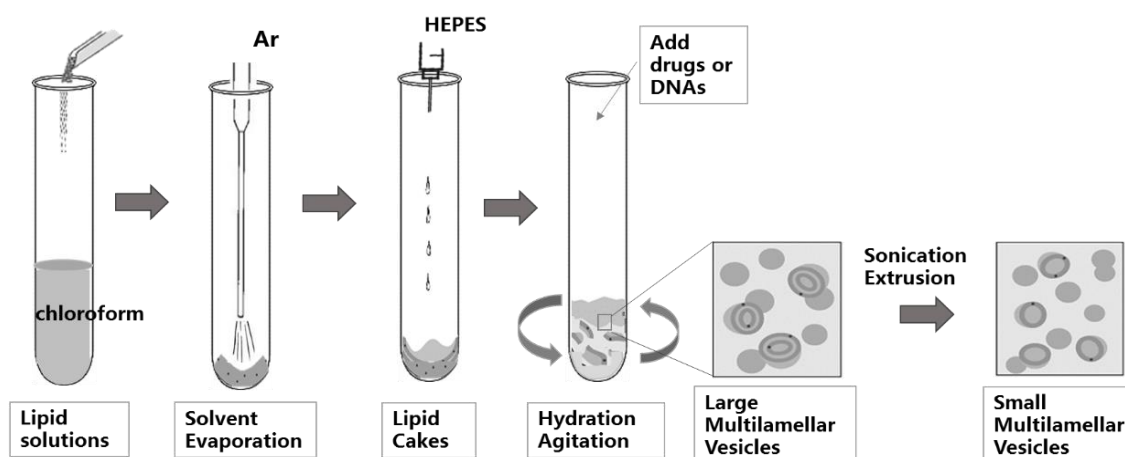


Figure 1-10 The illustration of thin-film preparation of liposome used in this thesis.

The structure of phosphoglycerides has glycerol-3-phosphate as a backbone and the glycerol molecules as the other part. Those two hydroxyl groups are easily esterified by fatty acids, forming a variety of phosphoglycerides⁶⁷. In this way the phosphate groups can have a variety of structures of small molecule compounds. Cholesterol is another important component of liposomes. Though it does not form a liposomal membrane structure, cholesterol has the effect to regulate membrane fluidity, known as liposome fluidity buffer, which is vital for improvement of the liposome stability⁶⁸.

1.3.3.2 Evaluation of the physical and chemical properties of liposomes

To effectively employ liposomes to deliver gene/drug, it's necessary to evaluate physicochemical properties including membrane fluidity, the surface charge, phase transition temperature, size distribution and so on.

(I) Mobility of liposome membranes

Mobility of membranes is an important physical entity of liposomes. The easier mobility of the membrane indicates the less structural stability and the faster drug release. Addition of cholesterol molecules usually reduce the fluidity of the liposome membrane when the temperature overpasses its phase transition temperature (T_m), thus improving the stability⁶⁸.

(II) Phase transition temperature

Orderly arrangement of hydrophobic chains in the liposomal bilayer can be turned to the disorderly arrangement when the temperature is increased, causing a series of property changes. The values of T_m that induces phase changes are determined by the types of phospholipid components⁶⁹. These liposomal membranes are composed of two or more phospholipids, each of which has a specific T_m value. Different phospholipids can coexist

with different phases at a certain temperature. At a certain T_m temperature, the fluidity of the liposomal membrane increases, enabling the encapsulated cargoes be released at the maximum rate⁷⁰.

(III) Electrical properties of the liposomal surface

Liposomal surface charge usually affects many properties of liposomes including the entrapment efficiency, drug loading, targeting ability to the specific sites, stability in targeted organs⁷¹. Conventional nanoparticles with negatively charged and without any surface modifications can be rapidly recognized and cleared by the reticuloendothelial system (RES) in the blood stream⁷². Suitable surface charge of lipid nanoparticles can improve their serum stability and targeting capability and eventually the therapeutic performance⁷³. For example, positively charged liposomes have higher binding preference to the nucleic acids owing to the strong electrostatic force. They can also have better interaction with the negatively charged biomembrane (eg. cell membrane), thus enhancing the uptake activity of these delivery systems⁷⁴.

(IV) Particle size

The size range of liposomes is relatively wide, from 20-80 nm in single-layer vesicle liposomes to multi-layer liposomes with a few microns. The application of liposomes varies somehow depending on different particle size. For example, liposomes with the diameter around 100 nm are commonly used in intravenous injections, whereas micron-sized liposomes are commonly used for oral administration or epidermis drug delivery system⁷⁵.

(V) Drug loading rate and encapsulation efficiency

The drug-loading rate refers to as the weight percentage of the drug contained in the liposome. The entrapment efficiency refers to as the amount of the entrapped drug substance⁷⁶. To obtain optimal encapsulation efficiency, the molar ratio of liposomes and loaded drugs needs to be adjusted during the synthesis⁷⁷.

1.3.3.3 Liposome classification

Based on the surface charges, liposomes are divided into neutral liposomes, negative liposomes and electropositive lipids. Neutral liposomes are consisted of lipid lecithin or other neutral phospholipids, therefore the surface of the liposomes are uncharged⁷⁸. Negatively charged liposomes incorporated acidic phospholipids such as phosphatidylserine in lipids. These two kinds of liposomes can reduce the non-specific adsorption during drug delivery process, thus allowing longer circulation time when used in *in vivo* applications, compared with positively charged liposomes⁷⁹. However,

electropositive liposomes containing positively charged lipids, can enhance the cellular uptake by interacting with negatively charged cell membrane. This enables their applicability for enhanced gene delivery and therapy.

Based on the structure and size, liposomes can be divided into small unilamellar liposome vesicle (SUVs) with the particle size of about 10 ~ 80nm, large unilamellar vesicles (LUVs) with particle size 100 ~ 1000 nm between the single-layer vesicles and multilamellar vesicle (MLVs) containing multiple bilayer with particle size ranging from 1 to 5 μm . When liposomes are used as drug carriers, each layer can in principle encapsulate hydrophobic drug molecules. The water-soluble drug can be encapsulated in the mid cavity of the vesicle. Generally speaking, LUVs can encapsulate the drug whose size is more than 10 times than that loaded inside SUVs⁸⁰. In addition, SUVs can be obtained after filtration of LUVs, which is considered as one of the special properties of liposomes that are superior to the general microcapsules as drug carriers (see Figure 1-11).

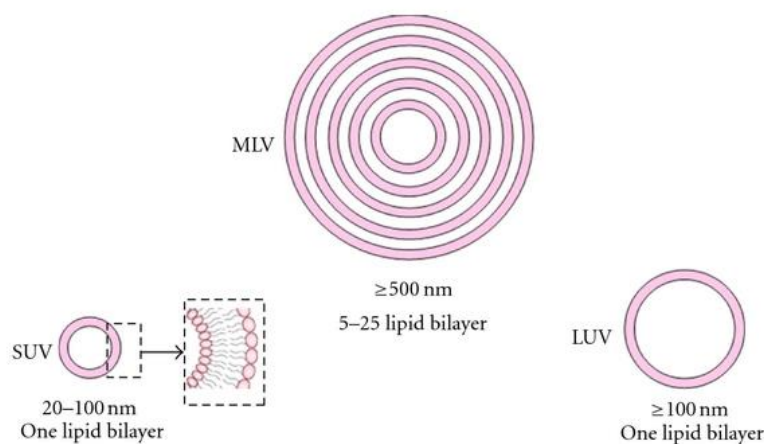


Figure 1-11 Classification of liposomes and their relative sizes. SUV: single unilamellar vesicles, MLV: multilamellar vesicles, LUV: large unilamellar vesicles⁸¹

1.3.3.4 Preparation methods

The preparation methods include thin film dispersion method, reverse phase evaporation method, ultrasonic dispersion method, freeze-dried method and injection method⁸².

(I) Film dispersion method

This method is mainly used for preparation of MLV liposomes. The phospholipids and cholesterol or other hydrophobic components are first dissolved in chloroform (or other

organic solvents) and then chloroform is evaporated using a rotary evaporator or under the inert gas stream to form a thin film laying on the inner wall of the flask. Subsequently, water-soluble drugs or other compounds in the hydrate buffer will be added to the dried lipid film, followed by constant stirring for liposome hydration.

(II) Reverse phase evaporation method

This method is mainly used to the prepare SUVs. The specific process is described as follows. Phospholipids are dissolved in an organic solvent such as chloroform, followed by addition of an aqueous solution of the drug for short-term sonication until a stable oil-in-water emulsion is formed. Evaporation under reduced pressure is conducted to remove the organic solvent. After reaching the colloidal state, the residue is purified by gel chromatography to remove the unencapsulated drugs.

(III) Ultrasonic dispersion method

This method is also mainly used for the preparation of SUVs. Briefly, the water-soluble molecules are dissolved in phosphate buffer and phospholipids, cholesterol or other fat-soluble drugs are dissolved in organic solvents. After that they were mixed together to form the microemulsion. The organic solvent is then removed by stirring and the residual solution is sonicated to form liposomes. The final product is obtained after separation and suspension in phosphorus acid salt buffer.

(IV) Injection method

Phospholipids, cholesterol (or other lipids) and fat-soluble drugs are co-dissolved in organic solvents (ether is generally used). The mixed solution is then passed through the syringe slowly into the phosphate buffer (which can contain water-soluble drugs) and heated to 50 degree, followed by constant stirring until the organic solvent was evaporated. The liposome suspension is then passed through the high-pressure homogenizer for twice, forming the SUVs with a small number of MLVs, with the majority of particle size of 2 microns or less.

(5) Some active liposomes (exclusive of light-triggered liposomes)

Liposomes can be divided into conventional and active types based on their properties and applications. Compared with conventional liposomes, active liposomes have more functions and improved therapeutic effects. They can be engineered to release payloads under certain triggering modality, such as thermosensitive liposomes, pH-sensitive liposomes, magnetic liposomes and photosensitive liposomes⁸³. I will discuss more about photosensitive liposomes in Part 4. Liposomes can also be designed to avoid the clearance

from the blood stream before reaching the target sites. Such liposomes were named “stealth liposomes”, which is usually modified by polymers of PEG⁸⁴.

(I) Thermosensitive liposomes⁸⁵

Thermosensitive liposomes possess the dual advantages of both temperature-activated release and hyperthermia effect when utilized for combination of chemotherapy and thermotherapy. The basic process can be understood as follows. At normal body temperature, the liposome membrane structure is closely arranged at the gelatinous state, therefore the loaded hydrophilic drugs hardly spread outside the liposomal entrapment. When the liposomes reach the targeted organ, the mobility of phospholipid molecules will be strengthened at the local high temperature. This movement turned the original arrangement of neat and dense gelatinous phospholipid bilayers into the loosely chaotic liquid crystal states, thus resulting in leakage of the encapsulated molecules for further therapeutic activities.

(II) pH-sensitive liposomes⁸⁶

After the pH-sensitive liposomes are endocytosed and entrapped into the endosomes, under the acidic microenvironment with lower pH value, they become instable and begin to release the loaded drugs or genetic materials. Because of this unique property, it is possible to release the contents outside the endo/lysosomal compartments into cytosol before enzymatic degradations, thus improving the cytosolic bifunctional effects of genes and drugs. In addition, there may be acidification phenomenon in areas of ischemia, inflammation, infection and in certain tumor tissues, therefore it is of great clinical value for the pH-sensitive liposomes to function at pH ranging from 7.4 to 6.5.

(III) Magnetic thermosensitive liposomes⁸⁷

There is another kind of novel gene/drug delivery system developed in recent years. They can simultaneously play the chemotherapeutic role in a magnetically enhanced manner. The whole carrier system can accumulate at the targeted tissue under the driven force of externally applied magnetic field during the blood circulation. In addition they can release the loaded drugs under the thermal effect to achieve targeted thermal chemotherapy. The triggering mechanism can be attributed as follows. Under the stimulation of an external magnetic field, the lipids are heated above a certain temperature, resulting in destabilization of liposomal structure and payload leakage.

(IV) Stealth liposomes⁸⁸

Traditional liposomes usually consist of phospholipid and cholesterol molecules without further modification, therefore their dwell time in the blood circulation is relatively short.

This is because most of them tend to be absorbed by the reticuloendothelial system before reaching the target site. Stealth liposomes are usually modified with PEG or polyacryloyl amines. Such modifications are prone to form three-dimensional flexible hydrophilic structures so that the liposomes cannot be easily identified. Therefore they are advantageous in extending the circulation time of liposomes and reduce the retention of drugs in the liver and spleen, which has been tremendously studied recently. It should be mentioned that circulation time of stealth liposomes in the blood stream usually depends on PEG molecular weight⁸⁴.

(V) Light responsive liposomes

These are discussed in the next section.

1.3.4 The transportation process and cellular uptake of the nanocarrier delivery system in human body

Synthetic nanocarriers in principle is able to transport genetic materials to the target sites. However there are some barriers and challenges during the transportation and cellular uptake of nanocarriers when used in *in vivo* applications. After administration of the nanocarriers, they are more likely to be cleared by albumin and taken up by macrophages during the circulation before entering the blood vessel associated with the targeted tissue⁸⁹. Therefore higher stability of these carriers in the physiological environment is usually required to avoid undesired clearance from the human body. After reaching the blood vessel, the carriers need to pass through the epithelial tissue and enter the targeted tissue⁹⁰. However, it is another challenge for those particles with diameter larger than 5 nm to cross the capillary epithelial⁸⁹. Therefore it is crucial to understand the cellular uptake mechanism especially in the epithelial cells, where the caveolin-mediated endocytosis (CvME) pathway is one of the most important endocytosis mechanisms⁹¹⁻⁹². After passing through epithelial layer, the carriers begin to attach cell membrane and they are internalized into cell plasma mainly via endocytosis⁹³. The dominant endocytosis pathways vary in different cell lines, resulting in different intracellular processes for the nonviral vectors⁹⁴. Thus the gene transfection efficiencies differ in various cell lines, even using the same delivery system⁹⁵. After internalized into the cytoplasm and then entrapped into the endolysosomal compartments, carriers eventually escape from the endosomes or lysosomes, followed by the release of genetic materials from the carriers into the cytoplasm⁹⁶. It should be

mentioned that pDNA has to be translocated in the nucleus for further transcriptions and translations to protein⁹⁷. The main route of nanocarriers is illustrated in Figure 1-12⁹⁸.

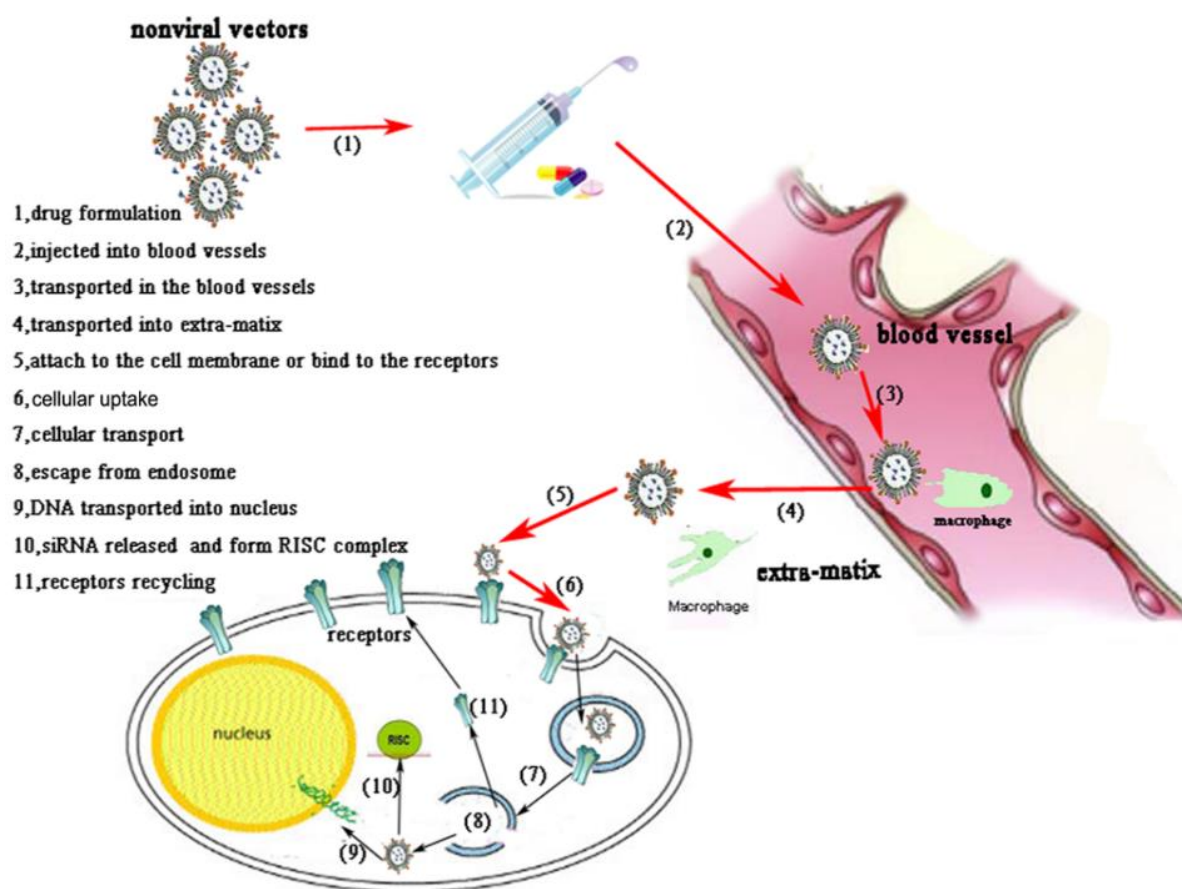


Figure 1-12 The biologic steps of nonviral vector transportation⁹⁸.

1.4 Light-induced release from synthetic nanocarrier delivery systems

In addition to the extracellular and paracellular barriers that the non-viral vectors encounter during their circulation, some intracellular issues including endosomal escape and on-demand release of genes need to be considered and addressed when used *in vivo* applications⁹⁹. Specifically, scientists have been focusing on the following questions: (1) What strategies can be employed to facilitate the endolysosomal escape and nuclear translocation of the loaded genes? and (2) how to achieve on-demand and precise release of genetic materials to enhance their biological functions?

1.4.1 Light triggered delivery systems

In order to address these abovementioned problems, stimulus-triggering delivery systems have been designed, with several strategies being developed for modulating the intracellular release of genes at specific timing and location. We have discussed other triggering modalities in Part 3, thus we will mainly focus on light triggering strategies in the following sections. Photolytic or photoresponsive triggers attracted extensive attention due to unique properties of light. First it can control the gene release in a non-invasive manner. In addition, visible light at an appropriate wavelength can penetrate the skin and tissue to a certain depth (up to 10 mm)¹⁰⁰⁻¹⁰¹ (Figure 1-13). Moreover, its parameters such as wavelength, power density, and illumination time can be adjusted for precise release of payloads from the carriers¹⁰². In recent years, enhanced cytoplasmic delivery of macromolecules by photochemical disruption of the endo/lysosomal membrane, referred to as photochemical internalization (PCI)¹⁰³, has been actively investigated in the context of gene delivery and pharmacotherapy¹⁰⁴. For example, Park *et al.* demonstrated endo/lysosomal escape of the therapeutic p53 gene carried by polymer/gene complex after illumination with a 671 nm laser¹⁰⁵. However, they did not quantitatively explain the endo/lysosomal escape process. By contrast, our study investigates such process through analysis of subcellular colocalization between the released DNA molecules and endo/lysosomes. The related work will be discussed in chapter 2.

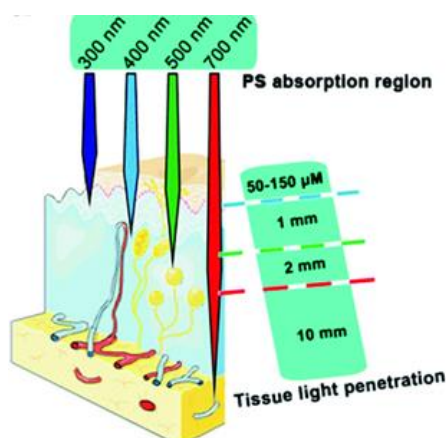


Figure 1-13 Correlation between the PS absorption range and the penetration depth of the light through the tissue¹⁰⁶

1.4.2 Mechanisms and applications of photo-induced gene release

Mechanisms of photo-induced gene release are generally attributed to the conversion of the electromagnetic radiation from light to other forms of energy by active molecules loaded inside nanocarriers (or attached to the surface)^{102, 107}(Figure 1-14a).

The main mechanisms include PCI process, photocrosslinking, photosensitization-induced oxidation, photothermal effects by gold nanoparticles, polymer backbone photo-degradation and photo de-crosslinking^{102, 108}. In the PCI process, the energy from a single photon of UV/visible light can induce photochemical reactions, which have been widely employed to design photo-responsive nanomaterials (Figure 1-14b). For example, under the illumination with a certain wavelength, photochromic groups such as spiropyran and azobenzenes can reversibly transform between their isomers (photoisomerization)¹⁰⁹. This transformation changes the hydrophobicity and polarity, thus resulting in structural disassembly of the nanocarriers¹¹⁰. In addition, some photochromic groups can be activated to remove the designed moieties of ‘caging groups or linkages’ by light trigger. For example, the hydrophobic 2-diazo-1,2-naphthoquinone (DNQ) group can form a hydrophilic 3-indenecarboxylic acid group via a Wolff rearrangement mechanism induced under UV illumination¹¹¹. This hydrophobicity change disrupts nanomaterials containing DNQ, which has been widely used in triggered release system¹¹²⁻¹¹³. In addition, the reversible inter-molecular crosslinking (photocrosslinking) induced by light, such as cycloaddition, can cause the shrinkage or disruption of the chemical structures, leading to a change of the uniformity of building blocks in nanocarriers and the release payloads¹¹³⁻¹¹⁴.

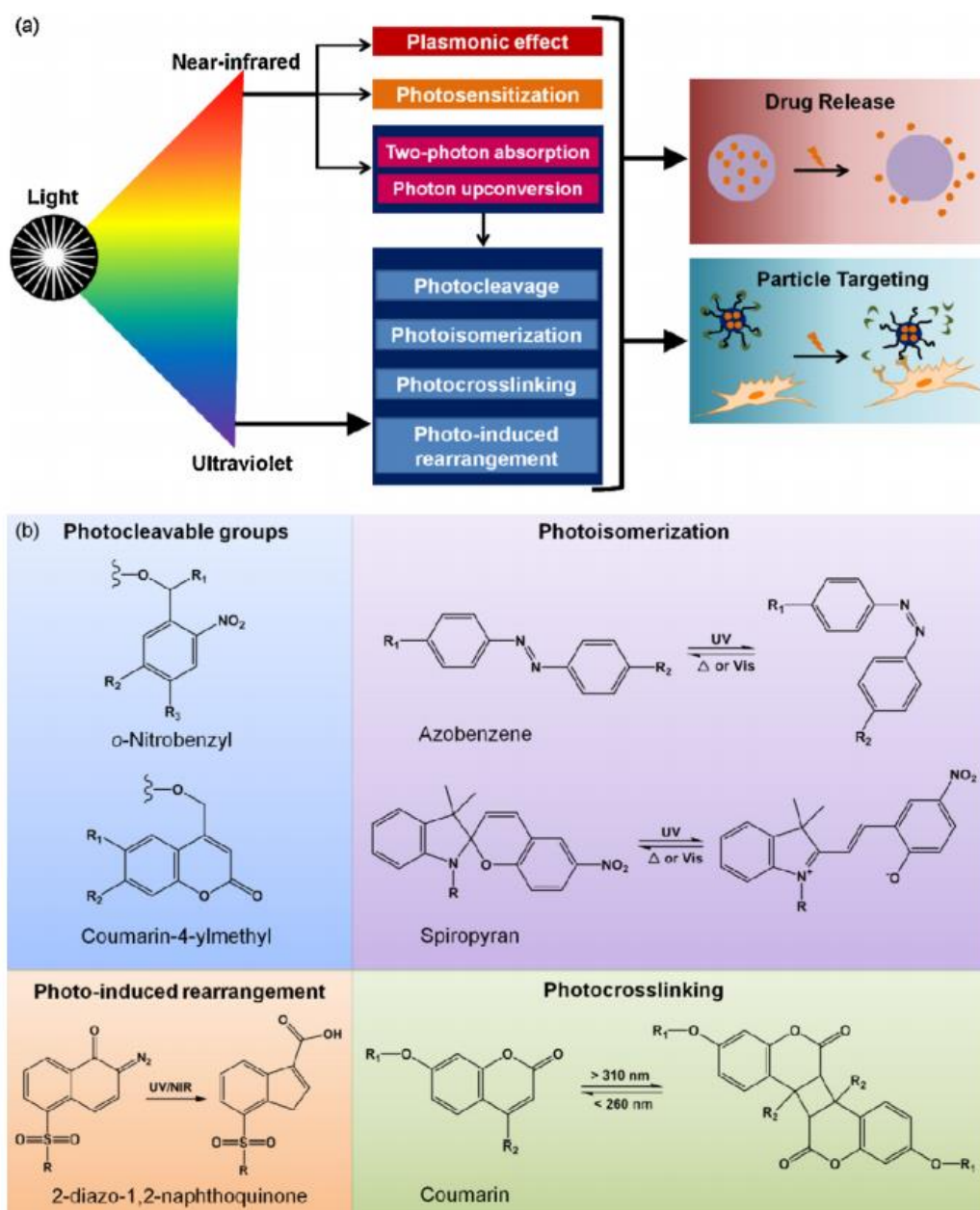


Figure 1-14 Mechanisms of phototriggered drug delivery. (a) Mechanisms of photoresponsiveness for nanoparticle targeting and drug release. (b) Selected chemical groups used for photochemical reactions, such as photocleavage, photoisomerization, photo-induced rearrangement, and photocrosslinking.

Light-triggered polymeric nanomaterial can be used in various applications including gene delivery and antitumour drug delivery. A classic study of light-induced gene transfer is shown in Figure 1-15 where the plasmid DNA was enveloped in a dendrimer carrier embedded with the photosensitiser¹¹⁵. Based on PCI-mediated photo triggering strategy, the ternary complex was designed to control the carrier internalization by the endocytosis, destabilise the endosomal membrane and release the polyplexes to the cytoplasm.

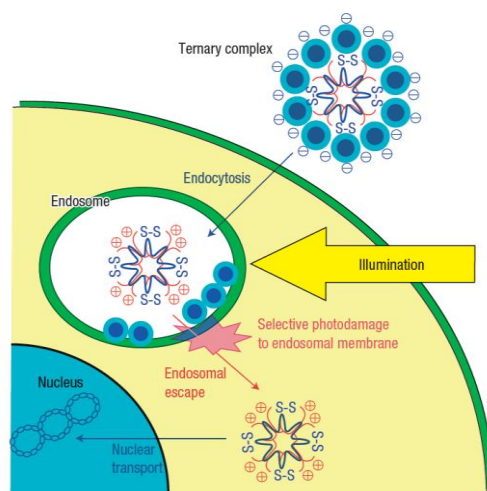


Figure 1-15 A scheme for PCI itinerary of the transgene expression using photoresponsive ternary complex¹¹⁵.

Another recent work¹¹⁶ on the PCI-induced gene release was reported that a star-shaped helical polypeptide with PS-embedding was used for enhanced gene release in melanoma-bearing mice. In this study (Figure 1-16), a PS molecule, 5, 10, 15, 20-Tetrakis-(4-aminophenyl) porphyrin (TAPP) was incorporated in the polypeptide, initiating the ring-opening polymerization (ROP) of N-carboxyanhydride (NCA) and enhancing the gene release under 661 nm laser irradiation. In my PhD work, light-triggered liposome systems were designed in which verteporfin was loaded inside the liposomal bilayers¹¹⁷. Verteporfin can be activated to generate ROS under light illumination at 360 nm or 690 nm wavelength. The generated ROS molecules further induce damages to the liposomal structure and endolysosome membranes stability by oxidizing lipids, leading to enhanced gene release and silencing.

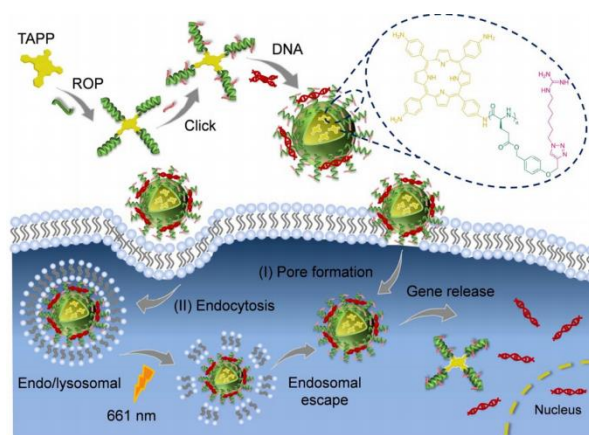


Figure 1-16 PCI-assisted endosomal rupture mediates intracellular gene release and delivery for gene transfection¹¹⁶.

1.4.3 PDT

Photosensitiser molecules are a key factor during PCI-mediated gene release process that investigated in my PhD study. Therefore in this section I will discuss in more details about PSs and PDT which is also based on PSs. PS molecules are widely used as PDT drugs to treat diseases with light illumination. They can absorb energy from light and generate ROS molecules, leading to serious cell damage and tissue necrosis. PDT is a new disease treatment based on the interaction of light, photosensitizers and oxygen¹¹⁸. The mechanism of PDT is shown in Figure 1-17. The excited triplet-state of PSs can be produced via Type-I and Type-II processes¹¹⁹. After the PS absorbs light, the electron shifts from a low-energy non-excited singlet state to a singlet state with high energy. This excited state loses energy by internal conversion (non-radiative decay) or by emitting a photon (fluorescence). The process, known as intersystem crossing, leads to a long-lived excited triplet state. In the presence of oxygen molecules, in Type I reactions superoxide hydroxyl radicals are produced, and singlet oxygen are formed in the Type II reactions. These ROS molecules can oxidize and damage most biomolecules (such as lipids, amino acids and nucleic acids)¹²⁰.

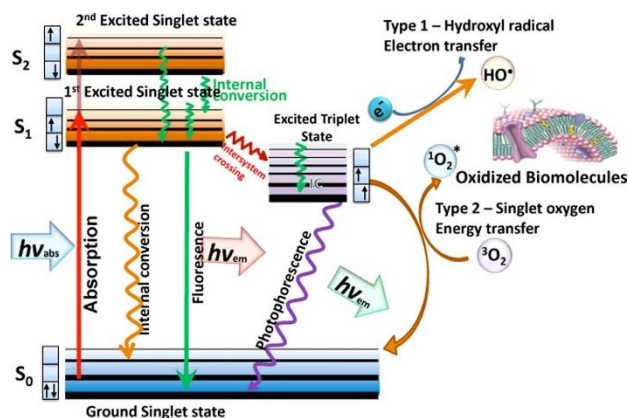


Figure 1-17 Mechanism of PDT processes¹²¹.

There are many types of PSs that have been widely developed and applied in clinical practice¹²². Among them, porfimer sodium was the first PS approved in the United States, Canada, the European Union, Japan and South Korea in 1993-1997¹²³. PDT has become widespread with the successful development of new PDT drugs and the improvement of laser technology. Many PSs have been approved by regulatory agencies for commercialization or clinical trials. Most PSs investigated so far possess the tetrapyrrole structures, such as chlorins, porphyrins, bacteriochlorin, phthalocyanines and their derivatives. In addition to these macrocycles, hypericin, hypocrellin A, rose bengal and methylene blue are also common PSs used in clinical trials for different indications¹²⁴.

In my projects, I loaded liposomes with the PS verteporfin (Benzoporphyrin derivative monoacid, BPD-MA), which belongs to the category of porphyrins¹²⁵. It is a FDA approved PDT drug that has been used for the treatment of macular degeneration. After light illumination at 360 nm or 690 nm, verteporfin generated the sufficient amount of ROS for destabilization of the liposomal structure and endo/lysosomal membranes, leading to enhanced gene release and silencing effect¹¹⁷.

1.5 Light-triggered liposomes for drug/gene delivery

Photo irradiation can act as a viable strategy for external control payloads release from liposomes. This can be realized by destabilizing the stability of the lipid bilayers via photo-induced polymerization, photoisomerization and photodegradation¹²⁶. However, most of these photoresponsive moieties are activated by ultraviolet or visible light illumination¹²⁷,

which restricts their applications due to limited tissue penetration of UV light source. Recently, NIR light was applied to trigger the on-demand cargo release from liposomes. NIR light is more suitable to biomedical applications as it penetrates tissues deeper (up to 10 mm)¹²⁸ with less photodamage to biological tissues¹²⁹, compared with UV and visible light. Table 1-2 summarized the examples of light inducible liposomal delivery systems. Although numerous NIR light responsive drug delivery carriers were reported in the past years, the incorporation of NIR responsive molecules into liposomes for nucleic acids delivery was seldom reported.

Table 1-2 The list of the light inducible liposome delivery systems

Photosensitive moieties	Lipid components	Mechanisms	Light sources (nm)	Applications	Ref
Photopolymerizable diacetylene phospholipid (DC8, 9PC)	DPPC, DSPE-PEG2000	Photopolymerization	254	Doxorubicin Delivery	130
Cinnamoyl Pluronic F127 (CP F127)	egg phosphatidylcholine	Photodimerization	254	Drug release	131
Photosensitizer aluminum phthalocyanine disulfonic acid (AlPcS2)	egg phosphatidylcholine	PCI	360	Release of fluorescein	132
Amino acid containing o-nitrobenzyl lipids	Synthetic lipids	Photocleavage	UV (>320)	Drug release	133
Azobenzene trimethylammonium bromide surfactant	Synthetic lipids	Photo-isomerization	350, 436	EGFP gene delivery in NIH 3T3 cells	134
1,1'-didodecyl-3,3,3,3'-tetramethylindocarbocyanine perchlorate (DiI)	DOPE SorbPC	Photopolymerization	550	Cytoplasmic release	135
Porphyrin-phospholipid	DSPC, DSPE-PEG2K, cholesterol	Light-absorbing monomer esterified	658	Doxorubicin delivery <i>in vivo</i>	136
Porphyrin-phospholipid	DSPE-PEG2k	Light-absorbing monomer esterified	665	Doxorubicin delivery <i>in vivo</i>	137
Hollow gold nanospheres	DPPC, DSPE-PEG ₂₀₀₀ -NH ₂	Photothermal effect	NIR laser	Doxorubicin delivery <i>in vivo</i>	138
Photosensitizer together with a lipophilic NIR dye 1,1'-dioctadecyl-3,3,3', 3'-tetramethylindotricarbocyanine iodide (DiR)	DPPC, DSPE-mPEG _{5k}	PCI	785	Anticancer drug delivery	139
Indocyanine green	DPPC, DSPE-PEG2k	Photothermal effect	808	Anticancer drug delivery	140
Gold nanostars	DOPE	Photothermal effect	656, 850	cytosolic drug delivery	141

1.6 Data Visualization of literature citation analysis on light-triggered gene release strategy by Citespace

CiteSpace is a freely available application for visualizing and analysing trends and patterns of the literatures in a certain field. It is a powerful tool for researchers to review the study topics and analyse the current trend of the fields of their interests¹⁴². More details and instructions can be found at <http://cluster.cis.drexel.edu/~cchen/citespace/>. Herein we mainly focused on the research topic of “light/laser related gene activities”. Data (up to 14th December 2017) from Web of Science (WOS) delivered 2660 hits of research articles. In order to obtain comprehensive records, we used the advanced searching language in the WOS database system (Table 1-3).

Table 1-3 Searching language used in the WOS database on the topics of “light/laser related gene activities”

Search language (Field Tags: TI = title, Booleans: AND, OR)	Database and timespan
“TI= (light OR photo* OR "laser") AND TI= ("gene delivery" OR "gene transfer" OR "DNA transfer" OR "DNA delivery" OR "nucleic acids delivery" OR "gene transfection" OR "gene therapy" OR "gene expression" OR "transcription" OR "CRISPR" OR "cas9" OR "gene editing" OR "genome editing" OR "TALEN" OR "ZFN" OR "gene silencing" OR "siRNA" OR "oligonucleotide" OR "gene activity" OR "*RNA")	LANGUAGE: (English) AND DOCUMENT TYPES: (Article) Timespan: 1997-2017. Indexes: SCI- EXPANDED, SSCI, A&HCI, CPCI-S, CPCI- SSH, BKCI-S, BKCI-SSH, ESCI, CCR-EXPANDED,

From the journal citation report shown in Figure 1-18, we can see a tremendous increase of citations in this research area. Table 1-4 shows the top 10 most cited articles (2007-2017, citation times are recorded from WOS), where the latest paper on the light-inducible CRISPR-Cas9 system published in 2015¹⁴³ has already attracted 135 citations within two years only. This indicates a research trend of the combination between the photo-induced systems and the cutting edge genome editing techniques.

Through simulation of records from WOS via the CiteSpace, Figure 1-19 further visualized the research topics within this field. Each big blue-coloured cluster represents a research keyword and the numerical order of the clusters implies the popularity of studies conducted

by scientists during these ten years. We can clearly find out that the topics of “microRNA”, “gene therapy”, “photochemical internalisation” and “photodynamic therapy” are highly relevant to this field and have been widely explored by researchers.

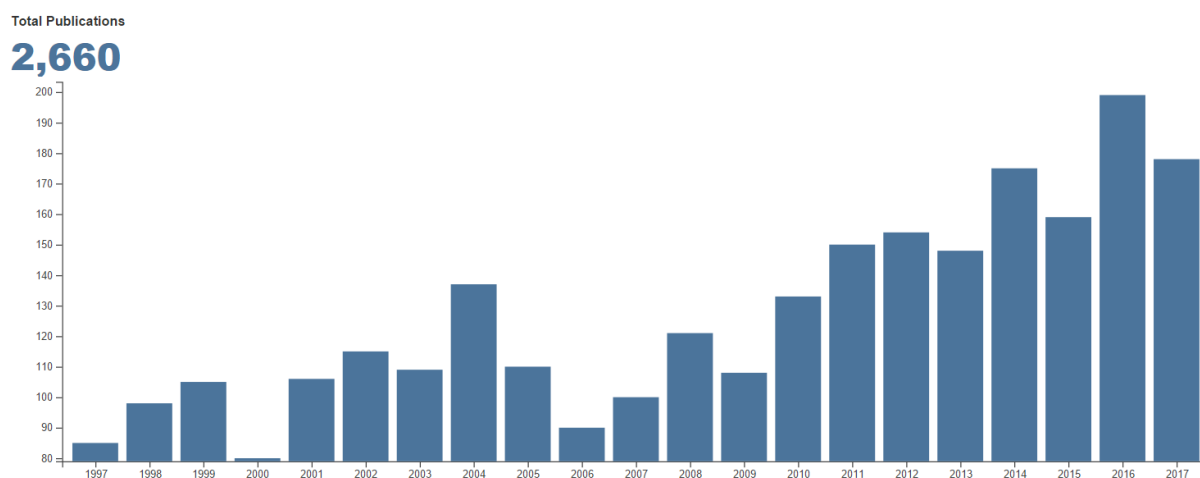


Figure 1-18 Journal citation report diagram.

Table 1-4 Top 10 most cited articles (2007-2017, citations are computed from WOS)

	Citations	Year	Article
1	191	2014	Lin, Li-Sen, et al. "Multifunctional Fe ₃ O ₄ @ polydopamine core-shell nanocomposites for intracellular mRNA detection and imaging-guided photothermal therapy." <i>ACS nano</i> 8.4 (2014): 3876-3883.
2	189	2010	Barbatti, Mario, et al. "Relaxation mechanisms of UV-photoexcited DNA and RNA nucleobases." <i>Proceedings of the National Academy of Sciences</i> 107.50 (2010): 21453-21458.
3	183	2011	Zhang, Yang, et al. "A highly efficient rice green tissue protoplast system for transient gene expression and studying light/chloroplast-related processes." <i>Plant methods</i> 7.1 (2011): 30.
4	180	2012	Wang, Xue, Xianjun Chen, and Yi Yang. "Spatiotemporal control of gene expression by a light-switchable transgene system." <i>Nature methods</i> 9.3 (2012): 266-269.
5	160	2013	Feng, Liangzhu, et al. "Polyethylene glycol and polyethylenimine dual-functionalized nano-graphene oxide for photothermally enhanced gene delivery." <i>Small</i> 9.11 (2013): 1989-1997.
6	160	2012	Msanne, Joseph, et al. "Metabolic and gene expression changes triggered by nitrogen deprivation in the photoautotrophically grown microalgae <i>Chlamydomonas reinhardtii</i> and <i>Coccomyxa</i> sp. C-169." <i>Phytochemistry</i> 75 (2012): 50-59.
7	150	2013	Lee, Jae Myung, et al. "Switchable gene expression in <i>Escherichia coli</i> using a miniaturized photobioreactor." <i>PloS one</i> 8.1 (2013): e52382.
8	143	2012	Akhavan, O., M. Choobtashani, and E. Ghaderi. "Protein degradation and RNA efflux of viruses photocatalyzed by graphene-tungsten oxide composite under visible light irradiation." <i>The Journal of Physical Chemistry C</i> 116.17 (2012): 9653-9659.
9	136	2012	Huschka, Ryan, et al. "Gene silencing by gold nanoshell-mediated delivery and laser-triggered release of antisense oligonucleotide and siRNA." <i>Acs Nano</i> 6.9 (2012): 7681-7691.

10	135	2015	Polstein, Lauren R., and Charles A. Gersbach. "A light-inducible CRISPR-Cas9 system for control of endogenous gene activation." <i>Nature chemical biology</i> 11.3 (2015): 198-200.
----	-----	------	--

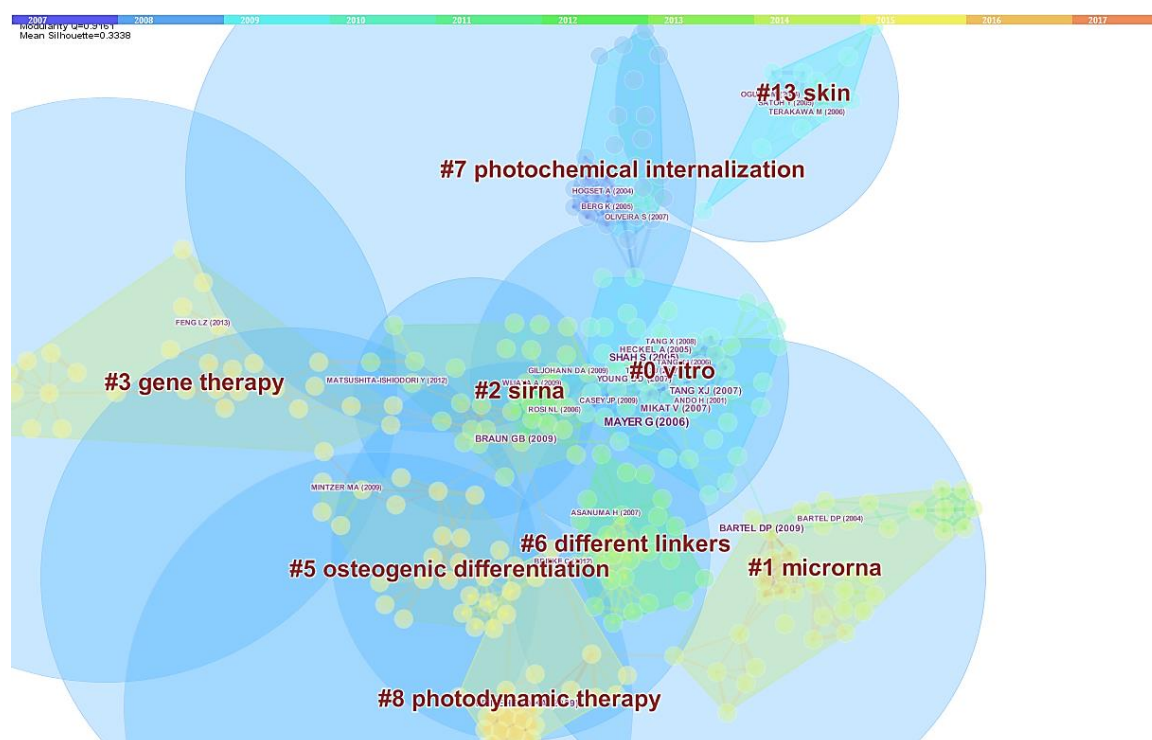


Figure 1-19 The research hotspots on the light regulated gene activities visualized by CiteSpace.

1.7 Thesis aims and outline

Based on the comprehensive literature review about the research topics on liposomes and light induced gene/drug transfer, it is hypothesized that traditional liposome mediated gene/drug delivery could be improved significantly and accurately using a light responsive manner. The aims of my PhD study are to (1) design and demonstrate the gene silencing effect from light-triggered liposome systems, (2) enhance the cancer cell killing effect of PDT by using polymers loaded with photosensitizers and (3) demonstrate *in vivo* therapeutic effect of chemotherapy induced by X-ray triggered liposomes. **Chapter 1** is mainly focused on literature review associated with my PhD work. Chapter 2, 3, 4 and 5 presented my main work in the format of published journal papers or online in press version. Chapter 6 is focused on the ongoing and future work. The detailed thesis outline was described as follows:

Chapter 2 is my first work published in the journal of *Molecular Therapy – Nuclei Acids*. It reports the successful construction and application of a light-triggerable liposome (lipVP) loaded with a photosensitizer verteporfin (VP). Such liposomes were employed as a DNA carrier for pituitary adenylyl cyclase-activating peptide (PACAP) receptor 1 (PAC1R) gene knockdown in PC12 cells. This has been done by incorporating PAC1R antisense oligonucleotides inside the lipVP cavity. PC12 cells which have taken up the lipVP gene delivery system were exposed to a UV light source at 360 nm wavelength. As a result of this exposure, reactive oxygen species (ROS) were generated from VP, destabilising the endo/lysosomal membranes and enhancing the liposomal release of antisense DNA into the cytoplasm. Endo/lysosomal escape of DNA was documented at different time points based on quantitative analysis of colocalization between fluorescently labelled DNA and endo/lysosomes. The antisense oligonucleotides thus released were found to silence PAC1R mRNA. The efficiency of this photo-induced gene silencing was demonstrated by a $74\pm 5\%$ decrease in PAC1R fluorescence intensity at 24 h after light treatment. Following the PAC1R gene knockdown, cell differentiation after exposure to two kinds of PACAP proteins was determined by counting cells exhibiting neurite outgrowth on day 4 after PACAP-38 and PACAP-27 treatment. These two treatments induced cell differentiation in $31\pm 9\%$ and $32\pm 5\%$ of cells treated with PACAP-38 and PACAP-27, respectively.

Work in **Chapter 3** further demonstrated EGFP gene transfection efficiency by using the stable and photoresponsive liposome-polycation-DNA (LPD) nanocomplexes in cancer cells via endolysosomal escape. The first-author manuscript is now published online by *Journal of Materials Chemistry B*. In this work, I engineered the photo-triggered LPD which incorporates verteporfin (VP) in a lipid bilayer and the complex of polyethylenimine (PEI)/plasmid DNA (pDNA) encoding EGFP (polyplex) in the central cavity of the liposome. The liposome was formulated with cationic lipid (DOTAP), PEGylated neutral lipid and cholesterol molecules, which improved liposome stability and cellular uptake in the cell media containing serum. We evaluated the nanocomplex stability by monitoring their size over six days, and assessed the nanocomplex cellular uptake by HCT116 cells under a confocal microscope. We also demonstrated the light-triggered pDNA release from the liposomes upon irradiation with a 690 nm LED light source. The release process was driven by the generation of reactive oxygen species (ROS) from VP after light illumination. These ROS oxidized and destabilized the liposomal and endolysosomal membranes, leading to the release of pDNA into the cytosol and subsequent gene transfer. Light-

triggered endolysosomal escape of pDNA at different time points was confirmed by quantitative analysis of colocalization between pDNA and endolysosomes. The increased expression of the reporter EGFP in HCT116 cells was also quantified after light illumination at various time points. The efficiency of this photo-induced gene transfection was demonstrated to be more than double compared to non-irradiated controls. Additionally, we observed reduced cytotoxicity of the LPD nanocomplexes compared with the polyplexes alone.

Work in **Chapter 4** explores another external triggering strategy by employing X-ray triggered PLGA polymers to PDT for deep tumour treatment. The manuscript is now published by *International Journal of Nanomedicine*. In this work, we engineered a poly (D, L-lactide-co-glycolide) (PLGA) polymer drug delivery system for dual triggering modalities. Verteporfin loaded inside PLGA matrix can be activated to generate cytotoxic singlet oxygen under both red light at 690 nm and 6 MeV X-ray radiation at 4Gy. The X-ray radiation used in this study allows this system to break through the PDT depth barrier, due to excellent penetration of 6 MeV X-ray radiation through biological tissue. In addition, the conjugation of the nanoparticles with folic acid moieties has enabled specific targeting of HCT116 cancer cells which overexpress the folate receptors.

Chapter 5 is the published paper in *Nature Communication* on X-ray triggered liposomal drug/gene release for enhanced antitumour effect, in which I contributed most of the animal and DNA work. The X-ray triggerable liposomes were developed by introducing gold nanoparticles and photosensitizer verteporfin inside the liposomal bilayer. The singlet oxygen generated from verteporfin destabilised the liposomal membrane, causing the release of cargos (gene silencing agents and/or drugs) from the liposomal cavity, under 6MeV X-ray radiation at 4 Gy. This was demonstrated by X-ray triggered PAC1R gene knockdown in rat PC12 cells. The same X-ray triggered liposomes loaded with a chemotherapy drug, doxorubicin killed human colorectal cancer HCT 116 cells more effectively than in the absence of X-ray triggering. Furthermore, such technique was demonstrated to control the colorectal cancer *in vivo*, which indicates the feasibility of a synergistic effect in the course of standard radiotherapy X-rays combined with chemotherapy delivered via X-ray triggered liposomes. My contributed work mainly includes *in vivo* antitumour effect by X-ray triggered liposomes.

Chapter 6 summarises the key novelties and outcomes of this thesis, and also envisions the future prospects of photo-induced gene delivery technology for development of advanced gene editing system *in vitro* and *in vivo*.

Reference

1. Xia, T.; Rome, L.; Nel, A. Nanobiology: particles slip cell security. *Nature materials* **2008**, *7* (7), 519-520.
2. Levy, L.; Sahoo, Y.; Kim, K.-S.; Bergey, E. J.; Prasad, P. N. Nanochemistry: synthesis and characterization of multifunctional nanoclinics for biological applications. *Chemistry of Materials* **2002**, *14* (9), 3715-3721.
3. Lu, W.; Lieber, C. M. Nanoelectronics from the bottom up. *Nature materials* **2007**, *6* (11), 841-850.
4. Kelkar, A. D.; Herr, D. J.; Ryan, J. G. *Nanoscience and Nanoengineering: Advances and Applications*, CRC Press: 2014.
5. Lieber, C. M. Nanoscale science and technology: building a big future from small things. *MRS bulletin* **2003**, *28* (7), 486-491.
6. Hayat, T.; Waqas, M.; Khan, M. I.; Alsaedi, A. Analysis of thixotropic nanomaterial in a doubly stratified medium considering magnetic field effects. *International Journal of Heat and Mass Transfer* **2016**, *102*, 1123-1129.
7. Rossi, L. M.; Costa, N. J.; Silva, F. P.; Wojcieszak, R. Magnetic nanomaterials in catalysis: advanced catalysts for magnetic separation and beyond. *Green Chemistry* **2014**, *16* (6), 2906-2933.
8. Kamyshny, A.; Magdassi, S. Conductive nanomaterials for printed electronics. *Small* **2014**, *10* (17), 3515-3535.
9. Shen, X. F.; Ding, Y. S.; Liu, J.; Cai, J.; Laubernds, K.; Zerger, R. P.; Vasiliev, A.; Aindow, M.; Suib, S. L. Control of Nanometer - Scale Tunnel Sizes of Porous Manganese Oxide Octahedral Molecular Sieve Nanomaterials. *Advanced Materials* **2005**, *17* (7), 805-809.
10. Ding, W.; Li, L.; Xiong, K.; Wang, Y.; Li, W.; Nie, Y.; Chen, S.; Qi, X.; Wei, Z. Shape fixing via salt recrystallization: a morphology-controlled approach to convert nanostructured polymer to carbon nanomaterial as a highly active catalyst for oxygen reduction reaction. *Journal of the American Chemical Society* **2015**, *137* (16), 5414-5420.
11. Marquis, F.; Chibante, L. Improving the heat transfer of nanofluids and nanolubricants with carbon nanotubes. *Jom* **2005**, *57* (12), 32-43.
12. Rapoport, L.; Fleischer, N.; Tenne, R. Fullerene - like WS₂ nanoparticles: Superior lubricants for harsh conditions. *Advanced Materials* **2003**, *15* (7 - 8), 651-655.

13. Xia, Y. Nanomaterials at work in biomedical research. *Nature materials* **2008**, 7 (10), 758-760.
14. Rizzo, L. Y.; Theek, B.; Storm, G.; Kiessling, F.; Lammers, T. Recent progress in nanomedicine: therapeutic, diagnostic and theranostic applications. *Current opinion in biotechnology* **2013**, 24 (6), 1159-1166.
15. Chiappetta, D. A.; Sosnik, A. Poly (ethylene oxide)–poly (propylene oxide) block copolymer micelles as drug delivery agents: improved hydrosolubility, stability and bioavailability of drugs. *European Journal of Pharmaceutics and Biopharmaceutics* **2007**, 66 (3), 303-317.
16. Torchilin, V. P. Passive and active drug targeting: drug delivery to tumors as an example. In *Drug delivery*; Springer: 2010; pp 3-53.
17. Danhier, F.; Feron, O.; Préat, V. To exploit the tumor microenvironment: passive and active tumor targeting of nanocarriers for anti-cancer drug delivery. *Journal of Controlled Release* **2010**, 148 (2), 135-146.
18. Kobayashi, H.; Choyke, P. L. Super enhanced permeability and retention (SUPR) effects in tumors following near infrared photoimmunotherapy. *Nanoscale* **2016**, 8 (25), 12504-12509.
19. Fang, J.; Nakamura, H.; Maeda, H. The EPR effect: unique features of tumor blood vessels for drug delivery, factors involved, and limitations and augmentation of the effect. *Advanced drug delivery reviews* **2011**, 63 (3), 136-151.
20. von Roemeling, C.; Jiang, W.; Chan, C. K.; Weissman, I. L.; Kim, B. Y. Breaking down the barriers to precision cancer nanomedicine. *Trends in biotechnology* **2017**, 35 (2), 159-171.
21. Zhang, L.; Gu, F.; Chan, J.; Wang, A.; Langer, R.; Farokhzad, O. Nanoparticles in medicine: therapeutic applications and developments. *Clinical pharmacology & therapeutics* **2008**, 83 (5), 761-769.
22. Thornton, P. D.; Mart, R. J.; Ulijn, R. V. Enzyme - Responsive Polymer Hydrogel Particles for Controlled Release. *Advanced Materials* **2007**, 19 (9), 1252-1256.
23. Yao, Y.; Wang, Y.; Huang, F. Synthesis of various supramolecular hybrid nanostructures based on pillar [6] arene modified gold nanoparticles/nanorods and their application in pH-and NIR-triggered controlled release. *Chemical Science* **2014**, 5 (11), 4312-4316.
24. Lee, B. Y.; Li, Z.; Clemens, D. L.; Dillon, B. J.; Hwang, A. A.; Zink, J. I.; Horwitz, M. A. Redox - Triggered Release of Moxifloxacin from Mesoporous Silica Nanoparticles Functionalized with Disulfide Snap - Tops Enhances Efficacy Against Pneumonic Tularemia in Mice. *Small* **2016**, 12 (27), 3690-3702.
25. Mura, S.; Nicolas, J.; Couvreur, P. Stimuli-responsive nanocarriers for drug delivery. *Nature materials* **2013**, 12 (11), 991-1003.
26. Naldini, L. Gene therapy returns to centre stage. *Nature* **2015**, 526 (7573), 351-360.
27. Sessa, M.; Lorioli, L.; Fumagalli, F.; Acquati, S.; Redaelli, D.; Baldoli, C.; Canale, S.; Lopez, I. D.; Morena, F.; Calabria, A. Lentiviral haemopoietic stem-cell gene therapy in early-onset metachromatic leukodystrophy: an ad-hoc analysis of a non-randomised, open-label, phase 1/2 trial. *The Lancet* **2016**, 388 (10043), 476-487.
28. Gaspar, H. B.; Buckland, K.; Carbonaro, D. A.; Shaw, K.; Barman, P.; Davila, A.; Gilmour, K. C.; Booth, C.; Terrazs, D.; Cornetta, K. C-8. Immunological and Metabolic Correction After Lentiviral Vector Gene Therapy for ADA Deficiency. *Molecular Therapy* **2015**, 23, S102-S103.
29. Approved Cellular and Gene Therapy Products. <https://www.fda.gov/BiologicsBloodVaccines/CellularGeneTherapyProducts/ApprovedProducts/default.htm>.

30. Jin, L.; Zeng, X.; Liu, M.; Deng, Y.; He, N. Current progress in gene delivery technology based on chemical methods and nano-carriers. *Theranostics* **2014**, *4* (3), 240.
31. Kay, M. A.; Glorioso, J. C.; Naldini, L. Viral vectors for gene therapy: the art of turning infectious agents into vehicles of therapeutics. *Nature medicine* **2001**, *7* (1), 33-40.
32. Viral Vectors. <http://www.genetherapy.net.com/viral-vectors.html>.
33. Naldini, L.; Trono, D.; Verma, I. M. Lentiviral vectors, two decades later. *Science* **2016**, *353* (6304), 1101-1102.
34. Kotterman, M. A.; Schaffer, D. V. Engineering adeno-associated viruses for clinical gene therapy. *Nature Reviews Genetics* **2014**, *15* (7), 445-451.
35. Wu, Z.; Asokan, A.; Samulski, R. J. Adeno-associated virus serotypes: vector toolkit for human gene therapy. *Molecular therapy* **2006**, *14* (3), 316-327.
36. Kotterman, M. A.; Chalberg, T. W.; Schaffer, D. V. Viral vectors for gene therapy: translational and clinical outlook. *Annual review of biomedical engineering* **2015**, *17*, 63-89.
37. Yin, H.; Kanasty, R. L.; Eltoukhy, A. A.; Vegas, A. J.; Dorkin, J. R.; Anderson, D. G. Non-viral vectors for gene-based therapy. *Nature Reviews Genetics* **2014**, *15* (8), 541-555.
38. Li, Y.; Lin, T.-y.; Luo, Y.; Liu, Q.; Xiao, W.; Guo, W.; Lac, D.; Zhang, H.; Feng, C.; Wachsmann-Hogiu, S. A smart and versatile theranostic nanomedicine platform based on nanoporphyrin. *Nature communications* **2014**, *5*.
39. Contreras-Ruiz, L.; Zorzi, G.; Hileeto, D.; Lopez-Garcia, A.; Calonge, M.; Seijo, B.; Sanchez, A.; Diebold, Y. A nanomedicine to treat ocular surface inflammation: performance on an experimental dry eye murine model. *Gene therapy* **2013**, *20* (5), 467-477.
40. Peer, D.; Karp, J. M.; Hong, S.; Farokhzad, O. C.; Margalit, R.; Langer, R. Nanocarriers as an emerging platform for cancer therapy. *Nature nanotechnology* **2007**, *2* (12), 751-760.
41. Nasongkla, N.; Bey, E.; Ren, J.; Ai, H.; Khemtong, C.; Guthi, J. S.; Chin, S.-F.; Sherry, A. D.; Boothman, D. A.; Gao, J. Multifunctional polymeric micelles as cancer-targeted, MRI-ultrasensitive drug delivery systems. *Nano letters* **2006**, *6* (11), 2427-2430.
42. Ferrari, M. Cancer nanotechnology: opportunities and challenges. *Nature Reviews Cancer* **2005**, *5* (3), 161-171.
43. Ganta, S.; Devalapally, H.; Shahiwala, A.; Amiji, M. A review of stimuli-responsive nanocarriers for drug and gene delivery. *Journal of controlled release* **2008**, *126* (3), 187-204.
44. Yuan, Y.; Zhang, C. J.; Liu, B. A Photoactivatable AIE Polymer for Light - Controlled Gene Delivery: Concurrent Endo/Lysosomal Escape and DNA Unpacking. *Angewandte Chemie International Edition* **2015**, *54* (39), 11419-11423.
45. Hill, A. B.; Chen, M.; Chen, C.-K.; Pfeifer, B. A.; Jones, C. H. Overcoming gene-delivery hurdles: physiological considerations for nonviral vectors. *Trends in biotechnology* **2016**, *34* (2), 91-105.
46. Kemp, J. A.; Shim, M. S.; Heo, C. Y.; Kwon, Y. J. "Combo" nanomedicine: Co-delivery of multi-modal therapeutics for efficient, targeted, and safe cancer therapy. *Advanced drug delivery reviews* **2016**, *98*, 3-18.
47. Chen, J.; Yu, Z.; Chen, H.; Gao, J.; Liang, W. Transfection efficiency and intracellular fate of polycation liposomes combined with protamine. *Biomaterials* **2011**, *32* (5), 1412-1418.
48. Yin, H.; Kauffman, K. J.; Anderson, D. G. Delivery technologies for genome editing. *Nature Reviews Drug Discovery* **2017**.
49. Benjaminsen, R. V.; Matthebjerg, M. A.; Henriksen, J. R.; Moghimi, S. M.; Andresen, T. L. The possible "proton sponge" effect of polyethylenimine (PEI) does not include change in lysosomal pH. *Molecular Therapy* **2013**, *21* (1), 149-157.

50. Werth, S.; Urban-Klein, B.; Dai, L.; Höbel, S.; Grzelinski, M.; Bakowsky, U.; Czubayko, F.; Aigner, A. A low molecular weight fraction of polyethylenimine (PEI) displays increased transfection efficiency of DNA and siRNA in fresh or lyophilized complexes. *Journal of controlled release* **2006**, *112* (2), 257-270.
51. Deng, R.; Yue, Y.; Jin, F.; Chen, Y.; Kung, H.-F.; Lin, M. C.; Wu, C. Revisit the complexation of PEI and DNA—How to make low cytotoxic and highly efficient PEI gene transfection non-viral vectors with a controllable chain length and structure? *Journal of Controlled Release* **2009**, *140* (1), 40-46.
52. Wiseman, J.; Goddard, C.; McLelland, D.; Colledge, W. A comparison of linear and branched polyethylenimine (PEI) with DCChol/DOPE liposomes for gene delivery to epithelial cells in vitro and in vivo. *Gene therapy* **2003**, *10* (19), 1654-1662.
53. Luten, J.; Van Steenis, J.; Van Someren, R.; Kemmink, J.; Schuurmans-Nieuwenbroek, N.; Koning, G.; Crommelin, D.; Van Nostrum, C.; Hennink, W. Water-soluble biodegradable cationic polyphosphazenes for gene delivery. *Journal of controlled release* **2003**, *89* (3), 483-497.
54. Zheng, M.; Zhong, Y.; Meng, F.; Peng, R.; Zhong, Z. Lipoic acid modified low molecular weight polyethylenimine mediates nontoxic and highly potent in vitro gene transfection. *Molecular pharmaceutics* **2011**, *8* (6), 2434-2443.
55. Zhan, Z.; Zhang, X.; Huang, J.; Huang, Y.; Huang, Z.; Pan, X.; Quan, G.; Liu, H.; Wang, L. Improved Gene Transfer with Functionalized Hollow Mesoporous Silica Nanoparticles of Reduced Cytotoxicity. *Materials* **2017**, *10* (7), 731.
56. Hirko, A.; Tang, F.; Hughes, J. A. Cationic lipid vectors for plasmid DNA delivery. *Current medicinal chemistry* **2003**, *10* (14), 1185-1193.
57. Nel, A. E.; Mädler, L.; Velegol, D.; Xia, T.; Hoek, E. M.; Somasundaran, P.; Klaessig, F.; Castranova, V.; Thompson, M. Understanding biophysicochemical interactions at the nano-bio interface. *Nature materials* **2009**, *8* (7), 543-557.
58. Lv, H.; Zhang, S.; Wang, B.; Cui, S.; Yan, J. Toxicity of cationic lipids and cationic polymers in gene delivery. *Journal of Controlled Release* **2006**, *114* (1), 100-109.
59. Wagner, E.; Zenke, M.; Cotten, M.; Beug, H.; Birnstiel, M. L. Transferrin-polycation conjugates as carriers for DNA uptake into cells. *Proceedings of the National Academy of Sciences* **1990**, *87* (9), 3410-3414.
60. Ward, C. M.; Read, M. L.; Seymour, L. W. Systemic circulation of poly (L-lysine)/DNA vectors is influenced by polycation molecular weight and type of DNA: differential circulation in mice and rats and the implications for human gene therapy. *Blood* **2001**, *97* (8), 2221-2229.
61. Park, T. G.; Jeong, J. H.; Kim, S. W. Current status of polymeric gene delivery systems. *Advanced drug delivery reviews* **2006**, *58* (4), 467-486.
62. Yingchoncharoen, P.; Kalinowski, D. S.; Richardson, D. R. Lipid-based drug delivery systems in cancer therapy: what is available and what is yet to come. *Pharmacological reviews* **2016**, *68* (3), 701-787.
63. Dawidczyk, C. M.; Kim, C.; Park, J. H.; Russell, L. M.; Lee, K. H.; Pomper, M. G.; Searson, P. C. State-of-the-art in design rules for drug delivery platforms: lessons learned from FDA-approved nanomedicines. *Journal of Controlled Release* **2014**, *187*, 133-144.
64. Brown, R. E. Sphingolipid organization in biomembranes: what physical studies of model membranes reveal. *Journal of cell science* **1998**, *111* (1), 1-9.
65. Henry, S. A.; Kohlwein, S. D.; Carman, G. M. Metabolism and regulation of glycerolipids in the yeast *Saccharomyces cerevisiae*. *Genetics* **2012**, *190* (2), 317-349.
66. Lipids. <https://www.khanacademy.org/science/biology/macromolecules/lipids/a/lipids>.
67. Watts, A. Membrane structure and dynamics. *Current opinion in cell biology* **1989**, *1* (4), 691-700.

68. Coderch, L.; Fonollosa, J.; De Pera, M.; Estelrich, J.; De La Maza, A.; Parra, J. Influence of cholesterol on liposome fluidity by EPR: relationship with percutaneous absorption. *Journal of Controlled Release* **2000**, *68* (1), 85-95.
69. Jing, Y.; Trefna, H.; Persson, M.; Kasemo, B.; Svedhem, S. Formation of supported lipid bilayers on silica: relation to lipid phase transition temperature and liposome size. *Soft Matter* **2014**, *10* (1), 187-195.
70. Mangiarotti, A.; Caruso, B.; Wilke, N. Phase coexistence in films composed of DLPC and DPPC: a comparison between different model membrane systems. *Biochimica et Biophysica Acta (BBA)-Biomembranes* **2014**, *1838* (7), 1823-1831.
71. Pérez-Herrero, E.; Fernández-Medarde, A. Advanced targeted therapies in cancer: drug nanocarriers, the future of chemotherapy. *European journal of pharmaceuticals and biopharmaceutics* **2015**, *93*, 52-79.
72. Rao, L.; Xu, J.-H.; Cai, B.; Liu, H.; Li, M.; Jia, Y.; Xiao, L.; Guo, S.-S.; Liu, W.; Zhao, X.-Z. Synthetic nanoparticles camouflaged with biomimetic erythrocyte membranes for reduced reticuloendothelial system uptake. *Nanotechnology* **2016**, *27* (8), 085106.
73. Kraft, J. C.; Freeling, J. P.; Wang, Z.; Ho, R. J. Emerging research and clinical development trends of liposome and lipid nanoparticle drug delivery systems. *Journal of pharmaceutical sciences* **2014**, *103* (1), 29-52.
74. Kabilova, T. O.; Shmendel, E. V.; Gladkikh, D. V.; Chernolovskaya, E. L.; Markov, O. V.; Morozova, N. G.; Maslov, M. A.; Zenkova, M. A. Targeted delivery of nucleic acids into xenograft tumors mediated by novel folate-equipped liposomes. *European Journal of Pharmaceutics and Biopharmaceutics* **2018**, *123*, 59-70.
75. Akbarzadeh, A.; Rezaei-Sadabady, R.; Davaran, S.; Joo, S. W.; Zarghami, N.; Hanifehpour, Y.; Samiei, M.; Kouhi, M.; Nejati-Koshki, K. Liposome: classification, preparation, and applications. *Nanoscale research letters* **2013**, *8* (1), 102.
76. Nii, T.; Ishii, F. Encapsulation efficiency of water-soluble and insoluble drugs in liposomes prepared by the microencapsulation vesicle method. *International journal of pharmaceutics* **2005**, *298* (1), 198-205.
77. Hattrem, M. N.; Kristiansen, K. A.; Aachmann, F. L.; Dille, M. J.; Draget, K. I. Ibuprofen-in-cyclodextrin-in-W/O/W emulsion-Improving the initial and long-term encapsulation efficiency of a model active ingredient. *International journal of pharmaceutics* **2015**, *487* (1), 1-7.
78. Imran, M.; Revol-Junelles, A.-M.; Paris, C.; Guedon, E.; Linder, M.; Desobry, S. Liposomal nanodelivery systems using soy and marine lecithin to encapsulate food biopreservative nisin. *LWT-Food Science and Technology* **2015**, *62* (1), 341-349.
79. Sercombe, L.; Veerati, T.; Moheimani, F.; Wu, S. Y.; Sood, A. K.; Hua, S. Advances and challenges of liposome assisted drug delivery. *Frontiers in pharmacology* **2015**, *6*.
80. Khuller, G.; Kapur, M.; Sharma, S. Liposome technology for drug delivery against mycobacterial infections. *Current pharmaceutical design* **2004**, *10* (26), 3263-3274.
81. Periyasamy, P. C.; Leijten, J. C.; Dijkstra, P. J.; Karperien, M.; Post, J. N. Nanomaterials for the local and targeted delivery of osteoarthritis drugs. *Journal of nanomaterials* **2012**, *2012*, 5.
82. Szoka Jr, F.; Papahadjopoulos, D. Comparative properties and methods of preparation of lipid vesicles (liposomes). *Annual review of biophysics and bioengineering* **1980**, *9* (1), 467-508.
83. Movahedi, F.; Hu, R. G.; Becker, D. L.; Xu, C. Stimuli-responsive liposomes for the delivery of nucleic acid therapeutics. *Nanomedicine: Nanotechnology, Biology and Medicine* **2015**, *11* (6), 1575-1584.

84. Immordino, M. L.; Dosio, F.; Cattel, L. Stealth liposomes: review of the basic science, rationale, and clinical applications, existing and potential. *International journal of nanomedicine* **2006**, *1* (3), 297.
85. Kneidl, B.; Peller, M.; Winter, G.; Lindner, L. H.; Hossann, M. Thermosensitive liposomal drug delivery systems: state of the art review. *International journal of nanomedicine* **2014**, *9*, 4387.
86. Zhao, Y.; Ren, W.; Zhong, T.; Zhang, S.; Huang, D.; Guo, Y.; Yao, X.; Wang, C.; Zhang, W.-Q.; Zhang, X. Tumor-specific pH-responsive peptide-modified pH-sensitive liposomes containing doxorubicin for enhancing glioma targeting and anti-tumor activity. *Journal of Controlled Release* **2016**, *222*, 56-66.
87. Pradhan, P.; Giri, J.; Rieken, F.; Koch, C.; Mykhaylyk, O.; Döblinger, M.; Banerjee, R.; Bahadur, D.; Plank, C. Targeted temperature sensitive magnetic liposomes for thermo-chemotherapy. *Journal of Controlled Release* **2010**, *142* (1), 108-121.
88. Moghimi, S. M.; Szebeni, J. Stealth liposomes and long circulating nanoparticles: critical issues in pharmacokinetics, opsonization and protein-binding properties. *Progress in lipid research* **2003**, *42* (6), 463-478.
89. Whitehead, K. A.; Langer, R.; Anderson, D. G. Knocking down barriers: advances in siRNA delivery. *Nature reviews Drug discovery* **2009**, *8* (2), 129-138.
90. Jevprasesphant, R.; Penny, J.; Attwood, D.; D'emanuele, A. Transport of dendrimer nanocarriers through epithelial cells via the transcellular route. *Journal of controlled release* **2004**, *97* (2), 259-267.
91. Wang, Z.; Tiruppathi, C.; Minshall, R. D.; Malik, A. B. Size and dynamics of caveolae studied using nanoparticles in living endothelial cells. *ACS nano* **2009**, *3* (12), 4110-4116.
92. Petros, R. A.; DeSimone, J. M. Strategies in the design of nanoparticles for therapeutic applications. *Nature reviews Drug discovery* **2010**, *9* (8), 615-627.
93. Harush-Frenkel, O.; Debotton, N.; Benita, S.; Altschuler, Y. Targeting of nanoparticles to the clathrin-mediated endocytic pathway. *Biochemical and biophysical research communications* **2007**, *353* (1), 26-32.
94. Iversen, T.-G.; Skotland, T.; Sandvig, K. Endocytosis and intracellular transport of nanoparticles: present knowledge and need for future studies. *Nano Today* **2011**, *6* (2), 176-185.
95. Yamano, S.; Dai, J.; Moursi, A. M. Comparison of transfection efficiency of nonviral gene transfer reagents. *Molecular biotechnology* **2010**, *46* (3), 287-300.
96. Blanco, E.; Shen, H.; Ferrari, M. Principles of nanoparticle design for overcoming biological barriers to drug delivery. *Nature biotechnology* **2015**, *33* (9), 941-951.
97. Lechardeur, D.; Verkman, A.; Lukacs, G. L. Intracellular routing of plasmid DNA during non-viral gene transfer. *Advanced drug delivery reviews* **2005**, *57* (5), 755-767.
98. Xiang, S.; Zhang, X. Cellular uptake mechanism of non-viral gene delivery and means for improving transfection efficiency. In *Gene Therapy-Tools and Potential Applications*; InTech: 2013.
99. Sauer, A. M.; Schlossbauer, A.; Ruthardt, N.; Cauda, V.; Bein, T.; Bräuchle, C. Role of endosomal escape for disulfide-based drug delivery from colloidal mesoporous silica evaluated by live-cell imaging. *Nano letters* **2010**, *10* (9), 3684-3691.
100. Ntziachristos, V.; Tung, C.-H.; Bremer, C.; Weissleder, R. Fluorescence molecular tomography resolves protease activity in vivo. *Nature medicine* **2002**, *8* (7), 757-761.
101. Pereira, P. M.; Korsak, B.; Sarmiento, B.; Schneider, R. J.; Fernandes, R.; Tomé, J. P. Antibodies armed with photosensitizers: from chemical synthesis to photobiological applications. *Organic & biomolecular chemistry* **2015**, *13* (9), 2518-2529.

102. Fomina, N.; Sankaranarayanan, J.; Almutairi, A. Photochemical mechanisms of light-triggered release from nanocarriers. *Advanced drug delivery reviews* **2012**, *64* (11), 1005-1020.
103. Berg, K.; Selbo, P. K.; Prasmickaite, L.; Tjelle, T. E.; Sandvig, K.; Moan, J.; Gaudernack, G.; Fodstad, Ø.; Kjølrsrud, S.; Anholt, H. Photochemical Internalization. *Cancer research* **1999**, *59* (6), 1180-1183.
104. Høgset, A.; Prasmickaite, L.; Selbo, P. K.; Hellum, M.; Engesæter, B. Ø.; Bonsted, A.; Berg, K. Photochemical internalisation in drug and gene delivery. *Advanced drug delivery reviews* **2004**, *56* (1), 95-115.
105. Park, S. j.; Park, W.; Na, K. Tumor Intracellular - Environment Responsive Materials Shielded Nano - Complexes for Highly Efficient Light - Triggered Gene Delivery without Cargo Gene Damage. *Advanced Functional Materials* **2015**, *25* (23), 3472-3482.
106. Agostinis, P.; Berg, K.; Cengel, K. A.; Foster, T. H.; Girotti, A. W.; Gollnick, S. O.; Hahn, S. M.; Hamblin, M. R.; Juzeniene, A.; Kessel, D. Photodynamic therapy of cancer: an update. *CA: a cancer journal for clinicians* **2011**, *61* (4), 250-281.
107. Gohy, J.-F.; Zhao, Y. Photo-responsive block copolymer micelles: design and behavior. *Chemical Society Reviews* **2013**, *42* (17), 7117-7129.
108. Rwei, A. Y.; Wang, W.; Kohane, D. S. Photoresponsive nanoparticles for drug delivery. *Nano Today* **2015**, *10* (4), 451-467.
109. Katsonis, N.; Lubomska, M.; Pollard, M. M.; Feringa, B. L.; Rudolf, P. Synthetic light-activated molecular switches and motors on surfaces. *Progress in Surface Science* **2007**, *82* (7), 407-434.
110. Alvarez - Lorenzo, C.; Bromberg, L.; Concheiro, A. Light - sensitive intelligent drug delivery systems. *Photochemistry and photobiology* **2009**, *85* (4), 848-860.
111. Goodwin, A. P.; Mynar, J. L.; Ma, Y.; Fleming, G. R.; Fréchet, J. M. Synthetic micelle sensitive to IR light via a two-photon process. *Journal of the American Chemical Society* **2005**, *127* (28), 9952-9953.
112. Liu, G.; Liu, W.; Dong, C.-M. UV-and NIR-responsive polymeric nanomedicines for on-demand drug delivery. *Polymer Chemistry* **2013**, *4* (12), 3431-3443.
113. Huang, Y.; Dong, R.; Zhu, X.; Yan, D. Photo-responsive polymeric micelles. *Soft Matter* **2014**, *10* (33), 6121-6138.
114. Shum, P.; Kim, J.-M.; Thompson, D. H. Phototriggering of liposomal drug delivery systems. *Advanced drug delivery reviews* **2001**, *53* (3), 273-284.
115. Nishiyama, N.; Iriyama, A.; Jang, W.-D.; Miyata, K.; Itaka, K.; Inoue, Y.; Takahashi, H.; Yanagi, Y.; Tamaki, Y.; Koyama, H. Light-induced gene transfer from packaged DNA enveloped in a dendrimeric photosensitizer. *Nature materials* **2005**, *4* (12).
116. Xu, X.; Li, Y.; Liang, Q.; Song, Z.; Li, F.; He, H.; Wang, J.; Zhu, L.; Lin, Z.; Yin, L. Efficient gene delivery mediated by helical polypeptide: controlling the membrane activity via multivalency and light-assisted photochemical internalization (PCI). *ACS applied materials & interfaces* **2017**.
117. Chen, W.; Deng, W.; Goldys, E. M. Light-Triggerable Liposomes for Enhanced Endolysosomal Escape and Gene Silencing in PC12 Cells. *Molecular Therapy-Nucleic Acids* **2017**, *7*, 366-377.
118. Gollavelli, G.; Ling, Y.-C. Magnetic and fluorescent graphene for dual modal imaging and single light induced photothermal and photodynamic therapy of cancer cells. *Biomaterials* **2014**, *35* (15), 4499-4507.
119. Foote, C. S. Mechanisms of photosensitized oxidation. *Science* **1968**, *162* (3857), 963-970.
120. Dickinson, B. C.; Chang, C. J. Chemistry and biology of reactive oxygen species in signaling or stress responses. *Nature chemical biology* **2011**, *7* (8), 504-511.

121. Abrahamse, H.; Hamblin, M. R. New photosensitizers for photodynamic therapy. *Biochemical Journal* **2016**, 473 (4), 347-364.
122. Allison, R. R.; Downie, G. H.; Cuenca, R.; Hu, X.-H.; Childs, C. J.; Sibata, C. H. Photosensitizers in clinical PDT. *Photodiagnosis and photodynamic therapy* **2004**, 1 (1), 27-42.
123. Triesscheijn, M.; Baas, P.; Schellens, J. H.; Stewart, F. A. Photodynamic therapy in oncology. *The oncologist* **2006**, 11 (9), 1034-1044.
124. Zhang, J.; Jiang, C.; Longo, J. P. F.; Azevedo, R. B.; Zhang, H.; Muehlmann, L. A. An updated overview on the development of new photosensitizers for anticancer photodynamic therapy. *Acta Pharmaceutica Sinica B* **2017**.
125. Runnels, J.; Chen, N.; Ortel, B.; Kato, D.; Hasan, T. BPD-MA-mediated photosensitization in vitro and in vivo: cellular adhesion and beta1 integrin expression in ovarian cancer cells. *British journal of cancer* **1999**, 80 (7), 946-953.
126. Ercole, F.; Davis, T. P.; Evans, R. A. Photo-responsive systems and biomaterials: photochromic polymers, light-triggered self-assembly, surface modification, fluorescence modulation and beyond. *Polymer Chemistry* **2010**, 1 (1), 37-54.
127. Zhang, H.; Chen, D.; Lv, X.; Wang, Y.; Chang, H.; Li, J. Energy-efficient photodegradation of azo dyes with TiO₂ nanoparticles based on photoisomerization and alternate UV– visible light. *Environmental science & technology* **2009**, 44 (3), 1107-1111.
128. O'Neal, D. P.; Hirsch, L. R.; Halas, N. J.; Payne, J. D.; West, J. L. Photo-thermal tumor ablation in mice using near infrared-absorbing nanoparticles. *Cancer letters* **2004**, 209 (2), 171-176.
129. Yang, Y.; Velmurugan, B.; Liu, X.; Xing, B. NIR photoresponsive crosslinked upconverting nanocarriers toward selective intracellular drug release. *Small* **2013**, 9 (17), 2937-2944.
130. Yavlovich, A.; Singh, A.; Blumenthal, R.; Puri, A. A novel class of photo-triggerable liposomes containing DPPC: DC 8, 9 PC as vehicles for delivery of doxorubicin to cells. *Biochimica et Biophysica Acta (BBA)-Biomembranes* **2011**, 1808 (1), 117-126.
131. Wang, M.; Kim, J.-C. Light-and temperature-responsive liposomes incorporating cinnamoyl Pluronic F127. *International journal of pharmaceutics* **2014**, 468 (1), 243-249.
132. Randles, E. G.; Bergethon, P. R. A photodependent switch of liposome stability and permeability. *Langmuir* **2013**, 29 (5), 1490-1497.
133. Chandra, B.; Subramaniam, R.; Mallik, S.; Srivastava, D. Formulation of photocleavable liposomes and the mechanism of their content release. *Organic & biomolecular chemistry* **2006**, 4 (9), 1730-1740.
134. Liu, Y.-C.; Le Ny, A.-L. M.; Schmidt, J.; Talmon, Y.; Chmelka, B. F.; Lee Jr, C. T. Photo-assisted gene delivery using light-responsive catanionic vesicles. *Langmuir* **2009**, 25 (10), 5713-5724.
135. Miller, C. R.; Clapp, P. J.; O'Brien, D. F. Visible light - induced destabilization of endocytosed liposomes. *FEBS letters* **2000**, 467 (1), 52-56.
136. You, J.; Zhang, P.; Hu, F.; Du, Y.; Yuan, H.; Zhu, J.; Wang, Z.; Zhou, J.; Li, C. Near-infrared light-sensitive liposomes for the enhanced photothermal tumor treatment by the combination with chemotherapy. *Pharmaceutical research* **2014**, 31 (3), 554-565.
137. Luo, D.; Carter, K. A.; Razi, A.; Geng, J.; Shao, S.; Giraldo, D.; Sunar, U.; Ortega, J.; Lovell, J. F. Doxorubicin encapsulated in stealth liposomes conferred with light-triggered drug release. *Biomaterials* **2016**, 75, 193-202.
138. Li, Q.; Tang, Q.; Zhang, P.; Wang, Z.; Zhao, T.; Zhou, J.; Li, H.; Ding, Q.; Li, W.; Hu, F. Human epidermal growth factor receptor-2 antibodies enhance the specificity and anticancer activity of light-sensitive doxorubicin-labeled liposomes. *Biomaterials* **2015**, 57, 1-11.

139. Feng, L.; Tao, D.; Dong, Z.; Chen, Q.; Chao, Y.; Liu, Z.; Chen, M. Near-infrared light activation of quenched liposomal Ce6 for synergistic cancer phototherapy with effective skin protection. *Biomaterials* **2017**, *127*, 13-24.
140. Lajunen, T.; Kontturi, L.-S.; Viitala, L.; Manna, M.; Cramariuc, O.; Róg, T.; Bunker, A.; Laaksonen, T.; Viitala, T.; Murtomäki, L. Indocyanine green-loaded liposomes for light-triggered drug release. *Molecular pharmaceutics* **2016**, *13* (6), 2095-2107.
141. Lajunen, T.; Viitala, L.; Kontturi, L.-S.; Laaksonen, T.; Liang, H.; Vuorimaa-Laukkanen, E.; Viitala, T.; Le Guével, X.; Yliperttula, M.; Murtomäki, L. Light induced cytosolic drug delivery from liposomes with gold nanoparticles. *Journal of controlled release* **2015**, *203*, 85-98.
142. Chen, C. Searching for intellectual turning points: Progressive knowledge domain visualization. *Proceedings of the National Academy of Sciences* **2004**, *101* (suppl 1), 5303-5310.
143. Polstein, L. R.; Gersbach, C. A. A light-inducible CRISPR-Cas9 system for control of endogenous gene activation. *Nature chemical biology* **2015**, *11* (3), 198-200.

2

Light triggerable liposomes for gene silencing

Chapter 2 Paper 1

Chen W, Deng W, & Goldys EM (2017). Light-triggerable liposomes for enhanced endolysosomal escape and gene silencing in PC12 cells. *Molecular Therapy-Nucleic Acids*, 7, 366-377.

Light-Triggerable Liposomes for Enhanced Endolysosomal Escape and Gene Silencing in PC12 Cells

Wenjie Chen,¹ Wei Deng,¹ and Ewa M. Goldys¹

¹ARC Centre of Excellence for Nanoscale BioPhotonics, Department of Physics and Astronomy, Macquarie University, Sydney, NSW 2109, Australia

Liposomes are an effective gene and/or drug delivery system, widely used in biomedical applications including gene therapy and chemotherapy. Here, we designed a photo-responsive liposome (lipVP) loaded with a photosensitizer verteporfin (VP). This photosensitizer is clinically approved for photodynamic therapy (PDT). LipVP was employed as a DNA carrier for pituitary adenyl cyclase-activating polypeptide (PACAP) receptor 1 (PAC1R) gene knockdown in PC12 cells. This has been done by incorporating PAC1R antisense oligonucleotides inside the lipVP cavity. Cells that have taken up the lipVP were exposed to light from a UV light source. As a result of this exposure, reactive oxygen species (ROS) were generated from VP, destabilizing the endolysosomal membranes and enhancing the liposomal release of antisense DNA into the cytoplasm. Endolysosomal escape of DNA was documented at different time points based on quantitative analysis of colocalization between fluorescently labeled DNA and endosomes and lysosomes. The released antisense oligonucleotides were found to silence PAC1R mRNA. The efficiency of this photo-induced gene silencing was demonstrated by a $74\% \pm 5\%$ decrease in PAC1R fluorescence intensity. Following the light-induced DNA transfer into cells, cell differentiation with exposure to two kinds of PACAP peptides was observed to determine the cell phenotypic change after PAC1R gene knockdown.

INTRODUCTION

Gene delivery and gene therapy rely on effective exogenous nucleic acids transfer into cells.¹ Due to the high transfection efficiency, viral carriers are a commonly used method of gene delivery.^{2,3} However, the development and application of viral carriers is hindered by a range of limitations including toxin production, limited size of transgenic DNA, packaging difficulties, and the risk of recombination.⁴ To overcome these limitations, synthetic non-viral gene delivery systems, in particular, nanomaterial-based systems, have been extensively studied and developed.⁵⁻⁷ Among these nanomaterials, liposomes, especially including cationic lipid components, have attracted significant interests as a drug and/or gene delivery vehicle since the 1980s.⁸⁻¹⁰ Up-to-date, various types of liposomes have been clinically used to improve the efficacy and biodistribution of drugs, including cancer therapeutics.^{11,12} In recent years, a number of studies reported the application of liposomal carriers to various gene-targeting strate-

gies in cancer gene therapy.^{3,13-16} For example, Mendonça et al.¹⁵ applied transferrin receptor-targeted liposomes encapsulating antisense oligodeoxynucleotides (asODNs) and small interference RNA (siRNA) into the treatment of chronic myeloid leukemia. Wu et al.¹⁶ demonstrated liposome-based synergetic treatment of insulin promoter-thymidine kinase gene therapy followed by ganciclovir pharmacotherapy, resulting in efficient ablation of the tumor size in mice. Therefore, liposomes can serve as an efficient technique for targeted gene transfer in cancer gene therapy.

Passive liposomal delivery is challenging due to biological extracellular and intracellular barriers such as enzyme degradation, pH change, and endolysosomal lysis.¹⁷ In order to overcome these barriers and enhance the efficacy of liposome-mediated gene and/or drug delivery, various strategies have been employed to develop active liposomes whose bilayer can be destabilized by using external stimuli, including temperature,¹⁸⁻²⁰ pH,²¹⁻²³ ultrasound,^{13,24} specific enzymes,^{25,26} magnetic field,²⁷⁻²⁹ and photo irradiation including UV light.³⁰⁻³⁴ Light is especially attractive as a triggering modality because it can be applied remotely with high spatiotemporal precision, while light parameters such as wavelength, power density, and illumination time can be adjusted to control the release platform.³⁵ In recent years, enhanced cytoplasmic delivery of macromolecular compounds by photochemical disruption of the endolysosomal membrane, referred to as photochemical internalization (PCI),³⁶ has been actively investigated in the context of gene delivery, including siRNA, peptide nucleic acids (PNAs), and plasmid DNA (pDNA),³⁷ and pharmacotherapy.³⁸⁻⁴² For example, Park et al.³⁹ demonstrated endolysosomal escape of the therapeutic p53 gene carried by polymer-gene complex after illumination with a 671 nm laser. Here, we used a similar strategy to deliver a gene to silence one of the pituitary adenyl cyclase-activating polypeptide (PACAP) receptors.

Received 28 November 2016; accepted 18 April 2017;
<http://dx.doi.org/10.1016/j.omtn.2017.04.015>

Correspondence: Wei Deng, Department of Physics and Astronomy, Macquarie University, Sydney, NSW 2109, Australia.

E-mail: wei.deng@mq.edu.au

Correspondence: Ewa M. Goldys, Department of Physics and Astronomy, Macquarie University, Sydney, NSW 2109, Australia.

E-mail: ewa.goldys@mq.edu.au

www.moleculartherapy.org

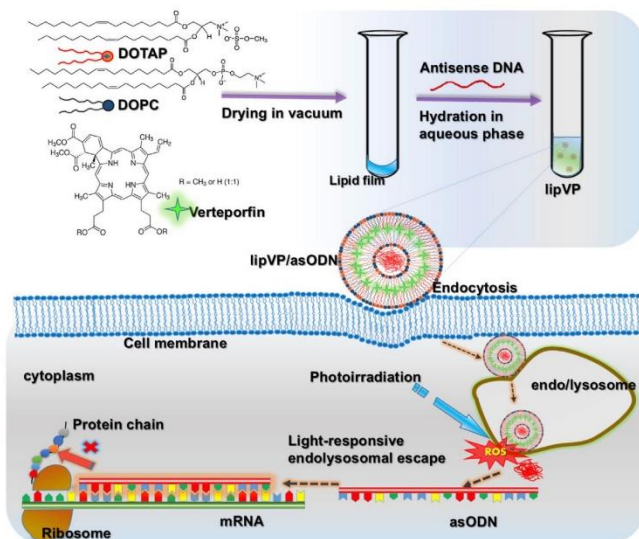


Figure 1. Schematic Diagram

Illustration of the lipVP preparation and light-triggered asODN release for gene silencing.

gene delivery because it is able to freely pass through negatively charged cell membranes.¹⁴ Verteporfin (VP), a highly potent photodynamic therapy (PDT) photosensitizer,⁵⁷ was loaded inside a liposomal bilayer, referred to as lipVP. asODN molecules of PAC1R were incorporated inside a liposomal cavity. These liposomes were endocytosed by cells, where they became entrapped in the endosomes and lysosomes.⁵⁸ VP was used to generate a sufficient amount of reactive oxygen species (ROS) for destabilization of the liposomal and endolysosomal membranes under light illumination.^{59,60}

Figure 1 illustrates the mechanism on asODN release from the endosomes and lysosomes by ROS. In particular, we quantitatively explain the endolysosomal escape process through sub-cellular colocalization analysis based on the released profiles of DNA molecules and endo-

somes and lysosomes. asODN molecules were then released from the endolysosomal compartments into the cytoplasm and silenced the PAC1R mRNA. To examine the response of PC12 cells to PACAP stimulation after gene silencing, we quantified the neurite outgrowth of cells treated with PACAP-27 and PACAP-38, respectively. For comparison, NGF was also added to the PC12 cells with the silenced PAC1R gene, and subsequent neurite outgrowth was assessed.

RESULTS

Characterization of Liposome Samples

The transmission electron microscopy (TEM) images of as-prepared lipVP exhibit fairly spherical liposome shapes with a size around 200 nm (Figure 2A). We determined the average sizes of lipVP-asODN complexes with different N/P ratios by the dynamic light scattering (DLS) method, ranging from 119.6 ± 0.6 nm to 121.7 ± 0.3 nm (Figure 2B). The polydispersity index (PDI) values decreased slightly from 0.204 ± 0.0036 to 0.178 ± 0.001 with an increased N/P charge ratio. The PDI values of nanoparticle suspension ranging from 0.1 to 0.25 indicate a narrow size distribution, and the value higher than 0.5 indicates a wide size distribution.⁶¹ Therefore, our PDI values indicated that as-prepared lipVP-asODN complexes were dispersed homogeneously with a relatively narrow size distribution. To obtain lipVP/asODN with an optimal N/P ratio used in this study, we conducted agarose gel retardation assays. The results shown in Figure 2C indicate that less DNA was detected with an increased N/P ratio. When the value of N/P ratio reached 25:1, free DNA could not be detected in the agarose gel. This finding suggests that the maximal amount of DNA molecules was loaded into the liposomes at an N/P ratio of 25:1. Additionally, the zeta potential of lipVP/asODN

PACAP is a member of the vasoactive intestinal polypeptide (VIP)-glucagon-growth hormone releasing factor-secretin superfamily, and it has two amidated forms: PACAP-38 and PACAP-27.⁴³ Broadly expressed in nerve cells, PACAP is a pleiotropic growth factor, affecting differentiation, proliferation, and maturation of most neural and non-neural cell types.⁴⁴ PACAP also plays a role in cancer cell proliferation.⁴⁵ It induces cell proliferation in small lung cancer cells and neuroblastoma cells,^{46,47} but it inhibits cell growth of lung cancer and breast cancer.^{48–50} Additionally, PACAP is an important neuropeptide that plays a vital role in the regulation of hypertension.⁵¹ The PACAP-specific cell membrane receptors include the PAC1, vasoactive intestinal peptide receptor (VPAC)1, and VPAC2. Among these receptors, PACAP receptor 1 (PAC1R) has the highest affinity for PACAP at physiological concentrations.⁵² Because PC12 cells only express PAC1R, this cell line was a good model to investigate the impact of PAC1R knockdown.⁵³ PC12 cells, a clonal cell line derived from a pheochromocytoma of the rat adrenal medulla, were used as the in vitro model for assessing differentiation and neurite growth because they can be stimulated for neurite outgrowth by the nerve growth factor (NGF).⁵⁴ PACAP, acting as a neurotransmitter, also induces PC12 cell differentiation, via a different signaling pathway from NGF.⁵⁵

In this study, we demonstrated PAC1R gene knockdown by light-triggerable liposomes and the effect of PACAP on PC12 cell differentiation following PACAP gene silencing. To prepare the liposomes, we chose 1, 2-dioleoyl-sn-glycero-3-phosphocholine (DOPC) as a neutral lipid⁵⁶ and 1, 2-di-(9Z-octadecenoyl)-3-trimethylammonium-propane (DOTAP) as a cationic lipid. The latter can enhance

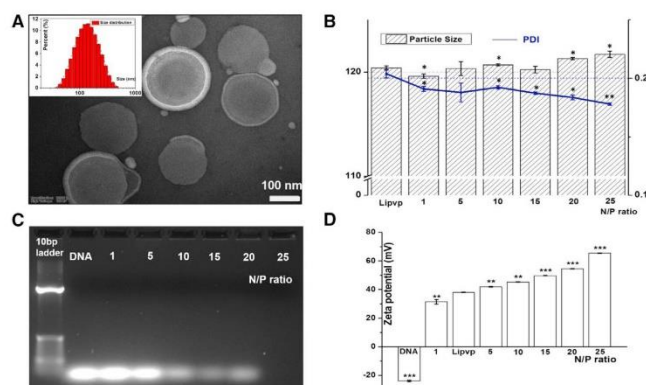


Figure 2. Characterizations of lipVP and lipVP-asODN Complexes

(A) A representative TEM image of lipVP; inset is the lipVP size distribution histogram. Scale bar, 0.1 μ m. (B) Average sizes and PDI of different lipVP-asODN complexes with different N/P ratios. The measurements of each were conducted in triplicates, * $p < 0.05$, ** $p < 0.01$ (t test) compared with the lipVP group. $n = 3$. (C) DNA agarose gel electrophoresis pattern of different lipVP-asODN complexes at different N/P ratios. Lane 1, 10 bp DNA ladder only; lane 2, pure asODN only; lanes 3–7, the N/P ratio = 1, 5, 10, 15, 20, and 25:1, respectively. (D) Zeta potential of different lipVP-asODN complexes at different N/P ratios. ** $p < 0.01$, *** $p < 0.001$ (t test) compared with the lipVP. $n = 3$.

with varying N/P ratios was also measured. As shown in Figure 2D, the zeta potential of the complexes increases with increasing N/P ratio. This increasing zeta potential enhances the cellular uptake of liposome-formulated DNA compared with free DNA molecules. The VP absorption peak at 700 nm was shifted to a shorter wavelength when loaded inside liposomes compared with VP alone (Figure S1), while the fluorescence spectrum of VP loaded inside liposomes was not obviously changed compared with pure VP (Figure S2). This indicates that VP was encapsulated in the liposomes. We also estimated the amount of VP loaded inside liposomes, which was approximately $143 \pm 0.36 \mu\text{g/mL}$.

Cellular Uptake of lipVP and Release of asODN under UV Light Illumination

Figure S3 shows the cellular uptake of lipVP with different incubation times (0.5, 1, 2, and 3 hr). After 2 and 3 hr incubation, higher red fluorescence signal from VP surrounding the nuclei (stained in blue color) was observed compared with cells treated for 0.5 and 1 hr. Therefore, we chose 2 hr incubation time in this study.

The DNA release test was first performed in test tubes with carboxy-fluorescein (FAM)-labeled DNA molecules encapsulated in the lipVP platform, as shown in Figure S4. FAM is a fluorescent dye that self-quenches at high concentration.⁶² This allows the detection of its release from the liposomes to the surrounding medium by monitoring the increase of FAM fluorescence.⁶³ Following light illumination, the FAM fluorescence intensity increases compared with the control without light treatment. The extent of this decrease was found to be related to the illumination period. However, an increase in the fluorescence signal was not observed when the same FAM-labeled DNA molecules were encapsulated into the liposomes without VP, as shown in the inset of Figure S4. Our results indicate that FAM-labeled DNA molecules were released from lipVP following light illumination. However, in liposomes without VP, the DNA molecules have not been released even when triggered by a light source. In order

to assess whether the light-induced ROS will damage the DNA, which is encapsulated into the lipVP compartment, the gel retardation assay was also carried out. As shown in Figure S5, the clear bands of DNA released from liposomes with 2, 4, 6, and 8 min of UV illumination can be observed, suggesting that ROS induced by light illumination did not significantly affect the entrapped DNA.

Having confirmed the ROS generation from lipVP under light illumination in a test tube, we evaluated intracellular ROS generation by using 2', 7'-dichlorofluorescein (DCF) diacetate (DCF-DA) assay where nonfluorescent DCF-DA can be oxidized by ROS to produce highly fluorescent DCF. As shown in Figure S6, the fluorescence intensity of DCF increased with light illumination time, indicating that a higher amount of ROS was generated from lipVP. Additionally, we assessed the in vitro DNA release profile by irradiating cells with the UV light (365 nm, 1.25 mW/cm²). As shown in Figure 3, an enhanced green signal from FAM was clearly observed after light illumination compared with the control sample without light treatment, with the maximum intensity achieved at 6 min illumination. Our results indicated that the increased ROS production resulted in more damage to endolysosomal membranes, and enhanced the release of DNA molecules from the endolysosomal compartments.

Quantitative Analysis of Endolysosomal Escape of asODN after Light Illumination

Subcellular distribution and endosomal escape of asODN from light-triggered lipVP was analyzed by using confocal laser scanning microscopy (CLSM) (Figure 4). After 1 hr incubation, FAM-labeled asODN was internalized in cells, which was confirmed by a green signal observed around the nucleus (Figure 4B). After 2 hr incubation, colocalization between the green signal from fluorescent asODN and red signal from the endosomes and lysosomes labeled by LysoTracker was clearly observed, indicating the entrapment of lipVP-asODN inside the endosomes and lysosomes (Figure 4C). Without light irradiation, some asODN molecules were able to escape from the endosomes and lysosomes, but most of them were still located inside the organelles after 4 hr incubation (Figure 4D). However, following

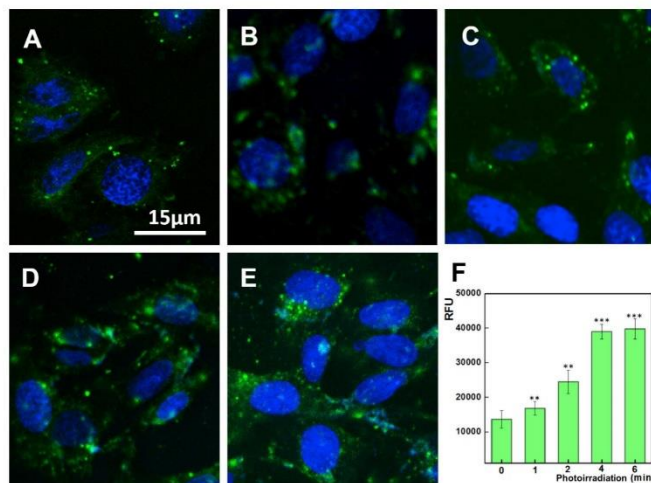


Figure 3. Light-Enhanced DNA Release in Cells

(A–E) CLSM images of FAM-labeled DNA release after 2 hr incubation with lipVP-asODN and photoirradiation for different periods: (A) 0, (B) 1, (C) 2, (D) 4, and (E) 6 min. (F) The amount of released DNA molecules during photoirradiation (in relative fluorescence units [RFU]; ** $p < 0.01$, *** $p < 0.001$ [t test]; $n = 3$ compared with the group without light treatment). Blue color indicates the nuclei stained with Hoechst 33342, and green color represents the FAM-labeled DNA.

4 min light irradiation after 2 hr incubation, most asODN molecules escaped outside the endosomes and lysosomes after a further 2 hr incubation, which was demonstrated by the green signal from asODN and almost no colocalization observed in Figure 4E. The light-triggered escape of asODN was also confirmed by the analysis of colocalization between the fluorescently labeled endosomes and lysosomes and fluorescent asODN molecules by using ImageJ (Figure 5). Colocalization was quantified using the Costes approach,⁶⁴ Mander's coefficient,⁶⁵ and Pearson's correlation coefficient (PCC).⁶⁶ Based on the Costes approach, a white overlay of the green signal from asODN and red signal from LysoTracker indicates the colocalization between asODN and endosomes and lysosomes. Figures 5A–5D show the Costes maps of Figures 5B–5E, respectively. Initially, the lipVP-asODN complexes were internalized into the cells and most of them had not reached the lysosomes. After 1 hr incubation, the white area was almost negligible (Figure 5A), indicating that asODN was not located within endolysosomal compartments. As the endocytosis process continued, after a 2 hr incubation time, a large white area was observed (Figure 5B), suggesting that most lipVP-asODN nanoparticles were internalized into the endosomes and lysosomes. Even after 4 hr incubation, some white spots were still observed, indicating the lipVP-asODN complexes were still entrapped in the endolysosomal compartments (Figure 5C). However, in a scenario of light illumination, at the same time point (4 hr incubation time), almost no white color was observed, suggesting that most lipVP-asODN molecules were then released from endolysosomal compartments into the cytoplasm (Figure 5D).

Based on the Costes colocalization analysis, the PCC value was also evaluated. The PCC ranges from -1 to 1 , with -1 indicating a nega-

tive correlation, 1 indicating a positive correlation, and 0 standing for no correlation. As shown in the inset table in Figure 5E, the PCC value was 0.305 after 2 hr incubation. However, it decreased to -0.036 after light illumination, consistent with the asODN release from endolysosomal compartments. For comparison purposes, the control experiments were also conducted where the cells were incubated only with lipVP-asODN for 4 hr but without light treatment. In this case, the PCC value was 0.023 , which indicated that some asODN molecules were still colocalized with lysosomes.

Furthermore, Mander's coefficient, varying from 0 to 1 , was calculated to determine the fraction of two overlapping channels. As shown in the inset table and the stack columns in Figure 5E, $M2$ was only 0.385 after light illumination compared with control cells without light illumination ($M2 = 0.988$), indicating that the DNA molecules escaped from endosomes and lysosomes after light treatment.

Additionally, the intensity correlation analysis (ICA) was also conducted by using the ImageJ plugin, JACoP Li,⁶⁷ as shown in Figure S7. In this figure the covariance of both channels is shown as the x value, and the intensity distribution of current channel is represented as the y value. The pixels scattered on the left side of the $x = 0$ line reflect the absence of colocalization or inversely correlated intensities, whereas those situated on the right side of the $x = 0$ line represent colocalization. These approaches present clear evidences of the dynamic process of light-enhanced endolysosomal escape.

PAC1R Gene Interference with Light-Triggered lipVP-asODN

To evaluate the expression level of the PAC1R protein following gene interference, the fluorescence intensity of stained PAC1R protein was measured with a microplate reader. In this case, a reduced fluorescence signal indicates higher silencing efficiency. As shown in Figure 6, the fluorescence signal decreased to a different extent with increased illumination time, with an approximately 2.5 times decrease achieved under 4 min illumination compared with control cells without light treatment. After 6 min

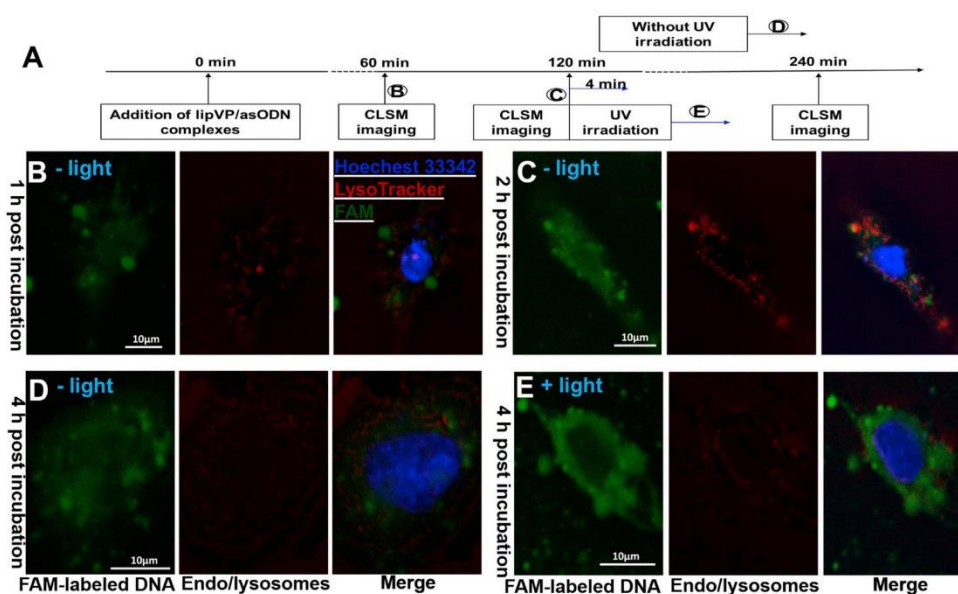


Figure 4. Light-Enhanced Endolysosomal Escape

(A) A time course showing the time points of transfection, photoirradiation, and CLSM imaging. (B–E) CLSM images of colocalization between the FAM-tagged DNA (green channel) and endosomes and lysosomes (LysoTracker, red channel); (B and C) images taken after 1 hr (B) and 2 hr (C) incubation with lipVP-asODN complexes (without light illumination); (D) images taken after 4 hr incubation with lipVP-asODN complexes (without light illumination); and (E) images taken after 4 hr incubation with lipVP-asODN and light illumination, which was done at 2 hr incubation time.

illumination, the remaining fluorescence did not change in a statistically significant fashion. These results are consistent with the DNA release profile under UV illumination shown in Figure 3. In addition, for comparison, free asODN molecules were delivered into the PC12 cells and UV light was then applied to cells under the same experimental conditions. As shown in Figure 6G, the fluorescence intensity of PAC1R remained unchanged with increased illumination time, indicating that an efficient gene knockdown was not triggered in this situation.

Assessment of Cell Differentiation after PAC1R Gene Interference

As the positive control of cell differentiation, a polypeptide, NGF, was also used to treat PC12 cells after the PAC1R gene knockdown. As shown in Figure 7, for control cells without light irradiation, at day 2 after addition of NGF, the PACAP-38 and PACAP-27 cells exhibited a high degree of differentiation ($65\% \pm 16\%$, $62\% \pm 7\%$, and $56\% \pm 5\%$, respectively) with many long neurites spreading out of the cells (Figure S7). On day 4, a higher percentage of neurite outgrowth was observed ($83\% \pm 4\%$, $72\% \pm 10\%$, and $66\% \pm 11\%$, respectively). For cells treated with 4 min light illumination, the PAC1R gene was silenced, but only to some extent, resulting in a

limited effect of PACAP on cell differentiation. Only $32\% \pm 5\%$ (PACAP-27-treated groups) and $31\% \pm 9\%$ (PACAP-38-treated groups) of cells showed an obvious neurite outgrowth at day 4 after PACAP treatment (Figure 7). We clarify that the siRNA molecules against PAC1R were not involved in this study. By contrast, the action of NGF on neurite outgrowth was not significantly affected by light illumination, with approximately 82% of cells in the NGF-treated groups at day 4 still exhibiting a high degree of cell differentiation (Figure 7). The corresponding morphologies of cell differentiation after light illumination are shown in Figures S9 and S10. These results suggested that the PACAP-dependent signaling pathway of neurite growth was interfered with to a different extent when the expression of receptor PAC1R was inhibited by gene silencing; on the other hand, NGF still played its role in neurite growth even when PAC1R was silenced.

Cellular Cytotoxicity Assay

A series of cell viability tests under various treatments were performed to estimate the potential toxicity effect on cells. To verify the potential light toxicity, we illuminated the cells with UV light from 0 to 6 min. As shown in Figure 8, the cell viability was not changed significantly compared with the controls (without the

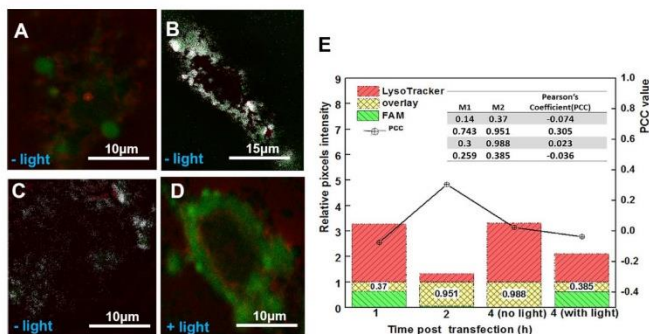


Figure 5. Co-localization Analysis with ImageJ Costes' Approach

(A), (B), (C), and (D) are Costes' maps of (B), (C), (D), and (E), respectively, with the white pixels overlay between the green (DNA molecules) and red channel (endosomes and lysosomes). (E) Stack graph of Manders' coefficient analysis and Pearson's coefficient (inset table).

UV treatment). We further assessed the toxicity of pure liposomes and the impact of both lipVP and light irradiation simultaneously. The liposomes at both higher (55.5 $\mu\text{g/mL}$) and lower concentration (5.55 $\mu\text{g/mL}$) did not significantly affect cell viability, even under photoradiation for different time periods. On the other hand, the lipVP showed increased cytotoxicity under longer illumination time. After 6 min illumination, about 19% and 17% of cells were killed by lipVP at higher (55.5 $\mu\text{g/mL}$) and lower concentration (5.55 $\mu\text{g/mL}$), respectively (Figure 8). These results suggested that cytotoxicity induced by both lipVP and UV exposure could be attributed to light-triggered ROS generation from VP. However, more than 80% of total cells were still alive in all tests, indicating the photo-triggered liposomes (or lipVP) are relatively biocompatible.

DISCUSSION

Non-viral gene vectors have recently attracted significant research interests because of their advantages for gene therapy including low toxicity of materials, cost-effectiveness, and ease of production and usage, compared with the viral vectors with inherent risks for clinical applications.^{4,68} The goal of this study was to develop a facile nanoparticle-based gene delivery system capable of being triggered with light to enable a higher level of control of gene release and interference. To this end, we developed a non-viral gene vector, based on engineered liposomes incorporating VP inside a liposomal bilayer and asODN inside a middle cavity. VP has a broad absorption band between 300 and 500 nm with one absorption peak at 350 nm, which can be activated to generate ROS with a UV light source. Considering the toxic effects of UV light on DNA molecules, we paid particular attention to the UV wavelength and power density used in this study. DNA easily absorbs UVB radiation (280–315 nm), compared with UVA (315–400 nm), while the UVA band causes sunburn on human skin.⁶⁹ The UV wavelength we used falls into the UVA region, where DNA molecules have almost no absorbance.⁷⁰ Additionally, a low-power density (1.25 mW/cm^2) and limited illumination time (no longer than 6 min) were also used to further minimize light toxicity. This is supported by Besaratinia's work,⁷¹ which demonstrated that UVA

safety issues related to the use of UV light in this study do not appear to be significant.

The endocytic pathway is one of the vital mechanisms of cellular uptake of nanoparticles. This pathway is regulated by a series of endosomes from early endosomes to late endosomes that mature and fuse with the intracellular organelles, lysosomes.⁷² After internalization of the delivery vehicles through the endocytic pathway, most of the vehicles are entrapped in endosomes and lysosomes where the enzymatic degradation usually takes place, resulting in deactivation of functional compounds before release or targeting other organelles.⁴¹ Therefore, endolysosomal escape of the vectors-DNA complexes is the main challenge for efficient gene transfection.⁷³ To overcome the issue of endolysosomal entrapment, we herein assessed the ability of ROS for endolysosomal damage. We first evaluated ROS generation from VP triggered by light in a test tube and at a cellular level by, respectively, conducting the FAM-labeled DNA release assay and the DCF-DA assay. Both enhanced FAM and DCF fluorescence was a clear indicator of light-triggered ROS production. After having confirmed that the ROS generation can be triggered, we further characterized the ROS-induced endolysosomal escape of asODN by confocal microscopy. This escape was demonstrated by documenting the illumination-induced change in the cells: the previously colocalized green fluorescence of asODN and red signal of LysoTracker became clearly separated after light illumination. We quantified this effect by using three different quantitative methods: the Costes approach, Mander's coefficient, and PCC. Taken together, these data demonstrated the enhanced endolysosomal escape induced by ROS.

To assess whether ROS-induced gene release can enhance the efficacy of gene knockdown, we evaluated the PAC1R protein level after gene silencing by comparing the effects of asODN loaded inside the liposomes incorporating VP and free asODN molecules. After light triggering, a decreased PAC1R level was clearly observed when cells were treated with lipVP-asODN, compared with free asODN molecules. Such enhancement of the gene knockdown was further confirmed

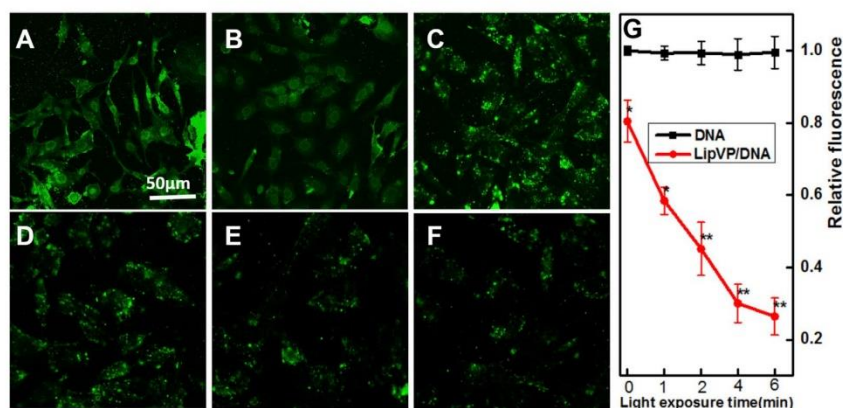


Figure 6. Immunofluorescence

(A–F) Representative CLSM images of indirect immunofluorescence staining of PAC1R in control cells without any treatment (A) and light-treated cells with different illumination times: 0 (B), 1 (C), 2 (D), 4 (E), and 6 min (F). (G) The relative PAC1R fluorescence intensity measured in cells treated with free DNA molecules (black squares) and lipVP-DNA (red circles) and light illumination. Data are presented as mean \pm SD, $n = 3$. * $p < 0.05$, ** $p < 0.01$ (t test) compared with groups treated with DNA molecules at the same light irradiation time.

by the neurite-inducing activity of PACAP in treated PC12 cells, where a limited neurite outgrowth was an indicator of the response to PAC1R gene knockdown achieved by using lipVP-asODN.

PACAP-induced differentiation of PC12 cells is generally investigated by either measuring the levels of signaling molecules involved in this processor or inhibiting the action of PACAP and its receptor with synthetic antagonists, including PACAP6-27 and PACAP6-38.^{74,75} However our light-triggered liposomal delivery platform incorporating VP provided another useful strategy to interfere with PACAP-induced cell differentiation. This method also has the potential to be applicable to studies on PACAP/PAC1R-mediated signaling pathways in the brain tissues.⁷⁶ Although our liposomes were applied to cell experiments only in this study, they will be able to be used in *in vivo* applications by surface modification with polyethyleneglycol (PEG) or cell-penetrating peptides (CCPs). PEG can dramatically extend the circulation time of liposomes and allow conjugation of liposomes with targeting ligands for a specific organelle target. CCPs will increase the delivery efficiency of gene⁷⁷ or drug⁷⁸ to the brain by passing the brain-blood barrier.⁷⁹

Apart from its neurotrophic action in PC12 cells, PACAP is also involved in many biological activities and regulations, including cardiovascular control,⁴⁷ psychiatric disorders, and stress responses.^{80,81} Although the exact mechanisms of PACAP-dependent regulation remain unclear, PACAP has the potential to be a therapeutic target for the treatment of the above disorders. Our approach, therefore, potentially offers another effective strategy for efficient gene therapy by delivering light-triggered liposomes incorporating PACAP gene and VP. It should be mentioned that our strategy has been designed

to be compatible with future clinical translation. The materials used in this study, such as VP and lipids, are clinically used in PDT treatment of tumors.

In summary, our light-responsive delivery strategy was able to achieve enhanced endosome and lysosome escape and the PAC1R gene silencing. Such light-triggered liposomes would be able to achieve spatiotemporal control of gene release, potentially offering a non-viral gene delivery platform for efficient gene therapy. Therapeutic agents such as siRNA or DNA would be able to be delivered and released in a more controllable way by taking advantage of such a vector model in combination with light.

MATERIALS AND METHODS

This project has obtained research ethics approval from the Institutional Biosafety Committee (IBC), Macquarie University.

Materials

Lipids (DOTAP: catalog no. 890890; DOPC: catalog no. 850375) were purchased from Avanti Polar Lipids. DMEM (catalog no. 11965-092), fetal bovine serum (FBS; catalog no. 10437-028), trypsin (catalog no. 15400054), LysoTracker (catalog no. L7528), Hoechst 33342 (catalog no. H3570), PBS (catalog no. 10010023) solution, Hank's balanced salt solution (HBSS; catalog no. 14175145), 4-(2-hydroxyethyl)-1-piperazineethanesulfonic acid (HEPES; catalog no. 14185052) buffer, and Opti-MEM (catalog no. 31985070) solution were purchased from Thermo Fisher. Uranyl acetate (catalog no. 73943), paraformaldehyde (catalog no. P6148), chloroform (catalog no. 372978), Fluoromount aqueous mounting medium (catalog no. F4680), and 2', 7'-dichlorofluorescein diacetate (DCF-DA) (catalog no. D6883)

www.moleculartherapy.org

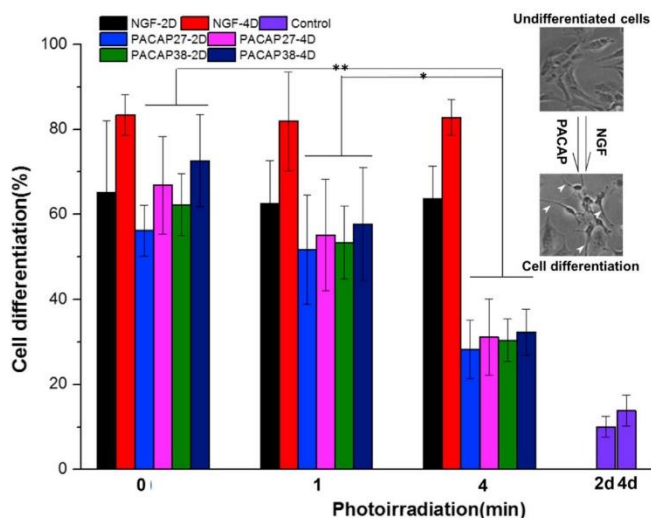


Figure 7. Cell Differentiation

The assessment of differentiation in PC12 cells induced by NGF and PACAP with and without light illumination; the control groups are cells only without any treatments. Cells growing at least a neurite with length no less than the cell body diameter were counted in five selective images. * $p < 0.05$, ** $p < 0.01$ (two-way analysis of variance with Fisher's least significant difference [LSD]). $n = 5$. Inset images illustrate the PC12 cell differentiation stimulated with NGF or PACAP peptides; white arrows indicate the outspread neurites.

amounts (moles of the amine groups of cationic polymers to those of the phosphate ones of DNA [N/P] ratios ranging from 1:1 to 25:1) were used to hydrate the lipid film by using the method described above.⁸³ The complexes were freshly prepared before further use.

Characterization

For TEM imaging, liposome samples were prepared by placing a drop of liposome suspension onto a copper grid and air-dried, followed by negative staining with 2% (w/v) uranyl acetate.⁸⁴

The samples were then imaged under a TEM with an acceleration voltage of 100 kV (Philips CM 10). Images were captured with an Olympus Megaview G10 camera and processed with ITEM software. The zeta potential and size distribution of liposome samples were determined by DLS using a Zetasizer 3000HSA (Malvern Instruments). Each sample was measured in triplicate after 2 min balance at 25°C, and data were collected as mean \pm SD. The absorption and fluorescence spectra of lipVP, pure liposomes, and pure VP were measured with a UV-VIS spectrometer (Cary 5000; Varian) and a Fluorolog-Tau3 System (HORIBA Scientific) with 425 nm Xe lamp excitation, respectively. To determine the encapsulation efficiency of VP loaded inside of liposomes, we added Triton X-100 (0.1%) to as-prepared liposome solution, resulting in VP release. The VP fluorescence (excitation/emission [ex/em]: 425 nm/690 nm) was recorded on a Fluorolog-Tau-3 system and compared with the corresponding VP standard curve. For the agarose gel (1.2%) assay of lipVP-asODN complexes with different N/P ratios, electrophoresis was carried out at 90 V for 45 min.

Cell Culture

The PC12 cell line was purchased from ATCC. DMEM supplemented with 10% FBS and 1% antibiotic-antimycotic was used as the culture medium. The cells were grown at 37°C in the humid atmosphere with 5% CO₂. When cells reached about 90% confluence, they were detached with trypsin and transferred into Petri dishes or well plates for different experimental purposes. For confocal microscopy imaging, glass coverslips with 12 mm diameter were placed at the bottom of each well in a 24-well plate; cells (5×10^4 /well) were then seeded onto the bottom of each well. For light irradiation experiments, the cells were cultured in a well plate or glass-bottom Petri dish and

were purchased from Sigma-Aldrich. asODN with 3' end modified by 6-carboxyfluorescein (FAM) was purchased from IDT Tech. We used the sequence 5'TGGTGCTTCCCAGCCACTAT3'-6-FAM. Goat anti-PAC1R primary antibody (catalog no. sczsc-15964) and donkey anti-goat IgG-FITC secondary antibody (catalog no. sczsc-2024) were purchased from Santa Cruz Biotechnology. PACAP-27 (catalog no. 05-23-2151) and PACAP-38 (catalog no. 05-23-2150) were purchased from Merck Millipore Pty.

Preparation of Pure Liposomes, Lipoplexes, and lipVP-DNA Complexes

For the synthesis of pure liposomes, 500 μ L of chloroform solution containing DOTAP and DOPC with a molar ratio of 1:1 (DOTAP 2.33 mg, DOPC 2.96 mg) was evaporated under argon gas stream, forming a thin lipid film at the bottom of a glass test tube. The lipid film was subsequently hydrated by adding 1 mL of HEPES buffer (40 mM [pH 7.4]) to the glass test tube, followed by vigorous stirring until the suspension was homogenized. For preparing liposomes loaded with asODN (lipoplexes), 1 mL of HEPES buffer containing asODN with varying concentration was added to the lipid film, followed by vigorous stirring for 10 min. After 24 hr aging, the lipoplex suspension was sonicated for 5 min, followed by extrusion 11 times in a mini-extruder (Avanti Polar Lipids) with two 1.0 mL glass syringes at 37°C. The pore size of the polycarbonate membrane (Avanti Polar Lipids) was 200 nm. When preparing lipVP-DNA complexes, DOTAP, DOPC, and VP were mixed in 500 μ L of chloroform with a molar ratio (DOTAP:DOPC:verteporfin) of 1:0.94:0.06.⁸² The lipid film was formed after evaporation of organic solvent by using the same procedure as described above. asODN molecules with varying

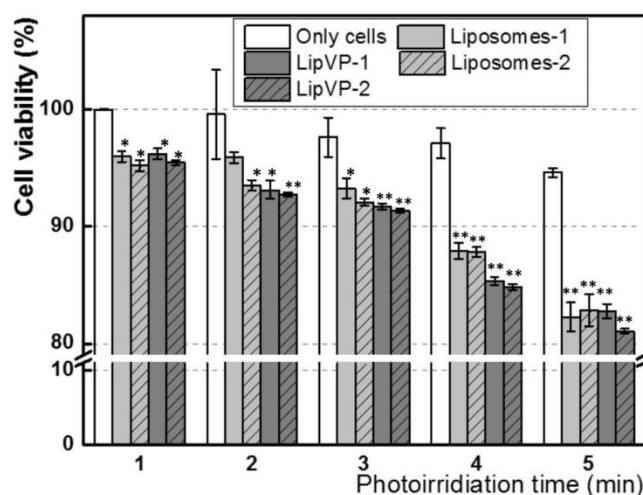


Figure 8. Cytotoxicity

In vitro toxicity assays of pure liposomes (Liposomes-1 and Liposomes-2), lipVP (LipVP-1 and LipVP-2), and light illumination on PC12 cells at 24 hr after treatment. The concentration of Liposomes-2 and LipVP-2 was 5.55 and 55.5 $\mu\text{g/mL}$, respectively. * $p < 0.05$, ** $p < 0.01$ (t test) compared with the control cells in each group at the same photoradiation time.

bated with 500 μL of the Opti-MEM solution containing lipVP (5.55 $\mu\text{g/mL}$). After 2 hr incubation at 37°C, the medium was removed and the cells were washed with 500 μL of 1 \times HBSS solution three times. A total of 200 μL of 1 \times HBSS containing DCF-DA (25 μM) was subsequently added to the cells, followed by incubation for 30 min at 37°C, while protected from light. After incubation, the cells were illuminated by UV light for different time periods. After light irradiation, the DCF-DA solution was removed from the cells. The cells were further imaged using a Leica SP2 CLSM system. For comparison, the

illuminated with UV light (365 nm, 1.25 mW/cm²) from a UV-LED source (Nichia) at various time points for 1, 2, 4, and 6 min, respectively.

Cellular Uptake of Liposomes and Endolysosomal Escape with a Light Trigger

Before incubation with the lipVP suspension, the cells (5×10^4 /well) were seeded onto 12 mm diameter glass coverslips placed at the bottom of each well in a 24-well plate. After reaching 70% confluence, the cells were incubated with 500 μL of Opti-MEM solution containing lipVP (5.55 $\mu\text{g/mL}$) for different periods. To observe the cellular uptake of lipVP, we washed the cells three times by using the PBS solution (1 \times [pH 7.4]), fixed with 2% paraformaldehyde for 10 min at 37°C, and stained with Hoechst 33342 (5 $\mu\text{g/mL}$) for 15 min at 37°C. For the assessment of light-triggered endolysosomal escape of asODN molecules from the liposomes, incubation with lipVP samples and light irradiation were sequentially carried out as per the schedule shown in Figure 4A. For the staining of endosomes and lysosomes, LysoTracker (50 nM) was added into the cell culture medium 1 hr before the cell fixation. After cell staining and fixation, each coverslip with fixed cells was washed by the PBS solution (1 \times [pH 7.4]) three times and transferred onto a glass slide with a drop of the mounting medium. The glass slide was then imaged using a Leica SP2 CLSM system. A violet laser operating at 405 nm and an argon laser at 496 and 570 nm were used for the excitation of VP, FAM-labeled asODN, and LysoTracker, respectively. The fluorescence emission was measured at 700 ± 25 nm for VP, 525 ± 25 nm for FAM, and 590 ± 10 nm for LysoTracker.

Detection of Cellular ROS Generation Using DCF-DA

The cells (5×10^4 /well) were attached to Petri dishes and incubated at 37°C for 24 hr. After removing culture medium, the cells were incu-

control cells were incubated with 100 μL of the Opti-MEM solution containing H₂O₂ at different concentrations (1, 10, and 100 μM) for 2 hr followed by addition of DCF-DA and CLSM imaging. For the determination of ROS, cells were cultivated in 96-well plates, instead of Petri dishes, followed by the same procedure as described above. After treatment, the DCF fluorescence intensity was measured using a FLUOstar Galaxy multi-mode microplate reader (BMG LABTECH Pty) with the 485/520 nm excitation/emission filter.

Cell Transfection and Immunofluorescence Staining of PAC1R

A total of 500 μL of the Opti-MEM solution containing lipVP-asODN (charge ratio N/P = 25, with 1 μg of asODN) was added to the cells in each well in a 24-well plate. After 2 hr incubation, the Opti-MEM medium was removed and the cells were washed with PBS three times, followed by incubation with a fresh culture medium (containing 10% FBS) for 24 hr. The cells were subsequently fixed with 2% paraformaldehyde for 10 min at 37°C and incubated with 0.1% Triton X-100 for another 10 min to achieve permeabilization, followed by 30 min blocking by using 5% BSA at ambient temperature. The cells were then incubated with goat anti-PAC1R primary antibody (1:50 dilution in PBS) for 90 min, followed by incubation with donkey anti-goat IgG secondary antibody conjugated with FITC (1:100 dilution in PBS) for 30 min at 37°C. The PAC1R fluorescence intensity was measured using a microplate reader with the 485/520 nm excitation/emission filter. The corresponding fluorescence images were obtained using a CLSM system with excitation at 496 nm and emission at 525 ± 25 nm.

NGF, PACAP-27, and PACAP-38 Stimulation for Neurite Outgrowth

After the treatment with liposomes and light irradiation, the cells were incubated with 100 μL of the Opti-MEM medium containing

www.moleculartherapy.org

NGF (50 ng/mL), PACAP-27 (10 nM), and PACAP-38 (10 nM), respectively. For comparison, the control groups were treated with same liposome samples but without light illumination. Cellular morphology analysis was performed based on the phase-contrast microscopy images taken under a microscope (Nikon Eclipse Ts100) at 2 and 4 days following the light treatment. Quantitative analysis based on light microscopy was used to assess the differentiation of PC12 cells.⁸⁵ We chose five images in each group to count the number of differentiated cells growing at least one neurite with length no less than a cell body diameter and to calculate their percentage.

Cell Viability after Treatment of Liposome Samples

The cells (1×10^4 /well) were seeded into 96-well plates and cultured for 24 hr at 37°C. When cells reached 70% confluence, the previous medium was removed and the Opti-MEM solution containing pure liposomes and lipVP with different concentrations were, respectively, added to the cells. After 2 hr of incubation with different liposome samples, the cells were washed with PBS three times to remove unbound liposomes. A fresh medium was then added to the cells, followed by another 24 hr incubation. For the light irradiation alone, the cells were exposed to UV light (365 nm, 1.25 mW/cm²) for 1, 2, 4, and 6 min, respectively. After light treatment, the fresh medium was added to the cells for another 24 hr incubation. The toxicity of the liposome samples and UV light in PC12 cells was assessed by the MTS test (Promega), as per manufacturer's instructions, and the results were compared with control cells without any treatment. Cell viability was then calculated as a percentage of the absorbance in treated cells compared with the untreated controls.

Statistical Analysis

All quantitative data were shown as mean \pm SD, $n \geq 3$, and the Student's *t* test was conducted between two sets of data. All data analysis and plotting were performed with OriginPro 8.5 software.

SUPPLEMENTAL INFORMATION

Supplemental Information includes Supplemental Materials and Methods and ten figures and can be found with this article online at <http://dx.doi.org/10.1016/j.omtn.2017.04.015>.

AUTHOR CONTRIBUTIONS

W.D. and E.M.G. conceived and supervised this project. W.D. and W.C. performed the data analysis. W.C. conducted experiments and wrote this manuscript.

CONFLICTS OF INTEREST

The authors declare no conflict of interest.

ACKNOWLEDGMENTS

This work was supported by the Australian Research Council (DECRA: grant DE130100894; ARC CoE: grant CE140100003) and the HDR Budget from the Department of Physics and Astronomy, Macquarie University. The authors thank Dr. Jenny Nhu Vo for her assistance work of DNA gel electrophoresis, and also thank the

Macquarie Microscopy Unit for the TEM microscope. W.C. thanks the iMQRES scholarship.

REFERENCES

- Naldini, L., Blömer, U., Gallay, P., Ory, D., Mulligan, R., Gage, F.H., Verma, I.M., and Trono, D. (1996). In vivo gene delivery and stable transduction of nondividing cells by a lentiviral vector. *Science* 272, 263–267.
- Kay, M.A., Glorioso, J.C., and Naldini, L. (2001). Viral vectors for gene therapy: the art of turning infectious agents into vehicles of therapeutics. *Nat. Med.* 7, 33–40.
- Zhang, Y., Satterlee, A., and Huang, L. (2012). In vivo gene delivery by nonviral vectors: overcoming hurdles? *Mol. Ther.* 20, 1298–1304.
- Luo, D., and Saltzman, W.M. (2000). Synthetic DNA delivery systems. *Nat. Biotechnol.* 18, 33–37.
- Shim, M.S., and Kwon, Y.J. (2012). Stimuli-responsive polymers and nanomaterials for gene delivery and imaging applications. *Adv. Drug Deliv. Rev.* 64, 1046–1059.
- Lee, D.-J., He, D., Kessel, E., Padari, K., Kempter, S., Lächelt, U., Rädler, J.O., Pooga, M., and Wagner, E. (2016). Tumoral gene silencing by receptor-targeted combinatorial siRNA polyplexes. *J. Control. Release* 244 (Pt B), 280–291.
- Moghim, S.M., Symonds, P., Murray, J.C., Hunter, A.C., Debska, G., and Szwedczyk, A. (2005). A two-stage poly(ethylenimine)-mediated cytotoxicity: implications for gene transfer/therapy. *Mol. Ther.* 11, 990–995.
- Semple, S.C., Akinc, A., Chen, J., Sandhu, A.P., Mui, B.L., Cho, C.K., Sah, D.W., Stebbing, D., Crosley, E.J., Yaworski, E., et al. (2010). Rational design of cationic lipids for siRNA delivery. *Nat. Biotechnol.* 28, 172–176.
- Mintzer, M.A., and Simanek, E.E. (2009). Nonviral vectors for gene delivery. *Chem. Rev.* 109, 259–302.
- Fraley, R., Subramani, S., Berg, P., and Papahadjopoulos, D. (1980). Introduction of liposome-encapsulated SV40 DNA into cells. *J. Biol. Chem.* 255, 10431–10435.
- Allen, T.M., and Cullis, P.R. (2013). Liposomal drug delivery systems: from concept to clinical applications. *Adv. Drug Deliv. Rev.* 65, 36–48.
- Su, B., Cengizeroglu, A., Farkasova, K., Viola, J.R., Anton, M., Ellwart, J.W., Haase, R., Wagner, E., and Ogris, M. (2013). Systemic TNF α gene therapy synergizes with liposomal doxorubicin in the treatment of metastatic cancer. *Mol. Ther.* 21, 300–308.
- Suzuki, R., Naimi, E., Oda, Y., Nishiie, N., Otake, S., Koshima, R., Hirata, K., Taira, Y., Utoguchi, N., Negishi, Y., et al. (2010). Cancer gene therapy by IL-12 gene delivery using liposomal bubbles and tumoral ultrasound exposure. *J. Control. Release* 142, 245–250.
- Yin, H., Kanasty, R.L., Eltoukhy, A.A., Vegas, A.J., Dorkin, J.R., and Anderson, D.G. (2014). Non-viral vectors for gene-based therapy. *Nat. Rev. Genet.* 15, 541–555.
- Mendonça, L.S., Firmino, F., Moreira, J.N., Pedrosa de Lima, M.C., and Simões, S. (2010). Transferrin receptor-targeted liposomes encapsulating anti-BCR-ABL siRNA or asODN for chronic myeloid leukemia treatment. *Bioconjug. Chem.* 21, 157–168.
- Wu, J.X., Liu, S.-H., Nemunaitis, J.J., and Brunicardi, F.C. (2015). Liposomal insulin promoter-thymidine kinase gene therapy followed by ganciclovir effectively ablates human pancreatic cancer in mice. *Cancer Lett.* 359, 206–210.
- Lin, G., Zhang, H., and Huang, L. (2015). Smart polymeric nanoparticles for cancer gene delivery. *Mol. Pharm.* 12, 314–321.
- Ewe, A., Schaper, A., Barnert, S., Schubert, R., Temme, A., Bakowsky, U., and Aigner, A. (2014). Storage stability of optimal liposome-polyethylenimine complexes (lipopolyplexes) for DNA or siRNA delivery. *Acta Biomater.* 10, 2663–2673.
- Needham, D., Anyambhatla, G., Kong, G., and Dewhirst, M.W. (2000). A new temperature-sensitive liposome for use with mild hyperthermia: characterization and testing in a human tumor xenograft model. *Cancer Res.* 60, 1197–1201.
- Ponce, A.M., Vigilanti, B.L., Yu, D., Yarmolenko, P.S., Michelich, C.R., Woo, J., Bally, M.B., and Dewhirst, M.W. (2007). Magnetic resonance imaging of temperature-sensitive liposome release: drug dose painting and antitumor effects. *J. Natl. Cancer Inst.* 99, 53–63.

21. Shi, G., Guo, W., Stephenson, S.M., and Lee, R.J. (2002). Efficient intracellular drug and gene delivery using folate receptor-targeted pH-sensitive liposomes composed of cationic/anionic lipid combinations. *J. Control. Release* 80, 309–319.
22. Zhang, Q., Tang, J., Fu, L., Ran, R., Liu, Y., Yuan, M., and He, Q. (2013). A pH-responsive α -helical cell penetrating peptide-mediated liposomal delivery system. *Biomaterials* 34, 7980–7993.
23. Obata, Y., Tajima, S., and Takeoka, S. (2010). Evaluation of pH-responsive liposomes containing amino acid-based zwitterionic lipids for improving intracellular drug delivery in vitro and in vivo. *J. Control. Release* 142, 267–276.
24. de Smet, M., Heijman, E., Langereis, S., Hijnen, N.M., and Grüller, H. (2011). Magnetic resonance imaging of high intensity focused ultrasound mediated drug delivery from temperature-sensitive liposomes: an in vivo proof-of-concept study. *J. Control. Release* 150, 102–110.
25. Meers, P. (2001). Enzyme-activated targeting of liposomes. *Adv. Drug Deliv. Rev.* 53, 265–272.
26. Torchilin, V.P. (2005). Recent advances with liposomes as pharmaceutical carriers. *Nat. Rev. Drug Discov.* 4, 145–160.
27. Ito, A., Shinkai, M., Honda, H., and Kobayashi, T. (2005). Medical application of functionalized magnetic nanoparticles. *J. Biosci. Bioeng.* 100, 1–11.
28. Hirao, K., Sugita, T., Kubo, T., Igarashi, K., Tanimoto, K., Murakami, T., Yasunaga, Y., and Ochi, M. (2003). Targeted gene delivery to human osteosarcoma cells with magnetic cationic liposomes under a magnetic field. *Int. J. Oncol.* 22, 1065–1071.
29. Marie, H., Lemaire, L., Franconi, F., Lajnef, S., Prapart, Y.-M., Nicolas, V., Frébourg, G., Trichet, M., Ménager, C., and Lesieur, S. (2015). Superparamagnetic liposomes for MRI monitoring and external magnetic field-induced selective targeting of malignant brain tumors. *Adv. Funct. Mater.* 25, 1258–1269.
30. Carter, K.A., Shao, S., Hoopes, M.L., Luo, D., Ahsan, B., Grigoryants, V.M., Song, W., Huang, H., Zhang, G., Pandey, R.K., et al. (2014). Porphyrin-phospholipid liposomes permeabilized by near-infrared light. *Nat. Commun.* 5, 3546.
31. Alvarez-Lorenzo, C., Bromberg, L., and Concheiro, A. (2009). Light-sensitive intelligent drug delivery systems. *Photochem. Photobiol.* 85, 848–860.
32. Wang, F., and Liu, J. (2014). Liposome supported metal oxide nanoparticles: interaction mechanism, light controlled content release, and intracellular delivery. *Small* 10, 3927–3931.
33. Hemphill, J., Borchardt, E.K., Brown, K., Asokan, A., and Deiters, A. (2015). Optical control of CRISPR/Cas9 gene editing. *J. Am. Chem. Soc.* 137, 5642–5645.
34. Polstein, L.R., and Gersbach, C.A. (2015). A light-inducible CRISPR-Cas9 system for control of endogenous gene activation. *Nat. Chem. Biol.* 11, 198–200.
35. Wu, Y.-C., Wu, T.-H., Clemens, D.L., Lee, B.-Y., Wen, X., Horwitz, M.A., Teitell, M.A., and Chiou, P.Y. (2015). Massively parallel delivery of large cargo into mammalian cells with light pulses. *Nat. Methods* 12, 439–444.
36. Berg, K., Selbo, P.K., Prasmickaite, L., Tjelle, T.E., Sandvig, K., Moan, J., Gaudernack, G., Fodstad, O., Kjolsrud, S., Anholt, H., et al. (1999). Photochemical internalization: a novel technology for delivery of macromolecules into cytosol. *Cancer Res.* 59, 1180–1183.
37. Berg, K., Weyergang, A., Prasmickaite, L., Bonsted, A., Høget, A., Strand, M.T., Wagner, E., and Selbo, P.K. (2010). Photochemical internalization (PCI): a technology for drug delivery. *Methods Mol. Biol.* 635, 133–145.
38. Bostad, M., Olsen, C.E., Peng, Q., Berg, K., Høget, A., and Selbo, P.K. (2015). Light-controlled endosomal escape of the novel CD133-targeting immunotoxin AC133-saporin by photochemical internalization - a minimally invasive cancer stem cell-targeting strategy. *J. Control. Release* 206, 37–48.
39. Park, S., Park, W., and Na, K. (2015). Gene delivery: tumor intracellular-environment responsive materials shielded nano-complexes for highly efficient light-triggered gene delivery without cargo gene damage. *Adv. Funct. Mater.* 25, 3472–3482.
40. Theodossiou, T.A., Gonçalves, A.R., Yannakopoulou, K., Skarpen, E., and Berg, K. (2015). Photochemical internalization of tamoxifen transported by a "Trojan-horse" nanoconjugate into breast-cancer cell lines. *Angew. Chem. Int. Ed. Engl.* 54, 4885–4889.
41. Bostad, M., Kausberg, M., Weyergang, A., Olsen, C.E., Berg, K., Høget, A., and Selbo, P.K. (2014). Light-triggered, efficient cytosolic release of IM7-saporin targeting the putative cancer stem cell marker CD44 by photochemical internalization. *Mol. Pharm.* 11, 2764–2776.
42. Maurice-Duelli, A., Ndoye, A., Bouali, S., Leroux, A., and Merlin, J.-L. (2004). Enhanced cell growth inhibition following PTEN nonviral gene transfer using polyethylenimine and photochemical internalization in endometrial cancer cells. *Technol. Cancer Res. Treat.* 3, 459–465.
43. Miyata, A., Jiang, L., Dahl, R.D., Kitada, C., Kubo, K., Fujino, M., Minamino, N., and Arimura, A. (1990). Isolation of a neuropeptide corresponding to the N-terminal 27 residues of the pituitary adenylate cyclase activating polypeptide with 38 residues (PACAP38). *Biochem. Biophys. Res. Commun.* 170, 643–648.
44. Vaudry, D., Falluel-Morel, A., Bourgault, S., Basille, M., Burel, D., Wurtz, O., Fournier, A., Chow, B.K., Hashimoto, H., Galas, L., and Vaudry, H. (2009). Pituitary adenylate cyclase-activating polypeptide and its receptors: 20 years after the discovery. *Pharmacol. Rev.* 61, 283–357.
45. Lee, J.-H., Lee, J.-Y., Rho, S.B., Choi, J.-S., Lee, D.-G., An, S., Oh, T., Choi, D.C., and Lee, S.H. (2014). PACAP inhibits tumor growth and interferes with clusterin in cervical carcinomas. *FEBS Lett.* 588, 4730–4739.
46. Moody, T.W., Zia, F., and Makheja, A. (1993). Pituitary adenylate cyclase activating polypeptide receptors are present on small cell lung cancer cells. *Peptides* 14, 241–246.
47. Gutiérrez-Cañas, I., Rodríguez-Henche, N., Bolaños, O., Carmona, M.J., Prieto, J.C., and Juarranz, M.G. (2003). VIP and PACAP are autocrine factors that protect the androgen-independent prostate cancer cell line PC-3 from apoptosis induced by serum withdrawal. *Br. J. Pharmacol.* 139, 1050–1058.
48. Zia, F., Fagarasan, M., Bitar, K., Coy, D.H., Pisegna, J.R., Wank, S.A., and Moody, T.W. (1995). Pituitary adenylate cyclase activating peptide receptors regulate the growth of non-small cell lung cancer cells. *Cancer Res.* 55, 4886–4891.
49. Leyton, J., Gozes, Y., Pisegna, J., Coy, D., Purdom, S., Casibang, M., Zia, F., and Moody, T.W. (1999). PACAP(6–38) is a PACAP receptor antagonist for breast cancer cells. *Breast Cancer Res. Treat.* 56, 177–186.
50. Leyton, J., Coelho, T., Coy, D.H., Jakowlew, S., Birrer, M.J., and Moody, T.W. (1998). PACAP(6–38) inhibits the growth of prostate cancer cells. *Cancer Lett.* 125, 131–139.
51. Farnham, M.M.-J., Lung, M.S., Tallapragada, V.J., and Pilowsky, P.M. (2012). PACAP causes PAC1/VPAC2 receptor mediated hypertension and sympathoexcitation in normal and hypertensive rats. *Am. J. Physiol. Heart Circ. Physiol.* 303, H910–H917.
52. Daniel, P.B., Kieffer, T.J., Leech, C.A., and Habener, J.F. (2001). Novel alternatively spliced exon in the extracellular ligand-binding domain of the pituitary adenylate cyclase-activating polypeptide (PACAP) type 1 receptor (PAC1R) selectively increases ligand affinity and alters signal transduction coupling during spermatogenesis. *J. Biol. Chem.* 276, 12938–12944.
53. Ravn, A., Bourgault, S., Lebon, A., Chan, P., Galas, L., Fournier, A., Vaudry, H., Gonzalez, B., Eiden, L.E., and Vaudry, D. (2006). The neurotrophic effects of PACAP in PC12 cells: control by multiple transduction pathways. *J. Neurochem.* 98, 321–329.
54. Vaudry, D., Chen, Y., Hsu, C.M., and Eiden, L.E. (2002). PC12 cells as a model to study the neurotrophic activities of PACAP. *Ann. N Y Acad. Sci.* 971, 491–496.
55. Vaudry, D., Stork, P.J., Lazarovici, P., and Eiden, L.E. (2002). Signaling pathways for PC12 cell differentiation: making the right connections. *Science* 296, 1648–1649.
56. Du, Z., Munye, M.M., Tagalakakis, A.D., Manunta, M.D., and Hart, S.L. (2014). The role of the helper lipid on the DNA transfection efficiency of lipopolyplex formulations. *Sci. Rep.* 4, 7107.
57. Aveline, B., Hasan, T., and Redmond, R.W. (1994). Photophysical and photosensitizing properties of benzoporphyrin derivative monoacid ring A (BPD-MA). *Photochem. Photobiol.* 59, 328–335.
58. Bareford, L.M., and Swaan, P.W. (2007). Endocytic mechanisms for targeted drug delivery. *Adv. Drug Deliv. Rev.* 59, 748–758.
59. Schmidt-Erfurth, U., and Hasan, T. (2000). Mechanisms of action of photodynamic therapy with verteporfin for the treatment of age-related macular degeneration. *Surv. Ophthalmol.* 45, 195–214.
60. Chen, J., Luo, J., Zhao, Y., Pu, L., Lu, X., Gao, R., Wang, G., and Gu, Z. (2015). Increase in transgene expression by pluronic L64-mediated endosomal/lysosomal escape through its membrane-disturbing action. *ACS Appl. Mater. Interfaces* 7, 7282–7293.

www.moleculartherapy.org

61. Wu, L., Zhang, J., and Watanabe, W. (2011). Physical and chemical stability of drug nanoparticles. *Adv. Drug Deliv. Rev.* 63, 456–469.
62. Chen, R.F., and Knutson, J.R. (1988). Mechanism of fluorescence concentration quenching of carboxyfluorescein in liposomes: energy transfer to nonfluorescent dimers. *Anal. Biochem.* 172, 61–77.
63. Antonsson, B., Conti, F., Ciavatta, A., Montessuit, S., Lewis, S., Martinou, I., Bernasconi, L., Bernard, A., Mermod, J.J., Mazzei, G., et al. (1997). Inhibition of Bax channel-forming activity by Bcl-2. *Science* 277, 370–372.
64. Costes, S.V., Daelemans, D., Cho, E.H., Dobbin, Z., Pavlakakis, G., and Lockett, S. (2004). Automatic and quantitative measurement of protein-protein colocalization in live cells. *Biophys. J.* 86, 3993–4003.
65. Manders, E.M., Stap, J., Brakenhoff, G.J., van Driel, R., and Aten, J.A. (1992). Dynamics of three-dimensional replication patterns during the S-phase, analysed by double labelling of DNA and confocal microscopy. *J. Cell Sci.* 103, 857–862.
66. Bolte, S., and Cordelières, F.P. (2006). A guided tour into subcellular colocalization analysis in light microscopy. *J. Microsc.* 224, 213–232.
67. Li, Q., Lau, A., Morris, T.J., Guo, L., Fordyce, C.B., and Stanley, E.F. (2004). A syntaxin 1, α -calmodulin, and N-type calcium channel complex at a presynaptic nerve terminal: analysis by quantitative immunocolocalization. *J. Neurosci.* 24, 4070–4081.
68. Jiang, X., Yu, H., Teo, C.R., Tan, G.S.X., Goh, S.C., Patel, P., Chua, Y.K., Hameed, N.B., Bertozzi, A., and Patzel, V. (2016). Advanced design of dumbbell-shaped genetic minimal vectors improves non-coding and coding RNA expression. *Mol. Ther.* 24, 1581–1591.
69. Kuluncsics, Z., Perdiz, D., Brulay, E., Muel, B., and Sage, E. (1999). Wavelength dependence of ultraviolet-induced DNA damage distribution: involvement of direct or indirect mechanisms and possible artefacts. *J. Photochem. Photobiol. B* 49, 71–80.
70. Sinha, R.P., and Hader, D.-P. (2002). UV-induced DNA damage and repair: a review. *Photochem. Photobiol. Sci.* 1, 225–236.
71. Besaratinia, A., Yoon, J.L., Schroeder, C., Bradforth, S.E., Cockburn, M., and Pfeifer, G.P. (2011). Wavelength dependence of ultraviolet radiation-induced DNA damage as determined by laser irradiation suggests that cyclobutane pyrimidine dimers are the principal DNA lesions produced by terrestrial sunlight. *FASEB J.* 25, 3079–3091.
72. Bissig, C., and Gruenberg, J. (2014). ALIX and the multivesicular endosome: ALIX in Wonderland. *Trends Cell Biol.* 24, 19–25.
73. Jayakumar, M.K.G., Bansal, A., Huang, K., Yao, R., Li, B.N., and Zhang, Y. (2014). Near-infrared-light-based nano-platform boosts endosomal escape and controls gene knockdown in vivo. *ACS Nano* 8, 4848–4858.
74. Kojro, E., Postina, R., Buro, C., Meiringer, C., Gehrig-Burger, K., and Fahrenholz, F. (2006). The neuropeptide PACAP promotes the α -secretase pathway for processing the Alzheimer amyloid precursor protein. *FASEB J.* 20, 512–514.
75. Gonzalez, B.J., Basille, M., Vaudry, D., Fournier, A., and Vaudry, H. (1997). Pituitary adenylate cyclase-activating polypeptide promotes cell survival and neurite outgrowth in rat cerebellar neuroblasts. *Neuroscience* 78, 419–430.
76. Hannibal, J. (2006). Roles of PACAP-containing retinal ganglion cells in circadian timing. *Int. Rev. Cytol.* 251, 1–39.
77. Gupta, B., Levchenko, T.S., and Torchilin, V.P. (2007). TAT peptide-modified liposomes provide enhanced gene delivery to intracranial human brain tumor xenografts in nude mice. *Oncol. Res.* 16, 351–359.
78. Pardridge, W.M. (2002). Drug and gene delivery to the brain: the vascular route. *Neuron* 36, 555–558.
79. Qin, Y., Chen, H., Zhang, Q., Wang, X., Yuan, W., Kuai, R., Tang, J., Zhang, L., Zhang, Z., Zhang, Q., et al. (2011). Liposome formulated with TAT-modified cholesterol for improving brain delivery and therapeutic efficacy on brain glioma in animals. *Int. J. Pharm.* 420, 304–312.
80. Stevens, J.S., Almlil, L.M., Fani, N., Gutman, D.A., Bradley, B., Norrholm, S.D., Reiser, E., Ely, T.D., Dhanani, R., Glover, E.M., et al. (2014). PACAP receptor gene polymorphism impacts fear responses in the amygdala and hippocampus. *Proc. Natl. Acad. Sci. USA* 111, 3158–3163.
81. Hashimoto, H., Shintani, N., Ago, Y., Hayata-Takano, A., Nakazawa, T., Hashimoto, R., Matsuzaki, S., Katayama, T., Tohyama, M., Matsuda, T., and Baba, A. (2016). Implications of PACAP signaling in psychiatric disorders. In *Pituitary Adenylate Cyclase Activating Polypeptide—PACAP*, D. Reglodi and A. Tamas, eds. (Springer), pp. 757–766.
82. Gross, N., Ranjbar, M., Evers, C., Hua, J., Martin, G., Schulze, B., Michaelis, U., Hansen, L.L., and Agostini, H.T. (2013). Choroidal neovascularization reduced by targeted drug delivery with cationic liposome-encapsulated paclitaxel or targeted photodynamic therapy with verteporfin encapsulated in cationic liposomes. *Mol. Vis.* 19, 54–61.
83. Wang, Y., Gao, S., Ye, W.-H., Yoon, H.S., and Yang, Y.-Y. (2006). Co-delivery of drugs and DNA from cationic core-shell nanoparticles self-assembled from a biodegradable copolymer. *Nat. Mater.* 5, 791–796.
84. Ruozi, B., Belletti, D., Tombesi, A., Tosi, G., Bondioli, L., Forni, F., and Vandelli, M.A. (2011). AFM, ESEM, TEM, and CLSM in liposomal characterization: a comparative study. *Int. J. Nanomedicine* 6, 557–563.
85. Das, K.P., Freudenrich, T.M., and Mundy, W.R. (2004). Assessment of PC12 cell differentiation and neurite growth: a comparison of morphological and neurochemical measures. *Neurotoxicol. Teratol.* 26, 397–406.

OMTN, Volume 7

Supplemental Information

Light-Triggerable Liposomes for Enhanced Endolysosomal Escape and Gene Silencing in PC12 Cells

Wenjie Chen, Wei Deng, and Ewa M. Goldys

Supplemental Figures

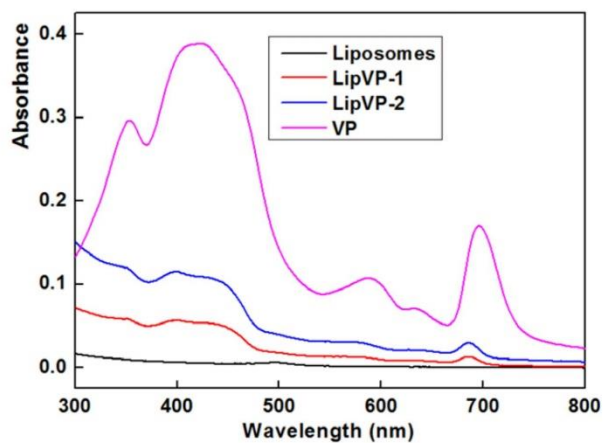


Figure S1 Absorbance spectra of liposomes alone, lipVP-1 (5.55 $\mu\text{g/mL}$), lipVP-2 (55.5 $\mu\text{g/mL}$) and free VP molecules.

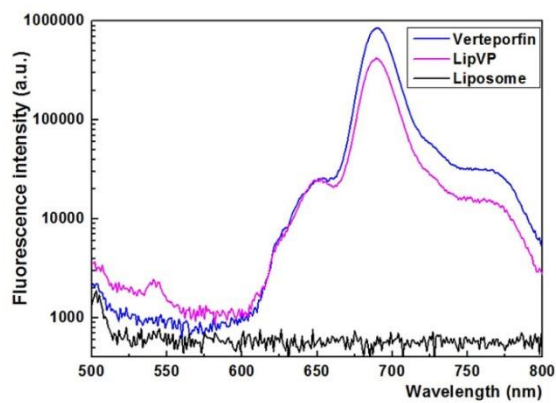


Figure S2 Fluorescence spectra of liposomes alone, lipVP and free VP molecules under 425 nm excitation.

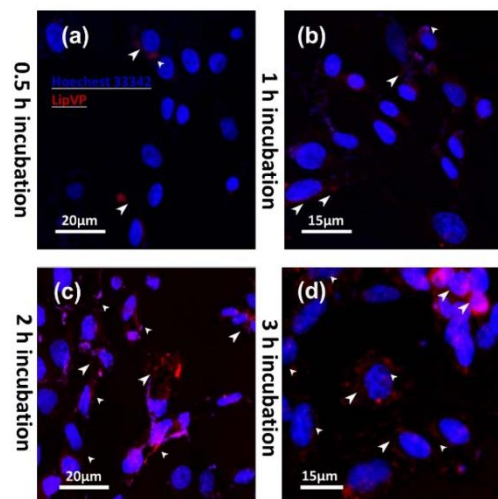


Figure S3 Cellular uptake. The confocal images of cellular uptake of lipVP in the serum-free medium at different incubation time points: (a) 0.5 h, (b) 1 h, (c) 2 h and (d) 3 h. White arrows refer to the lipVP nanoparticles surrounding the cell nucleus.

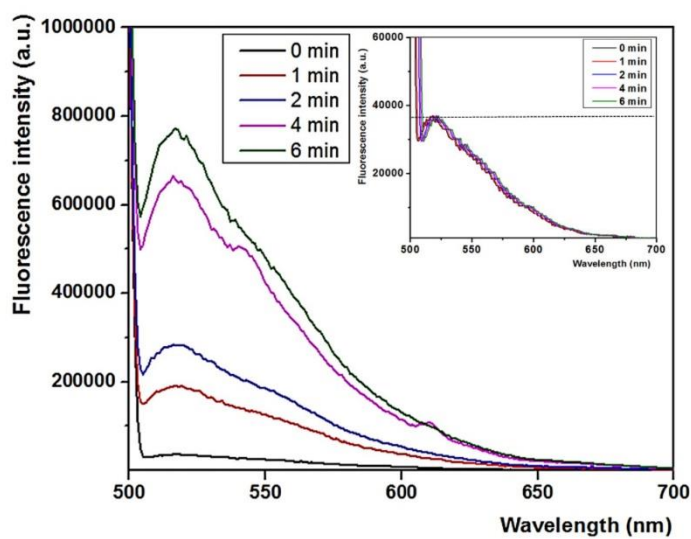


Figure S4 DNA release test. The release test of FAM labelled asODN encapsulated in lipVP and pure liposomes (inset) after UV illumination (365nm, 1.25mW/cm²) for different time periods. The fluorescence intensity of FAM was measured at 425nm excitation.

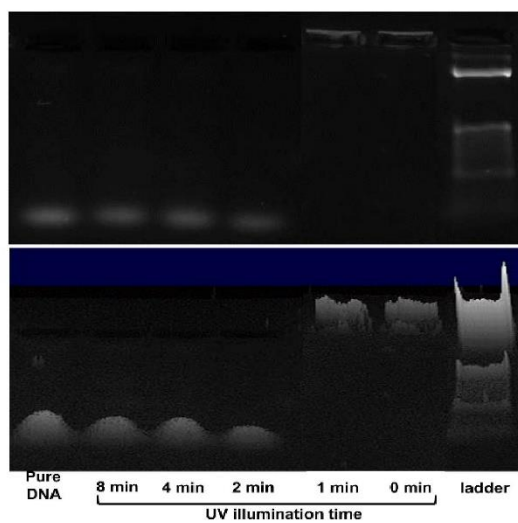


Figure S5 DNA damage assay. Agarose electrophoresis of lipVP/DNA complexes under different time of UV illumination. The below picture is the 3D version of the above.

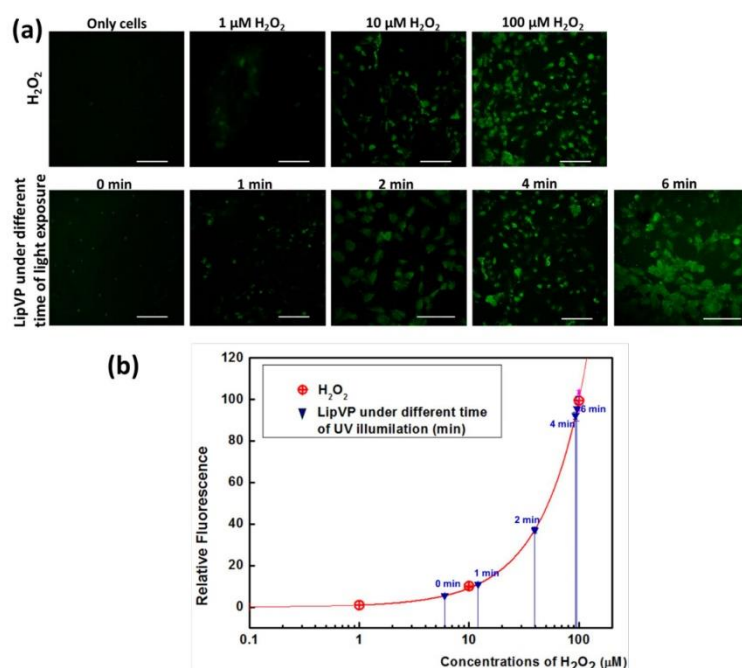


Figure S6 Detection of cellular ROS. (a) CLSM images of DCF fluorescence signal produced by the cellular ROS with and without light illumination. H₂O₂ solution with varying concentrations was added to cells in positive control groups. Scale bar, 120 μ m. (b) Quantitative assessment of DCF fluorescence intensity after light treatment compared with the H₂O₂ positive controls. The amount of ROS was calculated from the fitting curve of H₂O₂-treated groups. LipVP generated different amount of ROS in transfected cells after 0, 1, 2, 4 and 6 min of illumination, which was equivalent to the amount produced with the introduction of 6.0 μ M, 12.1 μ M, 39.6 μ M, 93.1 μ M and 96.1 μ M of H₂O₂, respectively.

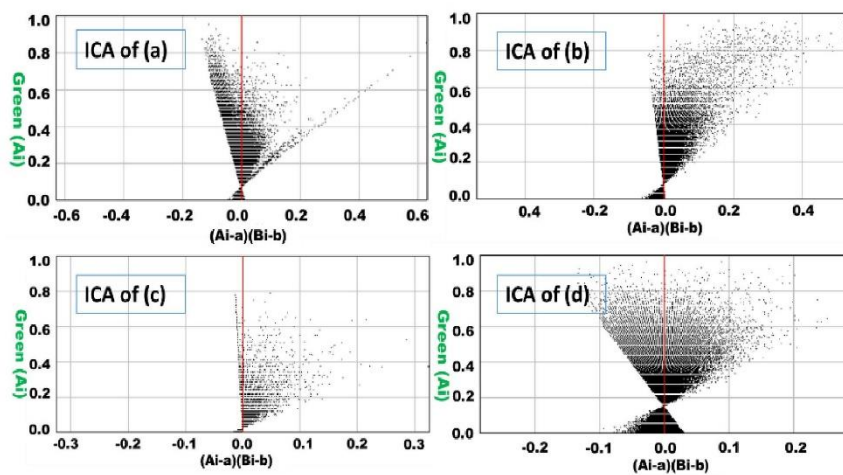


Figure S7 Intensity correlation analysis (ICA) of Figure4 a, b, c and d by using imageJ JACoP.

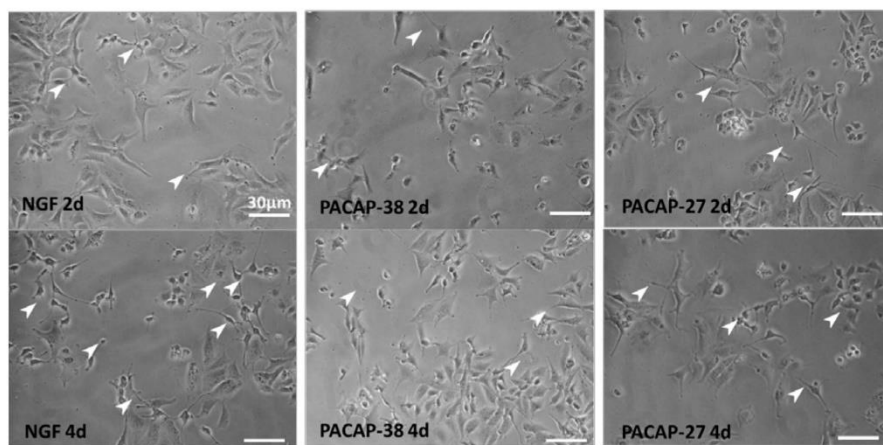


Figure S8 Phase contrast images of cell differentiation induced by NGF, PACAP-38 and PACAP-27 with 2-day and 4-day treatment. Scale bars: 30 μ m. White arrows indicate selected typical neurites.

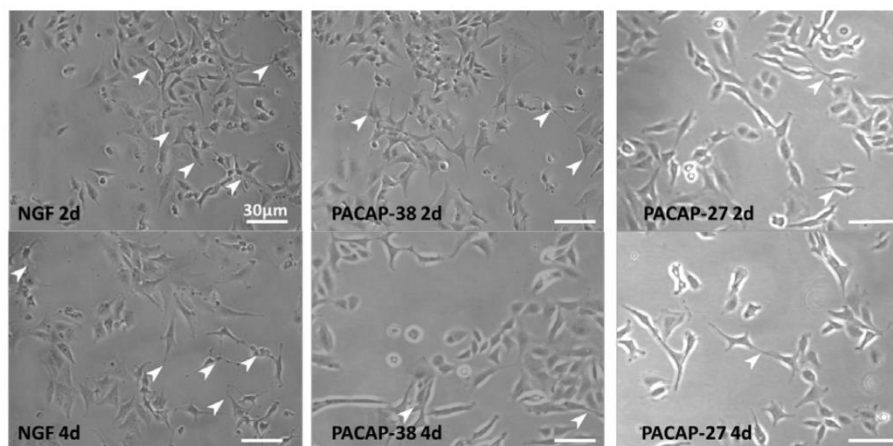


Figure S9 Phase contrast images of cell differentiation induced by NGF, PACAP-38 and PACAP-27 after transfection with lipVP-asODN complexes and UV illumination for 1 min. Scale bars: 30 μ m. White arrows indicate selected typical neurites.

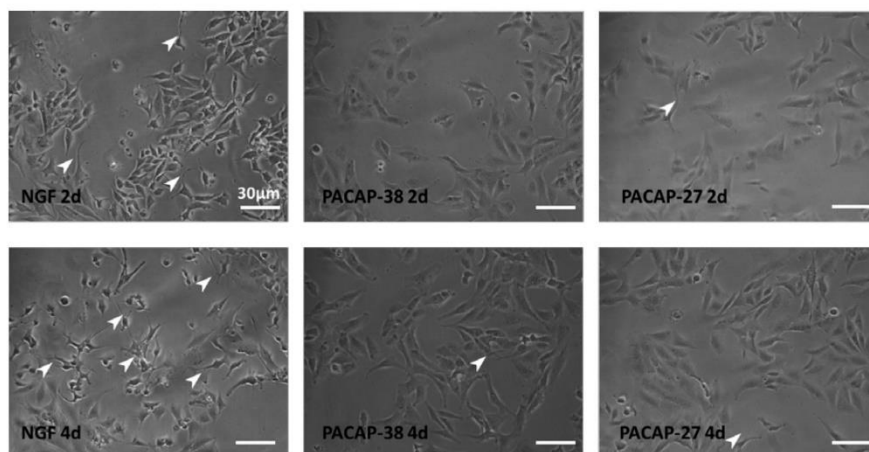


Figure S10 Phase contrast images of cell differentiation induced by NGF, PACAP-38 and PACAP-27 after transfection with lipVP-asODN complexes and UV illumination for 4 min. Scale bars: 30 μ m. White arrows indicate selected typical neurites.

Supplemental methods

To determine if generated ROS can obviously damage genes or not, we evaluated the performance of DNA release in solution after light illumination using gel electrophoresis. In each vial, 0.5 μ g of DNA was encapsulated into the as prepared lipVP to form the lipoplexes (lipVP/DNA at N/P ratio= 25), followed by 2, 4 and 8 min of UV illumination.

3

Liposome-polycation-DNA (LPD) for enhanced plasmid delivery

CHAPTER 3 Paper 2

Photoresponsive endosomal escape enhances gene delivery using liposome-polycation-DNA (LPD) nanovectors

Wenjie Chen, Wei Deng, Xin Xu, Xiang Zhao, Jenny Nhu Vo, Ayad G. Anwer, Thomas C. Williams, Haixin Cui, Ewa M. Goldys (2018) *Journal of Materials Chemistry B*, 6, 5269-5281.

Summary of author contributions to this paper.

	W.C.	W.D.	X.X.	X.Z.	JN.V.	AG.A.	TC.W.	H.C.	EM.G.
Project Design	●	●			●				●
Sample Preparation	●		●	●	●			●	
Experiment	●		●						
Data Analysis	●	●							
Manuscript	●	●		●		●	●	●	●



Cite this: *J. Mater. Chem. B*, 2018, 6, 5269

Photoresponsive endosomal escape enhances gene delivery using liposome–polycation–DNA (LPD) nanovectors†

Wenjie Chen,^a Wei Deng,^{a,b} Xin Xu,^c Xiang Zhao,^d Jenny Nhu Vo,^c Ayad G. Anwer,^a Thomas C. Williams,^{c,e} Haixin Cui^d and Ewa M. Goldys^{a,b}

Lipid-based nanocarriers with stimuli responsiveness have been utilized as controlled release systems for gene/drug delivery applications. In our work, by taking advantage of the high complexation capability of polycations and the light triggered properties, we designed a novel photoresponsive liposome–polycation–DNA (LPD) platform. This LPD carrier incorporates verteporfin (VP) in lipid bilayers and the complex of polyethylenimine (PEI)/plasmid DNA (pDNA) encoding EGFP (polyplex) in the central cavities of the liposomes. The liposomes were formulated with cationic lipids, PEGylated neutral lipids and cholesterol molecules, which improve their stability and cellular uptake in the serum-containing media. We evaluated the nanocomplex stability by monitoring size changes over six days, and the cellular uptake of the nanocomplex by imaging the intracellular route. We also demonstrated that light triggered the cytoplasmic release of pDNA upon irradiation with a 690 nm LED light source. Furthermore, this light triggered mechanism has been studied at the subcellular level. The activated release is driven by the generation of reactive oxygen species (ROS) from VP after light illumination. These ROS oxidize and destabilize the liposomal and endolysosomal membranes, leading to the release of pDNA into the cytosol and subsequent gene transfer activities. Light-triggered endolysosomal escape of pDNA at different time points was confirmed by a quantitative analysis of colocalization between pDNA and endolysosomes. The increased expression of the reporter EGFP in human colorectal cancer cells was also quantified after light illumination at various time points. The efficiency of this photo-induced gene transfection was demonstrated to be more than double compared to non-irradiated controls. Additionally, we observed a reduced cytotoxicity of the LPDs compared with the polyplexes alone. This study has thus shown that light-triggered and biocompatible LPDs enable an improved control of efficient gene delivery, which will be beneficial for future gene therapies.

Received 16th April 2018,
Accepted 18th July 2018

DOI: 10.1039/c8tb00994e

rsc.li/materials-b

1. Introduction

Gene therapies currently under development against cancer, genetic disorders, and other diseases utilize diverse genetic materials including antisense oligodeoxynucleotides (asODNs),

small interfering RNA (siRNA), plasmids and other forms of nucleic acids.^{1,2} While viral transfection remains the established method of their delivery, recently, various nanoscale nonviral vectors have been identified to deliver these genetic materials into cells with several advantages.^{3–5} Many of these are comparatively easy to prepare, and they have attractive properties such as minimal immunogenicity and excellent biocompatibility,⁶ as well as the ability of loading long DNA fragments.^{7–9} Besides, the enhanced permeability and retention (EPR) effect enables these nanoscale carriers to preferentially accumulate in tumour tissue,¹⁰ and they can also be molecularly targeted.^{11,12} This EPR effect can markedly reduce side-effects towards non-cancer tissue during therapy. All these advantages point to the possibility of nonviral carriers playing a vital role in future clinical gene/drug delivery systems.⁸

Among the nanoscale nonviral gene vectors, cationic phospholipids (lipoplexes), polymers (polyplexes) and lipid–polymer

^a ARC Centre of Excellence for Nanoscale BioPhotonics (CNBP), Department of Physics and Astronomy, Macquarie University, Sydney, New South Wales 2109, Australia

^b The Graduate School of Biomedical Engineering, University of New South Wales, Sydney, New South Wales 2052, Australia. E-mail: wei.deng@unsw.edu.au, e.goldys@unsw.edu.au

^c Department of Molecular Sciences, Macquarie University, Sydney, New South Wales 2109, Australia

^d Nanobiotechnology Research Centre, Institute of Environment and Sustainable Development in Agriculture, Chinese Academy of Agricultural Sciences, Beijing 100081, P. R. China

^e CSIRO Synthetic Biology Future Science Platform, Canberra, ACT 2601, Australia

† Electronic supplementary information (ESI) available. See DOI: 10.1039/c8tb00994e

hybrids (lipopolyplexes) have been widely developed for various delivery strategies.¹³ Lipopolyplexes are constructed from phospholipid molecules, which generally consist of hydrophobic tails and hydrophilic heads. These molecules reassemble to form liposomal or micellar structures able to encapsulate nucleic acids and prevent them from degradation.¹⁴ In cationic liposomal gene carriers, two main forces contribute to the lipoplex formation. One is the elasticity forces driven by the lipid hydrophobic moiety, the other is the electrostatic force between the negatively charged nucleic acid cargos and the positively charged groups in lipid molecules.¹⁵ Their relative balance may be correlated with lipoplex morphologies and the effectiveness of transfection.¹⁶ Moreover, the fusogenic mechanism induced by the liposomal structure affects the cellular internalization of liposomes within the endocytosis pathway, and it may promote endosomal escape *via* membrane destabilization, resulting in content release from the liposomes into the cytoplasm.^{17,18} To achieve on-demand content release, several types of stimulus-responsive liposomes have been designed whose bilayer can be destabilized by physiological and external stimuli.^{19–23} These triggering approaches include changes in pH,²⁰ temperature,²¹ ROS,²² magnetic fields,²⁴ ultrasound²⁵ or light.²³ Among these, the light-triggering modality has attracted intense interest, due to the precise control of different parameters of light, the feasibility of spatiotemporal manipulation (including optical fibre delivery directly into the body) and non-invasiveness of light irradiation. In addition to the controllability of lipid-like delivery systems, their stability in the physiological environment is also crucial for *in vivo* applications. This can be achieved by either the adjustment of lipid components or modification of the liposome surface. For instance, incorporating cholesterol (Chol) into liposomal formulations can improve resistance to liposome aggregation in a physiological environment, protect them from protein binding and mechanical breakage²⁶ and prolong their half-lives. Additionally, further surface modification with polyethylene glycol (PEG) improves the uptake by forming a mononuclear phagocyte system that extends their blood-circulation time by forming “stealth liposomes”.²⁷ Importantly, PEG groups may facilitate conjugation with different targeting ligands including folic acid, antibodies, and cell penetration peptides (CCPs).²⁸ All of these are important in *in vivo* applications.²⁹

Polycation vectors such as PEI³⁰ and poly-L-lysine (PLL)³¹ have been widely used for the formulation of DNA-polymer complexes (polyplexes) for improved DNA delivery into cells. The delivery of polyplexes into cells is facilitated by their high cationic charge density at physiological pH.³² Although PEI has good physical stability, is easy to manipulate and is moderately resistant to enzymatic degradation,³³ its drawbacks such as high cytotoxicity and limited transfection activity have hindered its applications *in vivo*.^{8,34,35} They are determined by the physicochemical properties of PEI structures and molecular weight. For example, branched PEI with a high molecular weight (for example, 25 kD) shows substantial transfection activity but suffers from greater cytotoxicity (80%, at 60 $\mu\text{g mL}^{-1}$ in Lovo cells),³⁶ compared with PEI of a lower molecular weight.^{37–39} To achieve the optimal balance between cytotoxicity and transfection

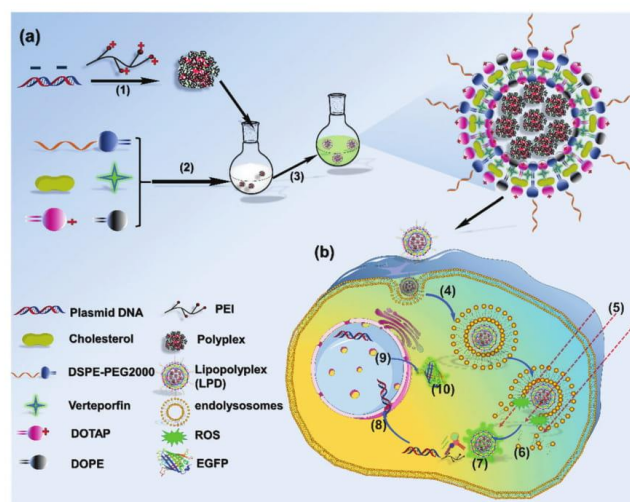
efficiency, different strategies for PEI modification have been explored, including combining the PEI/DNA complex with various phospholipids to form LPD complexes (named lipopolyplexes).⁴⁰

The purpose of our work is to further enhance the transfection efficiency of such LPD systems by using external stimuli, for example, light. To the best of our knowledge, few reports on photo-responsive LPD as a gene vector have been published. To this end, we herein developed PEGylated and light-triggered liposomes incorporating large PEI (branched, 25 kD)/pDNA (4.7 kbp) complexes based on our previous work.⁴¹ This photo-responsive LPD successfully delivered gene and achieved gene expression in the HCT116 cell line, which is considered as a typical *in vitro* model to study the gene therapy of colorectal cancer.⁴² The pDNA loading capability of LPD was assessed by gel electrophoresis at different N/P molar ratios (N indicates PEI nitrogen and P represents phosphate of pDNA). To enhance the stability of LPD, in addition to PEGylation, Chol was also added to the liposome formulations. The liposome stability with different Chol contents was measured by using dynamic light scattering (DLS) and differential scanning calorimetry (DSC). In order to enable light triggering, we used verteporfin (VP). VP is one of the photosensitizer drugs clinically used for photodynamic therapy. VP can rapidly and effectively generate reactive oxygen species (ROS) under 690 nm photoirradiation.⁴³ When VP is incorporated into the liposome, the ROS production upon irradiation can destabilise the liposomal membranes.⁴¹ We hypothesize here that after the liposomes have been endocytosed by cells where they eventually localize in the endosomes or lysosomes, the ROS can further destabilize the endolysosomal membranes, resulting in the escape of entrapped pDNA out of the endolysosomal compartments into the cytoplasm, in which the released pDNA can play the role of gene expression. To demonstrate this process of light activated release of pDNA from the endolysosomes, subcellular tracking of endolysosomal escape of pDNA was carried out by using confocal microscopy imaging and quantitative analysis of colocalization. Finally, light-enhanced transfection efficiency was examined using flow cytometry to determine the fraction of transfected, EGFP-expressing cells for different light illumination periods. The details of this approach are shown in Scheme 1.

2. Experimental

2.1 Materials

Lipids (DOTAP: Catalog No. 890890 and DOPE: Catalog No. 850375, DSPE-PEG (2000) Amine: Catalog No. 880128) were purchased from Avanti Polar Lipids (Alabaster, AL, USA). Dulbecco's modified Eagle's medium (DMEM: Catalog No. 11965-092), fetal bovine serum (FBS: Catalog No. 10437-028), trypsin (Catalog No. 15400054), LysoTracker (Catalog No. L7528), Hoechst 33342 (Catalog No. H3570), phosphate-buffered saline (PBS: Catalog No. 10010023) and Dulbecco's phosphate-buffered saline (DPBS: Catalog No. 14190250) solution, Hank's Balanced Salt Solution (HBSS: Catalog No. 14175145), 4-(2-hydroxyethyl)-1-piperazineethanesulfonic acid (HEPES: Catalog No. 14185052)



Scheme 1 (a) Schematic illustration of the preparation of LPD and (b) intracellular events in the course of light-triggered gene transfer: (1) polyplex complexation, (2) drying in a vacuum, (3) hydration, (4) cellular uptake, (5) 690 nm photoirradiation, (6) endolysosomal escape, (7) vector dissociation, (8) nuclear translocation, (9) gene transcription and (10) EGFP expression.

buffer, TAE Buffer (Tris-acetate-EDTA, 50×, Catalog No. B49) and optiMEM (Catalog No. 31985070) solution were purchased from Thermo Fisher (Scoresby, Vic, Australia). McCoy's 5A medium (product no: ATCC[®] 30-2007™) was purchased from the ATCC. Uranyl acetate (Catalog No. 73943), paraformaldehyde (Catalog No. P6148), chloroform (Catalog No. 372978), cholesterol (Catalog No. C8667), Fluoromount™ aqueous mounting medium (Catalog No. F4680), DNase I (deoxyribonuclease I, Catalog No. D5025), phosphotungstic acid (PTA, Catalog No. P4006) and 2',7'-dichlorofluorescein diacetate (DCF-DA) (Catalog No. D6883) were purchased from Sigma-Aldrich (Castle Hill, NSW, Australia).

2.2 Plasmid DNA and cell lines

The plasmid pEGFP-N1 (GenBank: U 55762.1) encoding the enhanced green fluorescence protein, EGFP (4.7 kbp), was obtained from the Chinese People's Liberation Army Military Academy of Medical Sciences (Beijing, China). It was amplified in the *E. coli* DH5α strain, extracted and purified using the Qiagen Plasmid Midi Kit. The concentration of the pEGFP-N1 solution was determined using NanoDrop 2000 (ThermoFisher, Vic, Australia). The fluorescein labelled pDNA was prepared using the Label IT[®] Nucleic Acid Labelling Reagents (Mirus Bio LLC., WI USA) as per the manufacturer's instructions.

The human colorectal cancer cell line HCT116 (product no: ATCC[®] CCL-247™) was purchased from ATCC (Manassas, VA USA). McCoy's 5A medium supplemented with 10% FBS and 1% antibiotic-antimycotic was used to culture the HCT116 cells. DMEM supplemented with 10% FBS and 1% antibiotic-antimycotic was used as the culture medium of the HCT116 cells. The cells were grown at 37 °C with 5% CO₂ in the cell incubator.

When the cells reached about 90% confluence, they were detached with trypsin and transferred into Petri dishes or well plates for different experimental purposes.

2.3 Preparation of liposomes and LPDs

Liposomes with different formulations were prepared *via* a thin-film method⁴⁴ with some modifications. Briefly, lipid components at different mole ratios were mixed with VP at a fixed amount in 5 mL of chloroform in a round flask (Scheme 1). The mixture solvent was then evaporated under an argon gas stream using a rotary evaporator (Buchi R-300, Flawil Switzerland) for 15 min at 50 °C. A thin lipid film formed at the bottom of the flask and it was subsequently hydrated with HEPES buffer (40 mM, pH 7.4) by vigorous stirring for 30 min until the suspension was homogenized. The hydrated liposome suspension was extruded 11 times through a 200 nm polycarbonate membrane in a mini-extruder (Avanti Polar Lipids). The final liposome suspension was purified by using 3000 MW dialysis tubes for 24 h at 37 °C in 500 μL of DI water prior to further use. To determine the encapsulation amount of VP loaded inside of the liposomes, we added Triton X-100 (0.1%) to the as-prepared liposome solution, resulting in VP release. VP fluorescence (excitation/emission: 425/690 nm) was recorded on a Fluorolog-Tau-3 system and compared with the corresponding VP calibration standard curve. To determine the encapsulation efficiency of VP loaded inside of the liposomes at different time points (6 h, 12 h, 24 h, 36 h and 48 h), dialysis was conducted. The leaked VP was calculated compared with the corresponding VP standard curve using a fluorophotometer measurement.

HN buffer (150 mM NaCl and 10 mM HEPES, pH 7.4) is the complexation buffer used for LPD formation. Polyplexes (PEI/pDNA complexes) with different N/P ratios⁴⁵ were prepared by incubation of pDNA with different amounts of PEI solution at 37 °C in HN buffer for 30 min. For the preparation of the LPD, the as-prepared lipid film was hydrated with the solution of preformed polyplexes for 30 min at room temperature. The hydrated lipopolyplex solution was freshly prepared prior to cell experiments and measurements.

2.4 Characterization

The zeta potential and size distribution of the liposome samples with and without PEGylation were determined by DLS using a Zetasizer 3000HSA (MALVERN Instruments, Worcestershire, UK). After 2 min balance at 25 °C, each sample was measured in triplicate and data were collected as the mean \pm standard deviation (SD). The sizes of liposome suspended in different solutions including HEPES buffer, optiMEM medium and 10% FBS solution were also measured at different time points.

Prior to transmission electron microscopy (TEM) imaging of the liposome samples, TEM grid specimens were prepared using the negative staining method. Briefly, a copper grid was placed onto a drop of 10 μ L of liposome, LPD or polyplex suspension, allowing the grid to absorb samples for 3 min, followed by staining with 2% (w/v) phosphotungstic acid for another 3 min. After air-drying the samples overnight, the grid specimens were then observed using TEM (Philips CM 10) at an acceleration voltage of 100 kV. Images were captured using an Olympus Megaview G10 camera and processed with iTEM software.

The absorption and fluorescence spectra of liposomes and pure VP were recorded on a UV-VIS spectrometer (Cary 5000, Varian Inc.) and a Fluorolog-Tau-3 System (HORIBA Scientific) with 425 nm Xe lamp excitation, respectively. To determine the encapsulation efficiency of VP loaded inside the liposomes, Triton X-100 (0.1%) was added to the as-prepared liposome solution, resulting in destabilization of the liposomal structure and VP release. VP fluorescence (Ex/Em: 425 nm/690 nm) was recorded on a Fluorolog-Tau-3 system and its concentration was calculated from the standard curve of free VP solution.

For the thermal stability measurement, differential scanning calorimetry (DSC2010, TA Instruments, Delaware, US) was used to characterize the temperature of the liposome phase transition (T_m). Briefly, about 10 μ L of each sample was placed on an aluminium pan, which was covered with an aluminium lid. The pan was heated over a linear gradient (1 °C min⁻¹, increasing from 25 to 100 °C) in a nitrogen environment, alongside a reference pan containing 10 μ L of HEPES buffer. The peak on each enthalpy graph indicated the T_m of each sample (data were acquired and exported from the Universal Analysis software).

2.5 Gel electrophoresis

To evaluate the pDNA loading ability of liposomes and determine the best N/P ratio, electrophoresis using 1% agarose gel (w/v) in TAE (1 \times) buffer was conducted. The complex solution with various N/P ratios was loaded into the agarose gel. The gel

was pre-stained with SYBR Safe DNA stain before running electrophoresis, which was carried out for 40 min at a constant voltage of 90 V. Electrophoresis images were then visualized using Gel Imaging U: Genius3 (Syngene, UK). The image acquisition was done using the software GeneSys.

2.6 Enzymatic degradation assay

To assess the capability of the LPD for the protection of pDNA from DNase I, an enzymatic digestion assay was conducted. The LPDs with different N/P ratios were suspended in 1 \times DNase I reaction buffer (10 mM Tris-HCl, 2.5 mM MgCl₂ and 0.5 mM CaCl₂, pH 7.6) to a final volume of 50 μ L. Two units of DNase I were then added and mixed thoroughly. The mixture solution was incubated at 37 °C for 10 minutes, followed by gel electrophoresis analysis described above.

2.7 Cellular uptake of liposomes and endolysosomal escape with light triggering

HCT116 cells (5×10^4 per well) were plated on the coverslips in a 24-well plate and incubated overnight at 37 °C in a humidified 5% CO₂ atmosphere. The cells were then incubated with 500 μ L of optiMEM solution containing LPD LPDs (10 μ g mL⁻¹) for different periods. After incubation, the old media were removed and the cells were washed three times with PBS solution (1 \times , pH 7.4). For the assessment of light-triggered endolysosomal escape of fluorescein labelled pDNA molecules, light irradiation (690 nm, 15 mW cm⁻²) using a red LED light source (Fedy, Shenzhen, China,) was carried out for 4 min after 2 h of incubation of cells with the LPD. For endolysosome staining, LysoTracker (50 nM in optiMEM) was added into the cell culture medium in each well and incubated for one hour before the cells were collected to be fixed. The cells were fixed with 2% paraformaldehyde (10 min, 37 °C) and stained with Hoechst 33342 (5 μ g mL⁻¹) (10 min, 37 °C). After staining, each coverslip was washed with PBS solution three times and then mounted onto a glass slide. The glass slide was imaged using a Leica SP2 confocal laser scanning microscopy (CLSM) system. The excitation wavelengths of 405 nm, 488 nm, and 543 nm were used for the confocal imaging of VP, fluorescein labelled pDNA and LysoTracker, respectively. Their fluorescence emission was imaged at 460 \pm 10 nm for Hoechst 33342, 525 \pm 25 nm for fluorescein, 590 \pm 10 nm for LysoTracker and 700 \pm 25 nm for VP.

2.8 Assessment of gene transfection after light illumination

HCT116 cells were seeded on a 24-well plate at a density of 1×10^5 cells per well, followed by overnight incubation. 500 μ L of optiMEM solution containing LPDs (N/P = 25) was added to each well. After 2 h incubation, the cells were exposed to the 690 nm LED light (0.15 mW cm⁻²) for 2 min, 4 min and 6 min, respectively, followed by an additional one hour incubation. The old medium was replaced by the fresh one and the cells were incubated for another 22 h. The EGFP expression in the cells was imaged using a CLSM system. The transfection efficiency of different samples was measured using flow cytometry (CytoFLEX S, Beckman Coulter, Australia). The cells were

washed twice and harvested in DPBS buffer at a concentration of 10^6 cells mL^{-1} , followed by flow cytometry measurements of the percentage of cells expressing EGFP.

2.9 Detection of cellular ROS generation after light illumination

DCF-DA is a non-fluorescent molecule, which can be rapidly oxidized by cellular ROS to the fluorescent DCF. This allows it to be the indicator of a broad range of ROS.⁴⁶ In order to quantify ROS generation upon light irradiation, the HCT116 cells (5×10^4 per well) were cultured in Petri dishes overnight. After removing the culture medium, the cells were incubated with 500 μL of the optiMEM solution containing LPDs ($10 \mu\text{g mL}^{-1}$). After 2 h incubation at 37°C , the medium was removed and the cells were washed with 500 μL of $1\times$ HBSS solution five times. 200 μL of $1\times$ HBSS containing DCF-DA ($25 \mu\text{M}$) was subsequently added to the cells, followed by incubation for 30 min at 37°C , while protected from light. After incubation, the cells were illuminated by 690 nm LED light for different time periods (2 min, 4 min and 6 min). After light irradiation, the DCF-DA solution was removed and the cells were washed with PBS three times, followed by imaging under a Leica SP2 CLSM system. For comparison, the control cells were incubated with 100 μL of the optiMEM solution containing H_2O_2 at different concentrations (1 μM , 10 μM and 100 μM) for 2 h followed by addition of DCF-DA and CLSM imaging. For the determination of ROS, the cells were cultivated in 96-well plates, instead of Petri dishes, followed by the same procedure as described above. After treatment, the mean DCF fluorescence intensity in each group was determined by flow cytometry.

2.10 Cell viability assays

HCT116 cells were seeded into 96-well plates (1×10^4 per well) and cultured for 24 h at 37°C . The old medium was then removed and the optiMEM solution containing liposomes (10 μg per well, encapsulating VP), lipopolyplex (10 μg per well) and pure PEI (10 μg per well) was added to each well. After 2 h of incubation, the cells were washed with PBS three times to remove unbound samples. Fresh medium was then added to the cells, followed by another 24 h incubation. For the light irradiation alone, the cells were exposed to a 690 nm light source (15 mW cm^{-2}) for 1 min, 2 min, 4 min and 6 min, respectively. After light treatment, fresh medium was added to the cells and incubated for another 24 h. The toxicity of the liposomes, LPDs, pure PEI solution and 690 nm light in cells was assessed using the MTS kit (Promega, WI, USA) as per the manufacturer's instructions. Cell viability was calculated as a percentage of the absorbance in treated cells compared with the untreated control cells.

2.11 Statistical analysis

All quantitative data are shown as mean \pm SD from at least three parallel groups. *P* values were determined by Student's *t*-tests or two-way ANOVA (analysis of variance) using Prism 5 (GraphPad). **p* < 0.05, ***p* < 0.01, ****p* < 0.001 and *****p* < 0.0001 were thought to be statistically significant.

3. Results and discussion

3.1 Characterization of pDNA and liposome samples

The morphology and optical properties of the pure pDNA molecules, polyplexes and LPD samples were determined by using spectrophotometry and TEM. A plasmid map was plotted using Vector NT and its absorption spectrum is shown (Fig. S1a, ESI†). The absorbance ratios between 260 nm and 280 nm (Abs260/Abs280) and between 260 nm and 230 nm (Abs260/Abs230) were calculated to be about 1.8 and 2.0, suggesting high purity of the DNA molecules.⁴⁷ The TEM images in Fig. 1 show the structures of liposomes loaded with VP (Fig. 1a), pDNA (Fig. 1b), polyplexes (Fig. 1c) and LPDs (Fig. 1d). The PEI/pDNA polyplexes (indicated by red arrows) were observed inside the liposomes as well as on the surface of the liposomes (Fig. 1d). In addition, the VP absorption peak at 690 nm was slightly blue-shifted to a shorter wavelength at 685 nm when loaded inside the liposomes compared to VP alone (Fig. 1e), which was consistent with the reported study that found that liposome encapsulation causes a blue shift of the loading cargoes.⁴⁸ However, the fluorescence spectrum of liposome-formulated VP was not obviously changed compared to the pure VP solution (Fig. 1f). These results indicated that VP was encapsulated in the liposomes. The amount of VP loaded inside liposomes was calculated to be approximately $112 \mu\text{g mL}^{-1}$.

3.2 Stability studies of liposome formulations

Size distribution and zeta potential of liposome formulations with varying Chol content were determined by the DLS method, as shown in Table S1 and Fig. S1b (ESI†). The mean size of liposomes increased with increasing Chol content, up to 150 nm for Chol levels exceeding 50%. These results are consistent with the literature.⁴⁹ All the PDI values of the nanoparticle suspension are around 0.40, varying slightly between groups with different Chol contents. These values indicate a relatively narrow size distribution of the as-prepared LPD.⁵⁰ The zeta potential reduced gradually with the increasing Chol%, because of an increase in the negatively charged hydroxyl group (–OH) on cholesterol.

Chol is a very important component in the liposomal structure that helps to control the rigidity of the lipid bilayer.⁵¹ In order to determine the optimized Chol% for the stabilized liposomes, DLS measurements over six days and DSC assay have been conducted. As shown in Fig. S2a and b in the ESI†, the size and corresponding PDI of liposomes with 33% Chol were largely unchanged over the 6 day incubation time, compared with other Chol contents; similar results were reported earlier.⁵² However, because cholesterol has a very small hydrophilic head and is, therefore, less efficient in shielding the hydrophobic interaction, the excess addition of Chol will lead to undesired destabilization of lipid bilayers.⁵³ Hence, 33% Chol was chosen to formulate liposomes for the following experiments.

In addition, the DSC heatflow diagram (Fig. S2c, ESI†) exhibits the phase transition temperature (T_m) of each liposome with various Chol%. In the absence of Chol, liposomes did not show any phase change peaks. However, when the Chol fraction reached 50%, the phase transition could be observed.

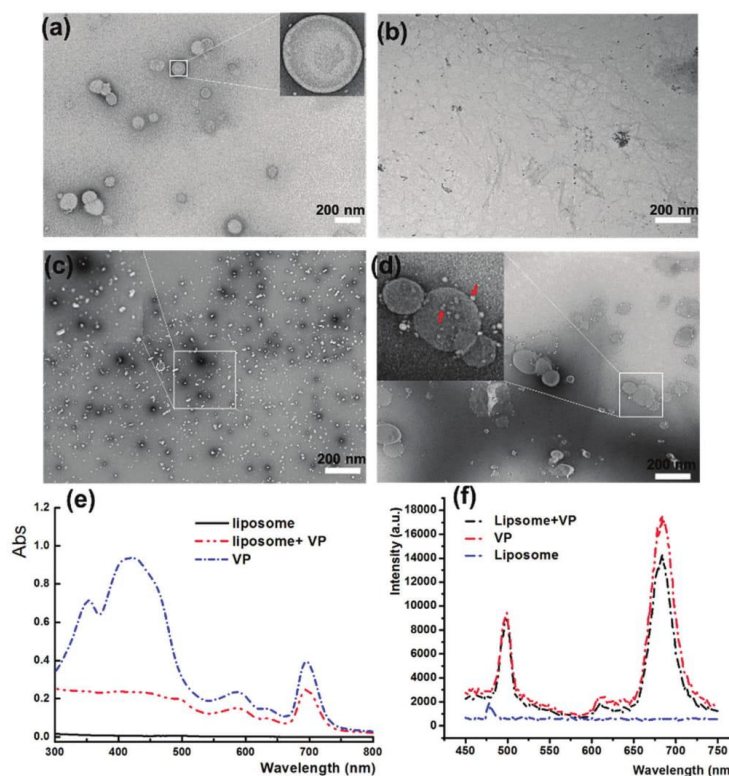


Fig. 1 Characterization of different liposome samples. Representative TEM images of (a) liposome loaded with VP, (b) pure pDNA, (c) polyplexes and (d) LPDs. The red arrows indicate the polyplexes. (e) Absorbance and (f) fluorescence spectra of pure liposomes, liposomes loaded with VP and pure VP.

This is because the higher content of cholesterol allows the formation of an anhydrous cholesterol domain in the bilayer structure,²⁶ which facilitates the phase transition from the solid-gel to a liquid crystal phase. Compared to the liposomes having 50% Chol where the T_m was 55 °C, the liposomes with a higher proportion of cholesterol (66.7%) exhibited a higher T_m of 72 °C. The increase in T_m confirms that the addition of cholesterol to the liposome formulation contributes to enhanced stabilization of the as-prepared liposomes.

To further investigate the stability of PEGylated liposomes in the physiological environment, DLS measurements were conducted to monitor the size changes of PEGylated and non-PEGylated liposomes in the serum-reduced medium (optiMEM) and serum-containing solution (10% FBS cell culture medium). As shown in Fig. S3 (ESI[†]), the size of the conventional liposomes increased by a factor of two after 6 h incubation in both the optiMEM medium and normal cell culture medium. However, the PEGylated liposomes showed a smaller size change compared to the non-PEGylated ones under the same experimental conditions. In addition, the change of encapsulation efficiency

(Fig. S3c, ESI[†]) of VP with different dialysis times also indicated that the PEGylated liposomes can undergo less leakage of the loaded VP molecules compared to the non-PEGylated groups. These findings indicate that PEGylation enhances the stability of liposomes during 6 h incubation compared to the liposomes without PEGylation. The optimal formulation of liposomes with higher stability is the molar ratio of 1:1:1:1 for DOTAP, DSPE-PEG, DOPE and Chol. In addition, VP release profiles of liposomes with and without PEGylation also indicated that PEGylated liposomes have higher stability compared to the non-PEGylated ones (Fig. 3c).

3.3 DNA loading capability of LPDs measured by gel electrophoresis

In the presence of polycations or cationic liposomes, the DNA molecules can self-assemble into polyplexes and/or lipopolyplexes due to electrostatic attraction. An ideal polycation-based gene carrier should have the capability to load a high amount of negatively charged DNA and facilitate cellular uptake. To determine the DNA loading capability of LPD with different N/P ratios

used in this study, agarose gel retardation assays were conducted. The naked DNA molecules without any loading vehicles were clearly observed from the gel, however, less DNA was detected with an increased N/P ratio (Fig. 2a). When the value of N/P ratio reached 25:1, free DNA could not be detected in the agarose gel lanes, indicating that the maximum amount of DNA molecules can be loaded into the PEI/pDNA polyplexes when the N/P ratio reached 25:1.

It is worth mentioning that the LPDs have a higher capacity of condensing negatively charged DNA, compared with the PEI/pDNA polyplex, which was confirmed by the fact that less DNA migrated from the gel wells than the polyplex at the same N/P ratio (Fig. 2a). The condensation of DNA molecules also contributes to the prevention of enzymatic degradation. To demonstrate the reduced enzymatic degradation of DNA in polyplexes and LPDs, DNase I, a strong endonuclease that non-specifically cleaves DNA, was respectively added into pDNA, polyplex and LPDs for the enzymolysis assay. As shown in Fig. 2b, DNA loaded inside the LPDs at all N/P ratios was clearly visualised in the gel wells even after the DNase I reaction, while DNA can only be observed in the polyplex at a high N/P ratio. For the polyplex at a low N/P ratio less than 20 and pure pDNA, there was no clear indication of DNA after enzymatic degradation. These results indicated that the encapsulation of polyplexes into the liposomal cavity can significantly reduce the enzymolysis effect on cleaving DNA molecules. Therefore, by using this LPD structure, exogenous genetic materials can be protected against undesired enzymatic degradation and delivered to the cells of interest. Additionally, the zeta potential of polyplexes and LPDs with varying N/P ratios was also measured. As shown in Fig. 2c, the zeta potential of different complexes increases with the increasing N/P ratio, with higher positive values for LPDs than the polyplex group. This increased positive charge of LPDs will facilitate their cellular uptake through an endocytosis pathway

due to the preferential interaction between the positively charged delivery platform and the negatively charged cell membranes.

3.4 Cellular uptake of LPDs, light-triggered ROS generation, and pDNA release

Fig. S4 (ESI[†]) shows representative CLSM images of the internalized LPDs in HCT116 cells after different periods of incubation (1, 2 and 3 h). After 3 h incubation, perinuclear rings with a red fluorescence signal from VP were clearly observed, compared with the cells after 1 h and 2 h incubation. Therefore, we chose the 3 h incubation time in this study.

Light-induced cellular ROS generation from LPDs was evaluated by using the DCF-DA assay. In principle, the cell-penetrable nonfluorescent DCF-DA molecules can be oxidized by ROS molecules, resulting in the production of fluorescent DCF. The fluorescence intensity of DCF increased with light illumination, indicating that a higher amount of ROS was generated from VP loaded inside LPDs than that in non-irradiated cells (Fig. S5, ESI[†]). By comparing with the H₂O₂-treated groups, which were considered as positive controls,⁵⁴ the DCF intensity in the cells treated with LPDs and 6 min illumination was almost equivalent to that produced by 100 μ M H₂O₂.

Additionally, cellular pDNA release from LPDs was assessed by irradiating cells with LED light (690 nm, 15 mW cm⁻²) for 2 and 4 min, respectively. As shown in Fig. 3, the increased green signal from the released pDNA (labelled with fluorescein) was clearly observed with light illumination, with the maximum intensity being achieved at 4 min illumination, compared with the absence of illumination. These data indicate that the release of pDNA molecules from the endolysosomal compartments can be enhanced by light irradiation. The reason could be attributed to the photochemical damage of endolysosomal membranes caused by increased ROS production due to light exposure.

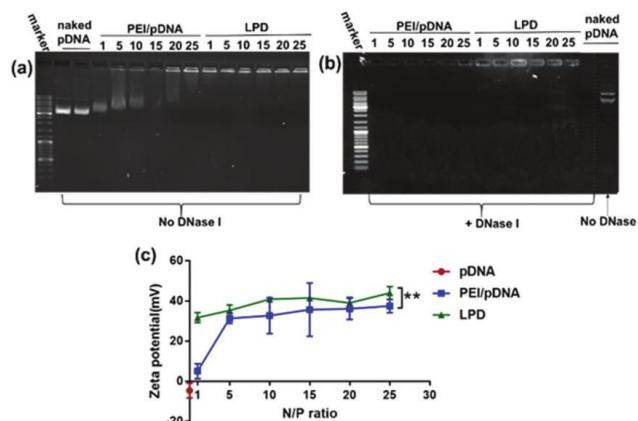


Fig. 2 Gel retardation assays of polyplexes and LPDs with different N/P ratios (a) without and (b) with DNase I digestion. (c) Zeta potentials of pDNA, PEI/pDNA and LPD with various N/P ratios. $**p < 0.01$.

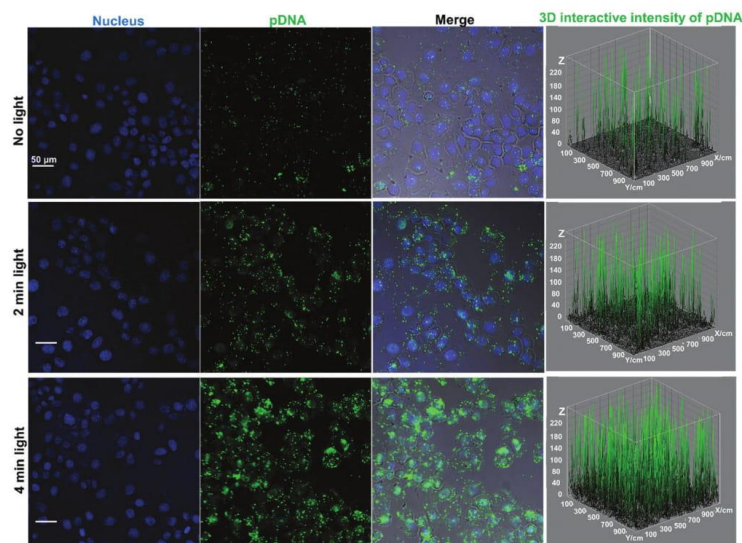


Fig. 3 CLSM images and 3D interactive intensity plots of fluorescein-labelled pDNA release after photoirradiation for different periods: 0, 2, and 4 min. The merge panels represent the images merged by the blue, green and bright field channels. Scale bars = 50 μm .

3.5 Quantitative analysis of endolysosomal escape of pDNA after light illumination

To further characterise the enhanced cellular release of pDNA from light-triggered LPDs, intracellular trafficking and

endolysosomal escape were recorded by using CLSM and analysed by the object-based colocalization of fluorescence intensity (Fig. 4), which was done by using the line profile in ImageJ software. After 2 h incubation, most fluorescein labelled

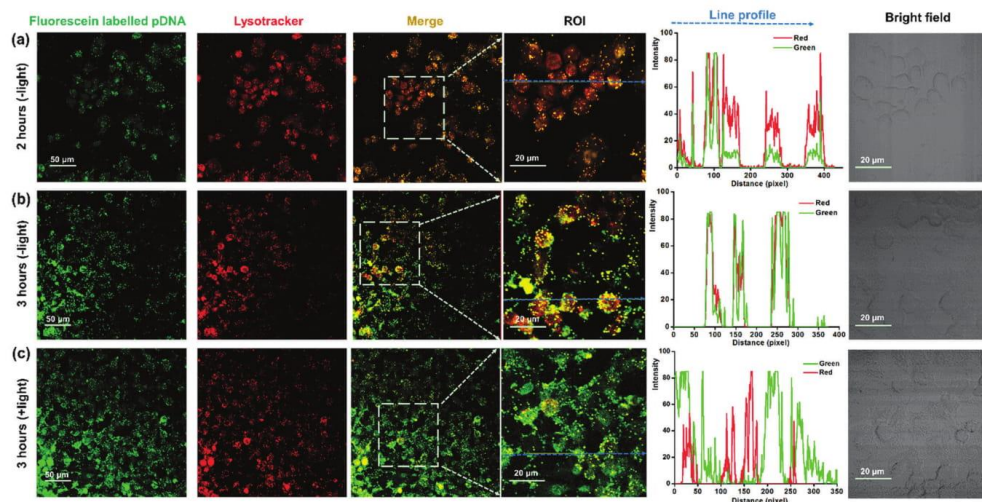


Fig. 4 CLSM images of colocalization between the endolysosomes (LysoTracker, red channel) and fluorescein-labelled pDNA (green channel) (a) after 2 h incubation, (b) after 3 h incubation and (c) after 3 h incubation and 4 min light illumination. The line profile plots indicate the intensity distribution of green and red channels through the blue lines in the magnified view of ROI in the merged panel. The right panel presents the bright field pictures of ROI.

pDNA was observed to be internalized in cells, which was confirmed by the pixel intensity profile (the line profile panel in Fig. 4). These data also show that most of the green signal from fluorescein (pDNA) overlaps with the red signal from LysoTracker (endolysosomes) although its intensity is lower than the LysoTracker signal (Fig. 4a). After 3 h incubation, a stronger overlap between the green and red signal was observed, indicating that the entrapment of LPDs inside the endolysosomes was enhanced after 3 h incubation, compared to 2 h incubation (Fig. 4b). However, after a subsequent 4 min light irradiation and another 1 h incubation, most pDNA molecules escaped the endolysosomal compartments. This was confirmed by the reduced overlap between the green and red channels, as shown in Fig. 4c.

To confirm the light-induced escape of pDNA, the colocalization of regions of interest (ROIs) shown in Fig. 4 was further quantified using the Costes' approach, Mander's coefficient and the Pearson's coefficient (PC) analysed by using ImageJ. Fig. 5a–c show the Costes' maps of the ROIs in Fig. 4a–c. Based on the Costes' approach, the colocalization between pDNA and

endolysosomes was represented by a white overlay of the red signal from LysoTracker and the green signal from fluorescein. A large white area was respectively observed after 2 h and 3 h incubation, suggesting that most LPD nanoparticles were internalized into the endolysosomes (Fig. 5a and b). However, in the presence of light illumination, green areas appeared and white areas were significantly reduced, indicating that most LPD nanoparticles were released from the endolysosomal compartments into the cytoplasm (Fig. 5c).

Based on the Costes' colocalization analysis, the PC value was also evaluated. The PC ranges from -1 to 1 , with -1 indicating a negative correlation, 1 indicating a positive correlation and 0 standing for no correlation. The PC value was 0.859 and 0.801 after 2 h and 3 h incubation without light illumination, respectively, which indicated that most pDNA molecules were colocalized with endolysosomes (Fig. 5d and e). However, the value of PC decreased to 0.633 after light illumination (Fig. 5f), consistent with the pDNA release from the endolysosome compartments.

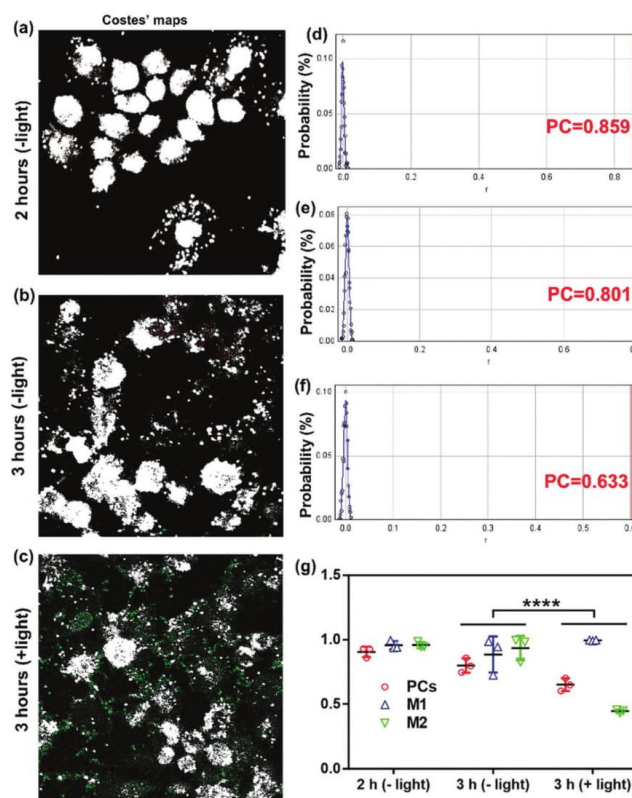


Fig. 5 (a), (b) and (c) are the Costes' maps of Fig. 4(a)–(c), respectively, showing colocalization between pDNA and endolysosomes. (d), (e) and (f) are plots of the distributions of the Pearson's coefficients (PCs) of (a), (b) and (c) respectively. (g) Manders' coefficient analysis and PCs. **** $p < 0.0001$.

Furthermore, the Mander's coefficient, varying from 0 to 1, was calculated to determine the overlap fraction of the two channels. Here, M1 is defined as the proportion of the green signal coincident with the red signal over its total intensity and M2 is the fraction of green signal coincident with the red one.⁵⁵ As shown in Fig. 5g, M2 (indicated by green triangles) was only 44.5% after light illumination, compared with the control cells without light illumination ($M2 = 99.6\%$), suggesting that more DNA molecules escaped from the endolysosomes after light treatment.

3.6 Gene transfection under light irradiation

The CLSM images and quantitative analysis of EGFP expression in HCT116 cells after light-triggered pDNA release are shown in Fig. 6. When the cells were treated with LPD ($N/P = 25$) alone, a slightly higher EGFP fluorescence intensity was observed, compared with the PEI/DNA ($N/P = 25$) treated cell group (Fig. 6b, c, and h). However, with light illumination, LPD produced enhanced transfection efficiency. The maximum EGFP expression level was achieved after 4 min illumination ($49.3 \pm 1.4\%$), to a value of over twice that in the LPD transfected cells without

light irradiation ($20.1 \pm 1.3\%$, Fig. 6h). It should be mentioned that compared with 2 min illumination, EGFP fluorescence after 4 min illumination shows only a slightly increased signal in the CLSM images (Fig. 6e and f), but its intensity changed in a statistically significant fashion (Fig. 6h, $*p < 0.5$). These results are consistent with the pDNA release profile under light irradiation shown in Fig. 3. For comparison purposes, the cells were also transfected with PEI/pDNA polyplexes ($N/P = 10$ and pure pDNA but without light illumination). A lower EGFP fluorescence intensity was observed in these groups, compared with cells transfected by LPDs (Fig. 6a, c, and g), indicating the limited transfection efficiency of the PEI/DNA complexes ($N/P = 10$) and pure DNA molecules. Additionally, we evaluated the EGFP fluorescence intensity in HCT116 cells transfected with pure DNA, PEI/DNA complexes and LPDs with and without light illumination by flow cytometry. The representative intensity histograms are shown in Fig. S6 (ESI[†]). The fluorescence intensity of the LPD-transfected groups increased with prolonged photoirradiation, which confirmed the enhanced transgene efficiency of LPD by photoirradiation.

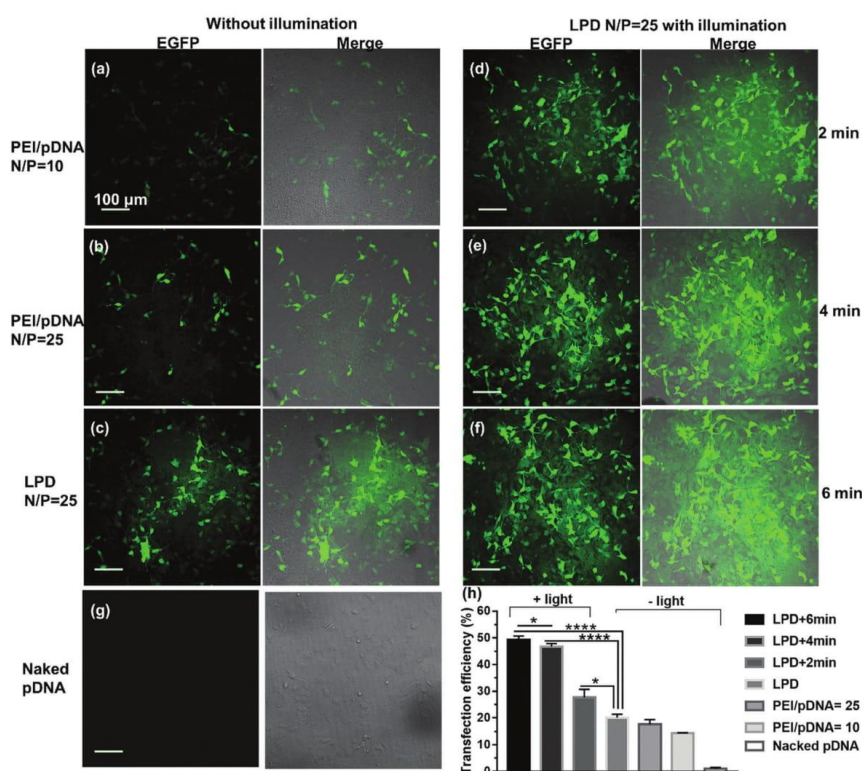


Fig. 6 CLSM images (a–h) of EGFP expression in HCT116 cells after 48 h transfection with and without light illumination. Scale bars = 100 μm . (h) Transfection efficiencies of different groups. $*p < 0.05$ and $****p < 0.0001$, compared to the LPD group without light.

The maximum transfection efficiency achieved in this study is comparable with previously published work where the combination of branched PEI (BPEI)/pDNA with reduced graphene oxide (rGO) was used to release pDNA under light illumination.⁵⁶ In this earlier work, the transfection efficiency of PEG-BPEI-rGO/pDNA (N/P = 20) nanocomplexes in PC-3 and NIH/3T3 cells (with 20 min irradiation at a wavelength of 808 nm and at a light irradiance of 6 W cm⁻²) was 2–3 times higher compared to the nanocomplexes alone. However, the involvement of graphene-based materials in this earlier study requires a detailed evaluation of the toxicity of these materials prior to clinical translation. In contrast, the liposome delivery system used in our work has a high potential for clinical translation due to the long and successful history of using liposomes for encapsulating agents such as Doxorubicin for clinical use.

3.7 Cellular cytotoxicity assays of different nanocomplexes and light illumination

A series of cell viability tests after the nanocomplex and light treatments was performed to estimate the potential toxicity effect on cells. As shown in Fig. 7, for the light treatment alone, the cell viability did not change significantly compared to the controls. Among the delivery systems considered in this work, with the same concentration at 10 µg per well, PEI shows a higher toxicity to cells, with about 32% cells being affected when treated with PEI and illuminated for 4 min. By contrast, the liposomes and LPDs did not affect cell viability, even under photoirradiation for different time periods. For example, about 17% cells were killed by LPDs after 6 min illumination. This could be a result of the light-triggered ROS generation from VP. However, more than 80% cells were still alive in the liposome and LPD groups, indicating that these delivery platforms are relatively biocompatible.

In this study, PEI polypeptides still exhibited their intrinsic cytotoxicity (around 70% cell viability under our experimental conditions). However, the cytotoxicity was significantly reduced by incorporating PEI/pDNA complexes into liposomes. The results

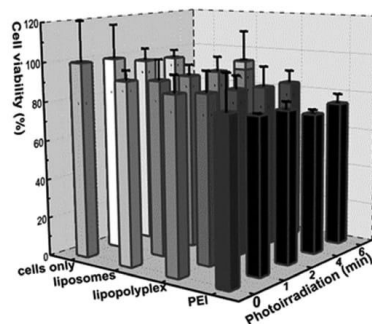


Fig. 7 Cytotoxicity of liposomes (10 µg per well), lipopolyplex (10 µg per well) and PEI (10 µg per well) on HCT116 cells in combination with photoirradiation.

of cell viability after treatment with our lipopolyplex and light illumination were even comparable with other liposome-PEI hybrid vectors alone (more than 80% cell viability).⁵⁷

4. Conclusions

In summary, a photoresponsive LPD system was developed for pDNA delivery and release *in vitro*. The complexation of DNA and PEI and the formation of the LPD nanoconstruct enhanced the loading capacity of pDNA into the liposomal vehicles. Subsequent encapsulation of polyplexes inside the liposomes overcame the disadvantage of the high cytotoxicity of PEI and the photosensitizer molecules. The addition of cholesterol and PEGylated lipids in the liposome formulation improved the stability and biocompatibility of the nanocomplexes in the physiological environment, which is very important for the use of light-triggered liposomes in *in vivo* applications, in particular, on-demand gene release. The VP molecules introduced into the liposome cavity generated ROS after light illumination, enabling endolysosomal escape of pDNA via a photochemical internalization mechanism. This dynamic process has been demonstrated by quantitatively analysing image-based colocalization between the nanocomplexes and endolysosomes. After light triggering, pDNA was released and modified the expression of encoded EGFP in HCT116 cells. The enhancement of the EGFP fluorescence intensity by a factor of two was achieved with the light-triggered LPD delivery system, compared with the control group without light illumination.

In this work, a 690 nm LED (15 mW cm⁻²) was used as a light source, whose maximum dosage (6 min irradiation) was calculated to be 5.4 J cm⁻². This is much lower than clinic and *in vivo* doses (25–500 J cm⁻²) of the light source used for activating VP in photodynamic therapy.^{58,59} In addition, the wavelength of 690 nm located within the “therapeutic window” can penetrate tissues deeper (5–10 mm) with less photodamage to biological tissues compared with visible light.⁶⁰ Given these excellent properties of this light source, we believe that this system could be feasible for *in vivo* work. In addition to pDNA used in this study, our light responsive LPD system can efficiently deliver other nucleic acids including siRNA, microRNA and larger plasmids with specific functions. These genetic materials can be delivered in a temporally controllable way by combining this delivery vehicle with light, thus providing the potential for enhanced transfection efficiency and therapeutic effect in gene therapy *in vivo*. Further clinical translation is also achievable with our liposomal nanocarrier since the key agents including lipids and VP are widely used in clinical practice.

Abbreviations

asODN	Antisense oligodeoxynucleotides
BPD-MA	Benzoporphyrin derivative monoacid
BPEI	Branched polyethylenimine
CLSM	Confocal laser scanning microscopy
DDS	Drug/gene delivery systems
DOPE	1,2-Dioleoyl- <i>sn</i> -glycero-3-phosphoethanolamine

Paper

Journal of Materials Chemistry B

DOTAP	<i>N</i> -[1-(2,3-Dioleoyloxy)propyl]- <i>N,N,N</i> -trimethylammonium methyl-sulfate
EGFP	Enhanced green fluorescent protein
FDA	Food and drug administration
LED	Light-emitting diode
LPEI	Linear polyethylenimine
NIR	Near-infrared
PCI	Photochemical internalization
pDNA	Plasmid DNA
PDT	Photodynamic therapy
PEG	Poly-(ethylene glycol)
PEI	Polyethylenimine
PLGA	Poly(<i>D,L</i> -lactide-co-glycolide)
PLL	Poly-L-lysine
ROS	Reactive oxygen species
siRNA	Small interference RNA
TEM	Transmission electronic microscopy
VP	Verteporfin
DLS	Dynamic light scattering
DCF	2',7'-Dichlorofluorescein
DCF-DA	2',7'-Dichlorofluorescein diacetate
PBS	Phosphate-buffered saline
HEPES	4-(2-Hydroxyethyl)-1-piperazineethanesulfonic acid
TAE	Tris-acetate-EDTA
HBSS	Hank's balanced salt solution
DMEM	Dulbecco's modified Eagle's medium
FBS	Fetal bovine serum
DPBS	Dulbecco's Phosphate-buffered saline
DSC	Differential scanning calorimetry
EPR	Enhanced permeability and retention
DMSO	Dimethyl sulfoxide
PTA	Phosphotungstic acid.

Conflicts of interest

There are no conflicts to declare.

Acknowledgements

This work was supported by the Australian Research Council (DECRA: DE130100894 and ARC CoE: CE140100003), the HDR Budget from Macquarie University, the Major National Scientific Research Program of China (2014CB932200) and the National Key Research and Development Program of China (2017YFD0500900). The authors thank Mr Kai Peng for his assistance of flow cytometry and also thank the Macquarie Microscopy Unit for TEM work.

References

- 1 R. C. Mulligan, *Science*, 1993, **260**, 926.
- 2 R. Srinivas, S. Samanta and A. Chaudhuri, *Chem. Soc. Rev.*, 2009, **38**, 3326–3338.
- 3 M. S. Shim and Y. J. Kwon, *Adv. Drug Delivery Rev.*, 2012, **64**, 1046–1059.
- 4 D.-J. Lee, D. He, E. Kessel, K. Padari, S. Kempter, U. Lächelt, J. O. Rädler, M. Pooga and E. Wagner, *J. Controlled Release*, 2016, **244**, 280–291.
- 5 D. Luo and W. M. Saltzman, *Nat. Biotechnol.*, 2000, **18**, 33.
- 6 H.-X. Wang, M. Li, C. M. Lee, S. Chakraborty, H.-W. Kim, G. Bao and K. W. Leong, *Chem. Rev.*, 2017, **117**, 9874–9906.
- 7 S.-d. Li and L.-y. Huang, *Gene Ther.*, 2000, **7**, 31.
- 8 H. Yin, R. L. Kanasty, A. A. Eltoukhy, A. J. Vegas, J. R. Dorkin and D. G. Anderson, *Nat. Rev. Genet.*, 2014, **15**, 541.
- 9 J. A. Kretzmann, D. Ho, C. W. Evans, J. H. Planí-Lam, B. Garcia-Bloj, A. E. Mohamed, M. L. O'Mara, E. Ford, D. E. Tan and R. Lister, *Chem. Sci.*, 2017, **8**, 2923–2930.
- 10 Z. Zhou, X. Liu, D. Zhu, Y. Wang, Z. Zhang, X. Zhou, N. Qiu, X. Chen and Y. Shen, *Adv. Drug Delivery Rev.*, 2017, **115**, 115–154.
- 11 L. S. Mendonça, F. Firmino, J. N. Moreira, M. C. Pedroso de Lima and S. Simões, *Bioconjugate Chem.*, 2009, **21**, 157–168.
- 12 J. Yang, A. Bahreman, G. Daudey, J. Bussmann, R. C. Olsthoorn and A. Kros, *ACS Cent. Sci.*, 2016, **2**, 621–630.
- 13 A. Ewe, A. Schaper, S. Barnert, R. Schubert, A. Temme, U. Bakowsky and A. Aigner, *Acta Biomater.*, 2014, **10**, 2663–2673.
- 14 R. N. Majzoub, K. K. Ewert, E. L. Jacovetty, B. Carragher, C. S. Potter, Y. Li and C. R. Safinya, *Langmuir*, 2015, **31**, 7073–7083.
- 15 V. Fehring, U. Schaeper, K. Ahrens, A. Santel, O. Keil, M. Eisermann, K. Giese and J. Kaufmann, *Mol. Ther.*, 2014, **22**, 811–820.
- 16 B. Ma, S. Zhang, H. Jiang, B. Zhao and H. Lv, *J. Controlled Release*, 2007, **123**, 184–194.
- 17 H. Deng, K. Song, X. Zhao, Y. Li, F. Wang, J. Zhang, A. Dong and Z. Qin, *ACS Appl. Mater. Interfaces*, 2017, **9**, 9315–9326.
- 18 L. Yin, H. Tang, K. H. Kim, N. Zheng, Z. Song, N. P. Gabrielson, H. Lu and J. Cheng, *Angew. Chem., Int. Ed.*, 2013, **52**, 9182–9186.
- 19 J. Liu, C. Detrembleur, S. Mornet, C. Jérôme and E. Duguet, *J. Mater. Chem. B*, 2015, **3**, 6117–6147.
- 20 L. Jiang, L. Li, X. He, Q. Yi, B. He, J. Cao, W. Pan and Z. Gu, *Biomaterials*, 2015, **52**, 126–139.
- 21 K. Kono, M. Takashima, E. Yuba, A. Harada, Y. Hiramatsu, H. Kitagawa, T. Otani, K. Maruyama and S. Aoshima, *J. Controlled Release*, 2015, **216**, 69–77.
- 22 X. Liu, J. Xiang, D. Zhu, L. Jiang, Z. Zhou, J. Tang, X. Liu, Y. Huang and Y. Shen, *Adv. Mater.*, 2016, **28**, 1743–1752.
- 23 K. A. Carter, S. Shao, M. I. Hoopes, D. Luo, B. Ahsan, V. M. Grigoryants, W. Song, H. Huang, G. Zhang and R. K. Pandey, *Nat. Commun.*, 2014, **5**, 3546.
- 24 R. Di Corato, G. Béalle, J. Kolosnjaj-Tabi, A. Espinosa, O. Clement, A. K. Silva, C. Menager and C. Wilhelm, *ACS Nano*, 2015, **9**, 2904–2916.
- 25 Y. Li, H. An, X. Wang, P. Wang, F. Qu, Y. Jiao, K. Zhang and Q. Liu, *Nano Res.*, 2018, **11**, 1038–1056.
- 26 S.-y. Yang, Y. Zheng, J.-y. Chen, Q.-y. Zhang, D. Zhao, D.-e. Han and X.-j. Chen, *Colloids Surf., B*, 2013, **101**, 6–13.
- 27 M. L. Immordino, F. Dosio and L. Cattel, *Int. J. Nanomed.*, 2006, **1**, 297.
- 28 E. Oh, J. B. Delehanty, K. E. Sapsford, K. Susumu, R. Goswami, J. B. Blanco-Canosa, P. E. Dawson, J. Granek, M. Shoff and Q. Zhang, *ACS Nano*, 2011, **5**, 6434–6448.

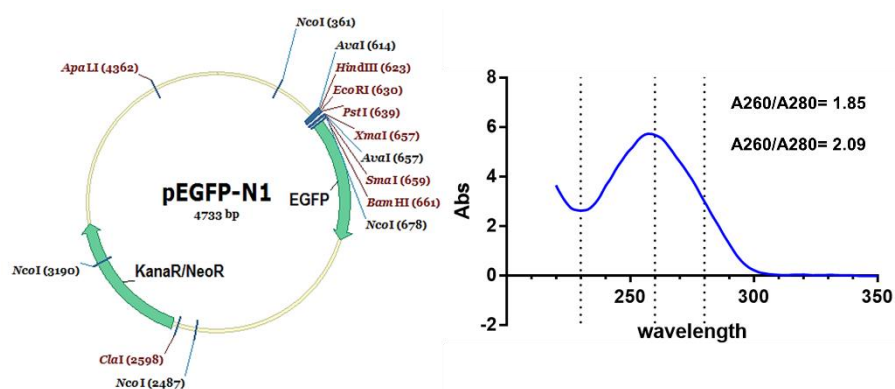
- 29 K. Maruyama, T. Yuda, A. Okamoto, S. Kojima, A. Suganaka and M. Iwatsuru, *Biochim. Biophys. Acta, Lipids Lipid Metab.*, 1992, **1128**, 44–49.
- 30 J. Kim, H. Kim and W. J. Kim, *Small*, 2016, **12**, 1184–1192.
- 31 M. A. Sheikh, Y. S. Malik, Z. Xing, Z. Guo, H. Tian, X. Zhu and X. Chen, *Acta Biomater.*, 2017, **54**, 58–68.
- 32 N. W. Kim, M. S. Lee, K. R. Kim, J. E. Lee, K. Lee, J. S. Park, Y. Matsumoto, D.-G. Jo, H. Lee and D. S. Lee, *J. Controlled Release*, 2014, **179**, 11–17.
- 33 Y. He, Y. Nie, G. Cheng, L. Xie, Y. Shen and Z. Gu, *Adv. Mater.*, 2014, **26**, 1534–1540.
- 34 S. P. Strand, S. Lelu, N. K. Reitan, C. de Lange Davies, P. Artursson and K. M. Vårum, *Biomaterials*, 2010, **31**, 975–987.
- 35 D. V. Schaffer, N. A. Fidelman, N. Dan and D. A. Lauffenburger, *Biotechnol. Bioeng.*, 2000, **67**, 598–606.
- 36 Z. Zhan, X. Zhang, J. Huang, Y. Huang, Z. Huang, X. Pan, G. Quan, H. Liu and L. Wang, *Materials*, 2017, **10**, 731.
- 37 V. Kafil and Y. Omid, *BioImpacts*, 2011, **1**, 23.
- 38 M. D. Giron-Gonzalez, R. Salto-Gonzalez, F. J. Lopez-Jaramillo, A. Salinas-Castillo, A. B. Jodar-Reyes, M. Ortega-Muñoz, F. Hernandez-Mateo and F. Santoyo-Gonzalez, *Bioconjugate Chem.*, 2016, **27**, 549–561.
- 39 W. Godbey, K. K. Wu and A. G. Mikos, *J. Biomed. Mater. Res.*, 1999, **45**, 268–275.
- 40 M. Rezaee, R. K. Oskuee, H. Nassirli and B. Malaek-Nikouei, *J. Controlled Release*, 2016, **236**, 1–14.
- 41 W. Chen, W. Deng and E. M. Goldys, *Mol. Ther. – Nucleic Acids*, 2017, **7**, 366–377.
- 42 A. Høgset, B. Ø. Engesæter, L. Prasmickaite, K. Berg, Ø. Fodstad and G. M. Mælandsmo, *Cancer Gene Ther.*, 2002, **9**, 365–371.
- 43 Z. Li, P. Agharkar and B. Chen, *Cancer Lett.*, 2013, **339**, 128–134.
- 44 A. Elhissi, M. O'Neill, S. Roberts and K. Taylor, *Int. J. Pharm.*, 2006, **320**, 124–130.
- 45 A. Ewe and A. Aigner, *Non-Viral Gene Delivery Vectors: Methods and Protocols*, 2016, pp. 187–200.
- 46 M. Diehn, R. W. Cho, N. A. Lobo, T. Kalisky, M. J. Dorie, A. N. Kulp, D. Qian, J. S. Lam, L. E. Ailles and M. Wong, *Nature*, 2009, **458**, 780.
- 47 K. Purdy, T. Embley, S. Takii and D. Nedwell, *Appl. Environ. Microbiol.*, 1996, **62**, 3905–3907.
- 48 A. Kunwar, A. Barik, R. Pandey and K. I. Priyadarsini, *Biochim. Biophys. Acta, Gen. Subj.*, 2006, **1760**, 1513–1520.
- 49 L. P. T. H. J. Liang, T. W. Chung and Y. Y. H. D. Z. Liu, *Jpn. J. Med. Electron. Biol.*, 2007, **27**, 29–34.
- 50 M. Instruments, MAN0317, 2004, 1.
- 51 D. Needham and R. S. Nunn, *Biophys. J.*, 1990, **58**, 997–1009.
- 52 D.-Z. Liu, W.-Y. Chen, L.-M. Tasi and S.-P. Yang, *Colloids Surf., A*, 2000, **172**, 57–67.
- 53 F. de Meyer and B. Smit, *Proc. Natl. Acad. Sci. U. S. A.*, 2009, **106**, 3654–3658.
- 54 W. Liu, Y. Wu, C. Wang, H. C. Li, T. Wang, C. Y. Liao, L. Cui, Q. F. Zhou, B. Yan and G. B. Jiang, *Nanotoxicology*, 2010, **4**, 319–330.
- 55 S. Bolte and F. Cordelieres, *J. Microsc.*, 2006, **224**, 213–232.
- 56 H. Kim and W. J. Kim, *Small*, 2014, **10**, 117–126.
- 57 M. Matsumoto, R. Kishikawa, T. Kurosaki, H. Nakagawa, N. Ichikawa, T. Hamamoto, H. To, T. Kitahara and H. Sasaki, *Int. J. Pharm.*, 2008, **363**, 58–65.
- 58 U. Schmidt-Erfurth and T. Hasan, *Surv. Ophthalmol.*, 2000, **45**, 195–214.
- 59 M. Azab, D. S. Boyer, N. M. Bressler, S. B. Bressler, I. Cihelkova, Y. Hao, I. Immonen, J. I. Lim, U. Menchini and J. Naor, *Arch. Ophthalmol.*, 2005, **123**, 448.
- 60 P. Agostinis, K. Berg, K. A. Cengel, T. H. Foster, A. W. Girotti, S. O. Gollnick, S. M. Hahn, M. R. Hamblin, A. Juzeniene and D. Kessel, *Photodynamic therapy of cancer: an update*, World Health Organization, 2011.

Supplementary material

Table S1 Average size, PDI and zeta potential of liposome formulations with different Chol% content.

Liposome formulations (DOTAP/DSPE-PEG/DOPE/Chol) (molar ratio)	Size (nm)	PDI	Zeta potential (mV)
1:1:1:0	121.6 ± 2.7	0.41 ± 0.01	17.5 ± 0.9
1:1:1:1	136.1 ± 4.7	0.40 ± 0.03	14.0 ± 1.7
1:1:1:3	150.1 ± 2.1	0.42 ± 0.02	13.6 ± 0.7
1:1:1:6	149.5 ± 1.5	0.45 ± 0.02	11.9 ± 0.5

a.



b.

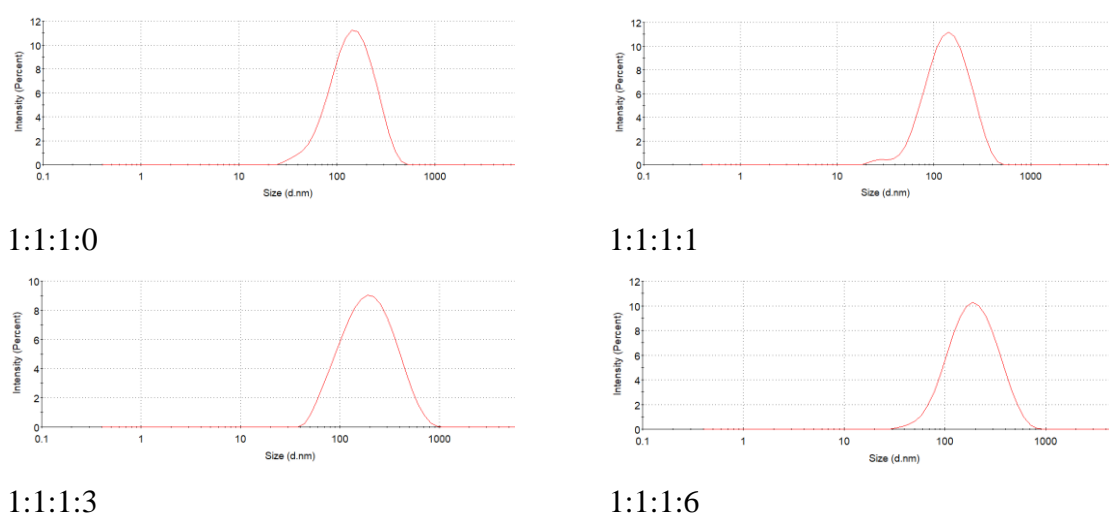


Figure S1 (a) Plasmid map of pEGFP-N1 (left) and absorbance spectra of the pDNA (right).

(b) The size distribution of liposomes with different formulations (molar ratio of DOTAP/DSPE-PEG/DOPE/Chol)

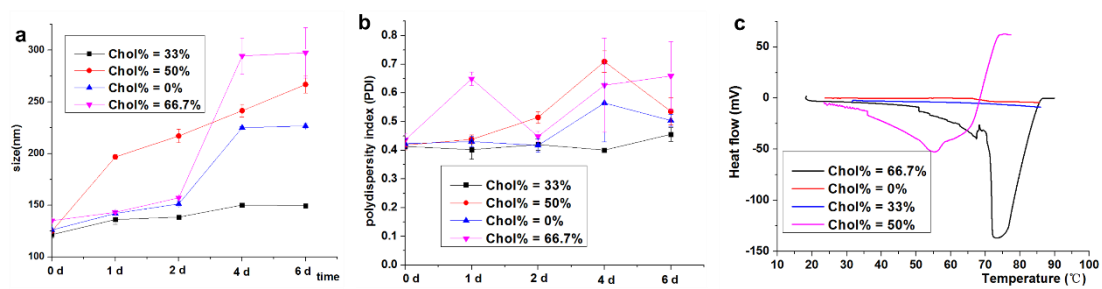


Figure S2 Size changes (a) and PDI changes (b) of liposomes with different Chol% in 6 days.

(c) DSC heatflow diagram of liposomes with different Chol%.

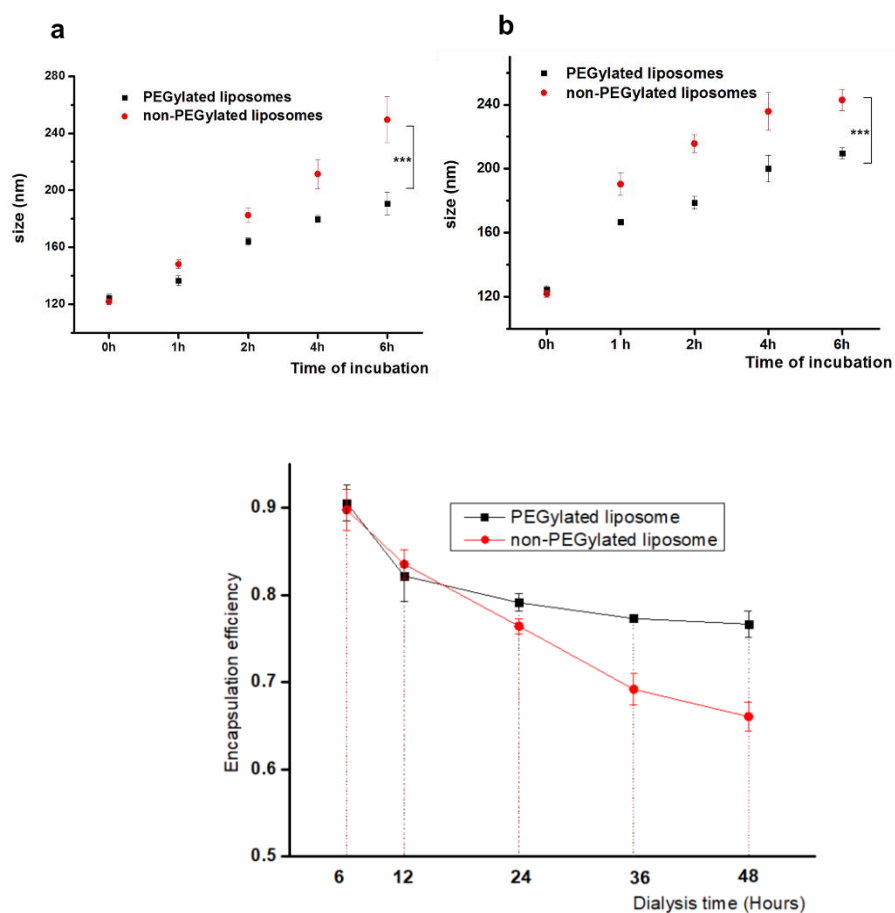


Figure S3 The size change of PEGylated and non-PEGylated liposomes at different time points after incubation with optiMEM (A) serum-contained culture medium (B) change of encapsulation efficiency of VP (C). *** $P < 0.0001$.

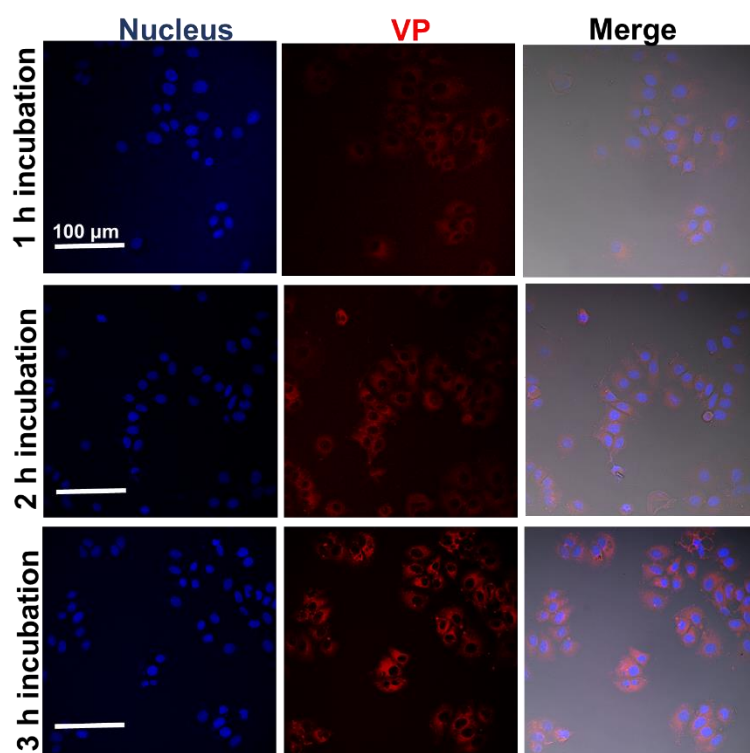


Figure S4. CLSM images of cellular uptake of lipopolyplexes loaded with VP molecules (red colour) at different incubation time points. The merge panel represent the images merged by the blue, red and bright field channels. Scale bars = 100 μm .

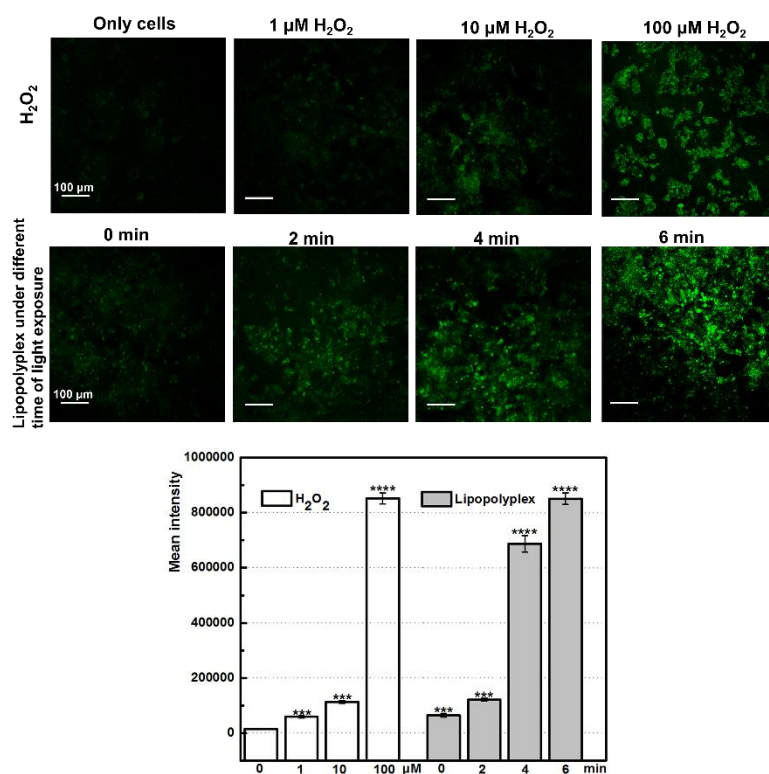


Figure S5. Cellular ROS detection from VP after light illumination. CLSM images of DCF fluorescence signal after cellular ROS generation with and without light illumination and quantitative assessment of DCF fluorescence intensity. Scale bars = 100μm. *** $p < 0.001$ and **** $p < 0.0001$ compared to the only cells group.

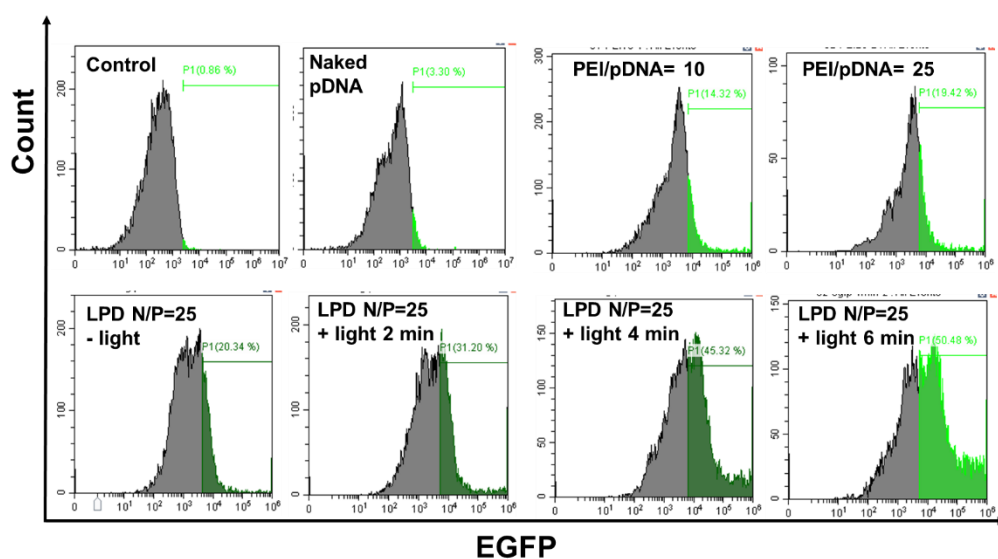


Figure S6 Representative flow cytometry histograms of EGFP intensity in HCT 116 cells transfected by pure pDNA, polyplexes at varying PEI/pDNA levels and LPDs with and without light illuminations.

4

X-ray radiation-induced and targeted photodynamic therapy

CHAPTER 4 Paper 3

X-ray radiation-induced and targeted photodynamic therapy with folic acid-conjugated biodegradable nanoconstructs

Sandhya Clement^{*†}, Wenjie Chen[†], Wei Deng, Ewa M. Goldys (2018). *International Journal of Nanomedicine*, 13, 3553.

[†] *These authors contributed equally.*

Summary of author contributions to this paper.

	S.C.	W.C.	W.D.	EM.G.
Project design	●	●	●	●
Nanomaterial	●			
Cell experiments		●		
Data analysis	●	●		
Manuscript	●	●	●	●

X-ray radiation-induced and targeted photodynamic therapy with folic acid-conjugated biodegradable nanoconstructs

This article was published in the following Dove Press journal:
International Journal of Nanomedicine

Sandhya Clement^{1,2,*}

Wenjie Chen^{1,*}

Wei Deng^{1,2}

Ewa M Goldys^{1,2}

¹Australian Research Council
Centre of Excellence for Nanoscale
BioPhotonics (CNBP), Department
of Physics and Astronomy, Macquarie
University, Sydney, NSW, Australia;

²The Graduate School of Biomedical
Engineering, University of New South
Wales, Sydney, NSW, Australia

*These authors contributed equally
to this work

Introduction: The depth limitation of conventional photodynamic therapy (PDT) with visible electromagnetic radiation represents a challenge for the treatment of deep-seated tumors.

Materials and methods: To overcome this issue, we developed an X-ray-induced PDT system where poly(lactide-co-glycolide) (PLGA) polymeric nanoparticles (NPs) incorporating a photosensitizer (PS), verteporfin (VP), were triggered by 6 MeV X-ray radiation to generate cytotoxic singlet oxygen. The X-ray radiation used in this study allows this system to break-through the PDT depth barrier due to excellent penetration of 6 MeV X-ray radiation through biological tissue. In addition, the conjugation of our NPs with folic acid moieties enables specific targeting of HCT116 cancer cells that overexpress the folate receptors. We carried out physicochemical characterization of PLGA NPs, such as size distribution, zeta potential, morphology and in vitro release of VP. Cellular uptake activity and cell-killing effect of these NPs were also evaluated.

Results and discussion: Our results indicate that our nanoconstructs triggered by 6 MeV X-ray radiation yield enhanced PDT efficacy compared with the radiation alone. We attributed the X-ray-induced singlet oxygen generation from the PS, VP, to photoexcitation by Cherenkov radiation and/or reactive oxygen species generation facilitated by energetic secondary electrons produced in the tissue.

Conclusion: The cytotoxic effect caused by VP offers the possibility of enhancing the radiation therapy commonly prescribed for the treatment of cancer by simultaneous PDT.

Keywords: PLGA nanoparticles, verteporfin, singlet oxygen generation, photodynamic therapy, X-ray PDT, folic acid targeting

Introduction

Photodynamic therapy (PDT), a minimally invasive therapeutic modality, primarily used to treat cancer, continues to attract research interest.^{1,2} PDT uses two entities, a photosensitizer (PS) drug and electromagnetic radiation of appropriate visible wavelength, to generate cytotoxic reactive oxygen species (ROS) such as singlet oxygen (¹O₂) to destroy cancer cells.^{3,4} The limited light penetration used in the established PDT with visible radiation allows treating only a limited range of superficial cancers such as skin cancers.^{5,6} Selecting PSs with absorption in a longer wavelength range of ~700 nm where tissue extinction is at its minimum (eg, Tookad[®]; Steba Biotech SA, Luxembourg) has been the main strategy used so far to enhance the penetration depth light used in PDT (up to 10 mm).^{6,7} However, the extinction coefficient in the tissue at ~700 nm and poor water solubility and low biocompatibility of these longer wavelength PSs limit their therapeutic efficacy as PDT agents.^{8,9} In addition, poor selectivity of PSs to tumors results

Correspondence: Sandhya Clement
The Graduate School of Biomedical
Engineering, University of New South
Wales, Sydney, NSW, 2052, Australia
Email sandyaclement@gmail.com

submit your manuscript | www.dovepress.com
Dovepress
<http://dx.doi.org/10.2147/IJN.S164967>

International Journal of Nanomedicine 2018:13 3553–3570

3553

© 2018 Clement et al. This work is published and licensed by Dove Medical Press Limited. The full terms of this license are available at <http://www.dovepress.com/terms.php> and incorporate the Creative Commons Attribution – Non Commercial (unported, v3.0) License (<http://creativecommons.org/licenses/by-nc/3.0/>). By accessing the work you hereby accept the Terms. Non-commercial uses of the work are permitted without any further permission from Dove Medical Press Limited, provided the work is properly attributed. For permission for commercial use of this work, please see paragraphs 4.2 and 5 of our Terms (<http://www.dovepress.com/terms.php>).

in undesired toxicity to healthy tissues, affecting therapeutic performance.¹⁰ Currently, the PDT for tumors located deeper in the tissue (more than 10 mm from the skin surface) is only possible with the aid of invasive delivery of light into tissue by inserted optical fibers.¹¹ To overcome these challenges, nanoparticle (NP)-formulated PS delivery systems have been developed, including those molecularly targeted to cancer-specific cell membrane proteins.^{12–14} In addition to carrying the PS cargo, some of these NPs may act as energy transducers for electromagnetic radiations and generate visible light to stimulate the PS molecules and enable ROS generation.^{3,15–19}

poly(D,L-lactide-co-glycolic acid) (PLGA) polymer is widely used in biomedical applications including drug delivery, bioimaging and diagnostics, cancer therapeutics and tissue engineering.²⁰ Biodegradability of PLGA is facilitated by the hydrolysis of its ester linkages in the presence of water, producing glycolic acid and lactic acid. These monomers undergo various metabolic processes in the human body under normal physiological conditions,²¹ owing to this property, PLGA has been clinically approved by the US Food and Drug Administration (FDA). PLGA can easily be formulated as a nanomaterial.²² The surface of PLGA NPs can be modified with various molecules such as polyethylene glycol (PEG) and chitosan.^{23,24} These NPs can passively accumulate in cancer tissue by virtue of the enhanced permeability and retention (EPR) effect.^{25–27} To enhance the efficiency of its cellular uptake, PLGA can be further functionalized and conjugated with molecularly targeting ligands for targeted drug or gene delivery.^{28–31} Among these targeting moieties, folic acid (FA) is an excellent choice because folate receptors (FRs) are overexpressed in most cancer cells, while they are almost absent in healthy tissues. The FR-mediated endocytosis has been reported in many human cancer cell lines.^{32–34} Therefore, cellular internalization of PS-bearing nanoparticles (NPs) conjugated with FA can be significantly enhanced in cancer cells, compared with healthy cells, leading to cancer-selective delivery of PS. In addition, deeply penetrating X-ray radiation, which is accompanied by in situ generated Cherenkov radiation and a cascade of energetic secondary electrons, was recently investigated by our group in the context of PS activation in deep tissues.^{35–37} In these studies, scintillating NPs were used as energy transducers providing scintillation photons for the PS molecules. Alternatively, the NPs themselves have also been used as PS.^{39,40} However, both these approaches used specialized inorganic materials, and the ensuing cytotoxicity of the NP when delivered in clinically meaningful doses represented a potential limitation for future clinical utilization of this approach.⁴¹ In contrast, in this study, we exclusively

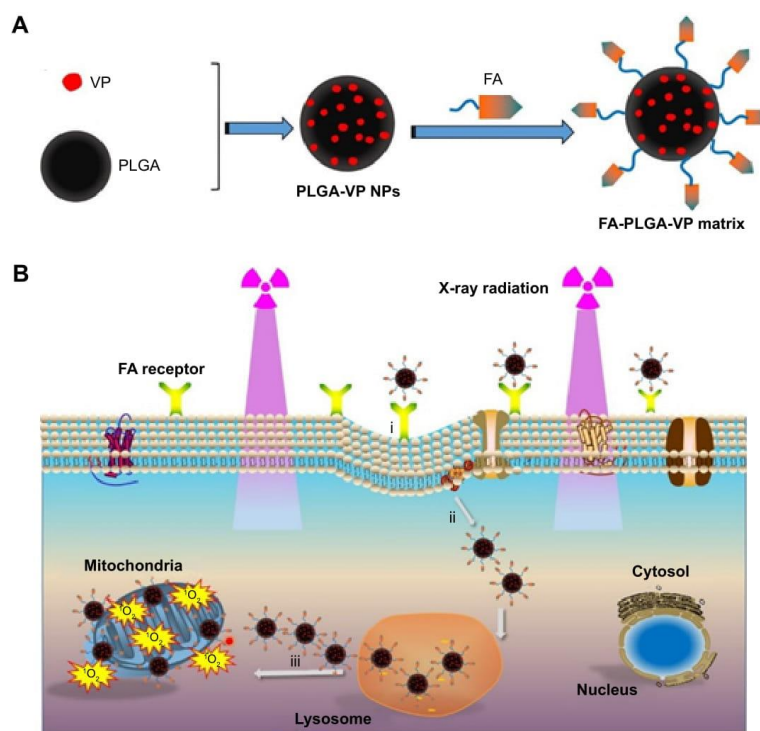
used chemical agents (PLGA and verteporfin [VP]) that are already clinically approved.

This study explores the therapeutic effect of a PLGA-encapsulated PS, VP, in combination with externally applied 6 MeV X-ray radiation as well as 690 nm light illumination. VP is a clinically approved PS for the treatment of macular degeneration with a strong absorption band near ultraviolet (UV)-blue region and a second weak band around 700 nm.^{42,43} The PLGA NPs with VP molecules encapsulated within PLGA-VP are conjugated with FA. The FA conjugate (FA-PLGA-VP) has high affinity for the FRs that are present on the surfaces of most human tumor cells.^{44,45} These FA-conjugated PLGA NPs were activated by both 6 MeV X-ray radiation and, for comparison, by 690 nm light irradiation usually used to stimulate VP. Light of a wavelength at 690 nm can directly excite the VP molecules to produce singlet oxygen, whereas 6 MeV X-ray radiation excites the VP molecule either by the induced CR in the biological media or due to the interaction of electrons with VP or both.⁴⁶ Singlet oxygen generated during PDT was monitored using singlet oxygen sensor green (SOSG), a chemical probe specifically designed for detecting ¹O₂.^{47,48} Cytotoxicity of the FA-PLGA-VP nanoconjugates exposed to X-ray radiation or light illumination was investigated in a colorectal cancer cell line, HCT116. Scheme 1 illustrates the formation of FA-PLGA-VP conjugates and their interaction with cells in targeted PDT of cancer.

Materials and methods

Materials

PLGA (50:50; molecular weight [MW]: 30,000–60,000; product no: P2191), poly(vinyl alcohol) (PVA; MW: 31,000–50,000; product no: 363138), dichloromethane (DCM; product no: 270997), VP (product no: SML 0534), FA (product no: F7876), 1-(3-(dimethylamino)-propyl)-3-ethyl carbodiimide hydrochloride (EDC; product no: 165344), *N*-hydroxysulfosuccinimide (NHS; product no: 130672), methanol (product no: 322415) and dimethyl sulfoxide (DMSO; product no: D2650) were purchased from Sigma-Aldrich Co. (St Louis, MO, USA). SOSG probe (product no: S-36002) and Live/Dead Cell Viability Kit (product no: L3224A) were purchased from Thermo Fisher Scientific (Waltham, MA, USA). Dulbecco's Modified Eagle's Medium (DMEM; product no: 11965092), fetal bovine serum (FBS; product no: 26140079), trypsin (product no: 12604-021), Hoechst 33345 (product no: H3570), Dulbecco's phosphate-buffered saline (DPBS; product no: 14190250), phosphate-buffered saline (PBS; product no: 10010023), opti-Minimal Essential Medium (MEM; reduced serum medium; product



Scheme 1 Illustration of conjugation and PDT mechanism.

Notes: (A) Synthesis of FA-PLGA-VP conjugates. (B) FA-PLGA-VP targeting and interacting with cancer cells following X-ray radiation exposure. (i) Specific binding to FRs overexpressed in cancer cells and cellular internalization. (ii) Cellular uptake of the conjugates via the FR-mediated endocytosis pathway. (iii) Endosomal escape and accumulation around the mitochondria of NPs as well as 1O_2 -induced cell killing with X-ray-triggered PDT.

Abbreviations: FA, folic acid; FR, folate receptor; NPs, nanoparticles; PDT, photodynamic therapy; PLGA, poly(D,L-lactide-co-glycolic acid); VP, verteporfin.

no: 31985062) and MitoTracker® Green FM (product no: M7514) were purchased from Thermo Fisher Scientific. McCoy's 5A medium (product no: ATCC® 30-2007™) and Eagle's Minimum Essential Medium (EMEM; ATCC® 30-2003™) were purchased from the American Type Culture Collection (ATCC, Manassas, VA, USA).

A human colorectal cancer cell line, HCT116 (product no: ATCC® CCL-247™), and a normal colorectal cell line, CCD 841 CoN (product no: ATCC® CRL-1790™) were purchased from the ATCC.

Methods

Preparation of PLGA NPs incorporating VP (PLGA-VP) and modification with FA (FA-PLGA-VP nanoconstruct)

In this study, we synthesized PLGA and PLGA-VP NPs by using a solvent evaporation single emulsion method with

slight modifications.^{49,50} Briefly, 2.5 mL of PLGA solution mixed with different amounts of VP stock solution (0 μ L, 50 μ L, 100 μ L, 200 μ L and 400 μ L) was added to 30 mL of 5% (w/v) PVA. The mixture was sonicated for 1.5 min at 200 W output using a microtip probe sonicator (Branson Digital Sonifier, S-250D; Emerson Industrial Automation, Danbury, CT, USA) followed by evaporation of DCM at room temperature under moderate magnetic stirring. The solution was purified by centrifugation (7,500 rpm for 10 min) and washed with water twice. The stock solution of the samples was prepared by suspension of NPs in 12 mL of water. The final concentration of VP in each sample (pure PLGA and PLGA-VP NPs; samples 1–5) was 0 μ M, 4.5 μ M, 15.9 μ M, 26.4 μ M and 39.6 μ M, respectively.

The conjugation of FA with PLGA-VP NPs was conducted based on a previously reported protocol with slight modifications.⁵¹ One milliliter of PLGA-VP stock solution

was centrifuged and washed with PBS three times and redispersed in 1 mL of PBS. Twelve milligrams of NHS and 20 mg of EDC were added to the solution, and it was vortexed in an orbital shaker for 1 h at 200 rpm. One hundred microliters of PBS containing FA (50 μ M) was subsequently added to the mixture followed by shaking in an orbital shaker (200 rpm) for another 18 h. The final product was washed with water twice and resuspended into 1 mL of water to make the stock solution.

Characterization of the conjugates

The size and the surface charge of different PLGA NPs were measured using a Zetasizer Nano ZS (Malvern Instruments, Malvern, UK). The absorption spectra of the pure PLGA and PLGA-VP samples were measured in Cary UV-VIS-NIR absorption spectrophotometer (Agilent, Santa Clara, CA, USA) by using a pair of 1 cm path length clean quartz cuvette. The fluorescence measurements were carried out using Cary Eclipse Spectrophotometer (Varian, Inc.) with xenon lamp excitation at room temperature. The as-prepared samples were diluted three times for carrying out the abovementioned measurements. The shape of the PLGA NPs was confirmed by carrying out transmission electron microscopy (TEM) imaging using the Philips CM10 system (Philips Electron Optics, Eindhoven, The Netherlands). The samples were negatively stained with uranyl acetate to enhance PLGA contrast in TEM. The conjugation of FA with PLGA-VP was confirmed by both absorption spectroscopy and Fourier transform infrared (FTIR) spectroscopy.

In vitro VP release from PLGA NPs

Five hundred microliters of PLGA-VP NPs (sample 3, with a VP concentration of 15.9 μ M) was centrifuged and redispersed in PBS with and without 10% FBS to mimic the physiological conditions. The solution was placed in a Lyzer tube (Midi Pur-A-Lyzer 6000 Dialysis Kit), and this tube was placed in a 50 mL tube with 15 mL of PBS in it followed by incubation at 37°C for different time intervals. An aliquot of PBS was taken for the fluorescence characterization of the released VP at different time points. The percentage of VP release from PLGA-VP NPs was calculated as follows:

$$\%VP \text{ release} = \frac{(VP_s)}{(VP_c)} \times 100$$

In this study, (VP_s) and (VP_c) represent the peak fluorescence emission intensities of VP in PBS and in control sample, respectively. The control sample was prepared by

the dispersion of the PLGA-VP NPs in 15 mL of PBS and 200 μ L of DMSO. The DMSO was added to dissolve the PLGA NPs.

Singlet oxygen detection using SOSG probe

Two different sources of electromagnetic radiation were used for singlet oxygen generation. We used a 690 nm red light-emitting diode (LED), at the power density of 15 mW cm^{-2} on the samples, for different exposure times. We also used a linear accelerator (LINAC; Elekta AB, Stockholm, Sweden) with an X-ray photon energy of 6 MeV generating various doses of X-ray radiation. The SOSG probe was used to detect the singlet oxygen generated in the samples. To this aim, 16 μ L of SOSG (4 μ M) was added to 2 mL of diluted samples (10 times dilution from the stock solution). The emission intensity from SOSG at 525 nm was measured after excitation at 488 nm wavelength. The increase in the fluorescence intensity is an indication of singlet oxygen generation.

Cell culture

McCoy's 5A medium was used to culture the HCT116 cells. EMEM supplemented with 10% FBS and 1% antibiotic-antimycotic was used as the culture medium of the CCD 841 CoN cells. The cells were grown at 37°C with 5% CO_2 in the cell incubator. When cells reached about 90% confluency, they were detached with trypsin and transferred into Petri dishes or well plates for different experimental purposes.

Cellular uptake of PLGA-FA-VP

To perform confocal microscopy cell experiments, HCT116 cells ($5 \times 10^4/\text{well}$) were seeded in 24-well plates with glass coverslips with 12 mm diameter placed in each well. When the cells reached 60% confluency, the previous medium was removed, and the reduced serum medium (opti-MEM) solution containing PLGA NPs was added to cells, while the same medium without additions was applied to the control groups. After 0.5, 1 and 3 h of incubation, the medium was removed and coverslips were washed twice with DPBS solution (pH 7.4). Then, cells were fixed with 2% paraformaldehyde (10 min, 37°C), washed twice with DPBS solution (pH 7.4), stained with MitoTracker® Green FM for 15 min at 37°C (50 nM) and stained with Hoechst 33345 for 15 min at 37°C (5 μ g mL^{-1}). After all staining procedures, each coverslip was rinsed by DPBS solution (pH 7.4) three times and transferred onto a glass slide with a drop of fluoromount mounting medium (Sigma-Aldrich Co.). The glass slides were then sealed and imaged using

a Leica SP2 confocal laser scanning microscopy system (Leica Microsystems, Wetzlar, Germany). The excitation wavelength of 405 nm was used for the excitation of VP loaded inside PLGA NPs, and their fluorescence emission was measured at 690 nm. The following imaging conditions were used: excitation 514 nm, emission of 590 nm for the labeled lysosomes and excitation 488 nm and emission 516 nm for the mitochondria.

FA receptor-mediated endocytosis uptake

For the observation of the FA receptor-mediated endocytosis uptake of FA-PLGA-VP, the HCT116 cells were incubated with NP matrix (10 times dilution in culture medium) for 0.5 h, 1 h, and 3 h at 37°C. To study the competitive effect of free FA on the endocytosis of NPs, the HCT116 cells were first incubated with the opti-MEM medium containing free FA (50 µg/mL) for blocking the FRs of the cells, followed by incubation with opti-MEM medium containing same amount of FA-PLGA-VP at 37°C. The cells without FA incubation served as the control group. After cell incubations with different treatments, cells were prepared in glass slides laser scanning confocal microscope imaging. Both the emissions from VP molecules in the conjugate and Hoechst 33342 were imaged by exciting at 405 nm.

Cell viability and in vitro PDT assays

To evaluate the toxicity of two external radiation sources (visible light and X-rays) on HCT116 and CCD 841 CoN cells, the MTS assays were carried out. Cells (1×10^4 /well) were seeded into 96-well plates and cultured for 24 h at 37°C. When the cells reached 70% confluency, they were exposed to X-ray radiation at different doses followed by another 24 h. The toxicity was assessed using the Cell Viability Assay Kit, MTS (Promega Corporation, Fitchburg, WI, USA) according to its protocol.

In X-ray PDT assays, HCT116 cells were divided into four groups: control cells without any treatment, cells incubated with PLGA NPs, cells incubated with PLGA-VP NPs and cells incubated with FA-PLGA-VP. Cells (1×10^4 cells/well) were seeded into 96-well plates and cultured for 24 h at 37°C. When the cells reached 70% confluency, the old medium was removed, and then opti-MEM solutions containing different NP samples were added. After 4 h of incubation, the old medium was removed and fresh serum-containing medium was added. For X-ray radiation PDT experiments, the cells incubated with different NP samples were, respectively, exposed to 6 MeV X-ray radiation with different doses. After treatments, cells were

further incubated for another 24 h. The cellular cytotoxicity of PDT was then assessed by the MTS assay (Promega Corporation) according to its protocol.

To confirm whether PLGA-VP NP-based PDT can be triggered with 690 nm (deep red) illumination, cytotoxicity of NPs on HCT116 cells was evaluated by using a Live/Dead Cell Viability Kit (product no: L3224A; Thermo Fisher Scientific). In brief, HCT116 cells (3×10^5) were seeded in glass bottom confocal dishes with 35 mm diameter and cultured with 1 mL McCoy's 5A medium. When cells grew to about 70% confluency, the dishes were divided into groups to undergo different treatments. Cells alone is considered as the control group. The other three groups are cells treated with light alone, cells treated with FA-PLGA-VP alone and cells treated with FA-PLGA-VP and light. After all treatments, the Live/Dead Cell Viability Kit was applied to all groups as per its manufacturer's instructions. Red fluorescent signal (excitation [Ex]/emission [Em] 528/617 nm) from dead cells and green signal (Ex/Em 494/517 nm) from live cells were imaged using a laser scanning confocal microscope (Leica SPM2).

Statistical analyses

All quantitative data are shown as mean \pm SD, $n \geq 3$. All data analyses and plotting were performed using and plotting were performed using Origin 8.5 software.

Results and discussion

Characterization of PLGA-VP nanoconstructs

We have first verified the loading capability of PLGA NPs with different concentrations of VP. This variable loading is qualitatively indicated by varying sample color (Figure 1A). The absorption spectra of PLGA-VP NPs, pure PLGA and VP are shown in Figure 1B. The VP absorption peaks from PLGA-VP samples were observed at 700 nm, and the increased peak extinction coefficient at these peaks confirmed an increased concentration of VP loaded into samples 2–5 compared with PLGA alone (sample 1). Using the absorption spectra, the final concentration of VP in each sample (2–5) was calculated approximately to be 4.5 µM, 15.9 µM, 26.4 µM and 39.6 µM, respectively.³ This loading capability was also confirmed by fluorescence emission intensity from VP in these samples at 425 nm excitation (Figure 1C).

The TEM image of pure PLGA NPs indicates that most of the particles were spherical in shape with a size of ~200 nm (Figure 1D). We further investigated the size

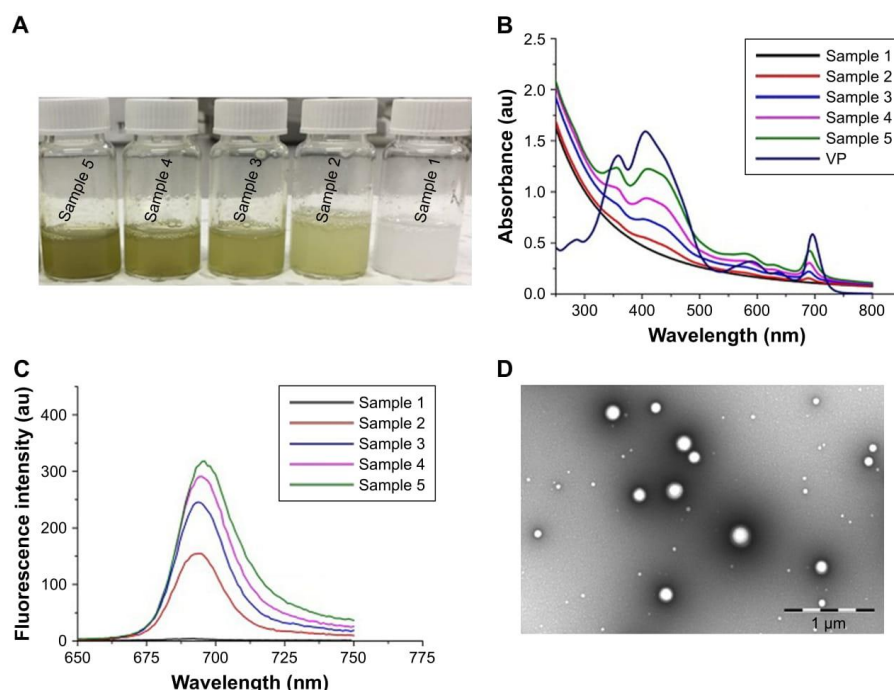


Figure 1 Characterization.

Notes: (A) Photographs of the synthesized PLGA NPs (sample 1) and PLGA-VP NP matrix with different VP concentrations (samples 2–5 with VP concentrations of 4.5 μM, 15.9 μM, 26.4 μM and 39.6 μM, respectively) in water. (B) Absorption spectra of VP, PLGA and different PLGA-VP NP solutions. (C) Fluorescence spectra of VP in PLGA samples with 425 nm excitation. (D) TEM image of PLGA NPs (scale bar: 1 μm).

Abbreviations: NPs, nanoparticles; PLGA, poly(D,L-lactide-co-glycolic acid); SOSG, singlet oxygen sensor green; TEM, transmission electron microscopy; VP, verteporfin.

and zeta potential of as-prepared PLGA-VP samples using dynamic light scattering (DLS; Table 1). The average size of the samples (sample 1–5) obtained from DLS was around 250 nm which is larger than the size observed by the TEM. All NPs have negative charge which slightly increased with increasing VP loading. The polydispersity index (PDI; Table 1) indicates that PLGA-VP samples are monodisperse and not aggregated.

Table 1 Mean size, zeta potential and PDI of synthesized PLGA samples

Sample number	Size (nm)	Zeta potential (mV)	PDI
1	241 ± 4	−20 ± 1	0.07 ± 0.03
2	241 ± 4	−22.6 ± 0.4	0.08 ± 0.03
3	245 ± 2	−21.8 ± 0.3	0.03 ± 0.01
4	248 ± 3	−20 ± 1	0.09 ± 0.02
5	252 ± 4	−23.2 ± 0.1	0.09 ± 0.01

Abbreviations: PDI, polydispersity index; PLGA, poly(D,L-lactide-co-glycolic acid).

Singlet oxygen generation under 6 MeV X-ray radiation

We first checked the feasibility of PS molecules to generate singlet oxygen under appropriate visible light illumination.⁵² SOSG was used for the detection of singlet oxygen generation. We observed the singlet oxygen generated from all samples (samples 1–5) under 690 nm excitation (Supplementary materials). We further evaluated the capability of PLGA samples for singlet oxygen generation under 6 MeV X-ray radiation at different radiation doses. Again, the same amount of SOSG as previously described was used in all samples. As previously indicated, the SOSG probe itself causes a small amount of singlet oxygen generation under X-ray radiation;⁵³ this was also observed in this study. The trend of the SOSG intensity measured in different samples as a function of radiation dose is shown in Figure 2A, and it is broadly similar to that for 690 nm irradiation. Singlet oxygen concentration in samples 2 and 3 increases with an increase in the concentration of

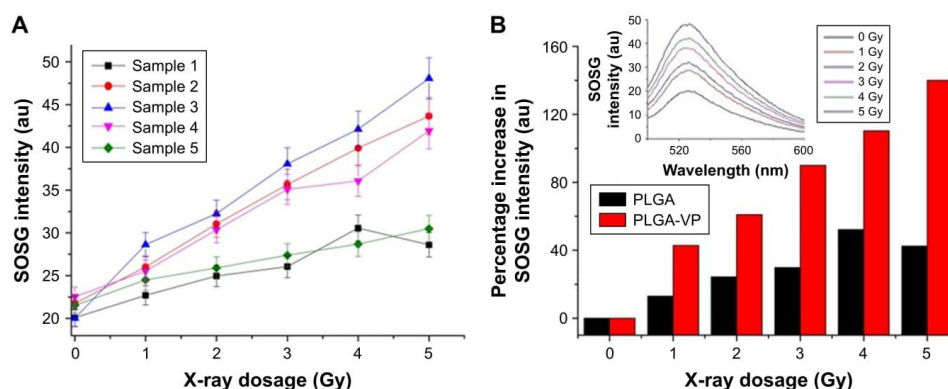


Figure 2 Single oxygen detection.

Notes: (A) Variation of SOSG intensity as a function of X-ray dose for different samples. (B) Comparison between the percentage increase in SOSG intensity of PLGA and PLGA-VP in the selected sample (sample 3). Inset shows the increase in fluorescence of SOSG for different radiation doses for PLGA-VP NPs (sample 3).

Abbreviations: NPs, nanoparticles; PLGA, poly(D,L-lactide-co-glycolic acid); SOSG, singlet oxygen sensor green; VP, verteporfin.

VP compared with the control (sample 1). Surprisingly, the amount of singlet oxygen was found to decrease for samples 4 and 5 under the same experimental conditions. This suggests concentration quenching of singlet oxygen generation, which is similar to well-established concentration quenching of fluorescence.⁵⁴ Figure 2B demonstrates that the percentage increase in SOSG intensity measured in sample 3 is much higher compared with sample 1 with increasing X-ray dose. The inset shows the SOSG fluorescence spectra of sample 3 for different radiation doses. In our previous study,⁵³ we reported that VP molecules themselves can generate singlet oxygen under different radiation doses at 6 MeV. This X-ray-induced singlet oxygen generation from VP molecules may be due to Cherenkov radiation and/or generation of energetic electron by the 6 MeV X-ray radiation, which then produce a cascade of ROS. Earlier reports confirm that 6 MeV LINAC can generate CR in biological media.⁴³ CR is electromagnetic radiation produced when charged particles move in a dielectric medium with a speed greater than phase velocity of light.⁵⁵ The featureless spectrum of CR spans the entire UV–visible region and beyond, and it fully overlaps with the strong absorption band of VP in the UV–blue region. This CR enables direct excitation of VP molecules and singlet oxygen generation from PLGA-VP samples. Simultaneously, the secondary electrons generated by the X-ray photons may directly interact with the available oxygen and generate ROS,⁵⁶ which may then react with VP. Direct interaction of these secondary electrons with the VP molecules is also possible. We ruled out the potential influence of ambient

light which was negligible in our X-ray PDT experiments (Supplementary materials).

Formation of FA-PLGA-VP nanoconstructs

To specifically target cancer cells with the NPs and enhance the uptake activity of the particle by the cancer cells, PLGA-VP (sample 3) was conjugated with FA moieties. We checked the stability of PLGA-VP NPs in biological conditions before performing the FA conjugation. The results indicate that these NPs were highly stable in the PBS containing 10% FBS for >50 h (Supplementary materials). The conjugation of NPs with FA was confirmed by the visible absorption spectra of the conjugates, where the absorption peaks of both VP and FA were observed (Figure 3A). The absorption feature at 270 nm in FA-PLGA-VP corresponded to the peak of pure FA at 280 nm with the spectral shift attributed to the underlying slope in the FA-PLGA-VP spectrum. This conjugation was additionally verified by the FTIR spectra as shown in Figure 3B. A detailed analysis of FTIR peaks for FA, PLGA and FA-PLGA-VP is provided in the “Supplementary materials” section.

Cellular uptake of FA-PLGA-VP nanoconstructs and colocalization between nanoconstructs and different cell organelles

To achieve the increased cellular uptake of NPs and target the FRs overexpressed in HCT116 cells, the PLGA-VP NPs were conjugated with FA using the EDC-NHS reaction.

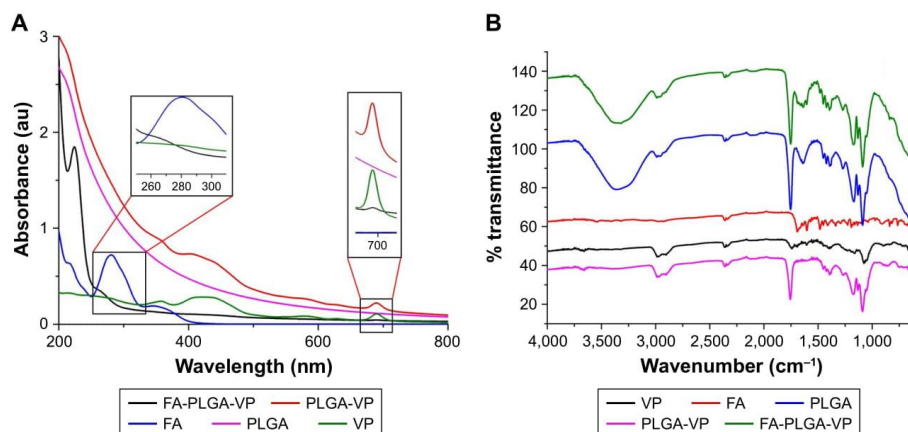


Figure 3 Confirmation of conjugation of FA with the PLGA-VP nanoconstructs using (A) absorption spectra (insets highlight the FA and VP peaks in FA-PLGA-VP sample) and (B) FTIR spectra.

Note: All graphs in the spectra are scaled for distinguishing the peaks.

Abbreviations: FA, folic acid; FTIR, Fourier transform infrared; PLGA, poly(D,L-lactide-co-glycolide); VP, verteporfin.

Figure 4 shows the confocal microscopy images of the uptake of FA-PLGA-VP conjugates by HCT116 cells at different incubation times. The uptake was monitored under two different conditions with and without FA blocking. As shown in Figure 4A, without the blocking of FRs, the red signal from VP was clearly observed after 1 h incubation with the conjugates. After 3 h incubation, most of nanoconstructs were taken up by cells, significantly increasing the red signal. We also evaluated the targeting property of the FA-PLGA-VP construct by blocking the FR overexpressed by HCT116 cells before incubation with conjugates. In this study, free FA

molecules were used to block the FRs.⁵⁷ Figure 4B shows red fluorescence from VP molecules after 0.5 h, 1 h and 3 h of incubation. Even after 3 h of incubation, the red signal from VP was much weaker (Figure 4B) compared with the signal without blocking (Figure 4A). These results indicate that FA-PLGA-VP conjugates were taken up by HCT116 cells via the FR-mediated endocytosis pathway.

Mitochondria are the main organelles implicated in cancer cell killing in antitumor PS therapy.^{58–61} To maximize the efficiency of PDT, the PSs should be spatially localized within the short (20 nm) diffusion distance of ROS in

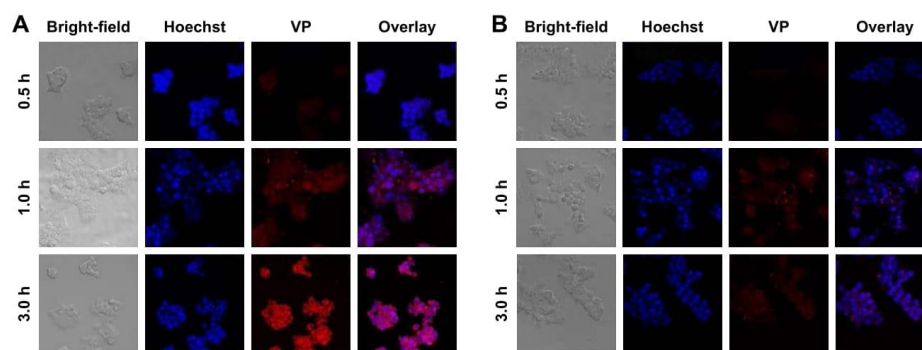


Figure 4 Confocal fluorescence images of cellular uptake of HCT116 cells with FA-PLGA-VP under (A) normal condition (B) with FR blocking.

Notes: Blue fluorescence, nuclei stained with Hoechst 33345; red fluorescence, emission of VP under 405 nm excitation. All images were taken with 20× magnification.

Abbreviations: FA, folic acid; FR, folate receptor; PLGA, poly(D,L-lactide-co-glycolic acid); VP, verteporfin.

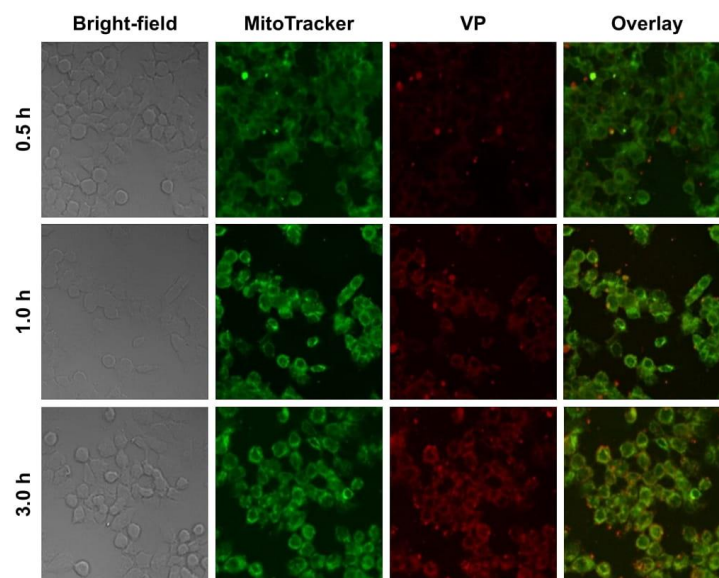


Figure 5 Confocal imaging of colocalization of FA-PLGA-VP in HCT116 cells.

Notes: Green fluorescence, MitoTracker; red fluorescence, emission of VP under 405 nm excitation. All images were taken with 40 \times magnification.

Abbreviations: FA, folic acid; PLGA, poly(D,L-lactide-co-glycolic acid); VP, verteporfin.

biological media.⁶² This proximity is shown in Figure 5, where the red signal from VP almost overlaps with the green signal from the MitoTracker, indicating that most of the released VPs were located at the mitochondria after 3 h of incubation.

We further quantitatively analyzed such colocalization by using the ImageJ software (<https://imagej.en.softonic.com>). As shown in Figure 6, the white/gray areas in the Costes map indicate the overlay of pixels of green color from the MitoTracker and red color from VP. A small number of white spots were observed after 0.5 h of incubation, indicating that some NPs were localized in the mitochondria. However, the white signal was significantly enhanced after 3 h of incubation, which means that most of the NPs were colocalized with the mitochondria.

These results were also confirmed by a scatter plot (middle panel) and cytofluorogram (Figure 6, right side panel). An increase in Pearson value and Manders coefficient indicates a good correlation between the MitoTracker fluorescence and VP fluorescence.^{63,64} In addition to mitochondria, the colocalization between FA-PLGA-VP and another organelle, lysosomes, was also documented and analyzed (Supplementary materials). The Pearson correlation coefficient (PCC) for

the lysosomes for 3 h of incubation (0.443) is much smaller than that obtained from colocalization between the NPs and mitochondria (0.7), which again confirms the localization of VP in the mitochondria rather than in lysosomes. This suggested that most of the NPs have escaped from the lysosomal compartments and eventually reached the mitochondria where they responded to photosensitization following irradiation. These results are in good agreement with previously published results for cellular localization of VP.^{65,66}

Cellular PDT with X-ray radiation

As discussed earlier, based on the singlet oxygen generation capability of PLGA-VP samples with different VP concentrations, we selected sample 3 for further surface conjugation with FA and cellular PDT using X-ray radiation in HCT116 cells prior to X-ray-triggered PDT; the viability of HCT116 and colon epithelial cells (CCD 841 CoN) incubated with PLGA, PLGA-VP and FA-PLGA-VP was evaluated (Supplementary materials). We also demonstrated the PDT effect on HCT116 cells incubated with FA-PLGA-VP under 690 nm irradiation (Supplementary materials).

Of particular interest, in this study, the results of cell viability in HCT116 and CCD 841 CoN cells are exposed to

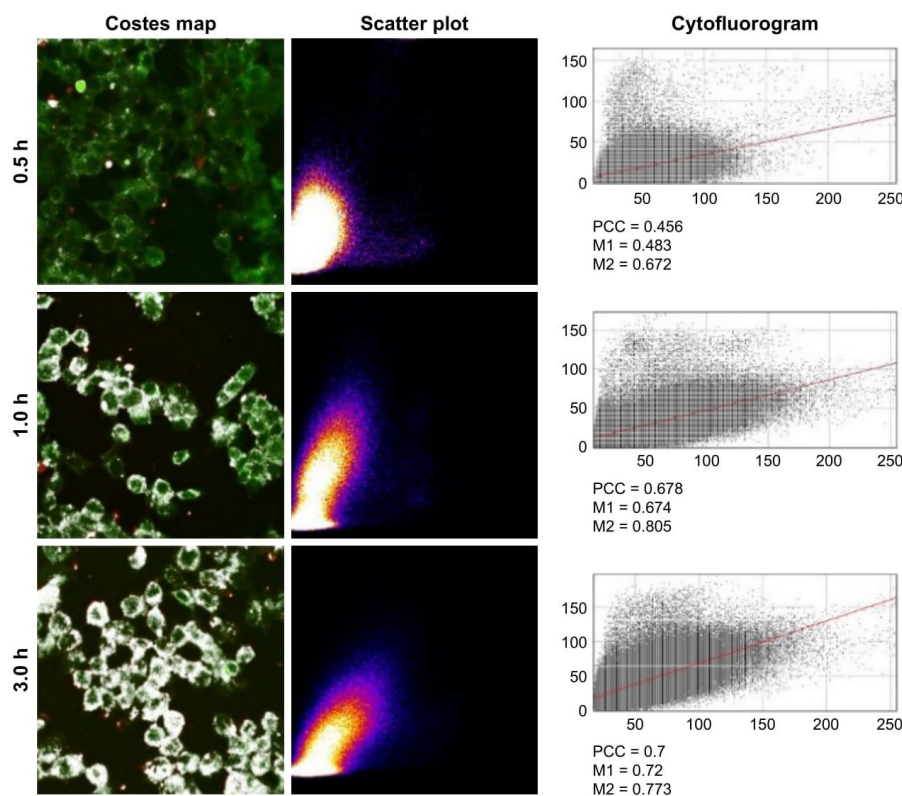


Figure 6 Image correlation analysis with ImageJ Costes map, scatter plot and cytofluorogram for the images as shown in Figure 5.

Notes: M1 and M2 represent the Manders correlation coefficients. All images were taken with 40 \times magnification.

Abbreviation: PCC, Pearson's correlation coefficient.

our conjugates in combination (Figure 7A); CCD 841 CoN cells were not visibly affected by X-ray radiation (>96%), while the viability of HCT116 cells was reduced with different doses with a decrease of 78% at 4 Gy radiation. The reduced viability of HCT116 cells under radiation may be due to their higher degree of dysregulation than normal cells and/or to different cell types. Figure 7B shows the viability of cancer cells after treatment with NPs and radiation. By comparing Figure 7A and B, it can be seen that the 4 Gy radiation alone can kill 22% of the cancer cells, whereas 67% of the cells were killed by a combination of radiation and FA-PLGA-VP constructs in these cells. This supports our hypothesis that X-ray-mediated PDT can enhance the cell-killing effect by exciting the PS drug encapsulated in the NPs compared with radiation alone. The likely mechanism for the singlet oxygen generation in

this X-ray PDT is explained in the "Introduction" section as well as in the "Singlet oxygen generation under 6 MeV X-ray radiation" section. In addition, there is a possibility of lower energy electrons to interact with the biomolecules, including DNA.⁶⁷ This kind of interaction can disrupt the DNA structure causing cell death.⁶⁸ Radiosensitizing effects of this type were reported for other porphyrin-type compounds such as photofrin II (PII), (hematoporphyrin) dimethyl ether (HPde) and hematoporphyrin derivative (HPD) in various cancer cell lines.^{69,70}

Our results of cell viability post PDT were comparable with earlier published study in X-ray and Cherenkov-mediated PDT. These earlier studies included our own study on CeF₃ NP conjugated with VP, where NP acted as an energy transducer for X-ray radiation and generated visible radiation to activate the PS to generate ROS.³⁵ In this study, we were

Dovepress

X-ray radiation-induced and targeted photodynamic therapy

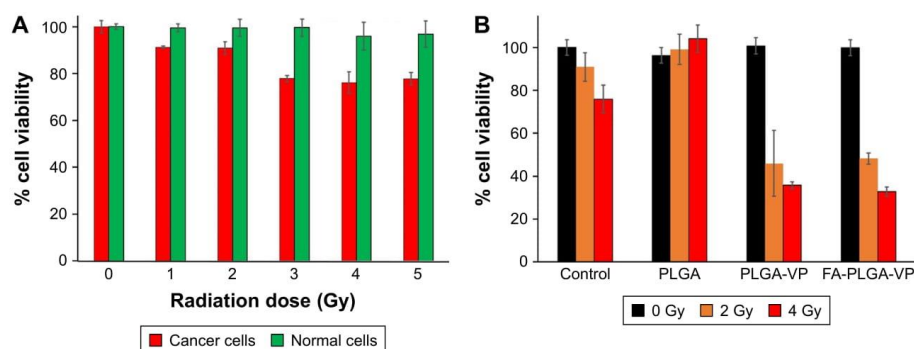


Figure 7 Cell viability under X-ray radiation.

Notes: (A) Viability of normal (CCD 841 CoN) and cancer cells (HCT116) toward different doses of 6 MeV X-ray radiation. (B) The viability of HCT116 cancer cells treated with different samples and different radiation doses.

Abbreviations: FA, folic acid; PLGA, poly(D,L-lactide-co-glycolic acid); VP, verteporfin.

able to kill 30% of Panc-1 cells with a 6 MeV X-ray with 6 Gy of radiation. In another study, >60% human glioblastoma cells (U87MG) were killed with PDT by using silica NPs incorporating $\text{SrAl}_2\text{O}_4:\text{Eu}^{2+}$ and the PS MC540 under 1.5 Gy of X-ray radiation.³⁹ These values are comparable with our current study where >65% of the cells were killed by FA-PLGA-VP nanoconjugate under 4 Gy dose of 6 MeV X-ray radiation. By comparison, 80% breast cancer cells (4T1) were damaged by the use of a radionuclide zirconium-89 (20 μCi , 909 keV, half-life: 78.4 h) and 20 μM chlorin e6 PS.³⁸ A similar study on Cherenkov-assisted radiotherapy on human fibrosarcoma (HT 1080) cells with TiO_2 -Tf nanoconstructs was reported using ^{18}F (0.2 mCi/0.1 mL, 633 keV, half-life: 1.83 h) and ^{64}Cu radionuclides (0.5 mCi/0.1 mL, 574 keV, half-life: 12.7 h).³⁷ In both these cases, a significant cell killing (>75%) was achieved. While these NP systems may be novel from a materials science perspective, their potential for translation to clinical use is currently unclear due to the lack of rigorous evaluation of their toxicity. Unlike previous study reported by other groups, our PLGA NPs and VP have been approved by FDA and are widely used in the clinical practice. Therefore, our results described in this study lay the foundations for a safe treatment modality, which is suitable for rapid translation to the clinic.

Conclusion

We have developed PLGA-VP NPs for efficient singlet oxygen generation by 6 MeV X-ray radiation. The successful conjugation of FA with the surface of PLGA-VP NPs enhanced cellular uptake, which was confirmed by confocal microscopy images and colocalization analysis between

NPs and mitochondria. Such NPs also demonstrated high stability by monitoring the VP release profile during certain time period. In vitro PDT assays suggest that the conjugates effectively kill HCT116 cells in the presence 6 MeV X-ray radiation. In X-ray radiation, the 6 MeV X-ray radiation from LINAC produces energetic secondary electrons and Cherenkov radiation in the samples, which in turn excite the VP molecules. Therefore, a stronger cytotoxic effect was observed as a result of combined radiation therapy with PDT. This X-ray-triggered PDT concept in combination with targeting ability of FA-PLGA-VP nanoconstructs offers a potential for treating deep-seated tumors with additionally enhanced cancer cell selectivity and reduced side effects to normal cells.

Acknowledgments

We acknowledge Ms Suzanne Lindsay, Manager, Microscopy Unit, Faculty of Science and Engineering at Macquarie University for helping us with the TEM images. We thank Mr Vaughan Moutrie and Mr Daniel Santos from Genesis Cancer Care for helping us with X-ray radiation experiments. We acknowledge PhD student Fei Wang from the Centre of Excellence for Nanoscale BioPhotonics at Macquarie University for supplying us with the cell lines. Wenjie Chen acknowledges the support of an iMQRES scholarship and the HDR budget from Macquarie University. This study is partially supported by Australian Research Council (ARC) through its Centre of Excellence Scheme (CE140100003) to EMG.

Disclosure

The authors report no conflicts of interest in this work.

References

- Brown SB, Brown EA, Walker I. The present and future role of photodynamic therapy in cancer treatment. *Lancet Oncol*. 2004;5(8):497–508.
- Ferreira-Strixino J, Debeve E. Photodynamic therapy in cancer treatment. In: de Freitas PM, Simões A, editors. *Lasers in Dentistry: Guide for Clinical Practice*. Hoboken: John Wiley & Sons, Inc.; 2015:346–350.
- Clement S, Sobhan M, Deng W, Camilleri E, Goldys EM. Nanoparticle-mediated singlet oxygen generation from photosensitizers. *J Photochem Photobiol A*. 2017;332:66–71.
- Nyman ES, Hynninen PH. Research advances in the use of tetrapyrrolic photosensitizers for photodynamic therapy. *J Photochem Photobiol B*. 2004;73(1–2):1–28.
- Wilson BC. Photodynamic therapy for cancer: principles. *Can J Gastroenterol Hepatol*. 2002;16:393–396.
- Allison RR, Downie GH, Cuenca R, Hu X-H, Childs CJ, Sibata CH. Photosensitizers in clinical PDT. *Photodiagnosis Photodyn Ther*. 2004;1:27–42.
- Zenkevich E, Sagun E, Knyukhto V, et al. Photophysical and photochemical properties of potential porphyrin and chlorin photosensitizers for PDT. *J Photochem Photobiol B*. 1996;33:171–180.
- Nyokong T, Ahsen V. *Photosensitizers in Medicine, Environment, and Security*. Berlin: Springer Science & Business Media; 2012.
- Olivo M, Bhuvaneshwari R, Lucky SS, Dendukuri N, Soo-Ping Thong P. Targeted therapy of cancer using photodynamic therapy in combination with multi-faceted anti-tumor modalities. *Pharmaceuticals (Basel)*. 2010;3(5):1507–1529.
- Brannon-Peppas L, Blanchette JO. Nanoparticle and targeted systems for cancer therapy. *Adv Drug Deliv Rev*. 2004;56(11):1649–1659.
- Beyer W. Systems for light application and dosimetry in photodynamic therapy. *J Photochem Photobiol B*. 1996;36(2):153–156.
- Peer D, Karp JM, Hong S, Farokhzad OC, Margalit R, Langer R. Nanocarriers as an emerging platform for cancer therapy. *Nat Nanotechnol*. 2007;2(12):751–760.
- Li S-Y, Cheng H, Qiu W-X, et al. Cancer cell membrane-coated biomimetic platform for tumor targeted photodynamic therapy and hypoxia-amplified bioreductive therapy. *Biomaterials*. 2017;142:149–161.
- Sun Y, Hu H, Zhao N, et al. Multifunctional polycationic photosensitizer conjugates with rich hydroxyl groups for versatile water-soluble photodynamic therapy nanoplateforms. *Biomaterials*. 2017;117:77–91.
- Chatterjee DK, Fong LS, Zhang Y. Nanoparticles in photodynamic therapy: an emerging paradigm. *Adv Drug Deliv Rev*. 2008;60(15):1627–1637.
- Idris NM, Gnanasammandhan MK, Zhang J, Ho PC, Mahendran R, Zhang Y. In vivo photodynamic therapy using upconversion nanoparticles as remote-controlled nanotransducers. *Nat Med*. 2012;18(10):1580–1585.
- Cheng Y, Meyers JD, Broome A-M, Kenney ME, Basilion JP, Burda C. Deep penetration of a PDT drug into tumors by noncovalent drug-gold nanoparticle conjugates. *J Am Chem Soc*. 2011;133(8):2583–2591.
- Bala I, Hariharan S, Kumar MR. PLGA nanoparticles in drug delivery: the state of the art. *Crit Rev Ther Drug Carrier Syst*. 2004;21(5):387–422.
- Gregoriadis G, Swain C, Wills E, Tavill A. Drug-carrier potential of liposomes in cancer chemotherapy. *Lancet*. 1974;1(7870):1313–1316.
- Lü J-M, Wang X, Marin-Muller C, et al. Current advances in research and clinical applications of PLGA-based nanotechnology. *Expert Rev Mol Diagn*. 2009;9(4):325–341.
- Athanasiou KA, Niederauer GG, Agrawal CM. Sterilization, toxicity, biocompatibility and clinical applications of polylactic acid/polyglycolic acid copolymers. *Biomaterials*. 1996;17(2):93–102.
- Gentile P, Chiono V, Carmagnola I, Hatton PV. An overview of poly(lactic-co-glycolic) acid (PLGA)-based biomaterials for bone tissue engineering. *Int J Mol Sci*. 2014;15(3):3640–3659.
- Cu Y, Saltzman WM. Controlled surface modification with poly(ethylene) glycol enhances diffusion of PLGA nanoparticles in human cervical mucus. *Mol Pharm*. 2008;6(1):173–181.
- Sharon JBL. *Surface Modification of PLGA Biomaterials for Site-Directed Immobilization of Growth Factors* [master's thesis]. Lexington: University of Kentucky; 2005.
- Matsumura Y, Maeda H. A new concept for macromolecular therapeutics in cancer chemotherapy: mechanism of tumorotropic accumulation of proteins and the antitumor agent smancs. *Cancer Res*. 1986;46(12 Pt 1):6387–6392.
- Acharya S, Sahoo SK. PLGA nanoparticles containing various anti-cancer agents and tumour delivery by EPR effect. *Adv Drug Deliv Rev*. 2011;63(3):170–183.
- Maeda H, Bharate G, Daruwalla J. Polymeric drugs for efficient tumor-targeted drug delivery based on EPR-effect. *Eur J Pharm Biopharm*. 2009;71(3):409–419.
- Cheng J, Teply BA, Sherifi I, et al. Formulation of functionalized PLGA-PEG nanoparticles for in vivo targeted drug delivery. *Biomaterials*. 2007;28(5):869–876.
- Makadia HK, Siegel SJ. Poly lactic-co-glycolic acid (PLGA) as biodegradable controlled drug delivery carrier. *Polymers (Basel)*. 2011;3(3):1377–1397.
- Bivas-Benita M, Romeijn S, Junginger HE, Borchard G. PLGA-PEI nanoparticles for gene delivery to pulmonary epithelium. *Eur J Pharm Biopharm*. 2004;58(1):1–6.
- Panyam J, Labhasetwar V. Biodegradable nanoparticles for drug and gene delivery to cells and tissue. *Adv Drug Deliv Rev*. 2003;55(3):329–347.
- Castillo JJ, Rindzevicius T, Novoa LV, et al. Non-covalent conjugates of single-walled carbon nanotubes and folic acid for interaction with cells over-expressing folate receptors. *J Mater Chem B*. 2013;1:1475–1481.
- Bhattacharya R, Patra CR, Earl A, et al. Attaching folic acid on gold nanoparticles using noncovalent interaction via different polyethylene glycol backbones and targeting of cancer cells. *Nanomedicine*. 2007;3:224–238.
- Zhang Y, Zhou J, Yang C, et al. Folic acid-targeted disulfide-based cross-linking micelle for enhanced drug encapsulation stability and site-specific drug delivery against tumors. *Int J Mol Med*. 2016;11:1119–1130.
- Clement S, Deng W, Camilleri E, Wilson BC, Goldys EM. X-ray induced singlet oxygen generation by nanoparticle-photosensitizer conjugates for photodynamic therapy: determination of singlet oxygen quantum yield. *Sci Rep*. 2016;6:19954.
- Misawa M, Takahashi J. Generation of reactive oxygen species induced by gold nanoparticles under x-ray and UV irradiations. *Nanomedicine*. 2011;7(5):604–614.
- Kotagiri N, Sudlow GP, Akers WJ, Achilefu S. Breaking the depth dependency of phototherapy with Cherenkov radiation and low-radiance-responsive nanophotosensitizers. *Nat Nanotechnol*. 2015;10(4):370–379.
- Kamkaew A, Cheng L, Goel S, et al. Cherenkov radiation induced photodynamic therapy using Chlorin e6-loaded hollow mesoporous silica nanoparticles. *ACS Appl Mater Interfaces*. 2016;8(40):26630–26637.
- Chen H, Wang GD, Chuang Y-J, et al. Nanoscintillator-mediated X-ray inducible photodynamic therapy for in vivo cancer treatment. *Nano Lett*. 2015;15(4):2249–2256.
- Ma L, Zou X, Chen W. A new X-ray activated nanoparticle photosensitizer for cancer treatment. *J Biomed Nanotechnol*. 2014;10(8):1501–1508.
- Maurer-Jones MA, Bantz KC, Love SA, Marquis BJ, Haynes CL. Toxicity of therapeutic nanoparticles. *Nanomedicine*. 2009;4(2):219–241.
- Brown DM, Kaiser PK, Michels M, et al. Ranibizumab versus verteporfin for neovascular age-related macular degeneration. *N Engl J Med*. 2006;355:1432–1444.
- Verteporfin in Photodynamic Therapy Study Group. Verteporfin therapy of subfoveal choroidal neovascularization in age-related macular degeneration: two-year results of a randomized clinical trial including lesions with occult with no classic choroidal neovascularization – verteporfin in photodynamic therapy report 2. *Am J Ophthalmol*. 2001;131(5):541–560.

44. Chen H, Ahn R, Van den Bossche J, Thompson DH, O'Halloran TV. Folate-mediated intracellular drug delivery increases the anticancer efficacy of nanoparticulate formulation of arsenic trioxide. *Mol Cancer Ther.* 2009;8(7):1955–1963.
45. Sudimack J, Lee RJ. Targeted drug delivery via the folate receptor. *Adv Drug Deliv Rev.* 2000;41(2):147–162.
46. Glaser AK, Zhang R, Davis SC, Gladstone DJ, Pogue BW. Time-gated Cherenkov emission spectroscopy from linear accelerator irradiation of tissue phantoms. *Opt Lett.* 2012;37(7):1193–1195.
47. Ragàs X, Jiménez-Banzo A, Sánchez-García D, Batllori X, Nonell S. Singlet oxygen photosensitisation by the fluorescent probe Singlet Oxygen Sensor Green®. *Chem Commun.* 2009:2920–2922.
48. Gollmer A, Arnbjerg J, Blaikie FH, et al. Singlet Oxygen Sensor Green®: photochemical behavior in solution and in a mammalian cell. *Photochem Photobiol.* 2011;87(3):671–679.
49. Deng W, Kautzka Z, Chen W, Goldys EM. PLGA nanocomposites loaded with verteporfin and gold nanoparticles for enhanced photodynamic therapy of cancer cells. *RSC Adv.* 2016;6:112393–112402.
50. Liu Y, Li K, Pan J, Liu B, Feng S-S. Folic acid conjugated nanoparticles of mixed lipid monolayer shell and biodegradable polymer core for targeted delivery of Docetaxel. *Biomaterials.* 2010;31(2):330–338.
51. Patel RH, Wadajkar AS, Patel NL, Kavuri VC, Nguyen KT, Liu H. Multifunctionality of indocyanine green-loaded biodegradable nanoparticles for enhanced optical imaging and hyperthermia intervention of cancer. *J Biomed Opt.* 2012;17(4):046003.
52. DeRosa MC, Crutchley RJ. Photosensitized singlet oxygen and its applications. *Coord Chem Rev.* 2002;233:351–371.
53. Clement S, Chen W, Anwer AG, Goldys EM. Verteporfin conjugated to gold nanoparticles for fluorescent cellular bioimaging and X-ray mediated photodynamic therapy. *Microchim Acta.* 2017;184(6):1765–1771.
54. Fonin AV, Sulatskaya AI, Kuznetsova IM, Turoverov KK. Fluorescence of dyes in solutions with high absorbance. Inner filter effect correction. *PLoS One.* 2014;9(7):e103878.
55. Bolotovskii BM. Vavilov-Cherenkov radiation: its discovery and application. *Phys Uspekhi.* 2009;52:1099–1110.
56. Murphy MP. How mitochondria produce reactive oxygen species. *Biochem J.* 2009;417(1):1–13.
57. Geng J, Li K, Ding D, et al. Lipid-PEG-folate encapsulated nanoparticles with aggregation induced emission characteristics: cellular uptake mechanism and two-photon fluorescence imaging. *Small.* 2012;8(23):3655–3663.
58. Trachootham D, Alexandre J, Huang P. Targeting cancer cells by ROS-mediated mechanisms: a radical therapeutic approach? *Nat Rev Drug Discov.* 2009;8(7):579–591.
59. Hoye AT, Davoren JE, Wipf P, Fink MP, Kagan VE. Targeting mitochondria. *Acc Chem Res.* 2008;41(1):87–97.
60. Yu Z, Sun Q, Pan W, Li N, Tang B. A near-infrared triggered nanophotosensitizer inducing domino effect on mitochondrial reactive oxygen species burst for cancer therapy. *ACS Nano.* 2015;9(11):11064–11074.
61. Yue C, Yang Y, Zhang C, et al. ROS-responsive mitochondria-targeting blended nanoparticles: chemo- and photodynamic synergistic therapy for lung cancer with on-demand drug release upon irradiation with a single light source. *Theranostics.* 2016;6(13):2352.
62. Yuan Y, Liu J, Liu B. Conjugated-polyelectrolyte-based polyprodrug: targeted and image-guided photodynamic and chemotherapy with on-demand drug release upon irradiation with a single light source. *Angew Chem Int Ed Engl.* 2014;53(28):7163–7168.
63. Dunn KW, Kamocka MM, McDonald JH. A practical guide to evaluating colocalization in biological microscopy. *Am J Physiol Cell Physiol.* 2011;300(4):C723–C742.
64. Adler J, Parmryd I. Quantifying colocalization by correlation: the Pearson correlation coefficient is superior to the Mander's overlap coefficient. *Cytometry A.* 2010;77(8):733–742.
65. Celli JP, Solban N, Liang A, Pereira SP, Hasan T. Verteporfin-based photodynamic therapy overcomes gemcitabine insensitivity in a panel of pancreatic cancer cell lines. *Lasers Surg Med.* 2011;43(7):565–574.
66. Runnels J, Chen N, Ortel B, Kato D, Hasan T. BPD-MA-mediated photosensitization in vitro and in vivo: cellular adhesion and beta 1 integrin expression in ovarian cancer cells. *Br J Cancer.* 1999;80(7):946–953.
67. Baskar R, Dai J, Wenlong N, Yeo R, Yeoh K-W. Biological response of cancer cells to radiation treatment. *Front Mol Biosci.* 2014;1:24.
68. Sanche L. Interaction of low energy electrons with DNA: applications to cancer radiation therapy. *Radiat Phys Chem.* 2016;128:36–43.
69. Luksiene Z, Labeikyte D, Juodka B, Moan J. Mechanism of radiosensitization by porphyrins. *J Environ Pathol Toxicol Oncol.* 2006;25(1–2):293–306.
70. Schaffer M, Schaffer PM, Jori G, et al. Radiation therapy combined with photofrin or 5-ALA: effect on Lewis sarcoma tumor lines implanted in mice. Preliminary results. *Tumori.* 2002;88(5):407–410.

Supplementary materials

Singlet oxygen generation at 690 nm irradiation

In this study, we exposed poly(D,L-lactide-co-glycolic acid) (PLGA) nanoparticles (NPs) incorporating verteporfin (VP; samples 1–5 with VP concentrations of 0 μM , 4.5 μM , 15.9 μM , 26.4 μM and 39.6 μM , respectively) to a 690 nm light-emitting diode (LED; 15 mW cm^{-2}) and used singlet oxygen sensor green (SOSG) for the detection of the generated singlet oxygen. A very weak SOSG fluorescence (maximum at 525 nm at 488 nm excitation) was observed in all samples prior to illumination in agreement with earlier reports. Figure S1A shows increased SOSG fluorescence signals at 525 nm as a function of irradiation time for different samples verifying singlet oxygen generation. The variation of SOSG fluorescence in sample 1 was not clearly observed compared with other samples (samples 2–5), which indicates that pure PLGA does not affect the singlet oxygen generation rate. Among these samples, sample 3 showed the most efficient singlet oxygen generation, and this sample was selected for further folic acid (FA) conjugation and cellular photodynamic therapy (PDT) investigations. Figure S1B shows the percentage increase in SOSG intensity in sample 3 as a function of light exposure time, which was significantly higher compared with sample 1 (pure PLGA). The inset shows the fluorescence spectra of SOSG measured from sample 3 for different irradiation times.

Singlet oxygen generation from VP molecules under 6 MeV X-ray radiation

Figure S2A shows the variation of SOSG intensity as a function of radiation dose in the pure SOSG solution and a mixture of SOSG with VP. SOSG alone shows a variation in its intensity with different radiation doses. The intensity variation of SOSG in VP solution is much higher than the SOSG alone. It means that VP is generating singlet oxygen in the presence of radiation. To further confirm that ambient light is not influenced by the measurements, we evaluated singlet oxygen generation from SOSG alone and a mixture of SOSG and VP by exposing samples to 5 Gy radiation in the presence and absence of aluminum (Al) foil. We wrapped the samples with Al foil to keep the samples away from the external ultraviolet (UV) and blue light. Figure S2B shows the SOSG intensity variation under these conditions. With Al foil protection, less singlet oxygen was generated from both SOSG and the mixture sample compared with the scenario in the absence of Al foil. These results indicate that the ambient light does not have any influence on singlet oxygen generation from VP.

In vitro VP release from PLGA-VP NPs

We evaluated the in vitro VP release from PLGA-VP NPs under physiological conditions. Figure S3 shows the percentage release of VP from NPs in biological media

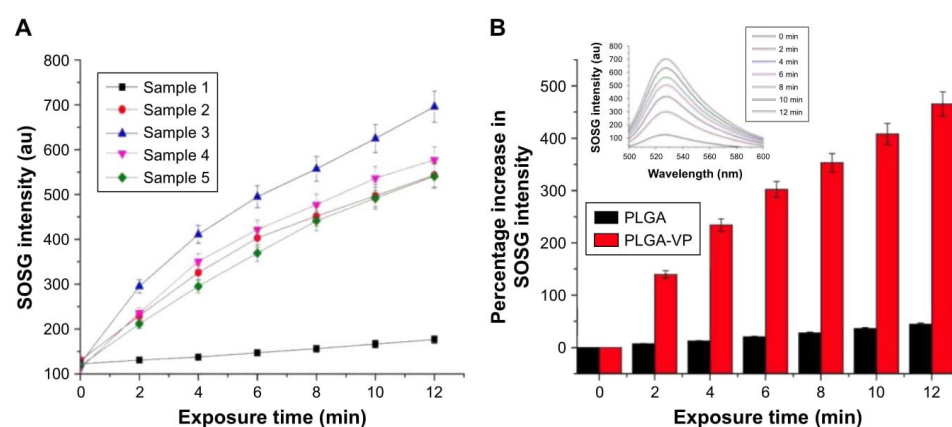


Figure S1 Singlet oxygen detection.

Notes: (A) Variation of SOSG intensity as a function of 690 nm light irradiation exposure time for different samples. (B) Comparison between the percentage increase in SOSG intensity of PLGA and the optimized PLGA-VP sample (sample 3). Inset shows the fluorescence spectra of SOSG for different exposure times used in these plots for PLGA-VP sample (excitation wavelength of 488 nm). Samples 1–5 are PLGA NPs with VP concentrations of 0 μM , 4.5 μM , 15.9 μM , 26.4 μM and 39.6 μM , respectively.

Abbreviations: PLGA, poly(D,L-lactide-co-glycolic acid); SOSG, singlet oxygen sensor green; VP, verteporfin.

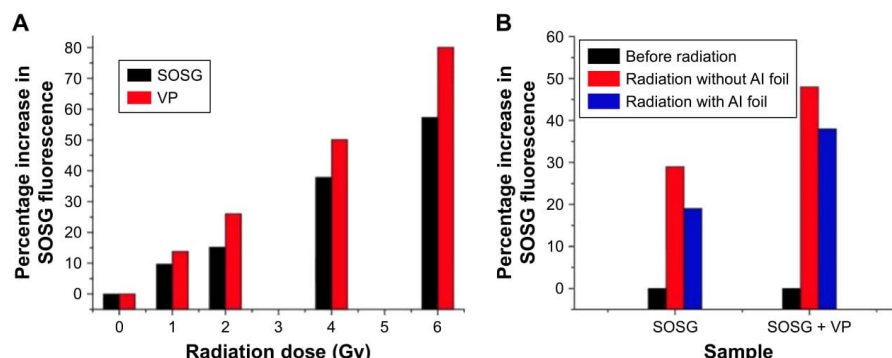


Figure S2 Singlet oxygen generation from pure VP.

Notes: (A) Variation of SOSG intensity as a function of radiation dose. (B) Variation of SOSG intensity from the control (SOSG) and VP sample in the presence and absence of Al foil. The applied radiation dose is 5 Gy.

Abbreviations: SOSG, singlet oxygen sensor green; VP, verteporfin.

(phosphate-buffered saline, PBS) with and without the presence of fetal bovine serum (FBS). Very little amount of VP was released with >95% of VP being trapped inside PLGA NPs even after 50 h. In addition, no burst release was observed during early hours of incubation. We attributed this stability to the hydrophobic nature of the VP molecules, which allowed the drug to stay inside the PLGA matrix rather than leaking to the surrounding environment. These results indicate that the as-prepared PLGA-VP sample (sample 3) is highly stable in biological conditions.

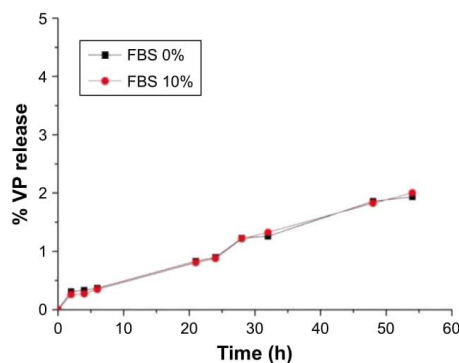


Figure S3 Percentage release of VP molecules from PLGA-VP sample as a function of time under different serum conditions (FBS 0% and FBS 10%).

Note: Data are shown for sample 3.

Abbreviations: FBS, fetal bovine serum; PLGA, poly(D,L-lactide-co-glycolic acid); VP, verteporfin.

FA conjugation

Figure S4 shows the Fourier transform infrared (FTIR) spectra of VP, FA, PLGA and PLGA-VP-FA nanoconstruct. The characteristic peaks of both FA and PLGA are highlighted.^{1,2} They were also observed in the spectra of FA-PLGA-VP nanoconstructs with a slight shift compared with pure PLGA and FA (Figure S4). The FTIR peaks in pure FA (3,324 cm^{-1} , 2,923 cm^{-1} , 1,603 cm^{-1} and 1,189 cm^{-1}) were also observed in FA-PLGA-VP albeit with a slight shift (3,329 cm^{-1} , 2,942 cm^{-1} , 1,600 cm^{-1} and 1,265 cm^{-1}).

Colocalization between nanoconstructs and lysosomes

Figure S5 shows the confocal images of colocalization between FA-PLGA-VP nanoconstructs and lysosomes in HCT116 cells. Lysosomes were labeled with LysoTracker™ Red DND-99, product number L7528; Thermo Fisher Scientific, Waltham, MA, USA. To differentiate the color between VP and LysoTracker, the VP fluorescence is shown with artificial green color. Three image analysis methods were conducted to determine the correlation between the red and green color images as shown in Figure S5, and the analysis results are demonstrated in Figure S6. As shown in Figure S6, the correlation was reduced as the incubation time was increased, which was confirmed by both the Pearson and Manders coefficients.

Cytotoxicity of NPs on HCT116 and CCD 841 CoN cells

Figure S7 shows the cellular viability after incubation with different NP samples with the same concentration of PLGA.

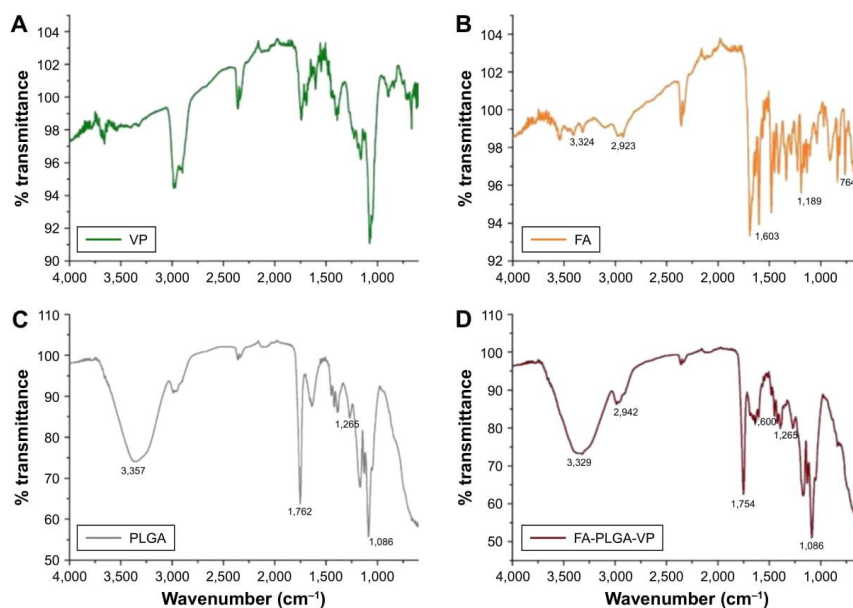


Figure S4 FTIR spectra corresponding to VP (A), FA (B), PLGA (C) and FA-PLGA-VP (D).

Abbreviations: FA, folic acid; FTIR, Fourier transform infrared; PLGA, poly(D,L-lactide-co-glycolic acid); VP, verteporfin.

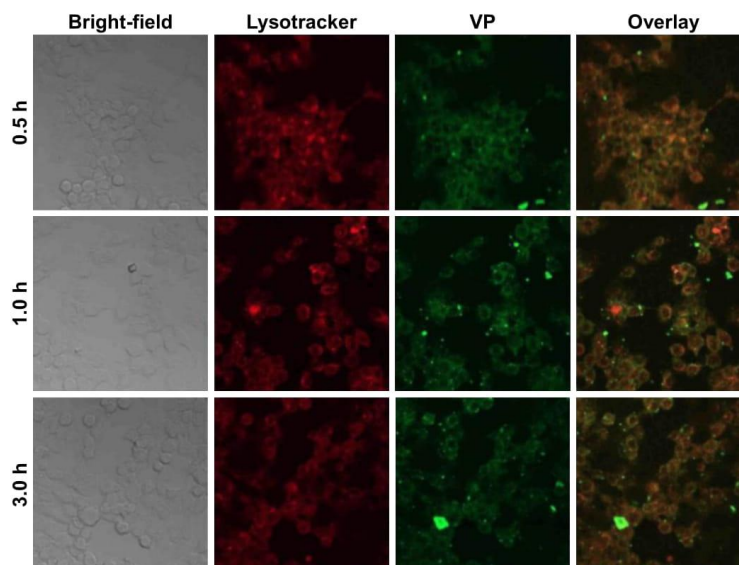


Figure S5 Colocalization of confocal imaging of FA-PLGA-VP in HCT116 cells.

Notes: Red fluorescence, Lysotracker; green fluorescence, emission of VP under 405 nm excitation. Image colors were modified to distinguish Lysotracker from the VP emission. All images were taken with 40 \times magnification.

Abbreviations: FA, folic acid; PLGA, poly(D,L-lactide-co-glycolic acid); VP, verteporfin.

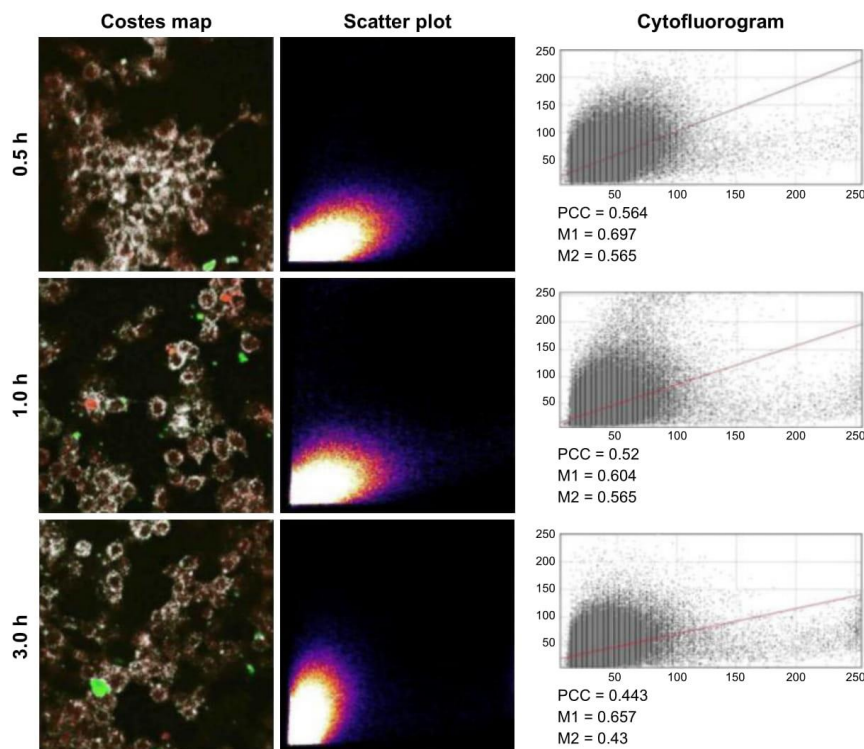


Figure S6 Colocalization of image correlation analysis with ImageJ Costes map, scatter plot and cytofluorogram for the images as shown in Figure S2. **Notes:** M1 and M2 represent the Manders correlation coefficients. All images were taken with 40 \times magnification. **Abbreviation:** PCC, Pearson's correlation coefficient.

The viability of both CCD 841 CoN and HCT116 cells was not visibly affected after treatment with >95% viability in all cell samples. Hence, we chose this concentration of NP samples for PDT experiments in this study.

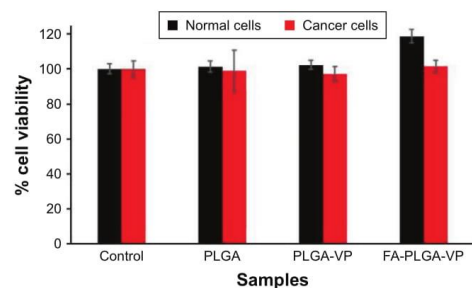


Figure S7 Viability of normal epithelial (CCD 841 CoN) and cancer cells (HCT116) toward PLGA, PLGA-VP and FA-PLGA-VP samples. **Abbreviations:** FA, folic acid; PLGA, poly(D,L-lactide-co-glycolic acid); VP, verteporfin.

PDT with 690 nm irradiation

This section demonstrated the PDT effect on colorectal cancer cell incubated with FA-PLGA-VP under 690 nm irradiation. Figure S8 shows the image of HCT116 cells with different treatments. The PDT effects were analyzed using the live/dead cell kit by differentially staining live and dead cells. The live cells are characterized by their ability to convert non-fluorescent calcein acetoxymethyl ester to fluorescent (green) calcein.³ This calcein remains in the cytoplasm, and its fluorescence can be imaged in laser scanning confocal microscopy at 494 nm excitation. On the other hand, dead cells are permeable, enabling access of ethidium homodimer-1 to the nuclei. Nuclei-bound ethidium homodimer-1 is fluorescent (red) at 528 nm excitation. Figure S8 shows that almost all cells are alive in control cells as well as cells exposed to light. Most of the cells are alive in the FA-PLGA-VP-treated sample, even though there is a red signal from dead cells in the FA-PLGA-VP-treated cells. The FA-PLGA-VP sample

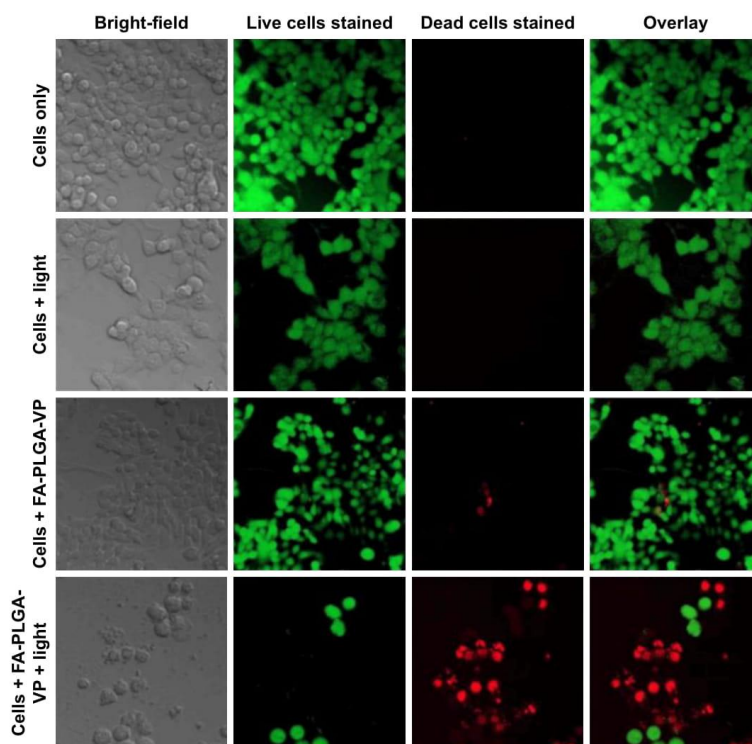


Figure S8 Confocal images of HCT116 cells after carrying out PDT under 690 nm for 10 min (15 mW cm^{-2}) using live/dead cell staining.

Notes: Green fluorescence, live cell staining with calcein AM (494 nm excitation); red fluorescence, dead cell staining with ethidium homodimer-1 (517 nm excitation). All images were taken with 40 \times magnification.

Abbreviations: AM, acetoxymethyl; FA, folic acid; PDT, photodynamic therapy; PLGA, poly(D,L-lactide-co-glycolic acid); VP, verteporfin.

treated with 690 nm light shows that most of the cells are dead after 10 min of irradiation. This is due to the fact that FA in the FA-PLGA-VP increased cellular uptake of NPs, whereas 690 nm irradiation triggered the VP in the mitochondria, thereby inducing a stronger cell-killing effect.

2. Chandrasekar D, Sistla R, Ahmad FJ, Khar RK, Diwan PV. Folate coupled poly (ethyleneglycol) conjugates of anionic poly (amidoamine) dendrimer for inflammatory tissue specific drug delivery. *J Biomed Mater Res A*. 2007;82(1):92–103.
3. Bourke S, Mason HS, Borok Z, Kim K-J, Crandall ED, Kemp PJ. Development of a lung slice preparation for recording ion channel activity in alveolar epithelial type I cells. *Respir Res*. 2005;6(1):1.

References

1. Hu Y, Zhao Z, Ehrich M, Fuhrman K, Zhang C. In vitro controlled release of antigen in dendritic cells using pH-sensitive liposome-polymeric hybrid nanoparticles. *Polymer*. 2015;80:171–179.

International Journal of Nanomedicine

Publish your work in this journal

The International Journal of Nanomedicine is an international, peer-reviewed journal focusing on the application of nanotechnology in diagnostics, therapeutics, and drug delivery systems throughout the biomedical field. This journal is indexed on PubMed Central, MedLine, CAS, SciSearch®, Current Contents®/Clinical Medicine,

Submit your manuscript here: <http://www.dovepress.com/international-journal-of-nanomedicine-journal>

Dovepress

Journal Citation Reports/Science Edition, EMBASE, Scopus and the Elsevier Bibliographic databases. The manuscript management system is completely online and includes a very quick and fair peer-review system, which is all easy to use. Visit <http://www.dovepress.com/testimonials.php> to read real quotes from published authors.

5

X-ray radiation-induced gene release and drug delivery *in vivo*

CHAPTER 5 Paper 4

Controlled gene and drug release from a liposomal delivery platform incorporating photosensitizers and gold nanoparticles triggered by X-ray radiation

Wei Deng^{*1,5}, Wenjie Chen ^{†1}, Sandhya Clement ^{†1}, Anna Guller², Zhenjun Zhao², Alexander Engel^{3,4,5} and Ewa M Goldys^{*1}(2018). *Nature Communication*, 9 (1), 2713.

Summary of author contributions to this paper.

	W.D.	W.C.	S.C.	A.G.	Z.Z.	A.E.	EM.G.
Project design	●					●	●
Nano material	●		●				
Animal experiment	●	●		●	●		
Data analysis	●	●	●				
Manuscript	●	●	●	●		●	●



ARTICLE

DOI: 10.1038/s41467-018-05118-3

OPEN

Controlled gene and drug release from a liposomal delivery platform triggered by X-ray radiation

Wei Deng^{1,7}, Wenjie Chen¹, Sandhya Clement^{1,7}, Anna Guller^{1,2,3,7}, Zhenjun Zhao², Alexander Engel^{4,5,6} & Ewa M. Goldys^{1,7}

Liposomes have been well established as an effective drug delivery system, due to simplicity of their preparation and unique characteristics. However conventional liposomes are unsuitable for the on-demand content release, which limits their therapeutic utility. Here we report X-ray-triggerable liposomes incorporating gold nanoparticles and photosensitizer verteporfin. The 6 MeV X-ray radiation induces verteporfin to produce singlet oxygen, which destabilises the liposomal membrane and causes the release of cargos from the liposomal cavity. This triggering strategy is demonstrated by the efficiency of gene silencing in vitro and increased effectiveness of chemotherapy in vivo. Our work indicates the feasibility of a combinatorial treatment and possible synergistic effects in the course of standard radiotherapy combined with chemotherapy delivered via X-ray-triggered liposomes. Importantly, our X-ray-mediated liposome release strategy offers prospects for deep tissue photodynamic therapy, by removing its depth limitation.

¹ARC Centre of Excellence for Nanoscale Biophotonics, Faculty of Science and Engineering, Macquarie University, North Ryde, 2109 New South Wales, Australia. ²Faculty of Medicine and Health Sciences, Macquarie University, North Ryde, 2109 NSW, Australia. ³Sechenov University, Moscow, 119992, Russia. ⁴Sydney Medical School, University of Sydney, Sydney, 2050 NSW, Australia. ⁵Department of Colorectal Surgery, Royal North Shore Hospital, St Leonards, 2065 NSW, Australia. ⁶Sydney Vital Translational Cancer Research, Kolling Institute of Medical Research, Northern Sydney Local Health District, St Leonards, 2065 NSW, Australia. ⁷Present address: The Graduate School of Biomedical Engineering, University of New South Wales, Sydney, Kensington, 2052 NSW, Australia. These authors contributed equally: Wenjie Chen, Sandhya Clement. Correspondence and requests for materials should be addressed to W.D. (email: wei.deng@mq.edu.au or (email: wei.deng@unsw.edu.au) or to E.M.G. (email: e.goldys@unsw.edu.au)

ARTICLE

NATURE COMMUNICATIONS | DOI: 10.1038/s41467-018-05118-3

The development and application of various nanomaterial designs for gene and drug delivery is currently one of the key focus areas in nanomedicine. Although viral carriers have been traditionally used as a gene/drug delivery method^{1,2}, their application is hindered by a range of limitations including immunogenicity, limited size of transgenic materials, packaging difficulties and the risk of recombination³. Furthermore, viral carriers do not offer any temporal control over transfection which, once introduced, cannot be deliberately stopped⁴. To overcome these limitations, synthetic nanomaterial-based systems have been extensively studied and developed. Among these nanomaterials, liposomes have been well established as an effective drug delivery system, due to simplicity of their preparation and unique characteristics^{5,6}. Liposomes consist of an aqueous core surrounded by a lipid bilayer similar to cell membranes, which facilitates cellular uptake of liposomes. The lipids forming liposomes are amphipathic, thus allowing the encapsulation of both hydrophobic and hydrophilic molecules or (and) colloidal particles⁷. Liposomes are usually biocompatible and biodegradable, which makes them suitable for clinical applications^{5,8}.

However conventional liposomes, for example, commercial lipofectamine 2000, are unsuitable for the on-demand content release, which limits their therapeutic utility, although they possess high efficiency of delivery. By contrast, triggerable liposomes are able to release genes/drugs in a more controlled manner, usually much faster and, depending on triggering modality, also to a specific area, and these properties contribute to their potentially greater clinical success. Several strategies have been previously employed to design responsive liposomes whose bilayer could be destabilised by using physiological and external stimuli. The triggering approaches previously reported include changes in pH (typical in cancer)^{9,10}, externally delivered heat, for example via alternating magnetic field or infrared light^{11,12}, enzymes^{13,14} and non-thermal effects caused by light irradiation^{15,16}. These approaches have certain limitations, in particular triggering of light-sensitive liposomes by visible light is limited by its relatively shallow (few mm) penetration of light into biological tissues¹⁷. As a result of this modest penetration depth, visible light can not activate photosensitizers (PS) located deeply in the body and generate sufficient amount of singlet oxygen (¹O₂) or other reactive oxygen species (ROS) to release the liposome cargo required for the therapeutic effects¹⁸. With its excellent tissue penetration depth, X-ray radiation explored in this work for liposome triggering offers an alternative approach to yield both spatial targeting (such as to a tumour site) via standard radiotherapy approaches such as the Gamma-knife¹⁹ and triggered release of encapsulated contents from the liposomes once they are located at the target site. Importantly, the X-ray liposome triggering can be used concurrently with radiation therapy, a common treatment modality in cancer.

Herein we design X-ray triggered liposomes by co-embedding photosensitizers and gold nanoparticles (3–5 nm) inside a lipid bilayer. Gold is chosen in this work as, due to its high atomic number, it strongly interacts with X-ray radiation as shown, for example, by gold nanoparticle-induced radiation enhancement inside biological tissue^{20–22}. Although in our design the photosensitisers are the primary source of reactive oxygen species (ROS) to oxidise unsaturated lipids and destabilise liposomal membranes, gold nanoparticles exposed to X-rays also generate some level of ROS²³. More complex effects are also possible; for example, secondary electrons produced during the interaction of X-rays with gold nanoparticles may transfer from gold to a photosensitizer and lead to PS-induced generation of ¹O₂ or other ROS^{24–26}. As a photosensitizer we choose verteporfin (VP), clinically approved for photodynamic therapy (PDT) of age-related macular degeneration^{27,28}. 1,2-dioleoyl-*sn*-glycero-3-

phosphocholine (DOPC) and 1, 2-di-(9Z-octadecenyl)-3-trimethylammonium-propane (DOTAP) are chosen as lipid components in the liposome formulation because DOPC can load highly hydrophobic molecules and DOTAP can facilitate cellular uptake due to its positive charge²⁹. The ¹O₂ generation from different liposome samples and destabilization of the lipid bilayer by ¹O₂ under 365 nm LED illumination with different time points (2, 4, 6, 8 and 10 min) and X-ray radiation with different dosage (1, 2 and 4 Gy) are assessed by using singlet oxygen green sensor (SOSG) and calcein release assays, respectively. SOSG is a commonly used and highly specific fluorescence probe for the detection of ¹O₂ generation³⁰. It is identified to be fluorescein covalently bound with an anthracene moiety³¹. Calcein is a fluorescent dye that self-quenches at high concentration^{32,33} which makes it possible to detect its release from the liposomes to the surrounding environment by monitoring the increase in calcein fluorescence intensity upon X-ray radiation^{34,35}. Additionally, ¹O₂ quantum yield under UV light illumination and the number of ¹O₂ generated as a result of X-ray radiation are also calculated based on experimental data^{36,37}. Triggered release of the liposome cargo by X-rays is verified by (a) demonstrating the efficiency of X-ray triggered gene silencing in vitro and (b) the increased effectiveness of chemotherapy in vivo (Fig. 1). For gene silencing, an antisense oligonucleotide complementary to a specific pituitary adenylate cyclase-activating polypeptide (PACAP) receptor, PAC1R, is encapsulated inside the liposomes. Following the liposome take-up by rat PC12 cells, the X-ray radiation at a dose of 4 Gy is applied. As a result of exposure to ionising radiation, the ¹O₂ generated in a lipid bilayer destabilises the liposomes, leading to the release of antisense oligonucleotides. This antisense nucleotide is then able to prevent the translation of the PAC1R mRNA by blocking the translation initiation complex. Gene knockdown is monitored by observing a decrease in the fluorescence intensity from indirect immunofluorescence staining

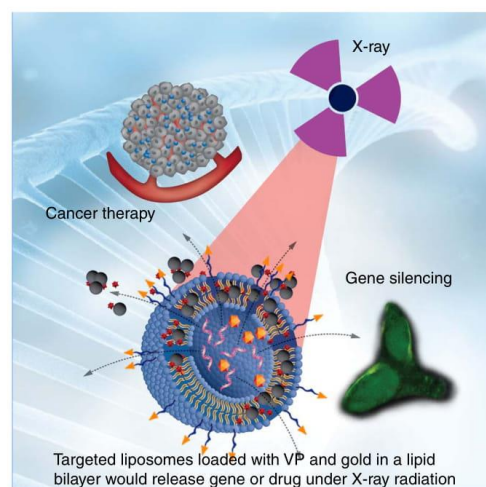


Fig. 1 The schematic illustration of gene silencing and cancer cell-killing by X-ray-triggered liposomes. This liposomal delivery platform incorporates verteporfin (VP) and gold nanoparticles. Two types of cargos, antisense oligonucleotide and Doxorubicin, are respectively entrapped inside a liposomal middle cavity for demonstration of in vitro gene release and in vivo drug delivery

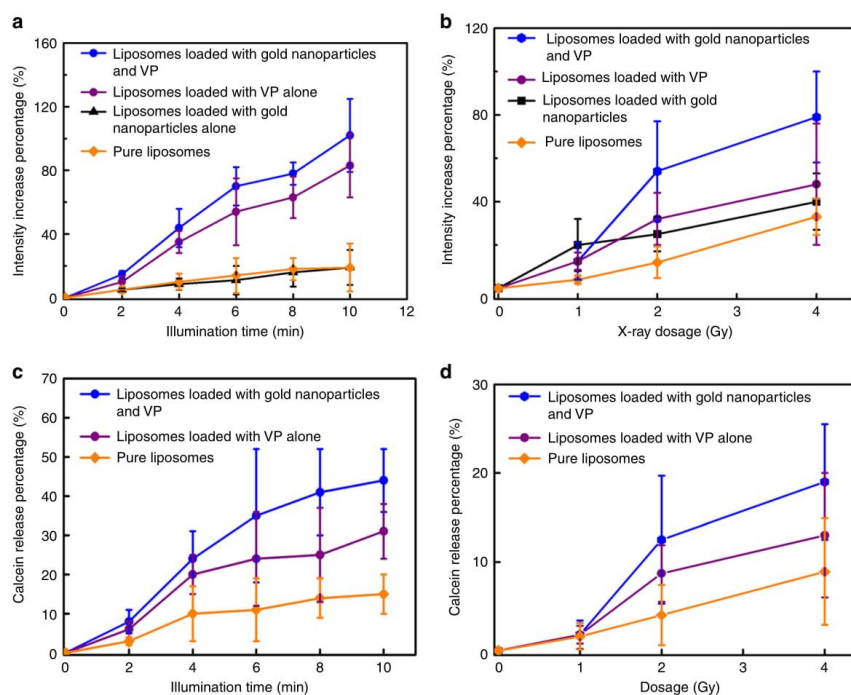


Fig. 2 Singlet oxygen generation and calcein release from liposomes under light and X-ray triggering. **a, b** Percentage increase of SOSG fluorescence intensities from different liposome samples under **(a)** 360 nm irradiation at different time points and **(b)** X-ray radiation with different doses. **c, d** Calcein release profiles from liposomes under **(c)** 360 nm irradiation and **(d)** X-ray radiation. Error bars show standard deviation from four measurements

of PAC1R in cells after X-ray irradiation. For X-ray-triggered chemotherapy, an antitumour drug, doxorubicin (Dox), is loaded into the liposomes. The liposomes are taken up by human colorectal cancer HCT 116 cells and X-rays applied. In vivo anti-tumour effect is evaluated by monitoring tumour development and body weight of mice bearing colorectal cancer xenografts and by conducting histological analysis of tumour tissues after the treatments.

Results

¹O₂ generation tests by using light and X-rays respectively. The generation of singlet oxygen is a key factor in the oxidation of unsaturated lipids, resulting in the disruption of the liposome structure²⁶. ¹O₂ generation was confirmed by using SOSG and monitoring the enhancement of fluorescence intensity at 488 nm excitation. ¹O₂ reacts with SOSG to produce endoperoxides which have a strong fluorescence signal at 525 nm for 488 nm excitation, while it has weak fluorescence in the absence of ¹O₂. The SOSG fluorescence intensity enhancement as a function of light illumination time and X-ray dose, respectively, is plotted in Fig. 2. Figure 2a shows that the liposomes loaded with gold nanoparticles and VP generate more singlet oxygen than the other samples, with an increase of about 102% after 10 min illumination. Singlet oxygen quantum yield (SOQY) from this sample (liposomes loaded with gold nanoparticles and VP) is calculated to be 0.75 ± 0.18 (mean value \pm standard deviation), indicating an enhancement factor of 1.42 compared with the

liposomes loaded with VP alone. The details of this calculation are explained in Supplementary Note 2. We attribute this enhancement of ¹O₂ generation from VP to near-field enhancement of electromagnetic field induced by gold nanoparticles^{38,39}. However such enhancement was dependent on one of experimental factors, the distance between gold and photosensitisers. In this study the distance between gold nanoparticles and VP molecules was not controllable under the current condition because both were randomly loaded in the liposomal bilayer, with some molecules less than optimally placed in terms of the distance for optimal enhancement of singlet oxygen generation. This may partially contribute to the singlet oxygen generation enhancement limited within a certain range as observed in this study. In particular, the interaction between gold and photosensitisers would not contribute to the singlet oxygen generation when they are extremely close^{40,41}.

Similarly, the enhancement of ¹O₂ generation was observed in liposomes loaded with gold nanoparticles and VP in our X-ray radiation experiments as well, but to a lesser extent. As shown in Fig. 2b, liposomes doped with gold nanoparticles and VP molecules generate the highest amount of ¹O₂, with a percentage increase of approximately 79% under X-ray radiation with 4 Gy, while liposomes containing gold nanoparticles alone and the sample containing VP alone produced a limited amount of ¹O₂, with a percentage increase of approximately 48% and 40%, respectively, under the same experimental conditions. We calculated the number of singlet oxygen generated from liposomes loaded with VP and gold nanoparticles under X-ray

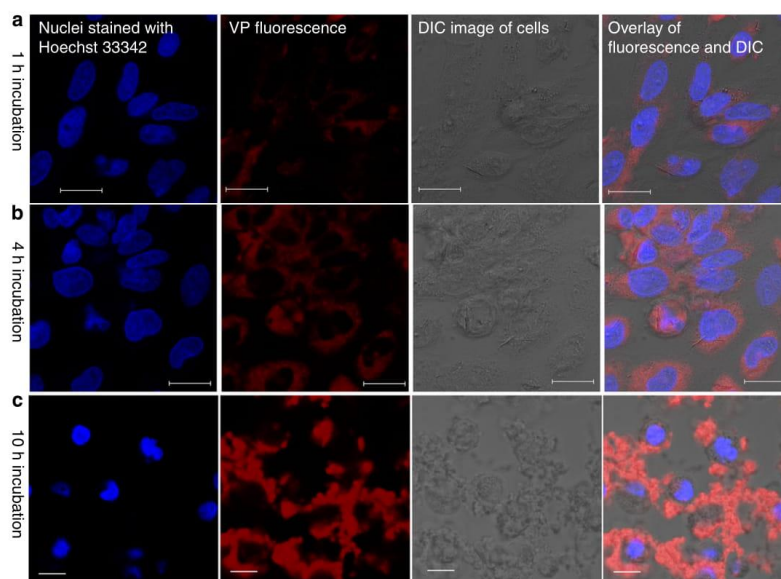


Fig. 3 Cellular uptake activity of liposomes in rat PC12 cells. **a–c** Representative confocal laser scanning microscopy images of PC12 cells incubated with liposome nanoparticles (25 μ M) for 1, 4 and 10 h, respectively. Scale bar is 20 μ m

radiation with 4 Gy, to be 7250 per a single liposome. The calculation is provided in Supplementary Note 3. The observed enhancement of X-ray induced $^1\text{O}_2$ generation in the presence of gold nanoparticles can be explained by the following mechanism. Gold is a heavy metal element strongly interacting with X-rays, which leads to a significant increase of energy deposition in biological tissues when irradiated with such rays^{42–44}. Therefore gold nanoparticles are well-known radiosensitizers able to amplify the radiation doses in tumour tissue^{45–47}. In addition, gold nanoparticles can selectively scatter and (or) absorb the high energy X-ray radiation^{20–22}, leading to enhanced energy transfer from X-ray to photosensitizers. With such contribution, the VP molecules in the presence of gold nanoparticles are able to interact more strongly with ionising radiation than the VP on its own, causing enhanced $^1\text{O}_2$ generation.

Calcein release assays under two external stimuli. Having confirmed the $^1\text{O}_2$ generation from VP entrapped inside liposomes using two stimulating modalities, we attempted to evaluate the liposome content release by using a calcein release assay, which is based on the principle of fluorescence self-quenching^{48,49}. Figure 2c,d shows the proportion of calcein release from different liposome samples under UV illumination and X-ray exposure, respectively. The amount of calcein released from liposomes doped with both gold nanoparticles and VP reaches a maximum of 44% after 10 min light illumination (Fig. 2c) and 19% after X-ray radiation with 4 Gy (Fig. 2d), respectively. However, lower leakage is observed in the controls (liposomes doped with VP alone), with only 31 and 13% of calcein being released at the same experimental conditions. Similarly to our results of the $^1\text{O}_2$ generation, our findings show that introduction of gold nanoparticles inside liposomes contributes to increased release of entrapped calcein, compared with samples

containing VP molecules only, under both UV illumination and X-ray radiation.

Cellular uptake of liposomes in PC12 cells. In order to investigate the cellular uptake of liposomes, the PC12 cells were treated with liposomes for 1 h, 4 h and 10 h. As shown in Fig. 3, higher red fluorescence signal from VP was observed after 4-h incubation compared with cells treated for 1 h. Detailed characterisation of the cellular uptake of liposomes after 4 h incubation with PC12 cells is provided in the Supplementary Fig. 6. In addition, green fluorescence from fluorescein amidite (FAM)-labelled oligonucleotide is also clearly observed after 4 h incubation (Supplementary Fig. 7). After 10 h incubation with liposomes, cells were surrounded by large red clusters, indicating a large amount of liposomes loaded with VP were internalised by cells. However, some clusters were also observed in other regions due to non-specific binding (Fig. 3). Therefore, we chose 4 h incubation time for PC12 cells. Based on the concentration of fluorescently labelled lipid internalised by cells, we estimated that 2550 ± 89 liposomes were internalised by each PC12 cell. The number of gold nanoparticles per liposome is estimated to be 156 ± 24 on the basis of the ICP-MS data. Therefore, the number of gold nanoparticles internalised by each PC12 cell is estimated to be 3.98×10^5 in this study. The detailed calculation of the number of liposome per cell and the number of gold nanoparticles per liposome is provided in Supplementary Note 4.

Cellular uptake of folate-conjugated liposomes. The folate receptor (FR) is significantly expressed in many types of cancer cells while its expression in most normal tissues is generally low⁵⁰. Folic acid (FA) has a very high affinity for the FRs with a minimal effect on its binding ability even after conjugation with other nanomaterials. Therefore FA can significantly enhance the

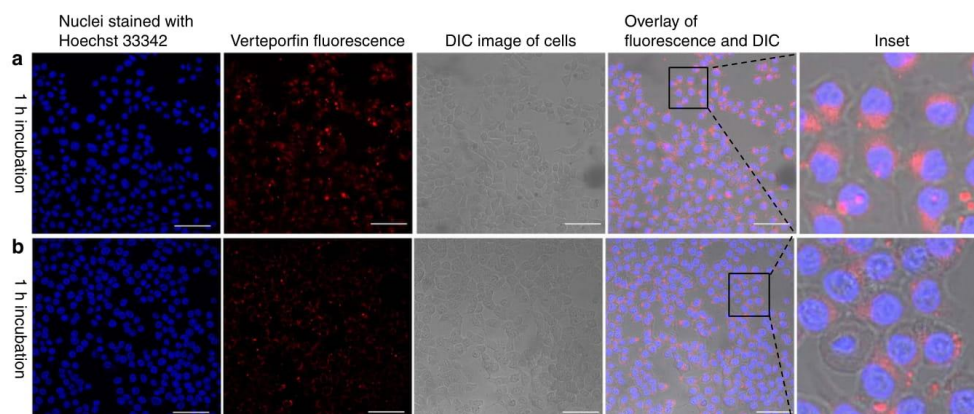


Fig. 4 Cellular uptake of folate-conjugated liposomes in HCT 116 cells and CCD 841 CoN cells. **a, b** Representative confocal laser scanning microscopy images of incubated (**a**) HCT 116 cells and (**b**) CCD 841 CoN cells with folate-conjugate liposomes (25 μ M) for 1 h. Scale bar is 75 μ m

capability of nanoparticle-based delivery systems to target cancer cells^{51,52}. In this study, we modified the liposome surface with folate and determined the average number of the folate molecules per liposome (estimated to be approximately 480) based on the total amount of folate and liposomes in the sample. To evaluate the targeting specificity of the folate-targeted liposomes to tumour cells, the uptake activity of liposomes by colorectal cancer HCT 116 cells, was compared to the uptake by normal human colonic cell line, CCD 841 CoN. As shown in Fig. 4a, cancer cells treated with folate-conjugated liposome nanoparticles clearly exhibited red signal from VP in the cytoplasm after 1 h incubation. By contrast, the level of liposome uptake by CCD 841 CoN cells is shown to be fairly low under the same experimental conditions (Fig. 4b). These results indicated that FA- induced specific binding to the folate receptor expressed on HCT 116 cell surface resulted in a higher internalisation rate of targeted liposomes, compared to the normal CCD 841 CoN cells.

X-ray triggered in vitro gene silencing and chemotherapy. We further applied the liposomes loaded with antisense oligonucleotide to carry out the PAC1R gene knockdown by delivering the liposomes to PC12 cells and applying 4 Gy of X-ray radiation. The fluorescently labelled PAC1R expressed by PC12 cells was imaged by using confocal microscopy at various time points. For comparison, the cells treated with liposomes alone, but without triggering were also imaged using the same imaging conditions. As shown in Fig. 5a, decreased fluorescence in cell samples was clearly observed 24 h after X-ray exposure, indicating that the antisense oligonucleotide released from liposomes effectively knocked down the PAC1R gene expression. For cells treated with liposomes alone, a decreased PAC1R fluorescence signal was also observed at 24 h after treatment, but the decrease was less pronounced compared to cells treated with X-ray radiation (Fig. 5b). We quantitatively analysed the PAC1R inhibition at different time points based on cellular fluorescence images. After 24 h since X-ray exposure the density of PAC1R decreased by about 45%, while the level of PAC1R in cells which were not exposed to X-rays but received the liposomes with antisense oligonucleotides decreased by only 30% (Fig. 5c, d).

In addition to the demonstration of gene silencing by using X-ray-triggered liposomes, we also investigated the in vitro cell-

killing effect of the liposomes loaded with varying amounts of antitumour drugs, Dox and etoposide (ETP), in HCT 116 cells. A series of drug-dilution assays presented in Supplementary Figure 8a reveals that 50% cell-killing (IC_{50}) was achieved at 1.6 μ M of Dox encapsulated in the liposomes (LipoDox) and triggered by X-ray radiation. However, the LipoDox alone, without X-ray triggering but with same Dox concentration of 1.6 μ M killed only about 10% of cancer cells (Supplementary Fig. 8b). This illustrates, not unexpectedly, that the efficacy of LipoDox for cell killing was higher with X-ray radiation, compared with LipoDox only. The results of our X-ray-triggered LipoDox treatment described here indicates that a combination of X-ray-triggered chemo- and radiotherapy with the same X-rays appears to produce an enhanced effect and it yields improved efficacy of cancer cell-killing. It should be mentioned that simultaneous chemo- and radiotherapy may result in the development of cardiotoxicity, whose incidence is associated with different factors, including the type of antitumour drugs⁵³. Therefore, we evaluated the cell-killing effect of a second chemotherapy drug, ETP, in combination with X-ray radiation. ETP is associated with reduced incidence of cardiotoxicity, compared with Dox⁵⁴. As shown in Supplementary Fig. 8c, higher cytotoxicity of LipoETP in HCT 116 cells was observed at 24 h after X-ray radiation of 4 Gy, compared with LipoETP alone.

Toxicity assays of liposomes and X-ray exposure. We first assessed the toxicity of liposomes doped with gold nanoparticles and VP. Compared with the control group, no significant change was observed in the viability of PC12 cells treated with liposome concentrations up to 50 μ M, higher than those used for gene and drug delivery in our study (Supplementary Fig. 9a). The liposome-formulated Dox designed in this study should also have minimal toxicity effect on normal cells without X-ray-triggering. To verify this, we examined the toxicity of LipoDox on CCD 841 CoN cells by varying Dox concentration. As shown in Supplementary Fig. 9b, we did not observe a noticeable reduction in cell survival (up to 14% cell death) at 24 h after incubation with liposome-formulated Dox samples (Dox concentration: 3 μ g mL⁻¹ and 2 μ g mL⁻¹), suggesting that under in vitro conditions, our LipoDox samples with these two Dox concentrations are likely not to affect the viability of CCD 841 CoN cells.

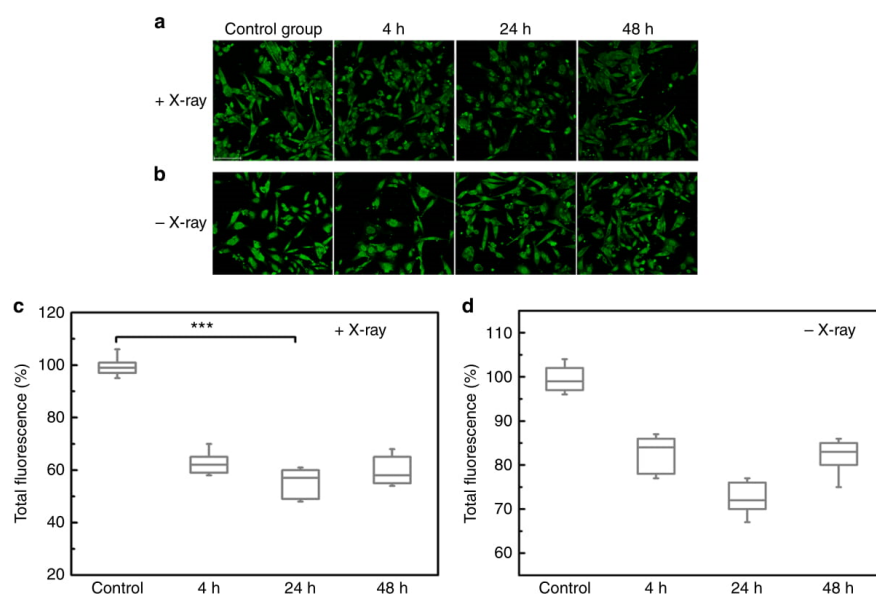


Fig. 5 In vitro gene silencing by X-ray triggered liposomes loaded with antisense oligonucleotide. **a, b** Representative confocal images of indirect immunofluorescence staining of PAC1R at different time points after cells were treated with **(a)** X-ray-triggered liposomes and **(b)** liposomes alone. The concentration of liposomes incubated with cells was 25 μ M. Scale bar was 75 μ m. Boxplots in **c, d** show quantitative assessment of PAC1R gene silencing induced by antisense oligonucleotide released from liposomes at different time points **(c)** with and **(d)** without X-ray radiation. Decreased PAC1R fluorescence intensity was expressed as percentage of the control. The box is bounded by the first and third quartile with a horizontal line at the median and whiskers extend to 1.5 times the interquartile range. The mean value was analysed using the *t* test (*n* = 5). *** *P* < 0.001, compared with the control group

It is well known that radiolysis of water molecules as a result of X-ray radiation damages DNA molecules by producing toxic radicals. Although cells attempt to repair the damage, complete repair may not be possible at higher doses⁵⁵. The surviving cells may suffer residual DNA damage, potentially contributing to adverse long-term health effects. In this study we assessed the X-ray-induced damage in both cultured cells and genetic materials. In cell experiments, the MTS test did not reveal a clear decrease in survival of PC12 cells, HCT 116 cells and CCD 841 CoN cells at 24 h and 48 h after X-ray exposure (Supplementary Fig. 9c). With regard to the X-ray effects on genes, the DNA gel electrophoresis did not show obvious dispersion of DNA bands after X-ray radiation compared to the control, indicating that X-ray radiation with our applied dosage did not cause obvious damage to the DNA molecules (Supplementary Fig. 9d).

In addition, we also checked the effect of the singlet oxygen on genetic material by irradiating a mixture solution of oligonucleotides and VP with X-ray. As shown in Supplementary Fig. 9d, there was no clear oligonucleotide damage observed compared with the control. Singlet oxygen is the primary cytotoxic agent responsible for photobiological activity involved in the PDT technique. It can damage cells by reacting with many biomolecules, including amino acids, nucleic acids and unsaturated fatty acids that have double bonds as well as sulphur-containing amino acids^{56,57}. Short lifetime of singlet oxygen prevents it from travelling larger distances, therefore it mainly causes localised⁵⁸, near the photosensitizer molecule where it was generated. In this study, singlet oxygen generated from VP loaded in a lipid bilayer

mainly destabilises the unsaturated lipids and consequently induces drug release. This reaction with lipids consumes singlet oxygen radicals⁵⁹. Therefore, adverse effect of singlet oxygen on oligonucleotides will be minimised.

Therapeutic effect of X-ray-triggered liposomes in vivo. To determine the efficacy of X-ray-triggered liposomes in vivo, we detected their ability to control tumour growth in a xenograft mouse model bearing HCT 1116 cells. Based on the in vitro work, 4 Gy was chosen for irradiation on mice. The sizes of tumours in mice treated with different conditions are presented in Fig. 6a. PBS-, liposome- and X-ray-treated tumours respectively increased 3.0-fold, 2.9-fold, and 3.4-fold during the study period (two weeks post treatment), indicating that these treatments failed to delay tumour progression. By contrast, in the group treated with X-ray-triggered liposomes the tumour sizes gradually shrunk over this period, with 74% reduction in tumour volume compared to the PBS control group. The size of tumours in mice exposed to different treatments were also photographed and presented in Supplementary Fig. 10a. This figure shows that tumours in mice treated with X-ray-triggered liposomes grew more slowly in comparison with PBS control, X-ray radiation alone, and liposomes alone. In addition, no mortality was observed during 14 days after treatment with X-ray-triggered liposomes, and no weight loss of treated mice was observed compared to the control, suggesting that this combined technique is well tolerated by mice under the present conditions (Fig. 6b). Histological analysis was also performed to further verify the tumour response to the

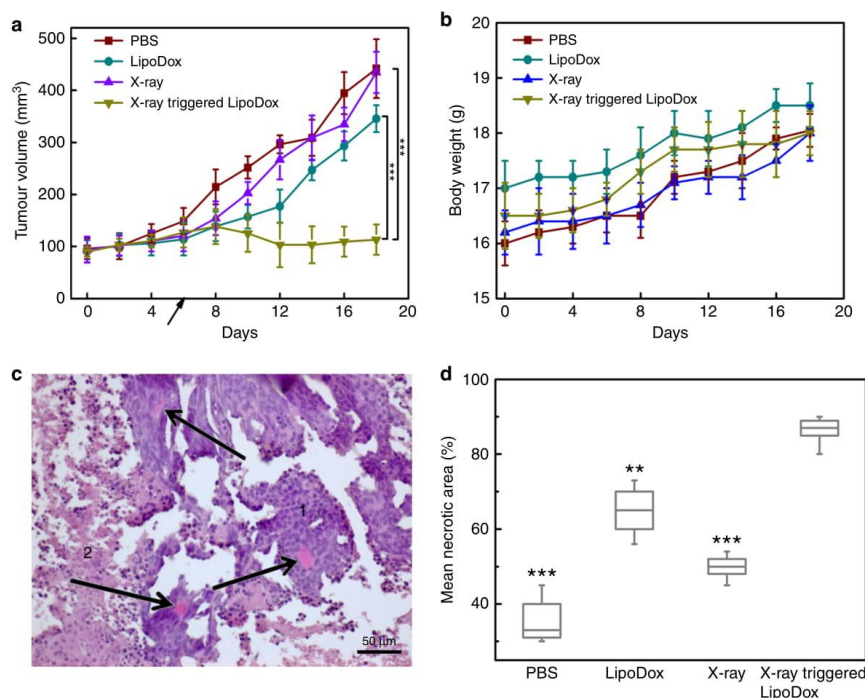


Fig. 6 Antitumour activity of X-ray triggered LipoDox in a xenograft model of colorectal cancer. **a,b** Changes of (a) tumours' volume and (b) mouse body weight after various treatments as indicated. A black arrow indicates the time of treatment administration. Error bars show standard deviation from four experiments. The mean tumour volumes were analysed using the *t* test ($n = 4$). * $P < 0.05$, ** $P < 0.01$, *** $P < 0.001$. **c** The structural components of treated tumour (H&E staining). Viable tumour tissues (1) were composed of uniform cells with basophilic (blue) cytoplasm and large roundish hyperchromatic nuclei. The areas of cellular paranecrosis and necrosis (2) were recognised by disorganised groups of tumour cells with eosinophilic (pink) cytoplasm, with and without nuclei, respectively. Arrows indicate congested blood vessels. Note the spatial association between the viable tumour tissue and blood vessels. Scale bar is 50 μm. **d** Boxplot shows morphometric analysis of the effect of the experimental treatment regimens on the structural composition of the xenograft tumours. The relative areas of the viable and non-viable (paranecrotic and necrotic) tumour tissues were measured using ImageJ open source software. The box is bounded by the first and third quartile with a horizontal line at the median and whiskers extend to 1.5 times the interquartile range. The mean tumour necrosis percentage was analysed using the *t* test ($n = 5$). * $P < 0.05$, ** $P < 0.01$, *** $P < 0.001$, compared with X-ray-triggered LipoDox-treated group

treatments. All tumours were found to be localised subcutaneously and surrounded by a thin capsule of connective tissue. No tumour invasion into the capsule tissue was observed. The tumours had a mixed histological structure, with various spatial combinations of viable, paranecrotic and necrotic tumour tissues (Fig. 6c). In general, viable tissues were localized mainly at the periphery of the tumours or near the blood vessels, while the non-viable elements were found more centrally, implying the contribution of intrinsic tumour hypoxia and the oxidative stress induced by the experimental treatments to the suppression of tumour growth. The mean percentage of necrotised tumour tissues showed statistically significant differences between the studied groups, with the maximal tumour necrosis being achieved when treated with X-ray triggered LipoDox (Fig. 6d). These findings further confirmed that this strategy can achieve better therapeutic effect compared with individual modality treatment. More detailed histological analysis for each treatment (PBS-, X-ray-, LipoDox-, and X-ray-triggered LipoDox-treated) is provided in Supplementary Note 6.

Discussion

X-ray radiation, as an external liposome triggering modality, was employed to activate a liposomal gene/drug delivery system in this study. Our X-ray-triggerable liposomes were designed by encapsulating a photosensitizer, VP, and gold nanoparticles in a liposomal bilayer. When these liposomes were exposed to X-rays, enhanced $^1\text{O}_2$ generation from VP was achieved due to the interaction between gold nanoparticles with incident X-rays. This $^1\text{O}_2$ oxidises unsaturated lipids and destabilises the membrane, allowing the release of entrapped cargos from the liposomes. We demonstrated that this release strategy has the capacity for in vitro gene knockdown and enhanced cancer cell-killing efficacy by releasing two kinds of cargos, antisense oligonucleotide against PAC1R gene and an antitumour drug (Dox) upon X-ray radiation. In animal experiments, X-ray-triggered liposomes were demonstrated to control colorectal tumour growth more effectively than other individual modality treatment conditions.

X-rays and other forms of ionising radiation are used to diagnose and treat medical conditions and are known to

ARTICLE

NATURE COMMUNICATIONS | DOI: 10.1038/s41467-018-05118-3

contribute to DNA mutations that may lead to dose-dependent and stochastic toxic effects. Compared with light, however, X-rays with the suitable energy can easily penetrate the human body, activating gene/drug release in deep tissues once the X-ray-triggered liposomes reach their target. This feature will open many opportunities for biomedical research and clinical medicine, from triggered gene therapies and chemotherapy, through to enhanced PDT which currently suffers from limited penetration depth of illumination light (usually in the UV and visible region).

Additionally, the strategy described here has been designed to be compatible with future clinical translation. The materials and approaches used in this study, such as VP, lipids, Dox, and X-rays, are clinically used in treatment of tumours. Although gold nanoparticles used in this study have not yet been approved by the regulatory agencies, their size is compatible with the requirements of renal clearance⁶⁰. In this way, long-term nanoparticle toxicity is likely to be minimised if not eliminated. Moreover, the ease of conjugation of targeting ligands to liposome surface with appropriate linkers, for example, lipid-polyethylene glycol (PEG)⁶¹, would be an added advantage when applied to the targeted therapy, in particular for tumour treatment. From a clinical point of view, it would be beneficial to have access to this multimodality treatment, given our evidence of better therapeutic effect (or, potentially, equal therapeutic effect) at diminished toxicity in the case when single modality treatment options alone can only produce desired therapeutic effects at a significant cost of short- and long-term toxicity.

Methods

Preparation of liposomes loaded with gold and VP. 350 μL of DOTAP (Avanti Polar Lipids, no. 890890 P) dissolved in chloroform (100 mg mL^{-1} , Sigma-Aldrich, no. 288306-1 L) was mixed with 370 μL of DOPC (Avanti Polar Lipids, no. 850375 P) dissolved in chloroform (100 mg mL^{-1}), followed by addition of 40 μL of gold nanoparticle suspension (Nanocomposix, Inc) and 50 μL of VP (Sigma-Aldrich, no. SML0534-5MG) dissolved in dimethyl sulfoxide (DMSO, 2.3 mg mL^{-1} , Sigma-Aldrich, no. 472301-500 ML). For the synthesis of empty liposomes, VP and gold nanoparticles were omitted in the mixture solution. The mixture was diluted to 1.0 mL in total volume using chloroform and vortexed gently for 10 min. Chloroform was evaporated off with a stream of Argon and the remaining DMSO was evaporated under freeze-drying, which was carried out in a freeze dryer (Alpha 1-4 LDplus, John Morris Scientific Pty Ltd). The lipid film was hydrated by adding 1.0 mL of DI water to a glass test tube, followed by vigorous stirring until the suspension was homogenised. The hydrated lipid suspension was left overnight to allow the maximal swelling of liposomes. The suspension was then extruded eleven times in an extruder (Avanti Polar Lipids, Inc) with two 1.0 mL glass syringes. The pore size of the polycarbonate membrane (Avanti Polar Lipids, Inc) was 200 nm. The resulting suspension was stored at 4 °C under argon. For encapsulation of calcein inside liposomes, 1.0 mL calcein solution (100 mM, Sigma-Aldrich, no. C0875-5G) was used as lipid hydration solution, instead of DI water. For encapsulation of oligonucleotides, 1.0 mL PBS (pH 7.4) solution containing antisense oligonucleotide (10 μM , 5'-TGGTGGCTTCCAGCCACTAT-3') with 3' FAM labelling against PAC1R gene (Integrated DNA Technologies Pte. Ltd.) was used to hydrate lipid film, followed by the hydration procedure described above. In order to remove calcein and oligonucleotides present in the supernatant after hydration, liposomes were then centrifuged at 14000 $\times g$ for 10 min by using Pall Nanosep centrifugal devices (Sigma-Aldrich) as per manufacturer's instructions.

Synthesis of LipoDox. The encapsulation of doxorubicin inside of liposomes was conducted as per a published protocol, using a gradient exchange method with minor modifications⁶². 1 mL ammonium sulphate (250 mM, Sigma-Aldrich, no. A4418-100G) was added to the glass test tube where the lipid film was produced after evaporation of organic solvent, followed by the hydration procedure described above. Free ammonium sulphate was removed by dialysis in the PBS solution (pH 7.4) with buffer exchange repeated four times. The Dox solution (10 mg mL^{-1} , Sigma-Aldrich, no. D1515-10MG) was subsequently added to hydrated liposome suspension with a drug to lipid mass ratio of 1:10, followed by incubation at 60 °C for 1 h. Unloaded Dox was removed by dialysis in PBS solution (pH 7.4) with four time buffer exchange.

Preparation of liposome incorporating ETP. Liposomes incorporating ETP, VP and gold nanoparticles were prepared by thin film hydration with some modifications. Briefly, 100 μL of DOTAP (50 mg mL^{-1} in chloroform) was mixed with 54 μL of DOPC (100 mg mL^{-1} in chloroform), followed by addition of 6 μL of gold

nanoparticle suspension, 7 μL of VP (2.3 mg mL^{-1} in DMSO) and 83.5 μL of ETP (Sigma-Aldrich, no. E1383-25MG, 1 mg mL^{-1} in chloroform and ethanol (1:1 V/V)). After evaporation of organic solvent, the lipid film was hydrated with 1 mL PBS (pH 7.4). The hydration and extrusion procedure was the same as described above. The unloaded etoposide was removed by dialysis in the PBS solution (pH 7.4) with buffer exchange repeated four times.

Preparation of folate-conjugated liposomes. Folate-conjugated liposomes were prepared by postinsertion of DSPE-PEG2000-Folate micelles into preformed liposomes with slight modifications^{63,64}. In brief, 1 mg DSPE-PEG2000-folate (Avanti Polar Lipids, no. 880124) was dissolved in 320 μL DMSO, followed by hydration with 3.1 mL of distilled water, producing 100 μM micelle suspension. The suspension was then dialysed three times in a 10000 MWCO dialysis tubing against 1 L water to remove DMSO. After this, 40 μL of micelles were added to 1 mL of the preformed liposome suspension in ammonium sulphate (250 mM) and heated at 60 °C for 1 h to produce folate-tethered liposomes. Leaked ammonium sulphate and unincorporated micelles were removed by dialysis. To determine the folate content conjugated with liposomes, bare liposomes was used in conjugation procedure instead of VP-loaded liposomes. After preparation, the folate amount was determined by measuring the UV absorbance at 285 nm after lysing liposomes with 0.1% Triton X-100 and comparing with a standard curve of folic acid with the known concentration.

Characterisation of liposomes. The extinction spectra of liposomes loaded with gold nanoparticles and VP, VP alone and gold nanoparticles alone were measured using a spectrophotometer (Cary 5000 UV-Vis-NIR, Varian Inc.). Size distribution and zeta potentials of liposomes were measured with a Zetasizer Nano Series from Malvern Instruments. The morphology of liposomes was documented using Transmission Electron Microscopy (TEM). For TEM imaging, the liposome samples were prepared by placing a drop of suspension onto a copper grid and air-dried, following negative staining with one drop of 2% aqueous Uranyl Acetate for contrast enhancement. The air-dried samples were then imaged using a PHILIPS CM 10 system at an accelerating voltage of 100 KV. Images were captured with an Olympus Megaview G10 camera and iTEM software. To determine the encapsulation efficiency of oligonucleotides, Dox and etoposide loaded inside of liposomes, Triton X-100 (0.1%, Sigma-Aldrich, no. T8787-50ML) was added to as-prepared liposome solution, resulting in the gene/drug release. The FAM fluorescence from oligonucleotides (Ex/Em: 494 nm/520 nm) and Dox fluorescence (Ex/Em 485/590 nm) was recorded on a Fluorolog-Tau-3 system (Jobin Yvon-Horiba, US) and compared with the corresponding oligonucleotide and Dox standard curves, respectively. The etoposide amount was determined by measuring the UV absorbance at 285 nm under Cary UV-VIS-NIR absorption spectrophotometer (Varian Inc.) and comparing with the etoposide standard curve.

¹O₂ generation tests with light and X-ray triggering. For light illumination, a 365 nm LED was used to illuminate the samples. 16 μL of SOSG (0.5 mM, Thermo Fisher Scientific Inc, no. S36002) was mixed with 3 mL of liposome suspension and the mixture was then placed in a cuvette, followed by illumination under a 365 nm LED (2.5 mW cm^{-2} , irradiation for 10 min). After illumination, the SOSG fluorescence at 525 nm upon 488 nm excitation was recorded using a fluorescence spectrophotometer. For X-ray radiation, a linear accelerator (6 MeV LINAC, Elekta AB, Sweden) was used to deliver different doses (1 Gy, 2 Gy and 4 Gy) to the samples. 96-well plates with 200 μL of liposome suspension and 2 μL of SOSG (0.5 mM) in each well were exposed to X-ray radiation. The irradiation of samples was carried out using 6 MeV X-ray photons from the anterior and posterior directed radiation fields. After irradiation, the SOSG fluorescence was recorded using a microplate reader (PHERAstar FS system, BMG LABTECH, Germany).

Calcein release assay with light and X-ray irradiation. Liposomes loaded with calcein were separated from free calcein molecules by using Pall Nanosep® centrifugal devices (Sigma-Aldrich) equilibrated with 10 mM Tris/HCl. They were then activated by light illumination and ionizing radiation, respectively. The experiment process was the same as described in the ¹O₂ generation test, apart from the omission of SOSG. The induced release and subsequent dilution of the calcein previously contained in the liposomes, leading to an increase of calcein fluorescence^{65,66}. The calcein fluorescence signal was recorded at 510 nm upon excitation at 485 nm. The percentage of calcein release ($R_i(\%)$) at various illumination time points or X-ray dosage was calculated as follows:

$$R_i(\%) = \frac{F_{i(d)} - F_0}{F_{\max} - F_0} \times 100\% \quad (1)$$

where F_i and F_0 respectively indicate the fluorescence intensity of calcein at various illumination time points and without illumination. F_{\max} refers to the total fluorescence intensity of calcein after the disruption of liposomes by adding 0.1% Triton X-100. For X-ray radiation, F_d is the fluorescence intensity of calcein at various radiation doses, d .

Serum and pH stability studies of PEGylated liposomes. 200 μL LipoDox samples with and without PEG modification were respectively diluted in PBS (pH 7.4) containing foetal bovine serum (FBS) with different concentrations (0%, 10%, 25 and 50%). All samples were dialyzed in Slide-A-Lyzer MINI dialysis devices (Thermo Fisher Scientific). These devices were then kept in 50 mL centrifuge tubes with 10 mL PBS at 37 °C for 48 h. At various time points (0 h, 2 h, 4 h, 18 h, 24 h and 48 h), an aliquot of PBS was taken for the fluorescence characterisation of the released Dox. The total Dox fluorescence was measured by disrupting liposomes with 0.1% Triton X-100. The percentage of Dox release at various time points was calculated by using the same formula as that applied to the calcein release assays. In our pH-triggered drug release studies, 200 μL Dox-loaded PEGylated liposome suspension was incubated with PBS (containing 10% FBS) with pH respectively adjusted to 7.4 (control), 6.0 and 5.0, followed by the same dialysis procedure and fluorescence measurement described above.

Cell preparation and ionizing radiation treatment of cells. Rat PC12 cells, human colon adenocarcinoma HCT 116 cells and normal human colon epithelial cells (CCD 841 CoN) were purchased from the American Type Culture Collection. PC12 cells were cultured in Dulbecco's modified Eagle's medium (DMEM); HCT 116 cells were cultured in McCoy's 5 A (modified) medium; CCD 841 CoN cells were cultured in Eagle's Minimum Essential Medium (EMEM). All culture media were supplemented with 10% foetal bovine serum and 1% antibiotic-antimycotic. The flasks were maintained in a 37 °C incubator with 5% CO₂ humidified air. The cells were detached with trypsin and transferred at appropriate dilutions into 96-well plates for cell viability assays or glass-bottom petri dishes for cell imaging. For X-ray radiation experiments, the cells were radiated by using the same accelerator as described in the ¹O₂ generation test.

Imaging and analysis of cellular uptake of liposomes. The PC12 cells ($3 \times 10^5 \text{ mL}^{-1}$) were attached to glass-bottom petri dishes and incubated at 37 °C for 24 h. After removing the culture medium, the cells were incubated with liposome suspension (25 μM) in culture medium supplemented with 10% FBS for 1 h, 4 h and 10 h. The cells were then washed with PBS (1 ×, pH 7.4) three times to remove free liposomes. To assess the uptake of liposome nanoparticles, the cells were fixed with 2.5% paraformaldehyde for 10 min at room temperature, washed twice with PBS (1 ×, pH 7.4) and stained with Hoechst 33342 (5 $\mu\text{g mL}^{-1}$) for 10 min at room temperature before imaging. The cells were imaged using a Leica SP2 confocal laser scanning microscopy system. A violet laser at 405 nm and an argon laser at 496 nm were used for the excitation of VP and FAM-labelled oligonucleotide entrapped inside liposomes, respectively. The imaging of uptake activity of FA-targeted liposomes into HCT 116 cells and CCD 841CoN cells were also conducted as mentioned above.

For quantitative analysis, fluorescently labelled DOTAP (Avanti Polar Lipids, no. 810890 P), was employed, instead of standard DOTAP in order to prepare fluorescent liposomes. PC12 cells ($1 \times 10^5 \text{ mL}^{-1}$) were cultured in petri dishes at 37 °C for 24 h. After removing the old culture medium, 1 mL of a fresh medium containing 10 μL of fluorescently labelled liposomes (0.5 mg mL^{-1}) was added to the petri dishes and the cells were incubated at 37 °C for a further 4 h. After incubation, the cells were washed with fresh medium three times to remove free liposomes, detached with trypsin from the petri dishes and counted using a cell counter (Countess II FL automated cell counter from Thermo Scientific). 100 μL NaOH (1 M) and 100 μL Triton X-100 (1% v/v) were subsequently added to 800 μL of cell suspension. The cells were lysed at R.T. for 2 h with constant shaking. After cell lysis, fluorescence (Ex/Em: 460/535 nm) was recorded on a Fluorolog-Tau-3 system and compared with the standard curve of free fluorescent DOTAP solution. A detailed calculation of the number of liposomes per cell is described in Supplementary Note 4.

Indirect immunofluorescence staining of PAC1R. The PC12 cells were fixed with 2.5% paraformaldehyde for 10 min and permeabilized with 0.1% Triton X-100 for another 10 min at room temperature, followed by blocking with 5% bovine serum albumin for 30 min. The cells were then incubated with goat anti-PAC1R primary antibody (1:50 dilution, Santa Cruz Biotechnology, no. sc-15964) for 90 min and donkey anti goat IgG secondary antibody (1:100 dilution, Santa Cruz Biotechnology, no. sc-2024) conjugated to FITC for 30 min at room temperature.

Cytotoxicity assays of X-ray-triggered LipoDox and LipoETP. The in vitro antitumour effect of X-ray-triggered LipoDox and LipoETP was evaluated using the MTS test. Before treatment, the HCT 116 cells ($2 \times 10^4 \text{ mL}^{-1}$) were grown on 96-well plates in the culture medium with 10% FBS for 24 h. After removing the old medium, the cells were respectively incubated with a series of LipoDox and LipoETP samples diluted in the culture medium with 10% FBS for 4 h. After incubation, the old medium was removed and a fresh medium was added to cells, followed by X-ray radiation with 4 Gy. The cytotoxicity of X-ray-triggered LipoDox and LipoETP on HCT 116 cells at various time points (0 h, 2 h, 4 h and 24 h) was determined by the MTS test (Promega Co., WI, USA, no. G3582) according to manufacturer's instructions and compared with control cells without any treatment. Cell viability was then calculated as a percentage of the absorbance of the untreated control sample. The latter was set to 100%. For comparison purposes, the

viability of cells treated with LipoDox alone was also evaluated in the same experimental conditions.

Toxicity assays of LipoDox and X-ray on cells and gene. The PC12, HCT 116 and CCD 841 CoN cells ($1-4 \times 10^4 \text{ mL}^{-1}$) were, respectively, grown on 96-well plates in a culture medium with 10% FBS for 24 h. For liposome and LipoDox treatment experiments, the PC12 cells and CCD 841 CoN cells were, respectively, incubated with different liposome and LipoDox samples for 4 h, followed by incubation in a fresh medium for further 24 h. For the X-ray exposure experiments on cells, all three types of cells were radiated with 4 Gy, followed by incubation in a fresh medium for further 24 and 48 h. Cell viability was assessed by using the same method as described above. For X-ray treatment of pure DNA molecules and mixture of DNA and verteporfin, 50 μL of antisense oligonucleotide solution (10 $\mu\text{g mL}^{-1}$) and 50 μL of mixture solution (10 $\mu\text{g mL}^{-1}$ DNA and 32 $\mu\text{g mL}^{-1}$ verteporfin) was respectively exposed to X-ray radiation with different dosages (1, 2 and 4 Gy). After treatment, the gel electrophoresis was carried out in 1.2 % agarose gel in Tris-acetate-EDTA (TAE) buffer at 95 V for 45 min. The gel was stained with SYBR Safe DNA Gel Stain (Thermo Fisher) and photographed under UV light using a Bio-Rad imaging system.

In vivo antitumour efficacy by X-ray-triggered drug release. All procedures were carried out with the approval from Macquarie University Animal Ethics Committee (animal ethics approval No. 2017/001). 6–7 weeks old BALB/c nu/nu female mice (The Animal Resources Centre, Perth, Australia) were injected subcutaneously with 5×10^6 HCT 116 cells, suspended in 100 μL McCoy's 5 A (modified) medium without FBS, to the flank. Tumours were measured every two days with a caliper and volume (V) was calculated by using the following formula:

$$V = \pi/6 \times L \times W^2 \quad (2)$$

where L and W are the length (large diameter) and width (short diameter) of the tumour. When tumour volume reached approximately 100 mm^3 , mice were randomly divided into 4 groups ($n = 4$ per group) for different treatments: Group A treated PBS via intratumour injection (20 μL); Group B treated with liposome suspension via intratumour injection (20 μL , 10 mg kg^{-1} , approximately 10 μM gold nanoparticles and 20 μM VP used for each mouse); Group C treated with X-ray radiation (4 Gy, single fraction) and Group D treated with liposome suspension via intratumour injection (20 μL , 10 mg kg^{-1}) and X-ray radiation (4 Gy, single fraction). Mice were then maintained for additional 2 weeks. Body weight and tumour volume were measured every other day. After two weeks, mice were sacrificed and tumours were removed, photographed and fixed with 10% neutral-buffered formalin for histological analysis. Tumour tissues were cryosectioned into serial sections of 6 μm in thickness and stained with haematoxylin and eosin (H&E) following conventional protocol. The histological preparations were examined using an upright research microscope Axio Imager Z2 (Zeiss, Germany) equipped with dry-air EC Plan-Neofluar ($5 \times / \text{NA}0.16$; $10 \times / \text{NA}0.30$; $20 \times / \text{NA}0.50$ Ph) and oil-immersion α Plan Apochromat ($100 \times / \text{NA}1.46$ oil) objectives (Zeiss, Germany). Images were recorded using a digital video camera AxioCam (1388×1040, Zeiss, Germany) in a single-frame and stitching modes.

Data availability. The relevant data generated and (or) analysed in the current study are available from the corresponding author upon reasonable request.

Received: 18 November 2016 Accepted: 24 May 2018
Published online: 13 July 2018

References

- Thomas, C. E., Ehrhardt, A. & Kay, M. A. Progress and problems with the use of viral vectors for gene therapy. *Nat. Rev. Genet.* **4**, 346 (2003).
- Zhang, Y., Satterlee, A. & Huang, L. In vivo gene delivery by nonviral vectors: overcoming hurdles? *Mol. Ther.* **20**, 1298–1304 (2012).
- Luo, D. & Saltzman, W. M. Synthetic DNA delivery systems. *Nat. Biotechnol.* **18**, 33–37 (2000).
- Liu, D., Yang, F., Xiong, F. & Gu, N. The smart drug delivery system and its clinical potential. *Theranostics* **6**, 1306 (2016).
- Allen, T. M. & Cullis, P. R. Liposomal drug delivery systems: from concept to clinical applications. *Adv. Drug Deliv. Rev.* **65**, 36–48 (2013).
- Pattni, B. S., Chupin, V. V. & Torchilin, V. P. New developments in liposomal drug delivery. *Chem. Rev.* **115**, 10938–10966 (2015).
- Khan, D. R., Rezler, E. M., Lauer-Fields, J. & Fields, G. B. Effects of drug hydrophobicity on liposomal stability. *Chem. Biol. Drug Des.* **71**, 3–7 (2008).
- Akbarzadeh, A. et al. Liposome: classification, preparation, and applications. *Nanoscale Res. Lett.* **8**, 102 (2013).
- Nahire, R. et al. pH-triggered echogenicity and contents release from liposomes. *Mol. Pharm.* **11**, 4059–4068 (2014).

ARTICLE

NATURE COMMUNICATIONS | DOI: 10.1038/s41467-018-05118-3

10. Ferreira, D. d. S., Lopes, S. C. d. A., Franco, M. S. & Oliveira, M. C. pH-sensitive liposomes for drug delivery in cancer treatment. *Ther. Deliv.* **4**, 1099–1123 (2013).
11. Dicheva, B. M. et al. Targeted and heat-triggered doxorubicin delivery to tumors by dual targeted cationic thermosensitive liposomes. *J. Control Release* **195**, 37–48 (2014).
12. Kono, K. et al. Highly temperature-sensitive liposomes based on a thermosensitive block copolymer for tumor-specific chemotherapy. *Biomaterials* **31**, 7096–7105 (2010).
13. Sarkar, N. R. et al. "Uncorking" of liposomes by matrix metalloproteinase-9. *Chem. Commun.* **0**, 999–1001 (2005).
14. Arouri, A. et al. Development of a cell-based bioassay for phospholipase A2-triggered liposomal drug release. *PLoS ONE* **10**, e0125508 (2015).
15. Leung, S. J. & Romanowski, M. Light-activated content release from liposomes. *Theranostics* **2**, 1020 (2012).
16. Puri, A. Phototriggerable liposomes: current research and future perspectives. *Pharmaceutics* **6**, 1–25 (2013).
17. Wilson, B. C. & Patterson, M. S. The physics, biophysics and technology of photodynamic therapy. *Phys. Med. Biol.* **53**, R61 (2008).
18. Shum, P., Kim, J.-M. & Thompson, D. H. Phototriggering of liposomal drug delivery systems. *Adv. Drug Deliv. Rev.* **53**, 273–284 (2001).
19. Begg, A. C., Stewart, F. A. & Vens, C. Strategies to improve radiotherapy with targeted drugs. *Nat. Rev. Cancer* **11**, 239–253 (2011).
20. Kwatra, D., Venugopal, A. & Anant, S. Nanoparticles in radiation therapy: a summary of various approaches to enhance radiosensitization in cancer. *Transl. Cancer Res.* **2**, 330–342 (2013).
21. Jain, S., Hirst, D. & O'sullivan, J. Gold nanoparticles as novel agents for cancer therapy. *Br. J. Radiol.* **85**, 101–113 (2012).
22. Apanasevich, V. et al. Enhance the absorption of gamma-ray energy inside the tumor using gold nanoparticles and iodine particles. *Cancer Oncol. Res.* **2**, 17–20 (2014).
23. Butterworth, K. T. et al. Evaluation of cytotoxicity and radiation enhancement using 1.9 nm gold particles: potential application for cancer therapy. *Nanotech* **21**, 295101 (2010).
24. Kotova, E. A., Kuzevanov, A. V., Pashkovskaya, A. A. & Antonenko, Y. N. Selective permeabilization of lipid membranes by photodynamic action via formation of hydrophobic defects or pre-pores. *Biochim. Biophys. Acta Biomembr.* **1808**, 2252–2257 (2011).
25. Yavlovich, A., Smith, B., Gupta, K., Blumenthal, R. & Puri, A. Light-sensitive lipid-based nanoparticles for drug delivery: design principles and future considerations for biological applications. *Mol. Membr. Biol.* **27**, 364–381 (2010).
26. Tejero, I., González-Lafont, A., Lluch, J. M. & Eriksson, L. A. Photo-oxidation of lipids by singlet oxygen: a theoretical study. *Chem. Phys. Lett.* **398**, 336–342 (2004).
27. Brodowska, K. et al. The clinically used photosensitizer Verteporfin (VP) inhibits YAP-TEAD and human retinoblastoma cell growth in vitro without light activation. *Exp. Eye Res.* **124**, 67–73 (2014).
28. Liu-Chittenden, Y. et al. Genetic and pharmacological disruption of the TEAD-YAP complex suppresses the oncogenic activity of YAP. *Genes Dev.* **26**, 1300–1305 (2012).
29. Chang, H.-I. & Yeh, M.-K. Clinical development of liposome-based drugs: formulation, characterization, and therapeutic efficacy. *Int. J. Nanomed.* **7**, 49 (2012).
30. Shen, Y. et al. in *Photonics Asia 2010* 78451F-78451F-78456 (International Society for Optics and Photonics, 2010).
31. Kim, S., Fujitsuka, M. & Majima, T. Photochemistry of singlet oxygen sensor green. *J. Phys. Chem. B* **117**, 13985–13992 (2013).
32. Allen, T. & Cleland, L. Serum-induced leakage of liposome contents. *Biochim. Biophys. Acta Biomembr.* **597**, 418–426 (1980).
33. Kundrot, C. E., Spangler, E. A., Kendall, D. A., MacDonald, R. C. & MacDonald, R. I. Sendai virus-mediated lysis of liposomes requires cholesterol. *Proc. Natl. Acad. Sci.* **80**, 1608–1612 (1983).
34. Yavlovich, A. et al. Design of liposomes containing photopolymerizable phospholipids for triggered release of contents. *J. Therm. Anal. Calorim.* **98**, 97–104 (2009).
35. Maherani, B., Arab-Tehrany, E., Kheiriloomoo, A., Geny, D. & Linder, M. Calcein release behavior from liposomal bilayer; influence of physicochemical/mechanical/structural properties of lipids. *Biochimie* **95**, 2018–2033 (2013).
36. Clement, S., Sobhan, M., Deng, W., Camilleri, E. & Goldys, E. M. Nanoparticle-mediated singlet oxygen generation from photosensitizers. *J. Photochem. Photobiol. A* **332**, 66–71 (2017).
37. Clement, S., Deng, W., Camilleri, E., Wilson, B. C. & Goldys, E. M. X-ray induced singlet oxygen generation by nanoparticle-photosensitizer conjugates for photodynamic therapy: determination of singlet oxygen quantum yield. *Sci. Rep.* **6**, 1–9 (2016).
38. Hutter, T., Huang, F. M., Elliott, S. R. & Mahajan, S. Near-field plasmonics of an individual dielectric nanoparticle above a metallic substrate. *J. Phys. Chem. C* **117**, 7784–7790 (2013).
39. Tanabe, K. Field enhancement around metal nanoparticles and nanoshells: a systematic investigation. *J. Phys. Chem. C* **112**, 15721–15728 (2008).
40. Conklin, D. et al. Electronic transport in porphyrin supermolecule-gold nanoparticle assemblies. *Nano. Lett.* **12**, 2414–2419 (2012).
41. Shaikh, A. J. et al. Binding strength of porphyrin–gold nanoparticle hybrids based on number and type of linker moieties and a simple method to calculate inner filter effects of gold nanoparticles using fluorescence spectroscopy. *J. Phys. Chem. A* **119**, 1108–1116 (2015).
42. Chithrani, D. B. et al. Gold nanoparticles as radiation sensitizers in cancer therapy. *Radiat. Res.* **173**, 719–728 (2010).
43. Hainfeld, J. F. et al. Gold nanoparticles enhance the radiation therapy of a murine squamous cell carcinoma. *Phys. Med. Biol.* **55**, 3045 (2010).
44. Rahman, W. N. et al. Enhancement of radiation effects by gold nanoparticles for superficial radiation therapy. *Nanomed. Nanotechnol. Biol. Med.* **5**, 136–142 (2009).
45. Cho, S. H. Estimation of tumour dose enhancement due to gold nanoparticles during typical radiation treatments: a preliminary Monte Carlo study. *Phys. Med. Biol.* **50**, N163 (2005).
46. Cooper, D. R., Bekah, D. & Nadeau, J. L. Gold nanoparticles and their alternatives for radiation therapy enhancement. *Front. Chem.* **2**, 86 (2014).
47. Hainfeld, J. F., Slatkin, D. N. & Smilowitz, H. M. The use of gold nanoparticles to enhance radiotherapy in mice. *Phys. Med. Biol.* **49**, N309 (2004).
48. Slepukhin, V. A. et al. Sterically stabilized pH-sensitive liposomes intracellular delivery of aqueous contents and prolonged circulation in vivo. *J. Biol. Chem.* **272**, 2382–2388 (1997).
49. Nam, J. et al. pH-responsive gold nanoparticles-in-liposome hybrid nanostructures for enhanced systemic tumor delivery. *Nanoscale* **5**, 10175–10178 (2013).
50. Parker, N. et al. Folate receptor expression in carcinomas and normal tissues determined by a quantitative radioligand binding assay. *Anal. Biochem.* **338**, 284–293 (2005).
51. Hong, E. J., Choi, D. G. & Shim, M. S. Targeted and effective photodynamic therapy for cancer using functionalized nanomaterials. *Acta Pharmacol. Sin. B* **6**, 297–307 (2016).
52. Zhang, S., Lu, C., Zhang, X., Li, J. & Jiang, H. Targeted delivery of etoposide to cancer cells by folate-modified nanostructured lipid drug delivery system. *Drug Deliv.* **23**, 1838–1845 (2016).
53. Bovelli, D., Plataniotis, G., Roila, F. & Group, E. G. W. Cardiotoxicity of chemotherapeutic agents and radiotherapy-related heart disease: ESMO Clinical Practice Guidelines. *Ann. Oncol.* **21**, v277–v282 (2010).
54. Nemade, H. et al. Cell death mechanisms of the anti-cancer drug etoposide on human cardiomyocytes isolated from pluripotent stem cells. *Arch. Toxicol.* **92**, 1507–1524 (2018).
55. Baskar, R., Dai, J., Wenlong, N., Yeo, R. & Yeoh, K.-W. Biological response of cancer cells to radiation treatment. *Front. Mol. Biosci.* **1**, 24 (2014).
56. Niedre, M., Patterson, M. S. & Wilson, B. C. Direct near-infrared luminescence detection of singlet oxygen generated by photodynamic therapy in cells in vitro and tissues in vivo. *Photochem. Photobiol.* **75**, 382–391 (2002).
57. DeRosa, M. C. & Crutchley, R. J. Photosensitized singlet oxygen and its applications. *Coord. Chem. Rev.* **233**, 351–371 (2002).
58. Krieger-Liszka, A. Singlet oxygen production in photosynthesis. *J. Exp. Bot.* **56**, 337–346 (2005).
59. Redmond, R. W. & Kojchevar, I. E. Spatially resolved cellular responses to singlet gen. *Photochem. Photobiol.* **82**, 1178–1186 (2006).
60. Rengan, A. K. et al. In vivo analysis of biodegradable liposome gold nanoparticles as efficient agents for photothermal therapy of cancer. *Nano. Lett.* **15**, 842–848 (2015).
61. Milla, P., Dosio, F. & Cattel, L. PEGylation of proteins and liposomes: a powerful and flexible strategy to improve the drug delivery. *Curr. Drug. Metab.* **13**, 105–119 (2012).
62. Li, X., Ding, L., Xu, Y., Wang, Y. & Ping, Q. Targeted delivery of doxorubicin using stealth liposomes modified with transferrin. *Int. J. Pharm.* **373**, 116–123 (2009).
63. Ishida, T., Iden, D. L. & Allen, T. M. A combinatorial approach to producing sterically stabilized (Stealth) immunoliposomal drugs. *FEBS Lett.* **460**, 129–133 (1999).
64. Yoshino, K. et al. Comparative studies of irinotecan-loaded polyethylene glycol-modified liposomes prepared using different PEG-modification methods. *Biochim. Biophys. Acta Biomembr.* **1818**, 2901–2907 (2012).
65. Shimanouchi, T., Ishii, H., Yoshimoto, N., Umakoshi, H. & Kuboi, R. Calcein permeation across phosphatidylcholine bilayer membrane: effects of membrane fluidity, liposome size, and immobilization. *Colloids Surf. B Biointerfaces* **73**, 156–160 (2009).
66. Han, H. D., Kim, T. W., Shin, B. C. & Choi, H. S. Release of calcein from temperature-sensitive liposomes. *Macromol. Res.* **13**, 54–61 (2005).

Acknowledgements

All TEM images in this work were performed in the Microscopy Unit, Faculty of Science and Engineering at Macquarie University. We thank Dr. Michael Grace, Dr. Vaughan Moutrie and Dr. Daniel Santos from Genesis Cancer Care NSW and Macquarie University Hospital, for helping us with X-ray radiation experiments. We also thank Mr Peter Wieland from the Department of Earth and Planetary Science at Macquarie University for his assistance in ICP-MS measurement. This work is supported by Discovery Early Career Researcher Award scheme (DE130100894), Centre of Excellence scheme (CE140100003) from the Australian Research Council and Sydney Vital Translational Cancer Research Centre. The experimental work was carried out at Macquarie University and Genesis Cancer Care NSW.

Author contributions

W. D. and E. G. designed this study, conducted experiments and draft the manuscript. W. C. conducted animal experiments, cell lysis experiments and gel electrophoresis. S. C. conducted calculation of SOQY and $^1\text{O}_2$ generation enhancement factor under light illumination and the number of $^1\text{O}_2$ generated under X-ray radiation. A. G. contributed to histological analysis and interpretation. Z. Z. helped with measurement of SOSG fluorescence intensity and calcein release assays after X-ray radiation. He also contributed to animal ethics application and experiments. A. E. contributed to manuscript preparation.

Additional information

Supplementary Information accompanies this paper at <https://doi.org/10.1038/s41467-018-05118-3>.

Competing interests: The authors declare no competing interests.

Reprints and permission information is available online at <http://npg.nature.com/reprintsandpermissions/>

Publisher's note: Springer Nature remains neutral with regard to jurisdictional claims in published maps and institutional affiliations.



Open Access This article is licensed under a Creative Commons Attribution 4.0 International License, which permits use, sharing, adaptation, distribution and reproduction in any medium or format, as long as you give appropriate credit to the original author(s) and the source, provide a link to the Creative Commons license, and indicate if changes were made. The images or other third party material in this article are included in the article's Creative Commons license, unless indicated otherwise in a credit line to the material. If material is not included in the article's Creative Commons license and your intended use is not permitted by statutory regulation or exceeds the permitted use, you will need to obtain permission directly from the copyright holder. To view a copy of this license, visit <http://creativecommons.org/licenses/by/4.0/>.

© The Author(s) 2018

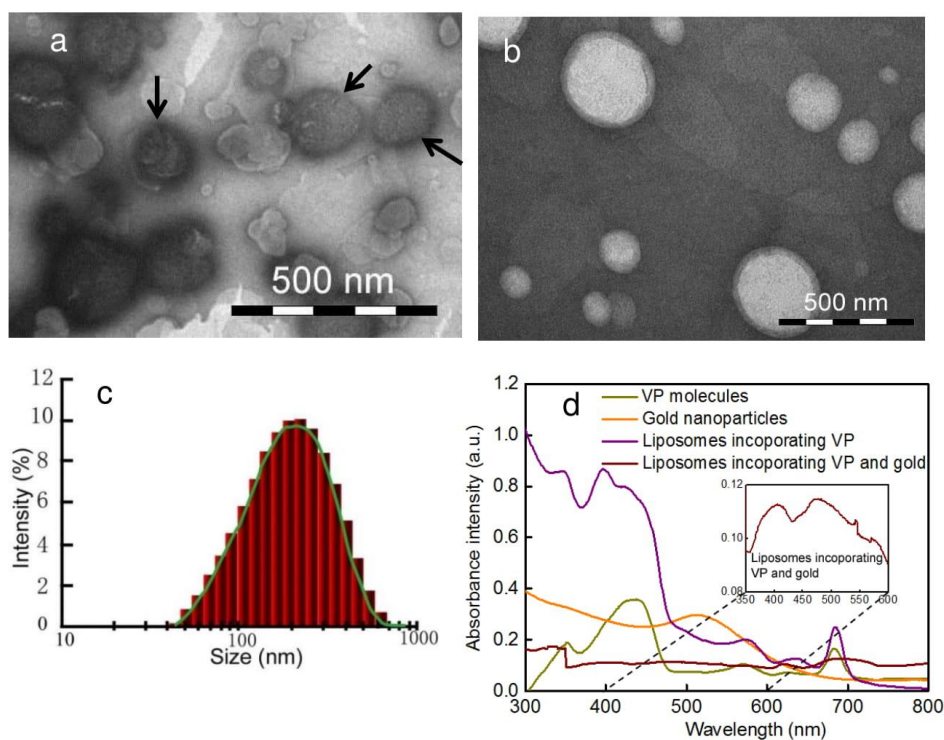
Supplementary Information

**Controlled gene and drug release from a liposomal delivery platform triggered by X-ray
radiation**

Deng W, et al

Supplementary Note 1: Characterization of liposome nanocomposites

Supplementary Fig.1a illustrates typical TEM images of liposomes containing gold nanoparticles and VP. Gold nanoparticle clusters were easily observed due to the higher electron density of metal gold compared with the pure liposomes (Supplementary Fig.1b). The average size of liposomes was about 165 nm determined by dynamic light scattering and the zeta potential was 37.3 ± 4 mV (Supplementary Fig.1c). Supplementary Fig.1d shows the absorption spectra of different liposome samples, where characteristic absorption peaks from both gold nanoparticles and VP were observed. We also estimated the encapsulation efficiency of oligonucleotide, Dox and epotoside loaded inside of liposomes, found to be approximately 37.5%, 44% and 77%, respectively.



Supplementary Figure 1 Characterisation of liposomes incorporating VP and gold nanoparticles. a and b TEM images of liposomes incorporating gold nanoparticles and pure

liposomes. Black arrows indicated gold nanoparticles loaded inside liposomes. c Size distribution determined by dynamic light scattering. d Absorption spectra of liposomes, pure VP and pure gold nanoparticles. The inset shows an enlargement of absorption spectrum of liposomes incorporating VP and gold between 350-600 nm.

Supplementary Note 2: Determination of Singlet oxygen quantum yield from liposomes loaded with VP and gold nanoparticles after illumination at 365 nm wavelength

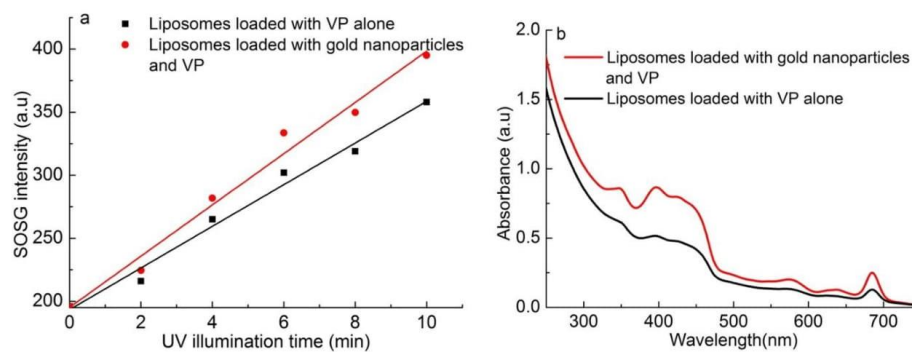
The singlet oxygen quantum yield (ϕ) is the ratio of the number of photons absorbed by a photosensitizer (PS) molecule to the number of singlet oxygen generated. The reference method is the most commonly used approach for calculating ϕ ¹. The singlet oxygen quantum yield of a PS (ϕ_{PS}) can be calculated based on a reference PS with a known quantum yield (ϕ_{REF}) using the equation²:

$$\phi_{PS} = \phi_{REF} \frac{\frac{r_{PS}}{(1-T_{PS})}}{\frac{r_{REF}}{(1-T_{REF})}} \quad 1$$

where r_{PS} and r_{REF} are the reaction rates of the fluorescent detection probe with singlet oxygen generated from PS and reference PS respectively. T_{PS} and T_{REF} represent the transmittance of the PS and the reference PS at the illumination wavelength.

In this case, we determine the singlet oxygen quantum yield ϕ of liposomes loaded with VP and gold nanoparticles at 365 nm by taking ϕ of VP alone as the reference PS (0.53 ± 0.06)². Supplementary Figure 2a shows the variation of SOSG intensity at 525nm as a function of UV illumination time for liposomes loaded VP alone and liposomes loaded with VP and gold nanoparticles. Their absorption spectra of these nanocomposites are shown in Supplementary Figure 2b. The transmittance value at 365 nm is calculated from absorbance of VP alone and liposomes loaded with VP and gold nanoparticles based on their absorption spectra. Using the equation 1 with the reaction rate and absorbance value obtained from Supplementary Fig.2, the singlet oxygen quantum yield ϕ of liposomes loaded with VP and gold nanoparticles obtained in this work was estimated as 0.75 ± 0.18 . This result shows that there is an enhancement in the quantum yield value of liposomes loaded with VP and gold nanoparticles by a factor of 1.42 compared with liposomes loaded with VP alone. This enhancement is

tentatively attributed to the electric field enhancement around the gold nanoparticles present in gold-loaded liposomes.



Supplementary Figure 2 Quantification of $^1\text{O}_2$ generation under UV illumination for liposomes loaded with VP and gold nanoparticles and liposomes loaded with VP alone. a SOSG intensity as a function of UV illumination time. b Absorption spectra of these samples.

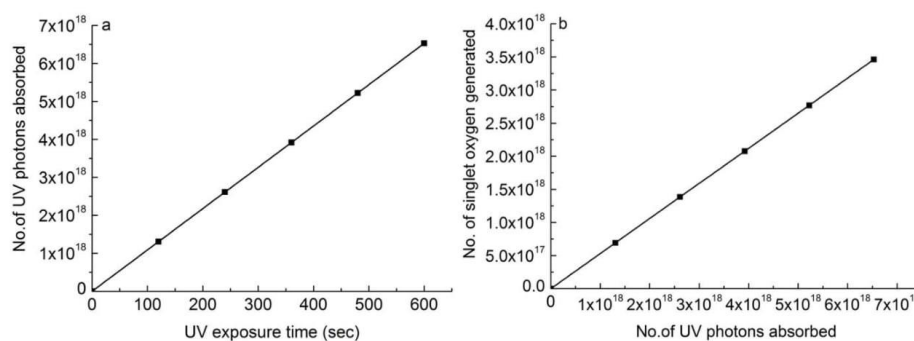
Supplementary Note 3: Quantification of singlet oxygen from liposomes loaded with VP and gold nanoparticles under X-ray radiation

To quantify the number of singlet oxygen generated from liposomes loaded with VP and gold nanoparticles under X-ray radiation for a particular dose, we established a relation between the number of singlet oxygen molecules generated by X-ray radiation and the intensity of SOSG fluorescence, in a way similar to our previous publication³.

We first calculated the number of UV photons absorbed ($N_{uv}(t)$) by liposomes loaded with VP alone as a function of time using the equation:

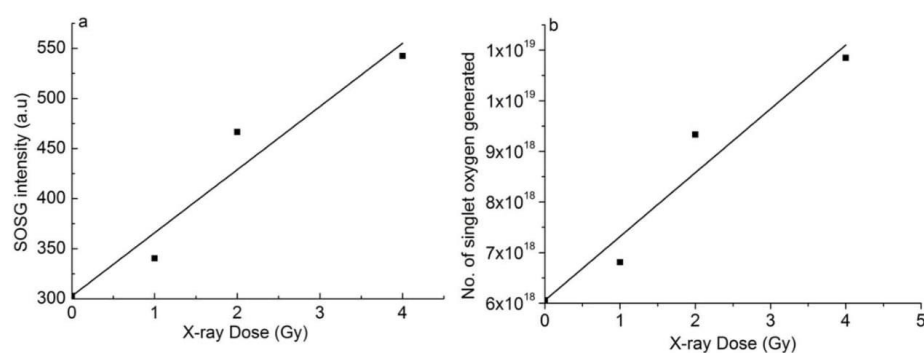
$$N_{uv}(t) = \frac{P}{E} * F * t \quad 2$$

where P is the optical power detected on the surface of the sample, E is the energy of 365 nm photons and t is the time of illumination. F is the absorption factor and is calculated from the absorption spectra of the sample. This $N_{uv}(t)$ is plotted against time as shown in Supplementary Fig. 3a. From the known singlet oxygen quantum yield ϕ of VP mentioned above and $N_{uv}(t)$ from Supplementary Fig. 3a, we calculated the number of singlet oxygen generated corresponding to each UV photons absorbed. If we compare this number with the SOSG intensity in Supplementary Fig. 2a, we will obtain a conversion factor which gives the calibration of the SOSG signal with respect to the number of singlet oxygen generated.



Supplementary Figure 3 Quantification of singlet oxygen from liposomes under light illumination. a Number of UV photons absorbed by liposomes loaded with VP alone as a function of time. b Number of singlet oxygen generated versus number of UV photons absorbed.

Supplementary Fig. 4a shows the SOSG intensity as a function of X-ray dose applied to liposomes loaded with VP and gold nanoparticles. By using the conversion factor estimated above, we now calculate the number of singlet oxygen generated corresponding to each X-ray dose. In this case, the number of singlet oxygen generated from liposomes loaded with VP and gold nanoparticles for 4 Gy is $\sim 2.9 \times 10^{18}$. By dividing the number of liposomes in this sample, we estimate the number of singlet oxygen generated from each liposome, which is about 7250. In this case, we took into account of the fact that SOSG shows some background fluorescence due to the presence of endoperoxides generated before the exposure to X-ray radiation.



Supplementary Figure 4 Quantification of singlet oxygen from liposomes under X-ray radiation. a SOSG intensity as a function of X-ray Dose for liposomes loaded with VP and gold nanoparticles. b Number of singlet oxygen generated corresponding to each X-ray dosage.

Supplementary Note 4: Calculation of the number of liposomes per cell and the number of gold nanoparticles per liposome

We first calculate the number of lipid molecules in each liposome as per the equation ⁴:

$$N_{tot} = \frac{4\pi(\frac{d}{2})^2 + 4\pi[\frac{d}{2} - h]^2}{a} \quad 3$$

where d is the diameter of a liposome, h indicates the thickness of a liposomal bilayer that was calculated as 4.7 nm for our lipid formulation ⁵, and a represents the average lipid head group area, whose value is calculated according to $a = a_1 N_1 + a_2 N_2 + a_3 N_3 + \dots$, where N is the molar fraction of each lipid component and a is 70Å for DOTAP ⁶ and 72.4 Å for DOPC ⁷ in our study.

The number of liposome for a known concentration of lipids is estimated by using the equation:

$$N_{lipo} = \frac{[lipid] \times N_A}{N_{tot} \times 1000} \quad 4$$

where $[lipid]$ is the lipid concentration, N_A is the Avogadro number ($6.023 \times 10^{23} \text{ mol L}^{-1}$) and N_{tot} is the total number of lipids per liposome.

The cell number is counted before incubation with liposomes. The total number of liposome is calculated based on Equation 3 and 4 after cell lysis and average number of liposomes taken up by each cell is obtained by dividing the total number of liposomes with the cell number.

For the number of gold nanoparticles per liposome, we first calculate the total number of gold atom (N_{atom}) in our liposome sample based on ICP-MS analysis and equation 5:

$$N_{atom} = \frac{[Au^{3+}] \times V}{M} \times N_A \quad 5$$

where $[Au^{3+}]$ is the concentration of Au (III), V stands for the sample volume, M indicates the atomic weight of gold and N_A is the Avogadro number ($6.023 \times 10^{23} \text{ mol L}^{-1}$).

The average number of gold atoms per gold nanoparticle (U) is also calculated by using the following equation ⁸:

$$U = \frac{2}{3} \times \pi \times \left(\frac{D}{\alpha}\right)^3 \quad 6$$

Where D refers to the diameter of gold nanoparticle and α is the edge of a unit cell whose value was 4.0786 \AA . Therefore the number of gold nanoparticles (N_{gold}) in a liposome sample is calculated based on the equation:

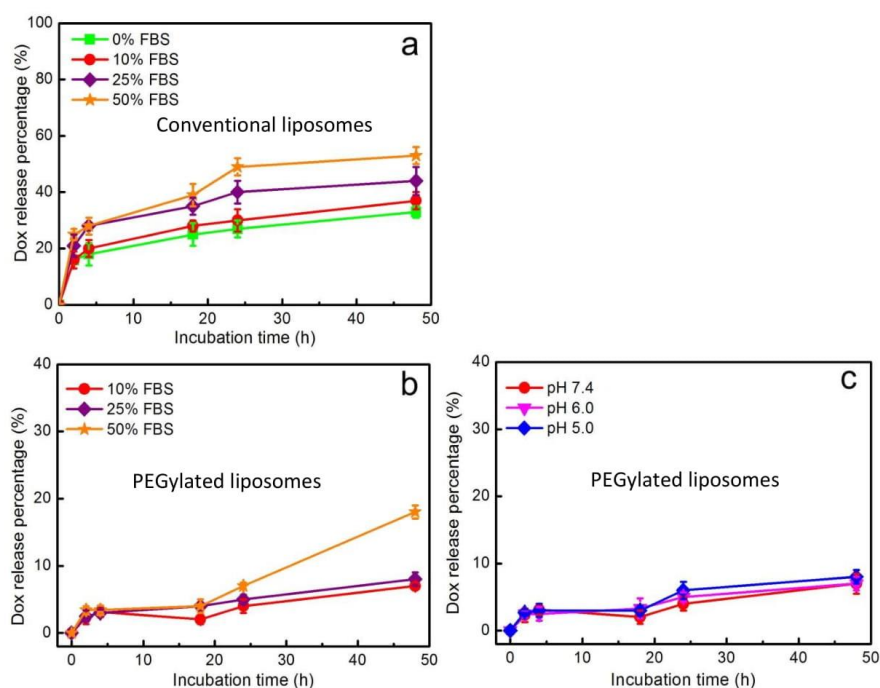
$$N_{gold} = \frac{N_{atom}}{U} \quad 7$$

Finally the number of gold nanoparticles per liposome (N) is estimated as per the equation:

$$N = \frac{N_{gold}}{N_{lipo}} \quad 8$$

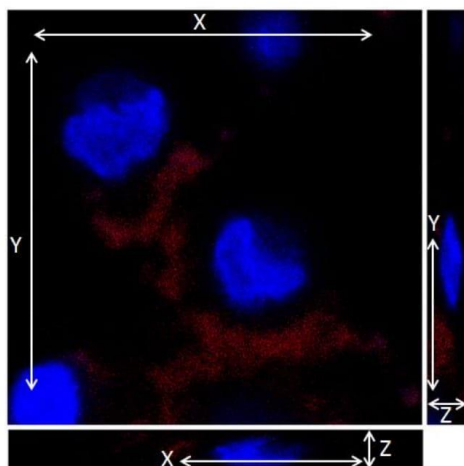
Supplementary Note 5: Serum and pH stability studies of PEGylated liposomes

For serum stability studies, the cumulative percentage of Dox released from liposomes with and without PEG modification is shown in Supplementary Fig.5a and 5b. Different amounts of Dox were released from conventional liposomes during 48 hr incubation, with the total amount being more than 30% and 50% at 48 hr when incubated in PBS with 10% and 50% FBS (Supplementary Fig.5a). However, the Dox release profile shown in Supplementary Fig.5b indicated that the release rates were reduced in the PEGylated liposomes, compared with liposomes without PEGylation. Liposomes still retained more than 90% and 80% of their initial drug content at 48 hr incubated in PBS with 10% and 50% FBS, indicating that PEG chains on the liposome surface would contribute to improved its stability in the blood circulation. Considering that decreased pH is a major feature of tumour tissue and, in principle, it may affect liposome stability and drug release from the liposomes. We also assessed Dox release triggered by different values of pH (Supplementary Fig.5c). These PEGylated liposomes showed a similar Dox release profile at different buffer pH values (7.4, 6.0 and 5.0). The overall amount of released Dox was less than 10% for 48 hr incubation even at pH 5.0. These findings suggested that the liposome formulation prepared in this study was largely unaffected by the decreased pH value. This indicates no stability change of liposomes in the tumour microenvironment before the application of light or X-ray to the tumour site.

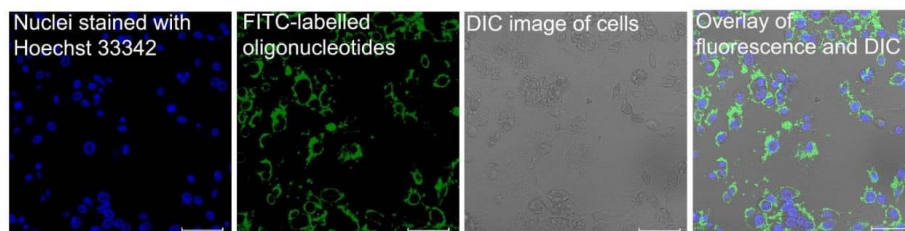


Supplementary Figure 5 Serum and pH stability studies of PEGylated liposomes. a-b The percentage of released Dox from (a) conventional liposomes and (b) PEGylated liposomes after 0 hr, 2 hr, 4 hr, 18 hr, 24 hr and 48 hr incubation in PBS (pH 7.4) containing FBS with various concentrations. c The percentage of released Dox from PEGylated liposome samples incubated in PBS (pH 7.4, 6.0 and 5.0) containing 10% FBS. Error bars show standard deviation from three measurements.

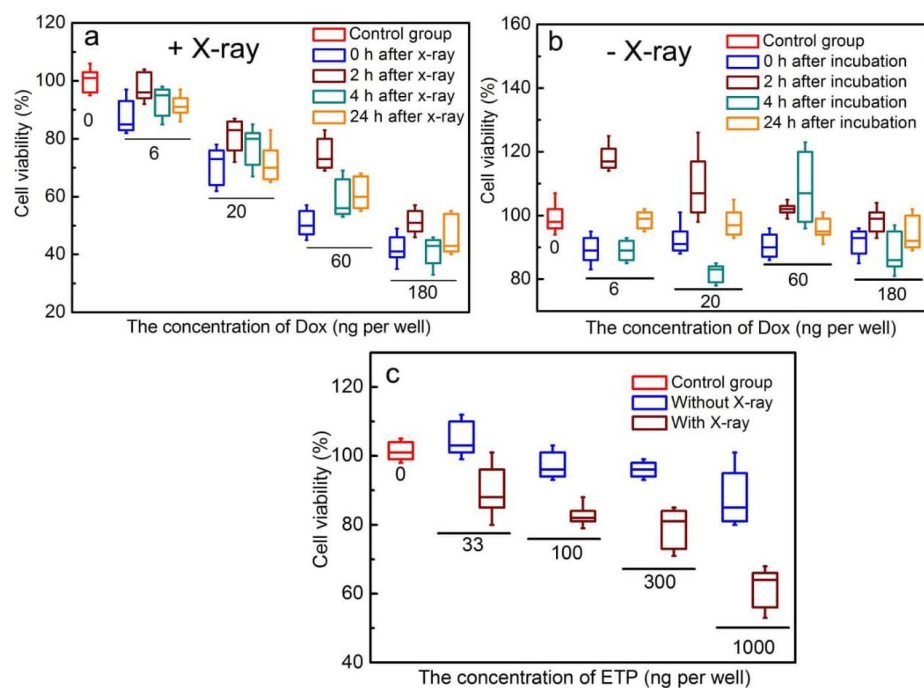
Supplementary Figure



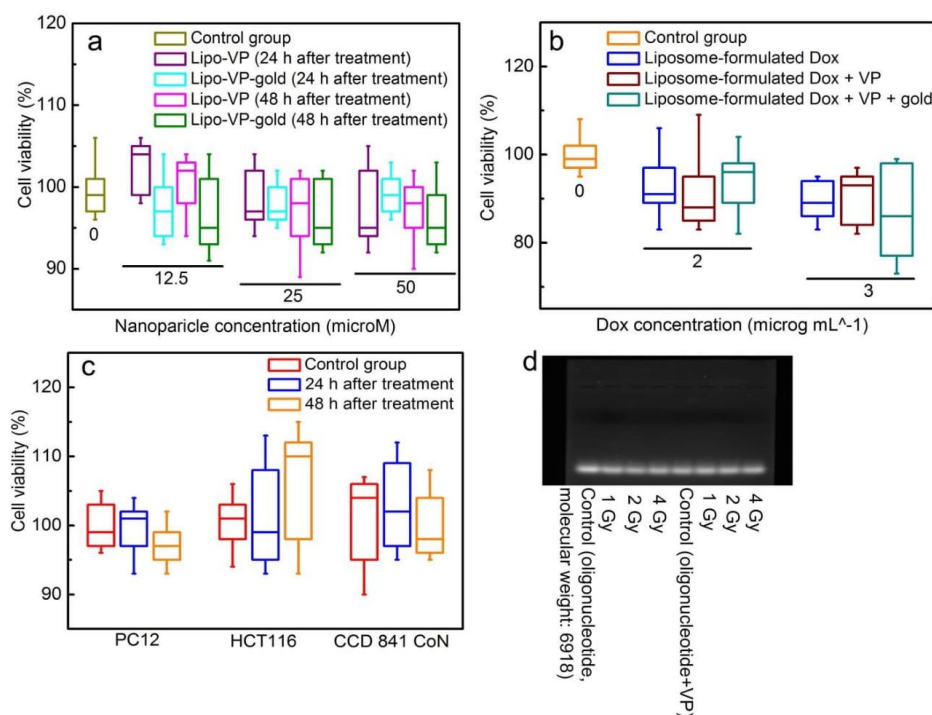
Supplementary Figure 6 Orthogonal views (XY, XZ and YZ) of cellular uptake of liposomes loaded with verteporfin after 4-h incubation with PC12 cells. The X-Y plane image was obtained at the centre of the Z-stack.



Supplementary Figure 7 Confocal laser scanning microscopy images of PC12 cells incubated with liposome nanoparticles (25 μM) loaded with fluorescent oligonucleotides for 4 hr. Scale bar is 75 μm .



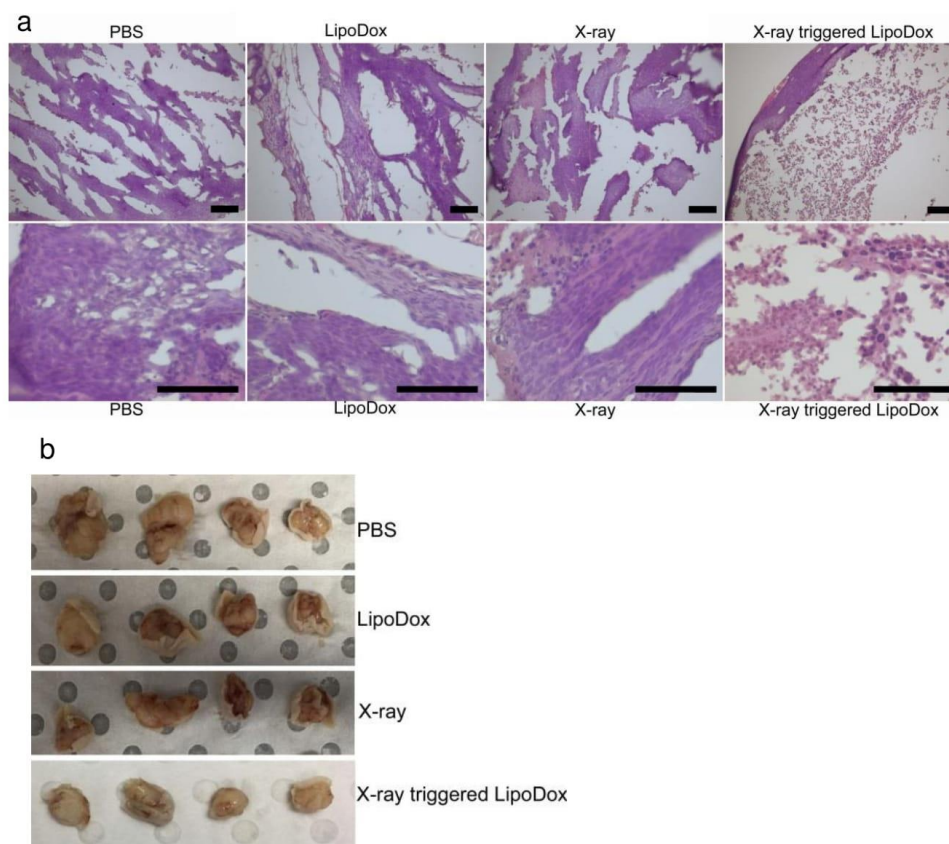
Supplementary Figure 8 X-ray triggered *in vitro* chemotherapy. a-b Cell-killing effect of LipoDox on HCT 116 (a) with and (b) without X-ray radiation of 4 Gy at various time points (0 hr, 2 hr, 4 hr and 24 hr). The concentration of Dox was 6, 20, 60 and 180 ng per well. c Cell-killing effect of LipoETP on HCT 116 at 24 hours after X-ray radiation of 4 Gy. The concentration of ETP was 33, 100, 300 and 900 ng per well. The box is bounded by the first and third quartile with a horizontal line at the median and whiskers extend to 1.5 times the interquartile range.



Supplementary Figure 9 *In vitro* toxicity assessment of liposome samples and X-ray radiation on cells and oligonucleotide. a Cell viability of PC12 cells at 24 hr and 48 hr after treatment with liposomes incorporating VP (Lipo-VP) and gold nanoparticles (Lipo-VP-gold). b Viability of CCD 841 CoN cells at 24 hr after treatment with liposome-formulated Dox. c Toxicity of X-ray of 4 Gy on PC12, HCT 116 and CCD 841 CoN cells at 24 hr and 48 hr after treatment. The box is bounded by the first and third quartile with a horizontal line at the median and whiskers extend to 1.5 times the interquartile range. d Agarose gel electrophoreses of antisense oligonucleotide ($10 \mu\text{g mL}^{-1}$) and mixture of oligonucleotide and VP ($10 \mu\text{g mL}^{-1}$ oligonucleotide and $32 \mu\text{g mL}^{-1}$ verteporfin) after X-ray exposure with different dosage. From left to right lane: control sample without treatment, 1 Gy, 2 Gy and 4 Gy.

Supplementary Note 6: Histological analysis of tumour tissues after each treatment

Supplementary Fig.10a demonstrates the histological images of tumour tissue under different treatment conditions. In the PBS-treated group, the internal region of the tumours mainly consisted of non-viable tumour residuals (about 1/3 of the whole volume of the lesion), while the outer part was formed by viable tumour cells. In the LipoDox-treated group, the viable tumour tissue formed a thinner outer rim (up to 0.5 mm below the capsule), but, in contrast to the PBS-treated group, it protruded towards the inner region as elongated cords and alternated with the necrotic and paranecrotic sites. The volume of non-viable tumour tissue in LipoDox group was about 60-70%. In the X-ray treated group, the difference between the outer and inner regions was less pronounced compared with other groups, and bigger fragments of viable tumour tissue of solid structure were surrounded by non-viable tumour tissue residuals. Finally, in the group treated by X-ray triggered LipoDox, the structure of the tumour resembles that observed in the LipoDox group, but with a significant reduction of the relative volume of viable tumour tissue. In particular, the outer rim of viable tumour tissue is much thinner (only 100-300 μm in thickness), and the amount of the viable tumour tissue spreading into the internal part of the tumour is significantly less than in any other experimental groups. In contrast to all other groups, the necrotic tumour tissue was visible even in the subcapsular zone. The average volume of necrotic tissue in the tumours was about more than 80%.



Supplementary Figure 10 *In vivo* antitumour effect by X-ray triggered LipoDox. a Representative histological images of tumour tissues after various treatments. H & E staining. The scale bar is 100 μm . b Photographs of tumours isolated at the endpoint.

Supplementary references:

1. Lin, H. et al. Feasibility study on quantitative measurements of singlet oxygen generation using singlet oxygen sensor green. *Journal of fluorescence* **23**, 41-47 (2013).
2. Clement, S., Sobhan, M., Deng, W., Camilleri, E. & Goldys, E.M. Nanoparticle-mediated singlet oxygen generation from photosensitizers. *Journal of Photochemistry and Photobiology A: Chemistry* (2016).
3. Clement, S., Deng, W., Camilleri, E., Wilson, B.C. & Goldys, E.M. X-ray induced singlet oxygen generation by nanoparticle-photosensitizer conjugates for photodynamic therapy: determination of singlet oxygen quantum yield. *Scientific reports* **6** (2016).
4. Güven, A., Ortiz, M., Constanti, M. & O'Sullivan, C.K. Rapid and efficient method for the size separation of homogeneous fluorescein-encapsulating liposomes. *Journal of liposome research* **19**, 148-154 (2009).
5. Small, D.M. Lateral chain packing in lipids and membranes. *Journal of Lipid Research* **25**, 1490-1500 (1984).
6. Koltover, I., Salditt, T. & Safinya, C. Phase diagram, stability, and overcharging of lamellar cationic lipid-DNA self-assembled complexes. *Biophysical Journal* **77**, 915-924 (1999).
7. Kučerka, N., Tristram-Nagle, S. & Nagle, J.F. Structure of fully hydrated fluid phase lipid bilayers with monounsaturated chains. *The Journal of membrane biology* **208**, 193-202 (2006).
8. Chithrani, B.D., Ghazani, A.A. & Chan, W.C. Determining the size and shape dependence of gold nanoparticle uptake into mammalian cells. *Nano letters* **6**, 662-668 (2006).

6

Conclusions and perspectives

CHAPTER 6 Conclusions and perspectives

6.1 Conclusions

The main aim of this thesis was to develop the light-triggered liposomal or polymeric nanocarriers for enhanced gene and drug delivery. It has been achieved using our synthetic lipid nanoparticles. Results demonstrated that light irradiation can significantly enhance the efficiency of gene transfection. This will facilitate the applications of (NIR) light irradiation for activated delivery vehicles due to its less phototoxicity and deep penetration in biological tissues. The enhanced endolysosomal escape of DNA molecules after light illumination was investigated by quantitative analysis of colocalisation between fluorescently labelled DNA molecules and endolysosomes. Enhanced PAC1R silencing and EGFP gene expression was respectively achieved by using two types of light-triggered liposomal delivery systems in rat PC12 cells and HCT116 human colorectal cancer cells. In addition, I was also involved in other work on X-ray triggered polymer and liposome delivery systems. The results have indicated the feasibility and therapeutic effect of these active nanocarriers for gene silencing and antitumour applications, extending their utility to treatments on deep-seated tumours. Further clinical translation is also achievable with our active nanocarrier since the key agents including lipids, polymers and photosensitiser are widely used in clinical practice.

6.2 Perspectives

Although many commercial gene/drug delivery systems based on cationic lipids and/or polymers have been well established, the customized functions of liposomes with particular aims such as specific targeting are still required for *in vivo* applications. When coming to *in vivo* applications, light activated lipid and/or polymeric nano DDSs can be further improved from the following aspects:

(1) NIR light triggering for liposome activation

Compared to the UV and visible light that used in this work, NIR light ranging from 700 to 900 nm has been adopted as the ideal light sources for in clinical applications due to its deeper penetration and less background for imaging¹. In my PhD work, red (~690 nm) and UV (~350 nm) light sources were used to trigger the verteporfin molecules for PDT or photochemical internalization for enhanced endosomal escape. In addition, X-ray irradiation was also used for activation of photosensitisers due to its excellent tissue penetrating ability. When considering

complicated operation and expensive cost of the X-ray facility, NIR light from the various commercial laser diodes can be another alternative. In this case, other PSs² (Figure 6-1) activated by NIR light irradiation can be incorporated to the nanocarrier systems to achieve NIR triggering purpose. This will enable photoactivation of PS even located in deep tissues as well as background-free live imaging³⁻⁵.

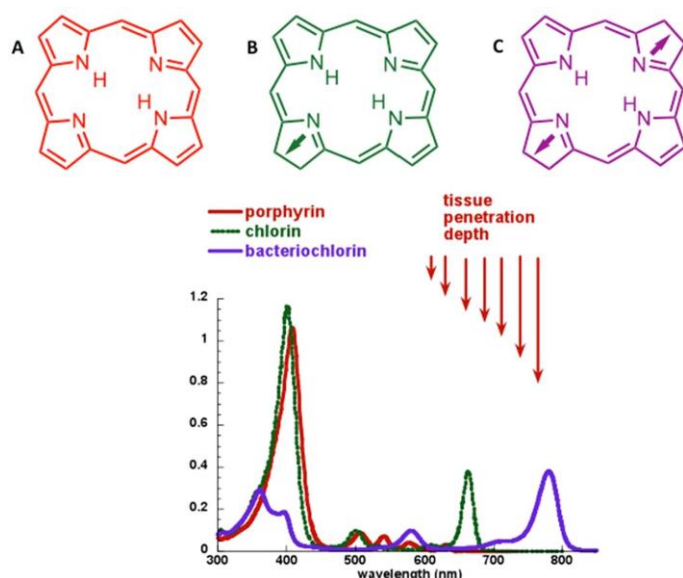


Figure 6-1 Structure and absorption spectra of tetrapyrrole photosensitizers: porphyrins (A), chlorins (B) and bacteriochlorins (C)².

(2) Development of capability for large genes and proteins

The developed light-triggered liposomal delivery systems also hold the potential to load and deliver other exogenous biomacromolecules including RNA molecules, large DNA fragments and proteins. This will be achieved by engineering various lipid components. Efficient delivery of various RNAs including sgRNA and larger pDNA remains a key challenge in the development of gene silencing, genome editing and RNA interference (RNAi) therapeutics⁶⁻⁸. Therefore the light activated nanosystems developed in this work will have a potential for the better release efficiency of these genetic materials.

Current approaches of protein delivery generally face some challenges including low tolerance for serum, instability and immunogenicity, poor endosomal escape and limited *in vivo* efficacy⁹. However, the light-triggered liposome delivery systems may offer a better solution to overcome these issues. In particular, lipid-based delivery of genome editing enzymes and transcription activators has become an efficient approach that mediates genome modification⁹.

6.3 Future work on light-triggered liposomal delivery systems

Recently, a new tool based on a bacterial CRISPR (clustered regularly interspaced short palindromic repeats)-associated protein-9 nuclease (Cas9) from a bacterium, *S. thermophiles*, has generated significant excitement and inspiration. This CRISPR/Cas9 system is an adaptive immune response system present in some prokaryotic cells, in which the Cas9 endonuclease is used by the CRISPR system to recognize and destroy foreign DNA entering into the cell¹⁰. To perform this task, Cas9 makes use of a short guide sequence of RNA (sgRNA), which targets the endonuclease to a particular sequence, and facilitates the gene modification (Figure 6-2). With such versatile guide sequences, Cas9/sgRNA complexes now can be constructed to target almost any gene. In addition, this gene silencing tool can completely knock out gene expression with minimal off-target effects, compared to the RNAi technique.

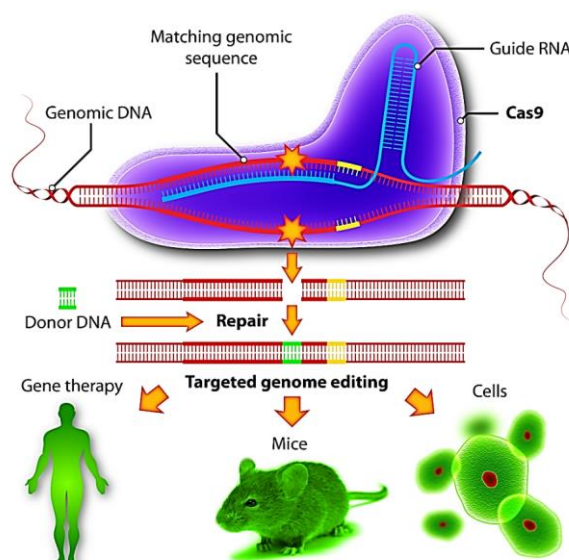


Figure 6-2 The scheme of different applications of targeted genome editing by using CRISPR/Cas9 systems.

Genome engineering technologies have enabled activation or repression of endogenous genes in mammalian cells using synthetic transcription factors that can be targeted to almost any DNA sequence¹¹. Most recently, researchers reengineered the CRISPR/Cas9 system of *Streptococcus pyogenes* to function in mammalian cells as a transcription factor¹². Thus, targeting the CRISPR/Cas9 system to new DNA sequences requires alteration of the short gRNA sequence only and does not involve reengineering a protein DNA-binding domain¹³. The simplicity of this system has enabled its rapid development as a tool for many diverse applications in biology. However a major roadblock to achieve the therapeutic potential of the CRISPR/Cas9 system is the lack of a safe and effective *in vivo* delivery method. Therefore, development of controllable

nanostructures as a delivery system of CRISPR/Cas9 will be very important for the safe and effective applications of gene editing.

Several studies of cationic lipid-based delivery of CRISPR/Cas9 delivery systems have already been reported for *in vivo* application. These includes the genome modification into the mouse inner ear cells⁹, liver¹⁴ and human cells for gene correction¹⁵. For example, cationic lipid-mediated delivery of unmodified Cas9:sgRNA nuclease complexes resulted in up to 80% genome modification and higher specificity compared to DNA transfection⁹.

Recently optically regulated CRISPR gene editing has been reported to use the photo-caging effect that the nucleic acids with inactivated groups turn to function upon UV light irradiation¹⁶. However, to the best of my knowledge, the CRISPR/Cas release by using the light-induced nonviral vectors has seldom been studied. Based on my PhD work on light-triggered liposomal delivery systems, external light activation may offer another option to remotely control CRISPR gene editing *in vivo*. Figure 6-3 illustrates my future work on genome editing by using light-activated liposomes. For comparison purpose, two kinds of agents will be delivered into the cells by the liposomes. One is the plasmid which express Cas9 nuclease and also transcript the sgRNA sequences; the other is the sgRNA and Cas9 complexes. This light-triggered liposomal gene editing system will be demonstrated in human cells HEK293 and zebrafish embryo with further phenotypic and molecular identification.

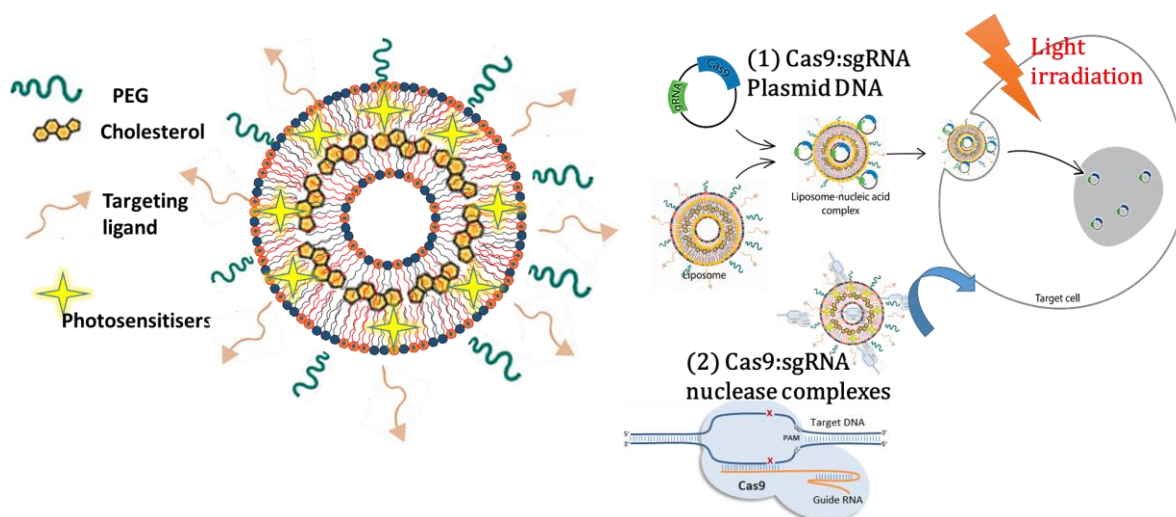


Figure 6-3 The schematic illustration of future work on the light-activated liposomes for controllable CRISPR/Cas9 delivery and release.

References

1. Weissleder, R. A clearer vision for in vivo imaging. *Nature biotechnology* **2001**, *19* (4), 316-316.
2. Abrahamse, H.; Hamblin, M. R. New photosensitizers for photodynamic therapy. *Biochemical Journal* **2016**, *473* (4), 347-364.
3. Yang, Y.; Liu, F.; Liu, X.; Xing, B. NIR light controlled photorelease of siRNA and its targeted intracellular delivery based on upconversion nanoparticles. *Nanoscale* **2013**, *5* (1), 231-238.
4. Jayakumar, M. K. G.; Idris, N. M.; Zhang, Y. Remote activation of biomolecules in deep tissues using near-infrared-to-UV upconversion nanotransducers. *Proceedings of the National Academy of Sciences* **2012**, *109* (22), 8483-8488.
5. Idris, N. M.; Gnanasammandhan, M. K.; Zhang, J.; Ho, P. C.; Mahendran, R.; Zhang, Y. In vivo photodynamic therapy using upconversion nanoparticles as remote-controlled nanotransducers. *Nature medicine* **2012**, *18* (10), 1580-1585.
6. Akinc, A.; Goldberg, M.; Qin, J.; Dorkin, J. R.; Gamba-Vitalo, C.; Maier, M.; Jayaprakash, K. N.; Jayaraman, M.; Rajeev, K. G.; Manoharan, M. Development of lipidoid-siRNA formulations for systemic delivery to the liver. *Molecular Therapy* **2009**, *17* (5), 872-879.
7. Hsu, S.-h.; Yu, B.; Wang, X.; Lu, Y.; Schmidt, C. R.; Lee, R. J.; Lee, L. J.; Jacob, S. T.; Ghoshal, K. Cationic lipid nanoparticles for therapeutic delivery of siRNA and miRNA to murine liver tumor. *Nanomedicine: Nanotechnology, Biology and Medicine* **2013**, *9* (8), 1169-1180.
8. Steyer, B.; Carlson-Stevermer, J.; Angenent-Mari, N.; Khalil, A.; Harkness, T.; Saha, K. High content analysis platform for optimization of lipid mediated CRISPR-Cas9 delivery strategies in human cells. *Acta biomaterialia* **2016**, *34*, 143-158.
9. Zuris, J. A.; Thompson, D. B.; Shu, Y.; Guilinger, J. P.; Bessen, J. L.; Hu, J. H.; Maeder, M. L.; Joung, J. K.; Chen, Z.-Y.; Liu, D. R. Cationic lipid-mediated delivery of proteins enables efficient protein-based genome editing in vitro and in vivo. *Nature biotechnology* **2015**, *33* (1), 73-80.
10. Cong, L.; Ran, F. A.; Cox, D.; Lin, S.; Barretto, R.; Habib, N.; Hsu, P. D.; Wu, X.; Jiang, W.; Marraffini, L. A. Multiplex genome engineering using CRISPR/Cas systems. *Science* **2013**, *339* (6121), 819-823.
11. Doudna, J. A.; Charpentier, E. The new frontier of genome engineering with CRISPR-Cas9. *Science* **2014**, *346* (6213), 1258096.
12. Polstein, L. R.; Gersbach, C. A. A light-inducible CRISPR-Cas9 system for control of endogenous gene activation. *Nature chemical biology* **2015**, *11* (3), 198-200.
13. Gaj, T.; Gersbach, C. A.; Barbas, C. F. ZFN, TALEN, and CRISPR/Cas-based methods for genome engineering. *Trends in biotechnology* **2013**, *31* (7), 397-405.
14. Xue, W.; Chen, S.; Yin, H.; Tammela, T.; Papagiannakopoulos, T.; Joshi, N. S.; Cai, W.; Yang, G.; Bronson, R.; Crowley, D. G. CRISPR-mediated direct mutation of cancer genes in the mouse liver. *Nature* **2014**, *514* (7522), 380-384.
15. Yin, H.; Song, C.-Q.; Dorkin, J. R.; Zhu, L. J.; Li, Y.; Wu, Q.; Park, A.; Yang, J.; Suresh, S.; Bizhanova, A. Therapeutic genome editing by combined viral and non-viral delivery of CRISPR system components in vivo. *Nature biotechnology* **2016**, *34* (3), 328-333.
16. Nihongaki, Y.; Kawano, F.; Nakajima, T.; Sato, M. Photoactivatable CRISPR-Cas9 for optogenetic genome editing. *Nature biotechnology* **2015**, *33* (7), 755-760.

List of publications

Peer-reviewed publications:

1. Deng W, **Chen W**, Clement S, Guller A, Zhao Z, Eagle A, Goldys EM (2018). X-ray triggered liposomal delivery system for gene knockdown and chemotherapy, *Nature Communication*, 9 (1), 2713.
2. **Chen W**, Deng W, Xu X, Zhao X, Vo JN, Anwer AG, Williams TC, Cui H, Goldys EM (2018). Stable and photoresponsive liposome-polycation-DNA (LPD) nanocomplexes for enhanced gene delivery in cancer cells via endolysosomal escape. *Journal of Materials Chemistry B*, 6, 5269-5281.
3. #Clement S, #**Chen W**, Deng W, Goldys EM (2018). Folic acid conjugated biodegradable nanoparticle – photosensitizer matrix for targeted deep tumour therapy, #co-first authors, *International Journal of Nanomedicine*, 13, 3553.
4. **Chen W**, Deng W, & Goldys EM (2017). Light-triggerable liposomes for enhanced endolysosomal escape and gene silencing in PC12 cells. *Molecular Therapy-Nucleic Acids*, 7, 366-377.
5. Clement S, **Chen W**, Anwer AG, & Goldys EM (2017). Verteporfin conjugated to gold nanoparticles for fluorescent cellular bioimaging and X-ray mediated photodynamic therapy. *Microchimica Acta*, 184(6), 1765-1771.
6. #Zhao X, #Meng Z, #Wang Y, **Chen W**, Sun, C, Cui, B, Yu M, Zeng Z, Guo S, Luo D, Cheng JQ, Zhang R, Cui H (2017). Pollen magnetofection for genetic modification with magnetic nanoparticles as gene carriers. *Nature Plants* 3, 956–964. #co-first authors.
7. Wang Y, Zhao X, Du W, Liu J, **Chen W**, Sun C, Cui B, Shen Y, Gao F, Wang A, Liu G, Cui H (2017). Production of transgenic mice through sperm-mediated gene transfer using magnetic nano-carriers. *Journal of Biomedical Nanotechnology* 13(12):1673-1681.
8. Ma K, Zhang F, **Chen W**, Anwer A, Care A, Xu B, Tian W, Goldys EM, Liu G (2017). "Turn-on" fluorescent aptasensor based on AIEgen labeling for the localization of IFN- γ in live cells.

ACS Sensor. In press. DOI: 10.1021/acssensors.7b00720.

9. Deng W, Kautzka Z, **Chen W**, & Goldys EM (2016). PLGA nanocomposites loaded with verteporfin and gold nanoparticles for enhanced photodynamic therapy of cancer cells. *RSC Advances*, 6(113), 112393-112402.
10. **Chen W**, Cui H, Zhao X, Cui J, Wang Y, Sun C, & Lei F (2015). Characterization and insights into the nano liposomal magnetic gene vector used for cell co-transfection. *Journal of Nanoscience and Nanotechnology*, 15(8), 5530-5536.
11. **Chen W**, Cui H, Zhao X, Cui J, Wang Y, Sun C, & Lei F (2015). Construction and characterization of liposomal magnetofection system in pig kidney cells. *Chin J Biotech*, 2014, 30(6): 972–981.
12. Zhao X, Cui H, **Chen W**, Wang Y, , Sun C, & Liu G Cui B (2014). Morphology, structure and function characterization of PEI modified magnetic nanoparticles gene delivery system. *PloS one*, 9(6), e98919.

Conference proceedings and abstracts:

1. **Chen W**, Deng W, Vo J, Goldys EM. Photochemically activated liposomal platform for enhanced nucleic acids delivery. Poster, ESGCT 25th Annual Congress 17-20 October 2017, Berlin. Human Gene Therapy (Vol. 28, No. 12, pp. A122-A123)
2. **Chen W**, Deng W, Vo J, Goldys EM. Enhanced plasmid DNA delivery from photo-triggered stealth liposomes. Molecular Therapy 2017, 25 (5), 220. Poster, ASGCT (American Society of Gene and Cell Therapy) 20th Annual Meeting, 10-13 May 2017, Washington. Molecular Therapy 2017, 25 (5), 220.
3. **Chen W**, Deng W, Goldys EM. Light enhances endosomal escape and DNA delivery. Oral, 2017 International Conference on BioNano Innovation 24-27 September 2017, Brisbane.
4. **Chen W**, Deng W & Goldys EM. Enhanced gene silencing mediated by photoresponsive liposomes. Deng W, Goldys EM. Enhanced gene silencing mediated by photoresponsive liposomes. Poster. SPIE BioPhotonics Australasia, 17-19 Oct 2016, Adelaide. DOI: 10.1117/12.2244465.
5. **Chen W**, Zhao X, Cui J, Cui H, Wang Y & Goldys EM. Characterization and Cell Co-Transfection Using Liposomal Magnetic Nanoparticles. 6th International Nanomedicine Conference. 6 - 8 July 2015, Sydney.

Short bio:

1. 2015-2018, PhD, “Light triggerable nanomaterial-mediated gene/drug delivery”, ARC Excellence Centre for Nanoscale BioPhotonics, Macquarie University, Sydney.
2. 2011-2014, MSC, Molecular Biophysics, Nanobiological Research Center, Chinese Academy of Agricultural Sciences (CAAS), Beijing, P. R. China.
3. 2007-2011, BSC, School of Pharmacy, China Pharmaceutical University, Nanjing, P. R. China.

Appendix

Research ethics clearance documents to this thesis are listed as appendix.

Appendix of this thesis has been removed as they may contain sensitive/confidential content